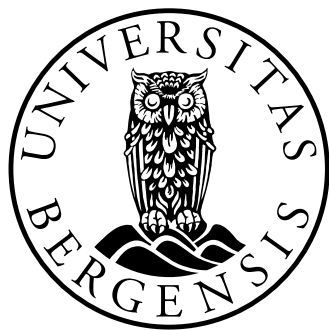


The Contour Deformation Method in Momentum Space, and Effective Interactions for Weakly Bound Nuclei

Gaute Hagen



Thesis submitted in partial fulfillment of the requirements
for degree Doctor Scientiarum

Department of Physics and Technology
University of Bergen
March 18, 2005

Contents

Acknowledgements	5
1 Introduction.	7
1.1 Few-Body Aspects of Dripline Nuclei.	7
1.2 Resonances in Quantum Mechanical Few-Body Systems.	9
1.3 Modern <i>Ab initio</i> Approaches to Nuclear Structure.	13
1.4 Exotic Many-Body States Embedded in a Continuum.	14
1.5 Outline of Thesis.	17
2 General Theory of Resonances and the Berggren Completeness.	19
2.1 Interpretation of Scattering Matrix Poles.	19
2.2 Regularizing Divergent Integrals of States on the Second Energy Sheet. . . .	24
2.2.1 Regularization by $e^{-\epsilon r^2}$	25
2.2.2 Regularization by Complex Scaling.	26
2.3 The Generalized Berggren Completeness; Proof and Discussion.	28
2.4 Interpretation of Complex Observables.	33
3 Contour Deformation Method (CDM) in Momentum Space; Theory and Applications.	37
3.1 The Momentum Space Schrödinger Equation.	37
3.2 Analytic Continuation of Momentum Space Schrödinger Equation by CDM. .	41
3.3 Single-Particle Resonances in a Deformed Field.	46
3.4 Two-Particle Resonances and Bound States Embedded in the Continuum in Complex Potentials.	56
3.5 Two-Particle Scattering; Isolating Resonance Phenomena by CDM.	61
3.5.1 Berggren representation of the t -matrix	62
3.5.2 Fredholm representation	63
3.6 Application of CDM to Resonance-Like Phenomena in nuclear matter.	67
3.6.1 2p2h Spectral Structures in a Nuclear Medium.	67
3.6.2 Pair Instabilities for the CD-Bonn interaction.	73
3.6.3 Calculation of Γ by CDM for the CD-Bonn Nucleon-Nucleon Interaction.	74

4 Effective Interactions and Many-Body Theory for Unstable Nuclei.	79
4.1 The Gamow Shell Model.	79
4.2 Lanczos Iteration Scheme for Many-Body Resonances.	82
4.3 Similarity Transformations and Effective Operators for Complex Interactions. .	88
4.4 Non-Hermitian Many-Body Perturbation Theory.	93
4.4.1 Single-Reference Perturbation Theory.	94
4.4.2 Multi-Reference Perturbation Theory.	100
4.5 Effective Interaction Scheme for Gamow Shell Model Calculations.	104
4.6 Inclusion of Realistic Nucleon-Nucleon Interactions in Gamow Shell Model Calculations.	106
5 Paper1.	115
5.1 Introduction to Paper 1.	115
5.2 <i>The contour deformation method in momentum space, applied to subatomic physics.</i>	116
6 Paper2.	149
6.1 Introduction to Paper 2.	149
6.2 <i>Effective Interaction Techniques for the Gamow Shell Model.</i>	150
7 Summary and perspectives.	175
A Left and right eigenvectors and bi-orthogonal sets.	187
B Three-body matrix elements in $j - j$ coupling	189

Acknowledgements

I would like to express gratitude to my supervisors Jan S. Vaagen and Morten Hjorth-Jensen for stimulating discussions and guidance during the work with my thesis. I owe a special thank to Morten Hjorth-Jensen for giving me thorough training in computational techniques, and organizing an exceptionally good work enviroment for me during my many stays at the Physics Department at the University of Oslo. Thanks also to the Research Council of Norway, for main economic support.

Also, I would like to thank Centre of Mathematics for Applications (CMA), at the University of Oslo, for letting me stay there for four months in the final stages of my work with this thesis.

I would also like to thank members of the RNBT collaboration, and in particular Boris V. Danilin Sergei Ershov and my good friend Maxim Kartamyshev for stimulating discussions on various topics related to my work.

Last but not least I would like to thank my family and girl friend Hanne Gøril Thomassen, who has been a great support to me for the last five years. Finally I would like to thank all my friends for giving me support and stimulating discussions.

Chapter 1

Introduction.

The complexity of the nuclear many-body problem has made nuclear physics a field driven by discoveries of outstanding phenomena. Tanihata's discovery in 1985 [1] of vastly spatially extended nuclei ($^{6,8}\text{He}$; ^{11}Li ; ^{11}Be) at the neutron dripline, renewed the interest in the study of weakly bound and resonance phenomena in few-body systems. With access to secondary exotic nuclear beams, the edges of the nuclear landscape itself are now being explored, *i.e.* the very limits of nuclear existence. At these limits, the so-called neutron (proton) *driplines*, additional neutrons(protons) literally drip out of the nucleus. Nuclei far from stability allow us to amplify and isolate particular aspects of the nuclear interaction and dynamics. Using what we learn from these nuclei we can then return to the nuclei of the world around us and understand them far better than ever before. Progress in nuclear structure is made at the various levels where one attempts to understand nuclear phenomena; (i) Experimental data and phenomenology, (ii) ‘Local models’ (effective models with few emergent degrees of freedom), (iii) ‘Global nuclear models’, (iv) Ab initio NN-interaction based procedures, (v) QCD. There is an overall effort to explain higher levels in terms of lower ones, but a more reductionist “deductive approach” is likely to have as precursor an approach which tries to isolate and understand the characteristic degrees of freedom.

1.1 Few-Body Aspects of Dripline Nuclei.

Nuclei along the dripline with an extreme dilute neutron skin have been labelled *halo nuclei*. Understanding the mechanisms underlying the formation of such nuclei has been a theoretical challenge, especially two-neutron Borromean¹ halos such as ^6He and ^{11}Li . The Borromean nuclei display extreme clusterization into an ordinary core nucleus and veil of halo nucleons – forming exceptionally dilute neutron matter. This clusterization has motivated few-body approaches such as the hyperspherical harmonic method and mo-

¹The three Borromean rings, the heraldic symbol of the Italian Borromeo family, are interlocked in such a way that if any of them were removed, the other two would also fall apart. The three intertwined Borromean rings are now widely used as the logo of the halo field.

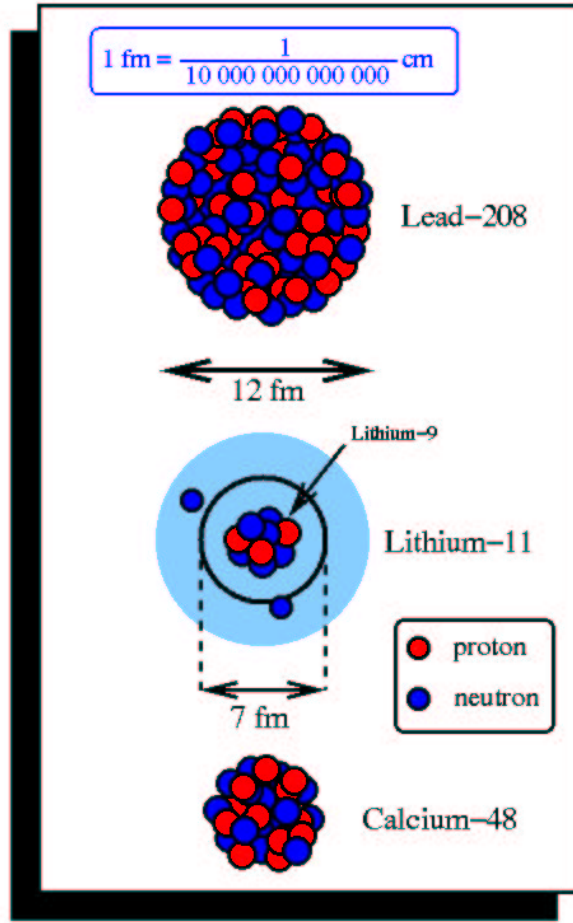


Figure 1.1: The matter size of ^{11}Li is compared to that of ^{48}Ca and ^{208}Pb

mentum space Faddeev equations, to these nuclei [2]. Borromean nuclei such as ^6He and ^{11}Li has been especially suitable for few-body models, they are characterized by pairwise constituents with no bound states whereas modelled as a three-body system they achieve binding. The extreme size of these dilute neutron excessive nuclei is mainly caused by the outermost neutrons being very loosely bound or even unbound, causing a large tail in their wave functions. Figure 1.1 shows the spatial extension of the Borromean nuclei ^{11}Li in comparison with the nuclei ^{48}Ca and ^{208}Pb . The spatial extension is huge, the rms matter radius of ^{11}Li is as large as that of ^{48}Ca , and the radius of the halo neutrons is as large as for the outermost neutrons in ^{208}Pb . To understand theoretically this abnormal feature of dripline nuclei has been a challenge over the years.

Borromean nuclei along the dripline have the property of being bound in their ground state. The ground-state properties of the Borromean nuclei ^6He has been well understood in terms of few-body modelling [2]. The α core of ^6He is stable and well bound, and it may be frozen in its ground state. The relevant degrees of freedom are then described

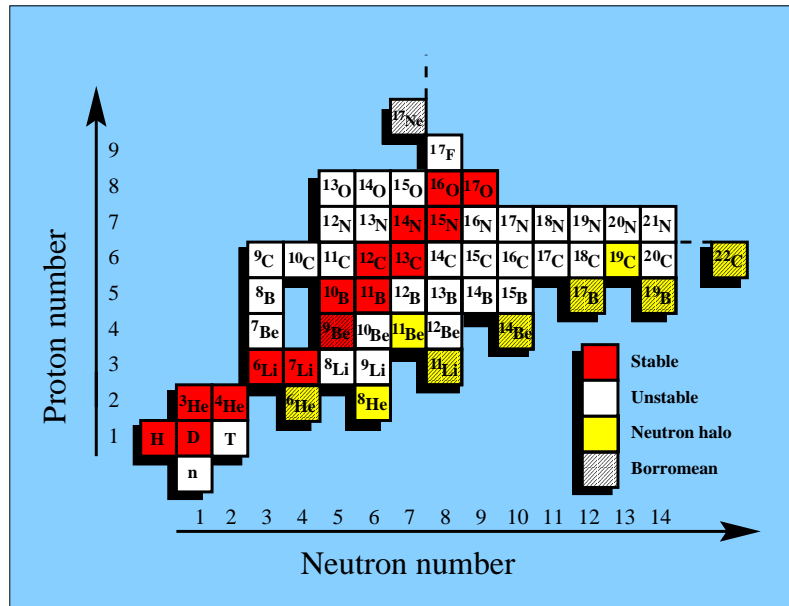


Figure 1.2: The nuclear chart exhibits the stability of Borromean nuclei among different isotope chains

by the two halo neutrons relative to the core. In three-body models of halo nuclei such as ^6He , Pauli blocking is needed to remove components of the halo wave function that would otherwise disappear under full antisymmetrization. This, and also other aspects of the composite nature of the clusters, make the challenge somewhat different from that of three-nucleon systems.

However, most nuclei along the dripline exhibit an unstable character, in that their ground state is embedded in the continuum, in the form of a resonance. The hadronic stability of Borromean nuclei is mainly due to strong pairing effects between the outermost neutrons. Figure 1.2 gives the hadronic stability of various isotope chains, and it is seen that while ^5He is unbound ^6He is bound, ^7He is unbound but ^8He is again bound. A recent review [3] looks at all the dripline nuclei. Dripline physics, which involves nuclei with one or a few weakly bound states, is physics of threshold phenomena where structure and reaction theory merge. Hence the development of methods for dealing with resonance and other continuum phenomena in such nuclei is of great importance. See my co-authored paper [4] for a more complete discussion of few body aspects of drip line nuclei.

1.2 Resonances in Quantum Mechanical Few-Body Systems.

The characteristic feature of exotic states embedded in the continuum is that they only exist for a limited time, before they fall apart into their decay products. Such states are labeled

quasi-stationary or resonant states. In a two-body picture, they may be understood as states trapped inside the centrifugal barrier for a limited time, before they tunnel through the barrier and decay. Such resonant structures are often called *shape resonances*, see figure 1.3. Considering the time dependent wave function, which satisfies the Schrödinger

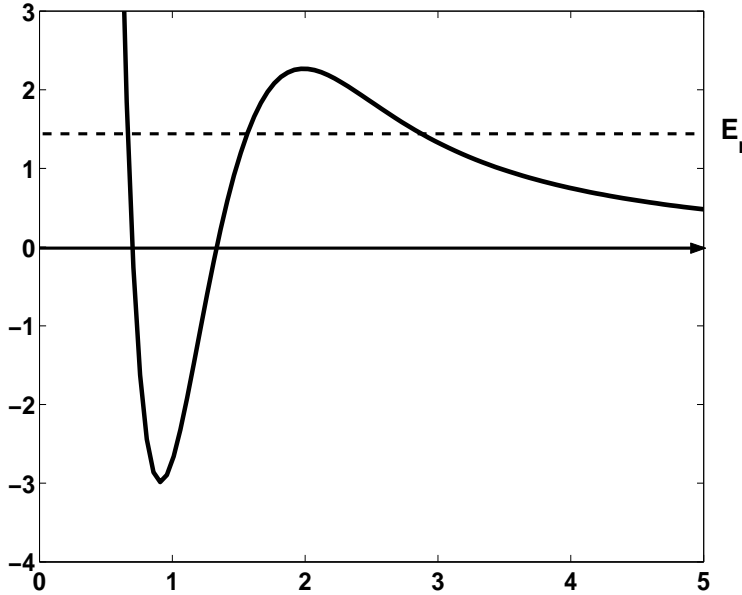


Figure 1.3: Confining potential in which a resonant state at real energy E_R is formed.

equation for a complex energy $z = E_R - i\Gamma/2$,

$$\Psi(\mathbf{r}, t) = \Phi(\mathbf{r}) \exp(-i \frac{z}{\hbar} t),$$

it is seen that the probability density at a point \mathbf{r} ,

$$|\Psi(\mathbf{r}, t)|^2 = |\Phi(\mathbf{r})|^2 \exp(-i \frac{\Gamma}{\hbar} t),$$

decreases exponentially with time only for $\Gamma > 0$. As already pointed out by Gamow in 1928 in his work on radioactive decay [5], this wave function is the only one appropriate for description of resonances or quasi-stationary states. Resonances are observed in experiments as enhancements in the cross section when plotted as a function of energy. In the case of isolated resonances, where the distance in energy between the resonances exceeds their widths, and the resonances are far from decay thresholds, the total cross section over the resonance peak may be parametrized by the Breit-Wigner formula [6],

$$\sigma \propto \frac{\frac{1}{4}\Gamma^2}{(E - E_R)^2 + \frac{1}{4}\Gamma^2}.$$

A detailed analysis of such data often reveals that this enhancement is due to one specific partial wave. To that extent, resonances have a definite set of quantum numbers just like bound states, the only differences being the fact that these states have a definite lifetime and thus correspond to complex energy eigenstates. Standard quantum mechanics is formulated for Hermitian operators. This raises the question of how a Hermitian Hamiltonian could give rise to a complex eigenvalue and whether such states should be included in our Hilbert space?

How to actually solve for single-particle resonances has been a separate study in many different areas of quantum physics over the years. The specialization trend within all disciplines of applied quantum physics makes it almost impossible to understand questions and problems raised within the different branches of quantum physics, on the other hand a methodological unification has taken place in many areas. The theory of resonances is such an example. The theory underlying the formation and decay of long lived states in molecules, atoms, nuclei, and condensed matter is from a quantum mechanical viewpoint methodologically basically the same. By recognizing this, it is possible to obtain new perspectives in various fields by adopting methods originally developed in different fields of physics. A variety of methods has been developed for understanding the basic mechanisms of formation of resonant states and processes taking place in the continuum. They are described in text books such as [7, 8, 9, 10]. All the methods have in common that they originate from standard scattering theory, and are based on the method of analytical continuation. The relevant equations are analytically continued from the physical energy sheet through the unitarity cuts onto the second energy sheet of the complex energy plane, where resonances may be located.

One of the more popular methods during the last decades has been the complex scaling method, originally formulated by Aguilar, Balslev and Combes in the early 70's [11, 12], and developed for examining the spectrum of the Green's function on the second energy sheet. Later this method has been adopted in other fields such as atomic and molecular fields to the study of resonances by complex scaling. In the context of complex coordinate scaling applied to quantum chemistry, Moiseyev [13, 14, 15] developed a generalized complex variational principle for resonant states. In reference [16] the complex scaling method where applied to the study of nuclear resonances, expanding the resonance wave function on complex scaled harmonic oscillator functions. During the last decade the complex coordinate method has seen several applications in nuclear physics, as interest in loosely bound nuclear halo systems has grown, see for example [17, 18, 19, 20] for an application to the resonant states of Borromean halo nuclei.

More recently a method based on exact differential equations for functions closely related to the Jost functions has been developed [21, 22]. The method exploits the idea of complex rotation of the coordinates, but differs from the traditionally used complex scaling methods using expansions and variational principles. The Jost function at a complex energy is obtained directly from exact equations, and resonances are associated with zeros of the Jost function on the second energy sheet.

Another popular approach is method based on analytic continuation in the coupling constant (ACCC) [8, 23]. The ACCC method uses analytic continuation in the coupling

strength of the potential instead of the usual continuation in energy. All these methods are usually formulated in coordinate representation.

One of the disadvantages of the coordinate space approach is that the boundary conditions have to be built into the equations, and convergence may be slow if the basis does not mirror the physical outgoing boundary conditions well. Instead, it is possible to represent the Schrödinger equation in momentum representation, invoking the Fourier transform. One of the most obvious advantages of this, is that the boundary conditions for bound and resonant states are automatically built into the transformed integral equations. Diagonalizing, using a plane wave basis is very accurate [24], since the convergence is only governed by the number of integration points.

As shown by Afnan [25] a rotation of the integration contour in the lower half complex k -plane is equivalent to the complex coordinate rotation method, and in this respect the coordinate and momentum space versions are complementary. It should be noted that the contour deformation method (CDM) formulated *in momentum space* is not new in nuclear physics. It was studied and applied in the 1960's and 1970's, see for example [26, 27, 28, 29], especially in the field of three-body systems. Most of these references applied a *contour rotation* in momentum space. By restricting oneself to a rotated contour certain limitations and restrictions however appear in the equations, determined by the analytical structure of the integral kernels and potentials. In [29] a more sophisticated choice of contour, based on rotation and translation, was applied to the three-nucleon momentum space Faddeev equation, for a separable Yamaguchi interaction. This choice of contour made it possible to avoid the logarithmic singularities of the Faddeev kernel and hence allowed for a continuation in energy to the non-physical energy sheet. The method has recently been revived to study anti-bound and resonant states in subatomic physics [24], where a general contour was considered.

The question now arises, whether resonant states can integrated into a complete set of states, appropriate for eigenfunction expansions. In the late 60's Berggren proved that for a finite range potential, a finite set of bound and resonant states together with a set of non-resonant continuum states form a complete set [30] of bi-orthogonal functions.

$$\mathbf{1} = \sum_n |\psi_{nl}\rangle\langle\psi_{nl}| + \int_{L^+} dk k^2 |\psi_l(k)\rangle\langle\psi_l(k)|. \quad (1.1)$$

This representation has later become known as the *Berggren basis*. The non-resonant continuum integral is defined along a contour in the fourth quadrant of the complex k -plane, and the discrete sum is over both bound and resonant states.

In this representation the usual inner-product is no longer Hermitian. The resonant states are not normalizable in the usual sense, as they oscillate and diverge exponentially along the real axis. As first shown by Zel'dovich [10], the inner product of a resonant state together with its complex conjugate, may be given a definite value by some regularization procedure. Expanding the scattering and reaction amplitudes in this basis, makes it possible to separate the resonance behaviour from the smooth non-resonant background in the scattering amplitudes. This is motivated by the fact that the most interesting phenomena taking place in the continuum are the resonance phenomena.

1.3 Modern *Ab initio* Approaches to Nuclear Structure.

In physics one often attacks a specific problem within a reductionist way of thinking. That is, the phenomena of the whole system should be described in terms of the theories and laws of the parts of the system.

In nuclear physics one would ideally like to start from nucleon degrees of freedom. The dominant philosophy within the nuclear theory community is that the nucleus (at low energies) as a whole may be fully described in terms of the interactions between these constituents. However, building up the nucleus from these basic constituents and their mutual interactions, the quantum mechanical description of the many-body system becomes extremely complex and hard to tackle as the number of nucleons increases.

In the history of nuclear structure the Shell Model has been very successful in describing properties of nuclei near the valley of stability. The traditional Shell Model has usually been formulated in a harmonic oscillator representation. This is based on the assumption that the single-particle motion within the nucleus is well described by harmonic oscillator orbitals. This is certainly true for well bound nuclei where the tail of the single-particle wave functions falls off rapidly. The harmonic oscillator wave functions are also favourable as they are given in terms of well known mathematical functions. However, the possibly most attractive aspect is that the Hamiltonian describing the motion of two particles in a harmonic oscillator potential may be written in separable form in both relative and center-of-mass coordinates and Shell Model coordinates. This is extremely favourable since the effective interaction between the nucleons is given in relative coordinates.

The Shell Model approaches to nuclear structure are usually not truly reductionistic. For heavier nuclei the number of degrees of freedom becomes too large to handle by modern computers. Therefore it has been customary to define an inert core of the nucleus which sets up a mean-field in which the valence nucleons move. Thus the nucleus ^{18}O may be modelled with two valence nucleons moving in the $s - d$ shell with respect to the closed shell nucleus ^{16}O acting as an inert core. As the number of valence particles grows the number of nucleon configurations within a valence space becomes larger and larger, making it difficult to handle numerically. Nevertheless, in the last decade one has experienced an extremely rapid development of computational power, making it possible to extend the Shell Model into regions previously inaccessible.

The growth of computational power has also induced a belief in *ab initio* calculations of nuclei, taking into account all degrees of freedom. The most ambitious of these ‘reductionist’ attempts are Green’s Function Monte Carlo (GFMC) calculations [31, 32, 33, 34, 35, 36, 37], extending previous variational Monte Carlo (VMC). According to the authors these are the first microscopic calculations that directly produce nuclear shell structure from realistic interactions that fit NN scattering data. Another line of approach is the large-basis no-core Shell Model (NCSM) calculations of Barrett’s group [38, 39, 40, 41], where the Shell Model is combined with microscopic effective interactions derived from modern nucleon-nucleon potentials.

The exponential growth of the configuration space as the number of active particles increases makes it extremely difficult to reach into the range of medium size nuclei, within these *ab initio* formalisms. The cost of matrix diagonalization increases with the third power of the number of basis states, and the memory required to store the Hamiltonian matrix increases with the square of the number of basis states. The practitioners have, however, already had success with their pioneering attempts. So far converged results for nuclei with up to $A = 12$ active particles have been reported. Further, GFMC and NCSM calculations for $A=6$ do produce an alpha-like core object, and two alpha-particles for ^8Be , both promising features.

Another *ab initio* approach which recently has proved promising in the medium size region of the nuclear chart, is the Coupled-Cluster method. The Coupled-Cluster method originated in nuclear physics in the 60's [42, 43], but has since that time only appeared sporadic within nuclear physics. On the other hand Coupled-Cluster theory has been extensively used, and with great success, in quantum chemistry over the years [44, 45]. Basically the Coupled-Cluster method is based on an exponential ansatz for describing correlations within a nucleus.

$$\Psi_{CC} = \exp(\hat{T})\Psi_0, \quad \hat{T} = \hat{T}_1 + \hat{T}_2 + \hat{T}_3 + \dots,$$

where \hat{T}_n are linear combinations of all n -type excitations. Including only single and double excitations (CCSD), the computational cost scales as N^7 where N is the size of the system. Instead of direct matrix diagonalization, a non-linear set of equations is solved iteratively. Very recently [46, 47, 48], converged Coupled-Cluster results for the ground- and first excited state of ^{16}O have been reported, using modern nucleon-nucleon interactions derived from effective field-theory.

1.4 Exotic Many-Body States Embedded in a Continuum.

All of the above mentioned many-body approaches have been formulated using a harmonic oscillator basis describing single-particle motion. Adopting a harmonic oscillator picture, one assumes from the very start that the interacting nucleons are isolated from an external environment of positive scattering states. The tremendous success of the multi-configurational Shell Model over the second part of the last century, in describing properties of nuclei where continuum aspects are more or less absent, has given little focus on mechanisms involved in the formation and decay of nuclei far away from the valley of *beta*-stability. However, approaching the drip-lines new aspects and properties of nuclei emerge, such as the instability of decay, enormous size of halo nuclei and the melt down of shell structures and new shell closures.

To bridge the gap between reaction and structure theory, microscopical Shell Model calculations using a Berggren representation for the single-particle states were proposed some years ago [49, 50]. The proximity of the scattering continuum in weakly bound and

unbound nuclei, implies that these nuclei cannot be properly described without taking into account the coupling between discrete states and the positive energy continuum. In other words, a proper description of loosely bound nuclei should take into account the coupling of the internal with the external environment, which has been totally neglected in classic Shell Model approaches. The coupling of the 'external' continuum of positive energy states, with the 'internal' nuclear states has for a long time been basic ingredient in nuclear reaction theory. Feshbach was the first to formulate a unified description of direct and compound nuclear reactions within the projection operator method [51, 52]. He showed that the coupling of the internal with the external environments could give rise to compound nuclear states, such as multi-channel resonances. As he was the first to formulate a general theory of such states, they became known as Feshbach resonances. Also in atomic physics Feshbach resonances are of great importance. In the early 60's, at the same time as Feshbach's work, Fano [53] discussed how the mixing of a configuration belonging to a discrete spectrum with configurations belonging to a continuous spectrum gives rise to the phenomena of *autoionization*, which is considered a multi-channel resonance or in other words a Feshbach resonance.

Entering the realm of weakly bound nuclei, it becomes evident that the standard separation of nuclear structure and nuclear reaction methods has to be abandoned. A merging of the two fields, where many-body methods from the structure community are united with reaction theory, where the importance of the continuum has been studied over several years, seems to be a fruitful approach. Treating the continuum aspects properly within existing many-body theories, is however much more difficult than when dealing with well bound nuclei. Existing many-body structure approaches have to be reformulated and developed further since the harmonic oscillator representation has to be abandoned. All the nice mathematical properties of the harmonic oscillator basis are non-existent in all other single-particle representations, e.g. the Woods-Saxon basis.

Having determined a single-particle basis consisting of bound, resonant and non-resonant continuum states, it is natural to again focus on the application of this basis in nuclear structure calculations of weakly bound and/or unbound nuclei. Ideally one would like an *ab initio* description of these nuclei, taking into account all relevant degrees of freedom. In the hyperspherical description of three-body Borromean and halo nuclei, the problem of treating core excitations and the anti-symmetrization between core and valence nucleons has not fully been solved. Treating such nuclei microscopically, a reformulation of the Shell Model using a single-particle basis of bound, resonant and scattering states may appear to be the most straightforward method. The recently developed Shell Model Embedded in the Continuum (SMEC), see e.g. references [54, 55, 56, 57], offers such a possibility. SMEC is closely related to the Feshbach projection operator technique. In SMEC the bound, resonant and scattering states are treated on equal footing, by introducing two sub-spaces and taking their coupling into account. However, most SMEC calculations have not taken into account coupling with decay channels containing more than one nucleon.

Restricting the theory to only one-nucleon decay channels, limits the applicability of SMEC along the drip-lines. Borromean nuclei for which the A and $A - 2$ nuclei are particle stable, while the nuclei $A - 1$ are not, requires a theoretical description which

takes into account decay channels involving all valence nucleons. That is, all many body configurations involving bound and scattering states should be considered. The newly developed Gamow Shell Model is devoted to such an approach, see for example references [58, 59, 60, 50, 61, 62, 63, 64, 65, 24]. The Gamow Shell Model starts with the Berggren representation (1.1) for single-particle states. A complete many-body Berggren basis may then be constructed from the discretized single-particle Berggren orbitals

$$\sum_n |\Psi_n\rangle\langle \tilde{\Psi}_n| = 1,$$

where the many body Slater determinants $|\Psi_n\rangle$ are constructed from the discrete bound, resonant and non-resonant continuum orbitals. This is in full analogy with the standard Shell Model using a harmonic oscillator basis. When the exact multi-particle resonance wave function is expanded in a complete set of Slater determinants consisting of discretized single-particle Berggren orbitals, an interpretation of these exotic multi-particle structures in terms of single-particle resonances becomes possible.

Intuitively one would expect that the Slater determinant built from single-particle resonances only, would be the major component in the fully correlated many body wave function. This is certainly true if the residual nucleon-nucleon interaction is weak compared with the mean-field in which the valence particles move. More interesting is the opposite case, where the residual interaction is strong. In this case it is not obvious that the pure pole configurations are the most important. However, the Gamow Shell Model may provide an answer to the question of how exotic structures, such as multi-particle resonances, embedded in the continuum are formed. The Gamow Shell Model is a promising many-body approach in the study of unstable nuclei along the drip-lines. And it is in the unifying spirit of scientific development, in that it reconciles the reaction and the structure part of the community. The Gamow Shell Model is in its early stages, and so there exists a vast area of applications and major theoretical and computational challenges to be dealt with. One of the first challenges and problems encountered in the Gamow Shell Model, was the *identification problem*, first addressed in [50, 61]. The physical multi-particle resonances will in many cases be embedded in a dense distribution of continuum states, depending on the contour on which the continuum states are defined. References [50, 61] related this *identification problem* to the problem of choosing a contour in the complex k -plane which in the case of several valence particles selects the physical interesting states from the dense continuum background. They found that in the two-particle case, choosing a *square-well* contour makes an identification of physical states based on inspection of the zeroth order energy surface possible. This solution is only applicable in the two-particle case, already in the tree-particle case the physical states get mixed in with the continuum states. In references [59, 62, 63] the problem of identifying multi-particle resonances was approached from a different angle. The proposed algorithm is a two step procedure. In the first step a diagonalization within the pole space, where all particles are in resonant single-particle orbitals, is performed. Secondly, a diagonalization within the complete configuration space undertaken. Under the assumption of weak coupling of the pole configurations with the configurations where at least one particle moves in a continuum orbital, the physical states

may be picked out unambiguously from the states obtained after a full diagonalization, using the criterion of largest overlap with the pole space. The weak coupling limit may not always be a valid assumption, as pointed out in Ref.[65] for the case of ^{11}Li the two-particle resonances may have a larger continuum component as compared to the pole component, depending on the strength of the residual nucleon-nucleon interaction. Presently one may conclude that the *identification problem* has not been solved generally, and developing an algorithm which picks out physical states unambiguously from the dense continuum background is still an open problem.

Another challenge for the Gamow Shell Model is the *dimensionality problem*. As the number of active particles moving in a valence space increases, the number of Slater determinants in the many-body Berggren basis increases dramatically. This explosion of many-body configurations is even more severe than in the standard Shell Model approach where only bound states appear. In the Gamow Shell Model one has for each partial wave a finite number of non-resonant continuum states which are absent in the standard Shell Model. In solving this problem, one has to take advantage of effective operator and perturbation method techniques typically used and developed for large scale Shell Model calculations using harmonic oscillator bases.

With further progress in computational power one may hope that *ab initio* calculations of light and medium size nuclei within the Berggren representation may become possible in the near future. Coupled-Cluster techniques has proven to be a promising method for microscopical calculations of medium size nuclei such as ^{16}O , a promising way of approach would be to generalize the Coupled-Cluster method to complex interactions, and at the first stage see how resonant structures are formed in light nuclei starting from an *ab initio* approach. Another interesting application would be to see how single-particle resonances are formed starting from a realistic nucleon-nucleon interaction. In conclusion, one may say that nuclear physicists are living in exciting times.

1.5 Outline of Thesis.

This thesis combines results which are published in international journals with results which appear only in this thesis. The main purpose of this thesis, may nevertheless be summarized in the two published papers *The contour deformation method in momentum space, applied to subatomic physics* and *Effective Interaction Techniques for the Gamow Shell Model*. However, since these papers deal with topics which may be less familiar to the audience, this thesis aims at giving a more detailed and thorough discussion of the formalisms and theories underlying this work. The outline of the thesis is the following.

Chapter 2 gives a detailed discussion of the scattering functions and Jost functions starting with the coordinate representation of the Schrödinger equation. The most general distribution of poles of the scattering matrix is discussed, together with their physical interpretations. Chapter 2 also discusses some typical regularization procedures for matrix elements involving resonant states. An outline of the proof of the general Berggren completeness which includes bound, anti-bound and resonant states is given, and a discus-

sion of the physical interpretation of expectation values of observable operators involving resonant states.

Chapter 3 starts with the momentum representation of the Schrödinger equation (section 3.1), and discusses how the Schrödinger equation may be analytically continued to the second energy sheet using the Contour Deformation Method (CDM) (section 3.2). A complete set of single-particle states, involving all kinds of poles, is obtained. Chapter 3 contains several applications which are not included in the published papers. Section 3.3 gives an application of the CDM to the problem of solving for resonances in a deformed field is given section 3.4 gives an application of CDM to resonances and bound states in complex absorptive and emitting potentials. Section 3.6.1 gives an application of CDM to the solution of pair instabilities of the CD-Bonn interaction in a infinite nuclear medium, and discusses how poles on the second energy sheet may be interpreted as resonance like states.

Chapter 4 discusses the application of a single-particle basis constructed by CDM may serve as a starting point for Gamow-Shell-Model studies. Section 4.2 discusses how the Lanczos iteration method may be applied to the calculation of multi-particle resonances in the Gamow Shell Model formulation. As numerical test study, the convergence of the 0^+ ground state and the 2^+ resonance energy of ${}^6\text{He}$ for each iteration is given. The results are promising for large-scale Gamow Shell Model calculations. Section 4.3 gives a formal derivation of the Lee-Suzuki similarity transformation method for complex interactions, and shows how a complex symmetric interaction may be obtained by a second similarity transformation. Section 4.4 discusses the use of Many-Body perturbation theory in Gamow-Shell-Model calculations. A derivation of the standard Rayleigh-Schrödinger perturbation expansion for a single model space state is given for the case of complex interactions. It is shown that the standard single-reference perturbation theory does not give satisfactory results when treating many-body resonance perturbatively. The Multi-Reference-Perturbation-Theory-Method (MRPTM) is subsequently derived. This theory differs from standard perturbation theory, in that it is a one-state-at-a-time perturbation theory. Section 4.5 gives an effective interaction scheme for the Gamow-Shell-Model which combines the Lee-Suzuki similarity transformation method with the one-state-at-a-time MRPTM. Finally, section 4.6 demonstrates how a complex scaled, renormalized nucleon-nucleon interaction ($V_{\text{low-}k}$) may be obtained invoking the Lee-Suzuki similarity transformation, this interaction may subsequently be input in microscopic calculations of resonances.

Chapter 5 gives a short introduction to the article *The contour deformation method in momentum space, applied to subatomic physics*.

Chapter 6 gives a short introduction to the article *Effective Interaction Techniques for the Gamow Shell Model*.

In Chapter 7 conclusions of the present work, and future perspectives are given.

Chapter 2

General Theory of Resonances and the Berggren Completeness.

2.1 Interpretation of Scattering Matrix Poles.

Resonance phenomena are associated with processes taking place in the continuum. Any quantum mechanical system may be experimentally found to be either in a bound stationary state or in a scattering state located in the positive continuum. Resonance states with definite lifetime are never directly observed, but instead the scattering states into which they decay are observed. It is therefore natural to start with the radial Schrödinger equation, for a spherically symmetric potential $V(r)$,

$$\left(-\frac{d^2}{dr^2} + v(r) + \frac{l(l+1)}{r^2} - k^2 \right) u_l(k, r) = 0, \quad (2.1)$$

here $v(r) = 2\mu V(r)/\hbar^2$ and the energy is related to the wavenumber by $k^2 = 2\mu E/\hbar^2$, where μ is the reduced mass of the system. There are four different types of physical states associated with this Schrödinger equation, bound, anti-bound, resonant and scattering states, differing in the boundary conditions imposed on the wave functions at large distances.

In the following an overview of the properties of the regular and irregular solutions of the Schrödinger equation, and their relation to the physical scattering wave function is given. For a more detailed review the reader is referred to the text books of Newton [7] or Sitenko [9] on scattering theory.

Next we assume that the central potential is less singular near the origin than r^{-2} and vanishes faster than r at infinity, that is,

$$\lim_{r \rightarrow 0} r^2 V(r) = 0, \quad \lim_{r \rightarrow \infty} r V(r) = 0. \quad (2.2)$$

From the theory of ordinary second order differential equations the condition that the potential $V(r)$ has a “weaker” singularity than r^{-2} at the origin, means that the point

$r = 0$ is a *regular singular point*. It is customary to label those solutions of equation (2.1) which vanish $r = 0$ *regular* and those which do not *irregular* solutions. The regular $\phi_l(k, r)$ and irregular solutions $f_l(k, r)$ to equation (2.1), are uniquely defined by the boundary conditions,

$$\begin{aligned} \lim_{r \rightarrow 0} (2l+1)!! r^{-l-1} \phi_l(k, r) &= 1, \\ \lim_{r \rightarrow \infty} \exp(ikr) f_l(k, r) &= i^l. \end{aligned} \quad (2.3)$$

The irregular solutions $f_l(k, r)$ are called the Jost solutions, and from the boundary condition it follows that they have the asymptotic form

$$f_l(k, r) \rightarrow \exp(-ikr), \quad r \rightarrow \infty. \quad (2.4)$$

The Jost solutions $f_l(k, r)$ and $f_l(-k, r)$ are linearly independent solutions of equation (2.1). This follows from the fact that the Wronskian of $f_l(k, r)$ and $f_l(-k, r)$ is non-vanishing,

$$W[f_l(k, r), f_l(-k, r)] = 2ik, \quad (2.5)$$

which is easily shown using the asymptotic forms of the Jost solutions as $r \rightarrow \infty$. Since $f_l(k, r)$ and $f_l(-k, r)$ are linearly independent solutions, the regular solutions $\phi_l(k, r)$ may be expressed as a linear combination of the Jost solutions. The coefficients of $f_l(k, r)$ and $f_l(-k, r)$ are determined from the boundary conditions imposed on the regular solutions $\phi_l(k, r)$ at $r = 0$, and it follows that

$$\phi_l(k, r) = \frac{1}{2} ik^{-l-1} [f_l(-k) f_l(k, r) - (-1)^l f_l(k) f_l(-k, r)]. \quad (2.6)$$

Here the Jost functions $f_l(k) = f_l(k, r = 0)$ and $f_l(-k) = f_l(-k, r = 0)$ have been introduced, and they are given by the Wronskian

$$f_l(k) = k^l W[f_l(k, r), \phi_l(k, r)], \quad (2.7)$$

which follows directly from equation (2.6). It can be shown [7, 9] that the regular function $\phi_l(k, r)$ is an entire function in the complex k -plane, while the irregular Jost solution $f_l(k, r)$ is an analytic function in the lower half complex k -plane. From the boundary conditions in equation (2.3) it follows for complex k that the regular and irregular solutions satisfy the following conditions,

$$\phi_l(k, r) = \phi_l^*(k^*, r), \quad f_l(k, r) = f_l^*(-k^*, r). \quad (2.8)$$

Further the regular solutions satisfy

$$\phi_l(k, r) = \phi_l(-k, r), \quad (2.9)$$

since the $\phi_l(k, r)$ is an everywhere regular function of k^2 .

The physical scattering solutions $u_l(k, r)$ of equation (2.1) are given for a mixed set of boundary conditions, regularity at $r = 0$ and the asymptotic behaviour of scattering wave functions as $r \rightarrow \infty$ [7], i.e.

$$u_l(k, r) \xrightarrow[r \rightarrow \infty]{} \sqrt{\frac{1}{2\pi}} i \left\{ e^{-ikr} - (-1)^l S_l(k) e^{ikr} \right\}. \quad (2.10)$$

Here $S_l(k)$ is the partial wave scattering matrix element, which determines the phase shift of the outgoing wave at infinity. Since all physical solutions are regular at the origin, they differ from the regular solutions $\phi_l(k, r)$ only by a normalization constant. However, different asymptotic behaviours of the regular solutions are specified at specific points on the complex k -plane. The proper boundary conditions for physical states are only given at certain points in the complex k -plane. If the regular solution $\phi_l(k, r)$ is known in the entire complex k -plane, all physical states are in principle known. From equation (2.6) it follows that the asymptotic form of the regular solutions is given by

$$\phi_l(k, r) \xrightarrow[r \rightarrow \infty]{} \frac{1}{2} ik^{-l-1} f_l(-k) \left\{ e^{-ikr} - (-1)^l \frac{f_l(k)}{f_l(-k)} e^{ikr} \right\}. \quad (2.11)$$

Comparing with equation (2.10) it is easily seen that the partial wave S -matrix element, $S_l(k)$, is given in terms of the Jost functions

$$S_l(k) = \frac{f_l(k)}{f_l(-k)}. \quad (2.12)$$

Comparing the asymptotics of the physical wave function with the asymptotics of the regular solution $\phi_l(k, r)$, the physical scattering function may be written in terms of the regular solution $\phi_l(k, r)$ and the Jost function $f_l(k)$,

$$u_l(k, r) = \sqrt{\frac{2}{\pi}} \frac{k^{l+1} \phi_l(k, r)}{f_l(-k)}, \quad (2.13)$$

which is delta-function normalized.

Knowing all analytic properties of the Jost functions, all analytic properties of $S_l(k)$ follow directly. From the definition of $S_l(k)$ given in equation (2.12) follows that

$$S_l(-k) = S_l^{-1}(k), \quad (2.14)$$

and from the symmetry property of the Jost functions given in equation (2.8) follows that

$$S_l^*(k^*) = S_l^{-1}(k), \quad (2.15)$$

where the latter property coincides with the unitarity condition for the scattering matrix for real values of k . Further, these properties establish a one-to-one correspondence between values of the scattering matrix in different quadrants of complex k -plane. Say that we know the value of scattering matrix at a point in the fourth quadrant of the complex k -plane,

$S_l(k) = S$. Then it follows immediately from equation (2.14) that $S_l(-k) = S^{-1}$, and from equation (2.15) $S_l(-k^*) = S^*$. Using again the symmetry relation in equation (2.14) it finally follows $S_l(k^*) = S_l^{-1}(-k^*) = S^{-1}$. This shows that knowing the values of $S_l(k)$ in one quadrant of the complex k -plane, the scattering matrix is automatically known in the whole complex k -plane.

The scattering wave function and the S -matrix element $S_l(k)$ have poles at the same location in the complex k -plane, given by the zeroes $k = k_n$ of the Jost function $f_l(-k) = 0$. Due to the symmetry of the Jost functions given in equation (2.8), for each pole $k = k_n$ there is in addition a pole located at $k = -k_n^*$. Furthermore the symmetry property in equation (2.14) of $S_l(k)$ implies that for each pole $k = k_n$ of $S_l(k)$, it has a zero at $k = -k_n$. The poles in the complex k -plane are divided into four categories depending on their location in the k -plane, and are often labeled by the letters $a - d$. Consider first the case where $S_l(k)$ has a zero for $k = -i\kappa$ for real $\kappa > 0$. Then both the regular solutions $\phi_l(k, r)$ and the physical wave functions $u_l(k, r)$ are square integrable functions since they fall off exponentially as $\exp(-\kappa r)$. Furthermore the corresponding energy is real and negative $E = -\hbar\kappa^2/2\mu$ corresponding to a bound state of the system. It can be shown that in the upper half-plane the scattering matrix $S_l(k)$ can have poles only on the imaginary axis [9]. These poles correspond to the boundary conditions of bound states at infinity, i.e. belonging to the L^2 functional space, with exponentially decaying tails, and are labeled b .

In the lower half-plane it can be shown that the poles can be positioned anywhere. Poles located in the fourth quadrant of the complex k -plane are associated with resonant states with outgoing boundary conditions at infinity, often called *decaying* resonances, labeled d . To see that they correspond to outgoing asymptotics consider the regular function in equation (2.6) at a pole of the scattering matrix ($f_l(-k_n) = 0$), at $r \rightarrow \infty$ i.e.

$$\phi_l(k_n, r) = \underset{r \rightarrow \infty}{\longrightarrow} \frac{-1}{2} (-1)^l ik^{-l-1} f_l(k_n) e^{ik_n r}. \quad (2.16)$$

For a pole $k = k_n = k_1 - ik_2$ in the fourth quadrant of the complex k -plane this gives the specific asymptotics

$$\phi_l(k_n, r) \rightarrow e^{ik_1 r} e^{k_2 r},$$

where $k_1, k_2 > 0$. This shows that the decay resonances correspond to outgoing asymptotics, furthermore they are not square integrable in the normal sense since they are exponentially increasing and oscillating functions. The corresponding energy of the decay states is written in the form

$$E_n = \mathcal{E} - i \frac{\Gamma}{2\mu} = \frac{\hbar^2}{2\mu} ((k_1^2 - k_2^2) - i2k_1 k_2). \quad (2.17)$$

Proper physical resonances are often defined as poles where $k_1 > k_2$, where it is seen that the real part of the energy given in equation (2.17) is positive. For poles where $k_2 > k_1$ the real part becomes negative and they are often called *unphysical* poles. The most interesting resonances physically, are the resonances which show up as sharp peaks

in the cross sections, and this occurs for $\Gamma \ll \mathcal{E}$. For resonance poles where the width Γ is large, the resonance contribution to the cross section tends to get smeared out within the continuum background.

For each pole located in the fourth quadrant there is a pole in the third quadrant symmetrically situated about the imaginary k - axis, these poles corresponds to resonant states with incoming boundary conditions at infinity, often called *capture* resonances, labeled c . That they are incoming waves is seen from equation (2.16),

$$\phi_l(k_n, r) \rightarrow e^{-ik_1 r} e^{k_2 r}, \quad k_1 > 0, \quad k_2 > 0,$$

Poles located on the imaginary axis in the lower half-plane correspond to anti-bound states, labeled a , often called virtual states. These states increases exponentially at large distances, contrary to the bound states, and are clearly not normalizable,

$$\phi_l(k_n, r) \rightarrow e^{\kappa r}, \quad \kappa > 0.$$

Figure 2.1 sums up the most general distribution of poles of the scattering matrix and the corresponding zeros.

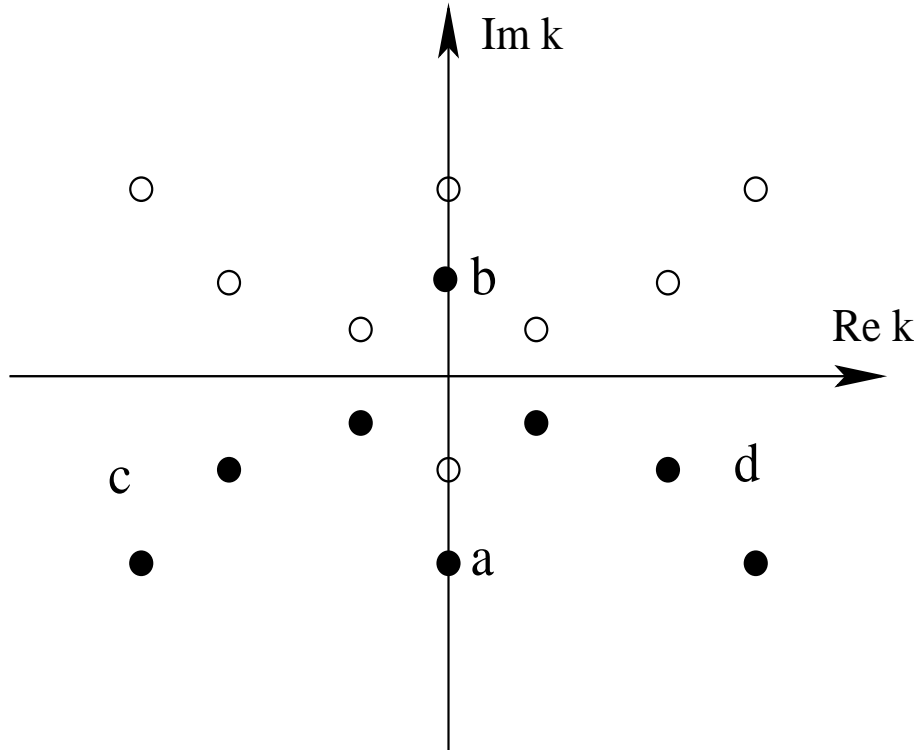


Figure 2.1: Distribution of S -matrix poles (filled circles) and corresponding zeroes (open circles) in the complex k -plane. a = anti-bound, b = bound, c = capture and d = decay.

2.2 Regularizing Divergent Integrals of States on the Second Energy Sheet.

The radial wave function $u_l(k, r)$ of a decay resonant state, with $k = k_n$ located in the fourth quadrant of the complex k -plane, satisfies the radial Schrödinger equation (2.1). The decay resonances are regular at the origin, $u_l(k, 0) = 0$, and have purely outgoing waves, $u_l(k, r) \rightarrow O_l(k, r)$, at infinity as boundary conditions. If the potential has a finite range, in the sense that it vanishes identically beyond some finite distance $r = a$. The outgoing solutions $O_l(kr)$ are given in terms of spherical Riccati-Hankel functions $h_l^{(+)}(kr)$. In the case of long-range potentials, such as the Coulomb potential, the asymptotic form of the wave functions are given by the more complicated Coulomb functions.

From the requirement that the wave functions and their derivatives should be continuous at the boundary of the potential $r = a$, follows that the logarithmic derivative should be continuous, giving the condition

$$u_l(k, a)O'_l(k, a) - u'_l(k, a)O_l(k, a) = 0. \quad (2.18)$$

For each pole $k = k_n$ in the fourth quadrant there is a pole $k = \tilde{k}_n = -k^*_n$ in the third quadrant associated with a capture resonance. The capture states, $u_l(\tilde{k}_n, r)$, are solutions of the complex conjugated version of the radial Schrödinger equation (2.1), with regularity at the origin and with purely incoming waves at infinity, $I_l(k, r)$. Where $I_l(kr)$ is given in terms of spherical Riccati-Hankel functions $h_l^{(-)}(kr)$. The corresponding boundary conditions for the capture states becomes,

$$u_l(\tilde{k}, a)I'_l(\tilde{k}, a) - u'_l(\tilde{k}, a)I_l(\tilde{k}, a) = 0. \quad (2.19)$$

In the following we define the the decay and capture states by

$$u_{nl}(r) \equiv u_l(k_n, r), \quad \tilde{u}_{nl}(r) \equiv u_l(\tilde{k}_n, r). \quad (2.20)$$

The capture and decay resonances are related through

$$\tilde{u}_{nl}(r) = u_{nl}^*(r), \quad \text{i.e. } \tilde{u}_{nl}^*(r) = u_l(r). \quad (2.21)$$

Normalization of the decay resonances through the usual Euclidean inner product,

$$\langle u_{nl}|u_{nl} \rangle = \int_0^\infty dr u_{nl}^*(r)u_{nl}(r) = \int_0^\infty \tilde{u}_{nl}(r)u_{nl}(r), \quad (2.22)$$

is not possible in the upper limit, since the integrand diverges exponentially as

$$\tilde{u}_{nl}(r)u_{nl}(r) \xrightarrow[r \rightarrow \infty]{} e^{2k_2 r}, \quad (2.23)$$

for $k_n = k_1 - ik_2$ and $k_1, k_2 > 0$. On the other hand, the fact the decay and capture resonances come in conjugate pairs, may suggest that they form a *bi-orthogonal* set of functions, and that the normalization integral,

$$\langle \tilde{u}_{nl}|u_{nl} \rangle = \int_0^\infty \tilde{u}_{nl}^*(r)u_{nl}(r) = \int_0^\infty u_{nl}^2(r), \quad (2.24)$$

may exist, and be given a definite value. The integrand of this integral still increases exponentially but oscillates as

$$\tilde{u}_{nl}^*(r)u_{nl}(r) \xrightarrow[r \rightarrow \infty]{} e^{2ir(k_1 - ik_2)}. \quad (2.25)$$

The hope is that the oscillations at large distances will cancel each other, such that

$$0 < |\langle \tilde{u}_l(k) | u_l(k) \rangle| < \infty. \quad (2.26)$$

2.2.1 Regularization by $e^{-\epsilon r^2}$.

From the theory of divergent integrals and series, see e.g. reference [66], many integrals which are divergent in the conventional sense, may be regularized by some regularization procedure. Zel'dovich [10] proposed the following integration procedure for regularizing integrals involving resonant states, which have an exponentially oscillating divergent tail along the real r -axis.

$$I = \lim_{\epsilon \rightarrow 0} \int_0^\infty dr e^{-\epsilon r^2} u_{nl}^2(r). \quad (2.27)$$

From the asymptotic behaviour of the resonant states in equation (2.25), it is natural to study the integral

$$I_n(k) = \lim_{\epsilon \rightarrow 0} I_n(k, \epsilon) = \lim_{\epsilon \rightarrow 0} \int_0^\infty dr e^{-\epsilon r^2} r^n e^{\kappa r}, \quad (2.28)$$

where $n = 0, 1$ and $\kappa = ik$. For a positive and finite value ϵ the regularizing factor $e^{-\epsilon r^2}$ decreases more rapidly than the exponential function $e^{\kappa r}$ increases for an arbitrary exponent κ , and the integral $I_n(k, \epsilon)$ converges. It is convenient to introduce a variable change in $I_0(k, \epsilon)$

$$t = r\sqrt{\epsilon}, \quad x = \frac{\kappa}{2\sqrt{\epsilon}}, \quad (2.29)$$

which gives

$$I_0(k, \epsilon) = \frac{1}{\sqrt{\epsilon}} e^{x^2} \int_{-x}^\infty dt e^{-t^2} = \sqrt{\frac{\pi}{\epsilon}} e^{x^2} [1 - 2\text{Erfc}(x)], \quad (2.30)$$

where

$$\text{Erfc}(x) = \frac{2}{\sqrt{\pi}} \int_x^\infty dt e^{-t^2}, \quad (2.31)$$

is the complementary error function [67]. As $\epsilon \rightarrow 0$ then $x \rightarrow \infty$, and using the asymptotic expansion of the error function [67], the integral $I_0(k, \epsilon)$ may be written as

$$\begin{aligned} I_0(k, \epsilon) &= \sqrt{\frac{\pi}{\epsilon}} e^{x^2} - \frac{1}{2x\sqrt{\epsilon}} \left(1 - \frac{1}{2x^2} + \frac{3}{4x^4} - \dots \right) \\ &= \sqrt{\frac{\pi}{\epsilon}} e^{-\frac{k^2}{4\epsilon}} + \frac{i}{k} - \frac{2\epsilon}{k^3} + O(\epsilon^2). \end{aligned} \quad (2.32)$$

The integral $I_1(k, \epsilon)$ is calculated using the relation,

$$I_1(k, \epsilon) = \frac{\partial}{\partial \kappa} I_0(k, \epsilon) = \frac{1}{2\epsilon} (\kappa I_0(k, \epsilon) + 1). \quad (2.33)$$

Inserting the asymptotic expansion for $I_0(k, \epsilon)$ in equation (2.32), gives for the $I_1(k, \epsilon)$ integral,

$$I_1(k, \epsilon) = -\sqrt{\frac{\pi}{4\epsilon^3}} i k e^{-\frac{k^2}{4\epsilon}} - \frac{1}{k^2} + O(\epsilon). \quad (2.34)$$

Dealing with regularization of integrals involving *proper* resonances, in which the real part of the resonance energy is positive, the restriction $|\operatorname{Re} k| > |\operatorname{Im} k|$ follows, and consequently $\operatorname{Re} k^2 > 0$. In this case the relation

$$\lim_{\epsilon \rightarrow 0} \epsilon^p e^{-\frac{k^2}{4\epsilon}} = 0, \quad (2.35)$$

is valid for any real p , and may be used to obtain the following finite expressions for the integrals $I_0(k)$ and $I_1(k)$,

$$I_0(k) = \frac{i}{k}, \quad I_1(k) = -\frac{1}{k^2}. \quad (2.36)$$

2.2.2 Regularization by Complex Scaling.

The regularization factor $e^{-\epsilon r^2}$ is not unique, and there exists a variety of other regularization procedures, all yielding the same unique finite result for the integrals $I_1(k)$ and $I_2(k)$. One such regularization procedure, more tractable from a numerical standpoint, is based on complex rotation in the complex r -plane, first discussed in reference [68]. Consider the zero contour integrals

$$\int_C dz e^{ikz} = 0, \quad \int_C dz z e^{ikz} = 0, \quad (2.37)$$

where the contour $C = C_1 + C_2 + C_3$ is defined by a rotation angle θ in the complex r -plane as shown in figure 2.2. For $R \rightarrow \infty$ the integral along the arc C_2 vanishes and by the Cauchy Riemann integral theorem it follows

$$\tilde{I}_0(k) = \int_0^\infty dr e^{ikr} = e^{i\theta} \int_0^\infty dr e^{ikr(\cos \theta + i \sin \theta)} \quad (2.38)$$

$$\tilde{I}_1(k) = \int_0^\infty dr r e^{ikr} = e^{2i\theta} \int_0^\infty dr r e^{ikr(\cos \theta + i \sin \theta)}. \quad (2.39)$$

(2.40)

For $k = k_1 - ik_2$ and $k_1, k_2 > 0$ these integrals converge for a rotation angle $\theta > \operatorname{atan}(k_2/k_1)$, and it is easily shown that they take the finite values

$$\tilde{I}_0(k) = I_0(k) = \frac{i}{k}. \quad (2.41)$$

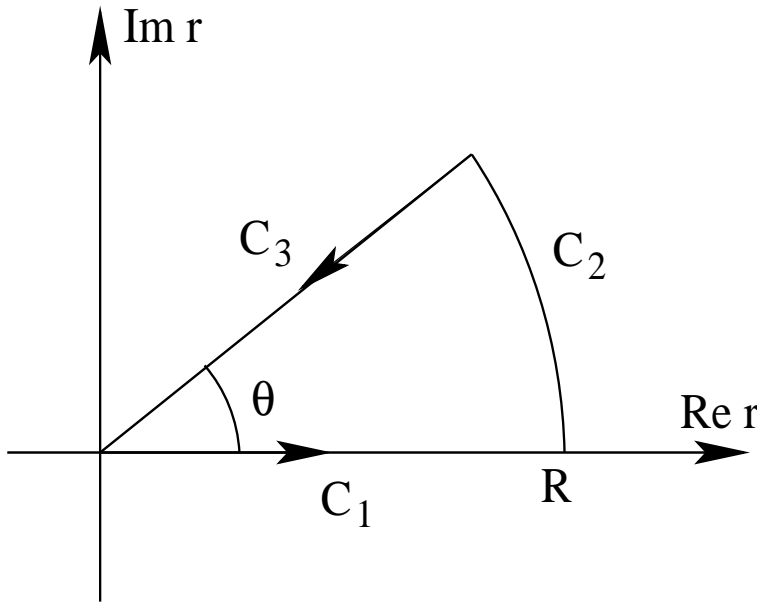


Figure 2.2: Integration contour in the complex r -plane used for regularization of integrals involving resonant states.

In the same way it is easily shown that the integral $\tilde{I}_2(k)$ takes the finite value

$$\tilde{I}_1(k) = I_1(k) = -\frac{1}{k^2}, \quad (2.42)$$

illustrating that different regularization procedures of divergent integrals must yield the same unique finite value, if it exists.

From the above analysis it is found that the innerproduct given in equation (2.27) of a d - and the corresponding conjugate c resonant state may be given a finite value, i.e. it is possible to normalize these states. It remains to examine whether resonant states at different energies, i.e. $k_{n_1} \neq k_{n_2}$, form a *bi-orthogonal* set. Starting with the Schrödinger equation for two different resonant states $u_{n_1l}(r)$ and $u_{n_2l}(r)$ and multiplying the left with $u_{n_2l}(r)$ and $u_{n_1l}(r)$ respectively, one obtains by subtracting the two equations,

$$\frac{d}{dr} [u_{n_2l}(r)u'_{n_1l}(r) - u'_{n_2l}(r)u_{n_1l}(r)] = (k_{n_2}^2 - k_{n_1}^2) \tilde{u}_{n_2l}^*(r)u_{n_1l}(r). \quad (2.43)$$

Multiplying from the left with $\int_0^\infty dr e^{-\epsilon r^2}$, one obtains the following expression by partial integration,

$$\begin{aligned} & \int_0^\infty dr e^{-\epsilon r^2} \frac{d}{dr} [u_{n_2l}(r)u'_{n_1l}(r) - u'_{n_2l}(r)u_{n_1l}(r)] = \\ & 2\epsilon \int_0^\infty dr r e^{-\epsilon r^2} [u_{n_2l}(r)u'_{n_1l}(r) - u'_{n_2l}(r)u_{n_1l}(r)] \\ & = (k_{n_2}^2 - k_{n_1}^2) \int_0^\infty dr e^{-\epsilon r^2} \tilde{u}_{n_2l}^*(r)u_{n_1l}(r), \end{aligned} \quad (2.44)$$

where the boundary condition $u_{nl}(r = 0) = 0$ has been used. From the asymptotic form of the integrand $re^{-\epsilon r^2} e^{i(k_{n_1} + k_{n_2})r}$ it is seen that the integrals in equation (2.44) are comparable with the finite result for the integral $I_1(k, \epsilon)$ as $\epsilon \rightarrow 0$. It follows that

$$(k_{n_2}^2 - k_{n_1}^2) \lim_{\epsilon \rightarrow 0} \int_0^\infty dr e^{-\epsilon r^2} \tilde{u}_{n_2 l}^*(r) u_{n_1 l}(r) = 0. \quad (2.45)$$

Defining the inner product of resonant states as this limit, we finally obtain

$$\langle \tilde{u}_{n_1 l} | u_{n_2 l} \rangle = \langle u_{n_1 l}^* | u_{n_2 l} \rangle = \delta_{n_1, n_2}, \quad (2.46)$$

which shows that the resonant states together with the bound states are orthogonal in this sense. In the case where bound states enter the inner product, there is no divergence problem since the bound states has an exponential decay as $r \rightarrow \infty$. This symmetric inner product is often called the *c*-product [15], which states that the resonances form a *bi-orthogonal* set. In the case where k_{n_1} and k_{n_2} are real, the *c*-product coincides with the usual Hermitian inner product.

2.3 The Generalized Berggren Completeness; Proof and Discussion.

We have shown that the regular solution $\phi_l(k, r)$ with $k = k_n$ being the poles of the scattering matrix or zeros of the Jost function, can be normalized by some regularization procedure. Further it was shown that regular solutions $\phi_l(k, r)$ located at different k_n in the complex k -plane are orthogonal to each other, through the symmetric inner product given in equation (2.46). This suggests that the regular solutions at the poles of the scattering matrix, are part of a complete set of *bi-orthogonal* states, which may serve as an expansion basis when dealing with processes taking place in the continuum regime. This is the subject of this section.

We start with the standard completeness relation defined along the real k -axis,

$$\sum_{n=b} u_{ln}(r) u_{nl}^*(r') + \frac{1}{2} \int_{-\infty}^\infty dk u_l(k, r) u_l^*(k^*, r') = \delta(r - r'), \quad (2.47)$$

where the discrete sum is over the bound state poles located along the positive imaginary k -axis, and the integral is over the continuum of scattering functions located along the real k -axis. Note that on the real axis we have $u_l^*(k^*, r') = u_l^*(k, r')$. A proof of this completeness is given by Newton in reference [7]. Newton considered the integral

$$I(r) = \int_C dk k \int_0^\infty dr' h(r') G_l(k; r, r'), \quad (2.48)$$

where $h(r)$ is a function part of the L^2 functional space and $G_l(k; r, r')$ is the complete Green's function or resolvent. The integration contour C , runs along the real k -axis from

$-\infty$ to ∞ , and is closed by a semicircle in the upper half k -plane. The Green's function has poles at the same locations in the complex k -plane as the scattering matrix, and using Cauchy's residue theorem the various contributions to the integral in equation (2.48) is evaluated by the residues at the bound state poles along the positive imaginary k -axis. In the end it is shown that a l^2 function $h(r)$ may be expanded in a complete set of bound- and scattering wave functions given in equation(2.47). The class of square integrable functions, includes those with exponential asymptotics, $h(r) \rightarrow e^{ikr}$, $r \rightarrow \infty$, where k is in the upper half complex k -plane.

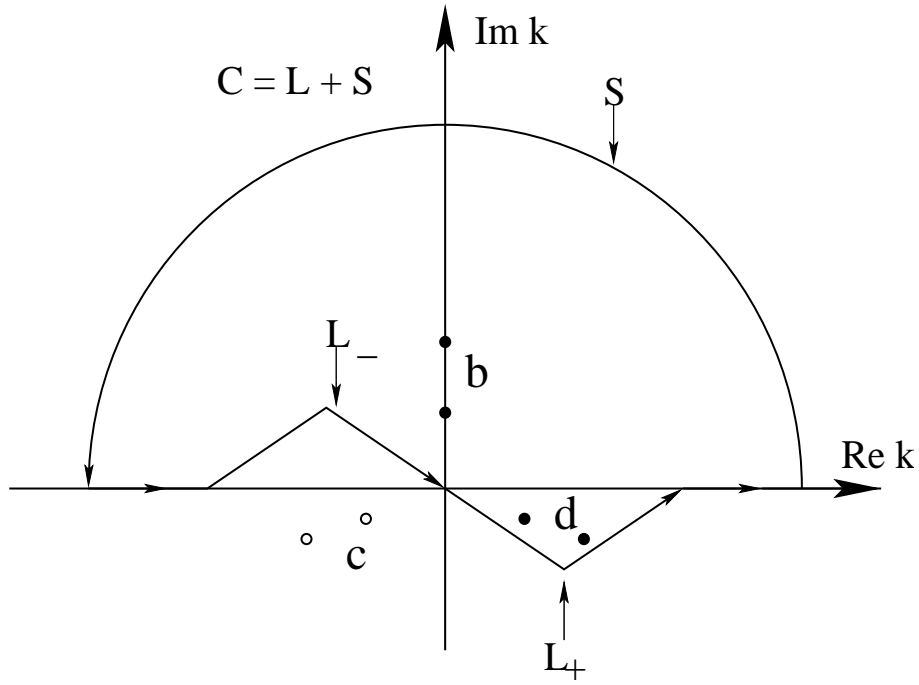


Figure 2.3: Integration contour $C = L + S$ used in deriving the Berggren completeness relation.

In reference [30] Berggren showed that there exist a modified completeness relation, where the resonant contributions hidden in the continuum integral were disentangled from the background of continuum states, and included in the discrete sum over bound states. The proof of Berggren, is based on the same complex analysis used by Newton, only that the integration contour C in equation (2.48) where modified to enclose not only the bound state poles, but in addition a set of *proper* resonant poles, see figure 2.3.

Later Lind [49] presented a straightforward method for deriving various completeness relations starting from the standard completeness relation given in equation (2.47). This method is based on analytic continuation of the integral over scattering functions, using the the known analytic properties of the scattering functions in the complex k -plane. As discussed in section 2.1, the scattering functions have poles wherever the Green's function $G_l(k)$ or the scattering matrix elements $S_l(k)$ have poles. Deforming the integration contour

defined along the real k -axis for the continuum integral in equation (2.47), one obtains by the Cauchy residue theorem

$$-\int_0^\infty dk u_l(k, r) \tilde{u}_l^*(k, r') + \int_{L^+} dk u_l(k, r) \tilde{u}_l^*(k, r') = 2\pi i \sum_{\substack{k=k_n \\ k_n \in \mathbf{C}}} \text{Res}_{k=k_n} u_l(k, r) \tilde{u}_l^*(k, r'), \quad (2.49)$$

where the contour L^+ is part of the inversion symmetric contour $L = L^- + L^+$, and is the deformation of the positive real k -axis. Here $\tilde{u}_l(k, r) = u_l(k^*, r)$ are associated with scattering functions on the conjugated contour L^* , which encloses the capture resonances which are orthogonal to the decay resonances enclosed by L . Inversion symmetric contour meaning that if k is on L , then so is $-k$. The product of scattering functions $u_l(k, r) \tilde{u}_l(k, r')$ is a meromorphic function of k with poles given by the Jost functions $f_l(-k) = 0$ and $f_l^*(-k^*) = 0$. The residue is evaluated at each pole $k = k_n$ of the scattering functions, located in the region between the contour L^+ and the real positive k -axis labeled \mathbf{C} . In writing equation (2.49) the inversion symmetry of L and the symmetry of the integrand in the continuum integral has been exploited to give

$$\int_{L^-} dk u_l(k, r) \tilde{u}_l^*(k, r') = \int_{L^+} dk u_l(k, r) \tilde{u}_l^*(k, r'). \quad (2.50)$$

In reference [49] the importance of choosing an inversion symmetric contour was discussed. If L is inversion symmetric, the complex continuum integral can be rewritten in terms of scattering functions, and the continuum integrals can be written using energy as the integration variable. In deriving the general Berggren completeness the residues in equation (2.49) have to be evaluated. Writing the physical wave function in terms of the regular solution and the Jost function, see section 2.1 for further details, one gets

$$u_l(k, r) = \sqrt{\frac{2}{\pi}} \frac{k^{l+1} \phi_l(k, r)}{f_l(-k)}, \quad (2.51)$$

and for the conjugate wave function $\tilde{u}_l(k, r)$,

$$\tilde{u}_l(k, r) = u_l(k^*, r) = \sqrt{\frac{2}{\pi}} \frac{(k^*)^{l+1} \phi_l(k^*, r)}{f_l(-k^*)} = \left(\sqrt{\frac{2}{\pi}} \frac{k^{l+1} \phi_l(k, r)}{f_l(k)} \right)^*, \quad (2.52)$$

where use has been made of the symmetry properties of the regular and Jost functions given in equation (2.8). The residue in equation (2.49) may then be written as

$$\text{Res}_{k=k_n} u_l(k, r) \tilde{u}_l^*(k, r') = \text{Res}_{k=k_n} \frac{2}{\pi} \frac{k^{2l+2} \phi_l(k, r) \phi_l(k, r')}{f_l(k) f_l(-k)}, \quad (2.53)$$

Making use of the property $\text{Res}_{z=z_0} h(z)/g(z) = h(z_0)/g'(z_0)$ where $h(z)$ and $g(z)$ are analytic functions at $z = z_0$, it is seen that following derivative has to be evaluated,

$$\frac{d}{dk} f_l(k) f_l(-k) \Big|_{k=k_n} = f_l(k_n) \frac{d}{dk} f_l(-k) \Big|_{k=k_n}, \quad (2.54)$$

here the fact that the Jost function $f_l(-k) = 0$ for $k = k_n$ has been used. The problem of determining the residue in equation (2.49) has now been reduced to the problem of determining the derivative of the Jost function at the resonance pole $k = k_n$. In reference [49] the derivative of the Jost function where proven to be

$$\frac{d}{dk} f_l(-k) \Big|_{k=k_n} = i4k_n^{2l+2} \text{Reg} \int_0^\infty dr r^2 \phi_l^2(k_n, r) = i4k_n^{2l+2} N^2, \quad (2.55)$$

where N is the norm of the regularized resonances wave functions appearing in the integral. The sum over residues in equation (2.49) now becomes,

$$\begin{aligned} 2\pi i \sum_{k_n \in \mathbf{C}} \text{Res}_{k=k_n} u_l(k, r) \tilde{u}_l^*(k, r') &= 4i \sum_{k_n \in \mathbf{C}} \frac{k^{2l+2} \phi_l(k_n, r) \phi_l(k_n, r')}{\frac{d}{dk} f_l(k) f_l(-k) \Big|_{k=k_n}} \\ &= \sum_{k_n \in \mathbf{C}} \frac{\phi_l(k_n, r) \phi_l(k_n, r')}{N^2} = \sum_{k_n \in \mathbf{C}} u_{nl}(r) \tilde{u}_{nl}^*(r'), \end{aligned} \quad (2.56)$$

inserting this into equation (2.49), one gets the following expression for the integral over scattering functions along the real k -axis (positive energy states),

$$\int_0^\infty dk u_l(k, r) \tilde{u}_l^*(k, r') = \sum_{k_n \in \mathbf{C}} u_{nl}(r) \tilde{u}_{nl}^*(r') + \int_{L^+} dk u_l(k, r) \tilde{u}_l^*(k, r'), \quad (2.57)$$

where it is explicitly seen that the resonant contributions hidden in the continuum integral along the real k -axis have been disentangled. In reference [49] it was shown for finite range potentials that the continuum integral along the contour L^+ produces a smooth background, but is in most cases non-negligible.

Switching to abstract vector notation, it has been shown that for a general inversion symmetric contour L , see figure 2.4, the generalized Berggren completeness becomes,

$$\mathbf{1} = \sum_{n=a,b,c,d} |u_{nl}\rangle \langle \tilde{u}_{nl}| + \int_{L^+} dk |u_l(k)\rangle \langle \tilde{u}_l(k)|. \quad (2.58)$$

The discrete sum includes all types of poles of the scattering matrix, i.e. anti-bound (a), bound (b), capture resonant (c) and decay resonant (d) states. This completeness can be used to expand all functions with exponential asymptotics, e^{ikr} , $r \rightarrow \infty$ where k is located within the closed contour $C = L + S$. Keeping only the discrete part of the completeness relation (2.58), one ends up with the pole-approximation. As shown in figure 2.4 a typical inversion symmetric contour cannot separate all poles from the continuum integral. In this particular case the red circles gives the poles which are not included in the discrete sum, while the black circles give the poles which are included in the sum. It is important to emphasize that completeness defined either along the real k -axis or along a distorted contour L in the complex k -plane are equivalent in the sense,

$$\begin{aligned} \mathbf{1} &= \sum_{n=a,b,c,d} |u_{nl}\rangle \langle \tilde{u}_{nl}| + \int_{L^+} dk |u_l(k)\rangle \langle \tilde{u}_l(k)| \\ &= \sum_{n=b} |u_{nl}\rangle \langle \tilde{u}_{nl}| + \int_0^\infty dk |u_l(k)\rangle \langle \tilde{u}_l(k)|, \end{aligned} \quad (2.59)$$

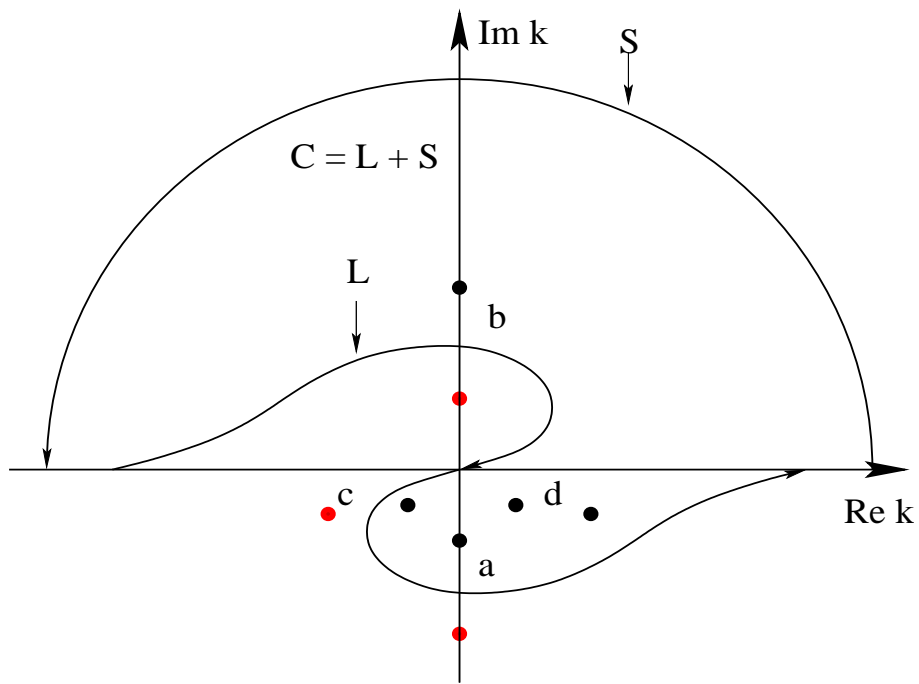


Figure 2.4: General inversion symmetric contour $C = L + S$ used in deriving the generalized Berggren completeness relation. The black circles represent the poles which are included in the discrete sum, while the red circles are poles which are embedded in the continuum integral along the contour L^+ .

the difference being that for a completeness defined along the real k -axis all the interesting processes taking place in the continuum are hidden as peaks within the continuum integral, while for a completeness defined along L the most interesting phenomena, i.e. the resonant contributions, are extracted out of the continuum integral and can be studied separately.

2.4 Interpretation of Complex Observables.

Turning to the interpretation of expectation values of observable operators involving resonant states, it is natural to ask what physical meaning one should assign to such expectation values. The resonant states are complex, yielding complex expectation values of the Hamiltonian H and any other Hermitian observable operator A . If resonant states are to be seen as excited states in which a particular system can undergo transition from and to, and such transitions are expected to be seen experimentally, a physical interpretation of the real and imaginary parts of $\langle A \rangle$ is necessary. This question was first raised by Berggren [30] and later by Gyarmati et. al. [69], where it was conjectured that the physical meaning of an expectation value $\langle A \rangle$ when the system is in a resonant state is given by the real part,

$$\langle A \rangle = \text{Re} \langle \tilde{u}_{nl} | A | u_{nl} \rangle. \quad (2.60)$$

A theoretical justification of this conjecture was given by Berggren in reference [70], where it was shown starting from scattering theory, that the real part of the complex cross section for populating a resonance is equal to the energy integral of the in-elastic continuum cross section across the resonance peak. The imaginary part of the cross section where identified with the strength of the resonance-background interference. In reference [71] this conclusion where generalized to hold for any observable operator A involving resonant states. To throw some light on this interpretation, consider the matrix element of an operator A with a scattering function defined on the real energy axis,

$$\langle \tilde{u}_l(k) | A | u_l(k) \rangle = \text{Re} \langle \tilde{u}_l(k) | A | u_l(k) \rangle. \quad (2.61)$$

Suppose now that the Jost function $f_l(-k)$ has a zero located close to the real k -axis, which is associated with a narrow resonance. Since the scattering wave functions have poles wherever the Jost functions have zeroes, see equation (2.13) of section 2.1, the matrix element (2.61) will display a sharp peak when it is plotted as a function of energy, and the energy traverses the real part of the resonance energy.

The momentum (energy)-integrated matrix element is,

$$\begin{aligned} & \int_0^{k_{\max}} dk \langle \tilde{u}_l(k) | A | u_l(k) \rangle = \\ & \int_C dk \langle \tilde{u}_l(k) | A | u_l(k) \rangle - 2\pi i \underset{k=k_n}{\text{Res}} \langle \tilde{u}_l(k) | A | u_l(k) \rangle, \end{aligned} \quad (2.62)$$

where C is a contour in the fourth quadrant of the complex k -plane enclosing the pole at $k = k_n$, and joining the real axis at $k = 0$ and $k = k_{\max}$, see figure 2.5. The residue in

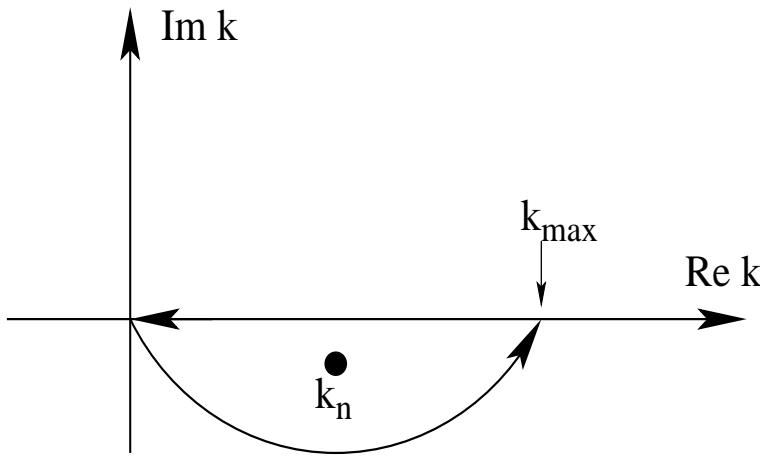


Figure 2.5: Integration contour used in evaluating the pure resonance contribution to the energy-integrated expectation value.

equation (2.62) is given by equation (2.53) from the previous section, and consequently,

$$\begin{aligned} \int_0^{k_{\max}} dk \langle \tilde{u}_l(k, r) | A | u_l(k, r) \rangle = \\ \int_C dk \langle \tilde{u}_l(k, r) | A | u_l(k, r) \rangle + \langle \tilde{u}_{nl} | A | u_{nl} \rangle = \\ \text{Re} \int_C dk \langle \tilde{u}_l(k) | A | u_l(k) \rangle + \text{Re} \langle \tilde{u}_{nl} | A | u_{nl} \rangle. \end{aligned} \quad (2.63)$$

Since the expectation value is by definition real, the imaginary parts of the contour integral of the scattering functions and the imaginary part of the matrix element involving the resonance at $k = k_n$ must cancel, in this way it is illustrated that the imaginary part of $\langle \tilde{u}_{nl} | A | u_{nl} \rangle$ may be interpreted as an interference effect with the continuum background.

Assuming now that equation (2.60) is a reasonable physical interpretation of the formal expectation value $\langle \tilde{u}_{nl} | A | u_{nl} \rangle$, what meaning should one assign the imaginary part? Let us start with the usual definition of the average deviation, or indeterminacy, of an operator A which is assumed to commute with the Hamiltonian H ,

$$(\Delta A)^2 = \langle A^2 - \langle A \rangle^2 \rangle = \langle A^2 \rangle - \langle A \rangle^2. \quad (2.64)$$

Using the definition of $\langle A \rangle$ in equation (2.60), it is easily found that

$$\langle A^2 \rangle = \text{Re} \langle \tilde{u}_{nl} | A^2 | u_{nl} \rangle = [\text{Re} \langle \tilde{u}_{nl} | A | u_{nl} \rangle]^2 - [\text{Im} \langle \tilde{u}_{nl} | A | u_{nl} \rangle]^2, \quad (2.65)$$

and

$$\langle A \rangle^2 = [\text{Re} \langle \tilde{u}_{nl} | A | u_{nl} \rangle]^2. \quad (2.66)$$

Inserting this into equation (2.64) yields,

$$(\Delta A)^2 = \langle A^2 - \langle A \rangle^2 \rangle = -[\text{Im} \langle \tilde{u}_{nl} | A | u_{nl} \rangle]^2. \quad (2.67)$$

Thus it is then formally shown that the imaginary part of the expectation value of an operator A in a resonant state, gives the uncertainty or indeterminacy of the measured result. This may also be understood from physical grounds. Resonant states have definite lifetimes, i.e. they decay in time. The lifetime of the resonant state is determined by the probability of tunneling through the potential barrier, in which the resonance is formed. The probability of decay is proportional to the imaginary part of the resonance pole or in other words the resonance width Γ . Let the operator A be the Hamiltonian of the system, $A = H$, then equation (2.67) becomes,

$$(\Delta H)^2 = \langle H^2 - \langle H \rangle^2 \rangle = -\frac{\Gamma^2}{4}, \quad (2.68)$$

where it is explicitly seen that by the definition of $\langle H \rangle$, the width Γ determines the uncertainty in energy measurements.

Chapter 3

Contour Deformation Method (CDM) in Momentum Space; Theory and Applications.

3.1 The Momentum Space Schrödinger Equation.

The Schrödinger equation in abstract vector (Dirac) representation is

$$(T + V) |\psi_n\rangle = E_n |\psi_n\rangle \quad (3.1)$$

Here T is the kinetic energy operator and V is the potential operator. The eigenstates form a complete orthonormal set according to

$$\mathbf{1} = \sum_n |\psi_n\rangle\langle\psi_n|, \quad \langle\psi_n|\psi_{n'}\rangle = \delta_{n,n'}.$$

The most commonly used representations of equation 3.1 are the coordinate (\mathbf{r}) and the momentum (\mathbf{k})¹ space representations. They correspond to completeness relations

$$\mathbf{1} = \int d\mathbf{r} |\mathbf{r}\rangle\langle\mathbf{r}|, \quad \langle\mathbf{r}|\mathbf{r}'\rangle = \delta(\mathbf{r} - \mathbf{r}'), \quad (3.2)$$

$$\mathbf{1} = \int d\mathbf{k} |\mathbf{k}\rangle\langle\mathbf{k}|, \quad \langle\mathbf{k}|\mathbf{k}'\rangle = \delta(\mathbf{k} - \mathbf{k}'). \quad (3.3)$$

Here the basis states in both \mathbf{r} - and \mathbf{k} -space are Dirac-delta function normalized. From this it follows that the plane-wave states are given by,²

$$\langle\mathbf{r}|\mathbf{k}\rangle = \left(\frac{1}{2\pi}\right)^{3/2} \exp(i\mathbf{k} \cdot \mathbf{r}), \quad (3.4)$$

¹Here we have used \mathbf{k} rather than $\mathbf{p} = \hbar\mathbf{k}$ as the conjugate Fourier variable.

²Some authors define the plane wave by $\langle\mathbf{r}|\mathbf{k}\rangle = \exp(i\mathbf{k} \cdot \mathbf{r})$, in which case $\langle\mathbf{k}|\mathbf{k}'\rangle = (2\pi)^3 \delta(\mathbf{k} - \mathbf{k}')$ and each $\int d\mathbf{k}$ is replaced by $(1/2\pi)^{3/2} \int d\mathbf{k}$.

which is a transformation function defining the mapping from the abstract $|\mathbf{k}\rangle$ to the abstract $|\mathbf{r}\rangle$ space. That the \mathbf{r} -space basis states are delta-function normalized follows from

$$\delta(\mathbf{r} - \mathbf{r}') = \langle \mathbf{r} | \mathbf{r}' \rangle = \langle \mathbf{r} | \mathbf{1} | \mathbf{r}' \rangle = \int d\mathbf{k} \langle \mathbf{r} | \mathbf{k} \rangle \langle \mathbf{k} | \mathbf{r}' \rangle = \left(\frac{1}{2\pi} \right)^3 \int d\mathbf{k} e^{i\mathbf{k} \cdot (\mathbf{r} - \mathbf{r}')}, \quad (3.5)$$

and the same for the momentum space basis states,

$$\delta(\mathbf{k} - \mathbf{k}') = \langle \mathbf{k} | \mathbf{k}' \rangle = \langle \mathbf{k} | \mathbf{1} | \mathbf{k}' \rangle = \int d\mathbf{r} \langle \mathbf{k} | \mathbf{r} \rangle \langle \mathbf{r} | \mathbf{k}' \rangle = \left(\frac{1}{2\pi} \right)^3 \int d\mathbf{r} e^{i\mathbf{r} \cdot (\mathbf{k} - \mathbf{k}')}. \quad (3.6)$$

Projecting equation 3.1 on momentum states³, the momentum space Schrödinger equation is obtained,

$$\frac{\hbar^2}{2\mu} k^2 \psi_n(\mathbf{k}) + \int d\mathbf{k}' V(\mathbf{k}, \mathbf{k}') \psi_n(\mathbf{k}') = E_n \psi_n(\mathbf{k}). \quad (3.7)$$

Here the notation $\psi_n(\mathbf{k}) = \langle \mathbf{k} | \psi_n \rangle$ and $\langle \mathbf{k} | V | \mathbf{k}' \rangle = V(\mathbf{k}, \mathbf{k}')$ has been introduced. The potential in momentum space is thus given by a double Fourier-transform of the potential in coordinate space, i.e.

$$V(\mathbf{k}, \mathbf{k}') = \left(\frac{1}{2\pi} \right)^3 \int d\mathbf{r} \int d\mathbf{r}' e^{-i\mathbf{k} \cdot \mathbf{r}} V(\mathbf{r}, \mathbf{r}') e^{i\mathbf{k}' \cdot \mathbf{r}'} . \quad (3.8)$$

Here it is assumed that the potential interaction does not contain any spin dependence. Instead of a differential equation in coordinate space, the Schrödinger equation has become an integral equation in momentum space. This has many tractable features. Firstly, most realistic nucleon-nucleon interactions derived from field-theory are given explicitly in momentum space. Secondly, the boundary conditions imposed on the differential equation in coordinate space are automatically built into the integral equation. And last, but not least, integral equations are easy to numerically implement, and convergence is obtained by just increasing the number of integration points. Instead of solving the three-dimensional integral equation given in equation (3.7), an infinite set of 1-dimensional equations can be obtained by invoking a partial wave expansion. The wave function $\psi_n(\mathbf{k})$ can be expanded in a complete set of spherical harmonics, i.e.

$$\psi_n(\mathbf{k}) = \sum_{lm} \psi_{nlm}(k) Y_{lm}(\hat{k}), \quad \psi_{nlm}(k) = \int d\hat{k} Y_{lm}^*(\hat{k}) \psi_n(\mathbf{k}). \quad (3.9)$$

By inserting equation 3.9 in equation 3.7, and projecting $Y_{lm}(\hat{k})$ from the left, the three-dimensional Schrödinger equation (3.7) is reduced to an infinite set of 1-dimensional angular momentum coupled integral equations,

$$\left(\frac{\hbar^2}{2\mu} k^2 - E_{nlm} \right) \psi_{nlm}(k) = - \sum_{l'm'} \int_0^\infty dk' k'^2 V_{lm,l'm'}(k, k') \psi_{nl'm'}(k'), \quad (3.10)$$

³In the literature the momentum states are often called plane-wave states.

where the angular momentum projected potential takes the form,

$$V_{lm,l'm'}(k, k') = \int d\hat{k} \int d\hat{k}' Y_{lm}^*(\hat{k}) V(\mathbf{k}, \mathbf{k}') Y_{l'm'}(\hat{k}'). \quad (3.11)$$

Here $d\hat{k} = d\theta \sin \theta d\varphi$. In many cases the potential is given in position space, so it is convenient to establish the connection between $V_{lm,l'm'}(k, k')$ and $V_{lm,l'm'}(r, r')$. Inserting position space completeness in equation (3.11) gives

$$\begin{aligned} V_{lm,l'm'}(k, k') &= \int d\mathbf{r} \int d\mathbf{r}' \int d\hat{k} \int d\hat{k}' Y_{lm}^*(\hat{k}) \langle \mathbf{k} | \mathbf{r} \rangle \langle \mathbf{r} | V | \mathbf{r}' \rangle \langle \mathbf{r}' | \mathbf{k}' \rangle Y_{lm}(\hat{k}') = \\ &= \int d\mathbf{r} \int d\mathbf{r}' \left\{ \int d\hat{k} Y_{lm}^*(\hat{k}) \langle \mathbf{k} | \mathbf{r} \rangle \right\} \langle \mathbf{r} | V | \mathbf{r}' \rangle \left\{ \int d\hat{k}' Y_{lm}(\hat{k}') \langle \mathbf{r}' | \mathbf{k}' \rangle \right\}. \end{aligned} \quad (3.12)$$

Since the plane waves depend only on the absolute values of position and momentum, $|\mathbf{k}|, |\mathbf{r}|$, and the angle between them, θ_{kr} , they may be expanded in terms of bipolar harmonics of zero rank [72], i.e.

$$e^{i\mathbf{k}\cdot\mathbf{r}} = 4\pi \sum_{l=0}^{\infty} i^l j_l(kr) \left(Y_l(\hat{k}) \cdot Y_l(\hat{r}) \right) = \sum_{l=0}^{\infty} (2l+1) i^l j_l(kr) P_l(\cos \theta_{kr}). \quad (3.13)$$

The addition theorem for spherical harmonics has been used in order to write the expansion in terms of Legendre polynomials. The spherical Bessel functions, $j_l(z)$, are given in terms of Bessel functions of the first kind with half integer orders [73, 74],

$$j_l(z) = \sqrt{\frac{\pi}{2z}} J_{l+1/2}(z).$$

Inserting the plane-wave expansion into the brackets of equation (3.12) yields,

$$\begin{aligned} \int d\hat{k} Y_{lm}^*(\hat{k}) \langle \mathbf{k} | \mathbf{r} \rangle &= \left(\frac{1}{2\pi} \right)^{3/2} 4\pi i^{-l} j_l(kr) Y_{lm}^*(\hat{r}), \\ \int d\hat{k}' Y_{lm}(\hat{k}') \langle \mathbf{r}' | \mathbf{k}' \rangle &= \left(\frac{1}{2\pi} \right)^{3/2} 4\pi i^{l'} j_{l'}(k'r') Y_{l'm'}(\hat{r}). \end{aligned}$$

The connection between the momentum- and position space angular momentum projected potentials is then given by,

$$V_{lm,l'm'}(k, k') = \frac{2}{\pi} i^{l'-l} \int_0^\infty dr r^2 \int_0^\infty dr' r'^2 j_l(kr) V_{lm,l'm'}(r, r') j_{l'}(k'r'), \quad (3.14)$$

which is known as a double Fourier-Bessel transform. The position space angular momentum projected potential is given by,

$$V_{lm,l'm'}(r, r') = \int d\hat{r} \int d\hat{r}' Y_{lm}^*(\hat{r}) V(\mathbf{r}, \mathbf{r}') Y_{l'm'}(\hat{r}'). \quad (3.15)$$

No assumptions of locality/non-locality or deformation of the interaction has so far been made, and the result in equation (3.14) is general. In position space the Schrödinger equation takes form of an integro-differential equation in case of a non-local interaction, in momentum space the Schrödinger equation is an ordinary integral equation of the Fredholm type, see equation (3.10). This is a further advantage of the momentum space approach as compared to the standard position space approach. If we assume that the interaction is of local character, i.e.

$$\langle \mathbf{r} | V | \mathbf{r}' \rangle = V(\mathbf{r})\delta(\mathbf{r} - \mathbf{r}') = V(\mathbf{r}) \frac{\delta(r - r')}{r^2} \delta(\cos \theta - \cos \theta') \delta(\varphi - \varphi'), \quad (3.16)$$

then equation (3.15) reduces to

$$V_{lm,l'm'}(r, r') = \frac{\delta(r - r')}{r^2} \int d\hat{r} Y_{lm}^*(\hat{r}) V(\mathbf{r}) Y_{l'm'}(\hat{r}), \quad (3.17)$$

and equation (3.14) reduces to

$$V_{lm,l'm'}(k, k') = \frac{2}{\pi} i^{l'-l} \int_0^\infty dr r^2 j_l(kr) V_{lm,l'm'}(r) j_{l'}(k'r), \quad (3.18)$$

where

$$V_{lm,l'm'}(r) = \int d\hat{r} Y_{lm}^*(\hat{r}) V(\mathbf{r}) Y_{l'm'}(\hat{r}). \quad (3.19)$$

In the case that the interaction is central, $V(\mathbf{r}) = V(r)$, then

$$V_{lm,l'm'}(r) = V(r) \int d\hat{r} Y_{lm}^*(\hat{r}) Y_{l'm'}(\hat{r}) = V(r) \delta_{l,l'} \delta_{m,m'}, \quad (3.20)$$

and

$$V_{lm,l'm'}(k, k') = \frac{2}{\pi} \int_0^\infty dr r^2 j_l(kr) V(r) j_{l'}(k'r) \delta_{l,l'} \delta_{m,m'} = V_l(k, k') \delta_{l,l'} \delta_{m,m'}, \quad (3.21)$$

where the momentum space representation of the interaction finally reads,

$$V_l(k, k') = \frac{2}{\pi} \int_0^\infty dr r^2 j_l(kr) V(r) j_l(k'r). \quad (3.22)$$

For a local and spherical symmetric potential, the coupled momentum space Schrödinger equations given in equation (3.10) decouple in angular momentum, giving

$$\frac{\hbar^2}{2\mu} k^2 \psi_{nl}(k) + \int_0^\infty dk' k'^2 V_l(k, k') \psi_{nl}(k') = E_{nl} \psi_{nl}(k). \quad (3.23)$$

Here we have written $\psi_{nl}(k) = \psi_{nlm}(k)$, since the equation becomes independent of the projection m for spherical symmetric interactions. The momentum space wave functions $\psi_{nl}(k)$ define a complete orthogonal set of functions, which spans the space of functions with a positive finite Euclidean norm (also called l^2 -norm), $\sqrt{\langle \psi_n | \psi_n \rangle}$, which is a Hilbert space. The corresponding normalized wave function in coordinate space is given by the Fourier-Bessel transform

$$\phi_{nl}(r) = \sqrt{\frac{2}{\pi}} \int dk k^2 j_l(kr) \psi_{nl}(k) \quad (3.24)$$

3.2 Analytic Continuation of Momentum Space Schrödinger Equation by CDM.

In Chapter 2 it was shown how the generalized Berggren completeness relations may be derived from the completeness relation defined on the physical energy sheet using analytic continuation techniques to reach into the non-physical energy sheet. Having obtained a generalized completeness relation, the corresponding eigenvalue problem may easily be deduced. On the other hand one may start with the eigenvalue problem for bound- and scattering states, and investigate under which conditions the Schrödinger equation may be continued to the non-physical energy sheet where the most interesting continuum phenomena, i.e. the resonance phenomena, are located. In this section we outline a method which analytically continues the momentum space Schrödinger equation through the unitarity cut onto the second Riemann sheet of the complex energy plane, which is based on deforming the integration contour. This method is known as the *contour deformation (distortion) method* (CDM). The contour deformation method was first introduced in the study of the full off-shell scattering amplitudes in two- and three particle scattering in the early 60's, see references [75, 76, 77, 27]. A rotation of the integration contour in the momentum space integral equations extended the domain over which the integral kernel is a compact (Hilbert-Schmidt)-operator. This has numerical advantages as the kernel is no longer singular. Already in 1954 Wick [78] introduced the method of contour rotation in momentum space; in transforming the equation to the imaginary axis the strong singularities of the interaction kernel were avoided. A rotation of the contour in momentum space has therefore often been referred to as Wick rotation. The contour deformation method has therefore two important applications, first the Schrödinger equation is analytically continued onto the non-physical sheet revealing resonant structures and secondly it provides a method for making the integral kernels compact enabling stable numerical solutions for the scattering amplitudes.

In the following we consider the momentum space Schrödinger equation given in equation (3.10) where the potential is assumed spherically symmetric and with no spin- or tensor components. Equation (3.23) may be rewritten as an integral equation for the bound states

$$\psi_{nl}(k) = \frac{1}{E_{nl} - k^2/2\mu} \int_0^\infty dk' k'^2 V_l(k, k') \psi_{nl}(k'). \quad (3.25)$$

For real k, k' this equation is defined on the physical energy sheet, i.e. in the upper half complex k -plane. If this equation is to describe a resonant or antibound state, it has to be analytically continued through the branch cut along the real energy axis and onto the non-physical energy sheet, defined as the lower half complex k -plane.

The most straightforward method of analytic continuation is by use of power series. Consider a function $f(z)$ analytic in the domain D , and let f_1 and f_2 be Taylor series of $f(z)$ about z_0 and z'_0 on domains D_1 and D_2 , respectively,

$$f_1(z) = \sum_{n=0}^{\infty} a_n (z - z_0)^n, \quad f_2(z) = \sum_{n=0}^{\infty} b_n (z - z'_0)^n.$$

Both domains D_1 and D_2 are in D , and the radius of convergence is determined by the distance from z_0 and z'_0 to the nearest point on the boundary of analyticity region D . Further suppose that the intersection $D_1 \cap D_2$ is not empty and that $f_1 = f_2$ on $D_1 \cap D_2$. Then f_2 is called an analytic continuation f_1 of to D_2 , and vice versa. This procedure may be iterated to obtain the values of $f(z)$ in the entire domain D based on its values in the subdomains D_1, D_2, \dots .

Consider now the analytic continuation of the bound state equation given in equation (3.25). In analytic continuation of integral equations we state the general rule, see for example [8, 7]:

Continuing an integral in the complex plane, the moving singularities of the integrand must not intercept the integration contour.

First of all, it is seen that the analytic properties of $\psi_{nl}(k)$ is determined by the interaction, $V_l(k, q)$ entering the integral kernel. The analytic continuation of equation (3.25) to the lower half complex energy plane is a stepwise process where overlapping domains of analyticity are created. Each step of analytic continuation of the bound state Schrödinger equation to the lower half complex energy plane involves the following three steps:

1. The analyticity domain, D_1 , for the wave function $\psi_{nl}(k)$ is determined. The analyticity of $\psi(k)$ is given by the potential $V(k, q)$, where in the first step q is defined along the real axis.
2. Having determined the analyticity region D_1 in the lower half k -plane, the integration in q along the real axis may be distorted onto a contour L_1^+ in the lower half complex k -plane, using the Cauchy integral formula. All points on the contour L_1^+ must be contained in the analyticity domain D_1 .
3. A new analyticity domain D_2 is determined for the wave function $\psi(k)$. The domain D_2 is again determined by the singularity structure of the potential $V(k, q)$ where q is now on the distorted contour L_1^+ . If and only if the contour L_1^+ also lies in the new domain of analyticity D_2 , we may choose k on L_1^+ as well. This gives a closed integral equation, and the Schrödinger equation is transformed onto the contour L_1^+ .

This process of analytic continuation may be continued iteratively, uncovering larger domains of interest in the complex energy plane. The contour L^+ starts at $k = 0$, and is therefore by definition part of the inversion symmetric contour $L = L^- + L^+$. The analytically continued equation (3.23) on a general inversion symmetric contour then takes the form

$$\frac{\hbar^2}{2\mu} k^2 \psi_{nl}(k) + \int_{L^+} dk' k'^2 V_l(k, k') \psi_{nl}(k') = E_{nl} \psi_{nl}(k). \quad (3.26)$$

Here both k and k' are defined on the inversion symmetric contour L^+ in the lower half complex k -plane, giving a closed integral equation.⁴ The analytically continued wave functions $\psi_{nl}(k)$ defines a complete bi-orthogonal set of functions, which spans the space

⁴See Paper 1 for an application of CDM to the solution of anti-bound and resonant states and scattering in the Malfliet-Tjon potential.

of functions with exponential asymptotics in the domain above the inversion symmetric contour L^+ , see also Chapter 2. The wave functions are normalized according to the generalized inner product (c-product), see e.g. [15, 79]

$$\int_{L^+} dk k^2 \psi_{nl}(k) \psi_{n'l}(k) = \delta_{n,n'}. \quad (3.27)$$

The corresponding normalized wave function in coordinate space is given by the Fourier-Bessel transform

$$\phi_{nl}(r) = \sqrt{\frac{2}{\pi}} \int dk k^2 j_l(kr) \psi_{nl}(k). \quad (3.28)$$

The orthogonality of the coordinate wave functions is easily proved using the orthogonality of the spherical Bessel functions [73],

$$\int dr r^2 j_l(kr) j_l(k'r) = \frac{\pi}{2} \frac{\delta(k - k')}{kk'}. \quad (3.29)$$

Equation (3.26) is analytically solvable for only a limited class of potentials. Newton [7] proved that for all separable potentials, equation (3.26) admits solutions in closed forms. In most practical applications the solutions have to be approximated numerically. This is for example the case for the Woods-Saxon potential which is widely used in nuclear physics. In solving equation 3.26 numerically, one chooses a set of N grid points in k -space by some quadrature rule, e.g. Gauss-Legendre. The integral is then discretized by $\int dk \rightarrow \sum_{i=1}^N w_i$. On the chosen grid, equation 3.26 takes the form

$$\frac{\hbar^2}{2\mu} k_i^2 \psi_{nl}(k_i) + \sum_j^N w_j k_j^2 V_l(k_i, k_j) \psi_{nl}(k_j) = E_{nl} \psi_{nl}(k_i). \quad (3.30)$$

This equation represents a non-symmetric eigenvalue problem which is easily solved numerically. As most diagonalization routines are optimized for specific classes of matrices, it would be preferable to obtain a symmetric matrix, in the complex case the computational cost is drastically reduced if the matrix to be diagonalized can be made symmetric, see e.g. [80, 81, 82]. Equation 3.30 is easily made symmetric by multiplying through with $\sqrt{w_i} k_i$. Defining $\psi_{nl}(i) \equiv \sqrt{w_i} k_i \psi_{nl}(k_i)$, one gets the symmetric eigenvalue problem,

$$\frac{\hbar^2}{2\mu} k_i^2 \psi_{nl}(i) + \sum_j^N \sqrt{w_i w_j} k_i k_j V_l(k_i, k_j) \psi_{nl}(j) = E_{nl} \psi_{nl}(i). \quad (3.31)$$

The norm integral in equation (3.27) becomes the discrete sum

$$\delta_{n,n'} = \sum_{i=1}^N \psi_{nl}(i) \psi_{n'l}(i) = \sum_{i=1}^N w_i k_i^2 \psi_{nl}(k_i) \psi_{n'l}(k_i), \quad (3.32)$$

and the discretized completeness relation then takes the form

$$\mathbf{1} = \sum_n^N |\psi_{nl}\rangle \langle \psi_{nl}^*| = \sum_n^N \sum_{i=1}^N \psi_{nl}(i) \psi_{nl}(i). \quad (3.33)$$

Changing from a continuous to a discrete plane-wave basis, it becomes transparent that the coordinate wave function is an expansion in a basis of spherical Bessel functions

$$\phi_{nl}(r) = \sqrt{\frac{2}{\pi}} \sum_{i=1}^N \sqrt{w_i} k_i j_l(k_i r) \psi_{nl}(i), \quad (3.34)$$

where $\psi_{nl}(i)$ are the expansion coefficients. Defining the functions

$$f_l(k_i r) = \sqrt{\frac{2}{\pi}} \sqrt{w_i} k_i j_l(k_i r), \quad (3.35)$$

and using the discrete representation of the Dirac-delta function

$$\delta(k - k') \rightarrow \frac{\delta_{k_i, k_j}}{\sqrt{w_i w_j}}, \quad (3.36)$$

we get the expansion

$$\phi_{nl}(r) = \sum_{i=1}^N \psi_{nl}(i) f_l(k_i r). \quad (3.37)$$

Here it is seen that the functions $f_l(k_i r)$ are orthogonal for different k_i and normalized according to

$$\int dr r^2 f_l(k_i r) f_l(k_j r) = \delta_{k_i, k_j}, \quad (3.38)$$

where δ_{k_i, k_j} is the Kronecker delta. The eigenfunctions satisfy the general Berggren completeness relation discussed in the previous sections, and constitute a *bi-orthogonal* set and are normalized according to the general *c*-product. Collecting the results from the discussion on the Berggren completeness relation in the previous section, and on the analytic continuation of the momentum space Schrödinger equation by CDM, the choice of contour in the complex k -plane must therefore be based on the following.

- The contour must be *inversion symmetric*.
- The contour must be located in overlapping domains of analyticity, see step (iii) above, and the wave function must admit analytic continuation onto the contour L^+ .
- The choice of contour must be based on an *a posteriori* knowledge of poles in each partial wave of the scattering matrix.

In figure 3.1 a plot of the $l = 1$ trajectory of the imaginary part of the bound and antibound state poles in the complex k -plane as a function of interaction strength ν_A is given, for the Malfliet-Tjon potential. Figure 3.2 gives a plot of how the $l = 1$ bound state in the Malfliet-Tjon potential approaches the scattering threshold and develop into decay resonant states for decreasing interaction strength ν_A . See Paper 1 for further details on the potential parameters.

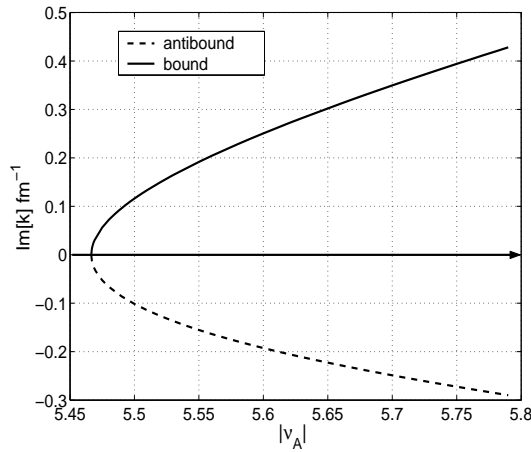


Figure 3.1: Plot of the bound and antibound state pole trajectory for the $l = 1$ component of Malfliet-Tjon interaction. The location of the poles along the imaginary k -axis is plotted as a function of interaction strength ν_A .

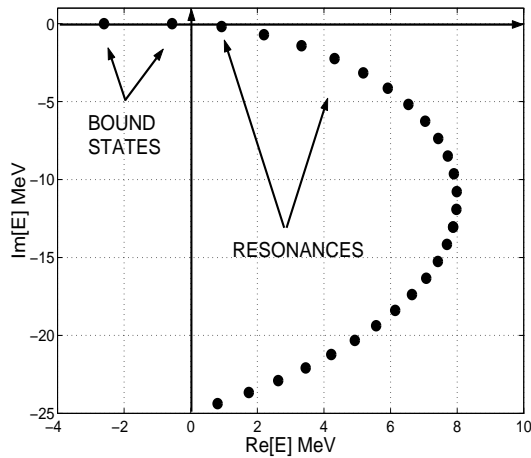


Figure 3.2: Plot of pole trajectory in the complex energy plane for the $l = 1$ partial wave solution of the Malfliet-Tjon interaction for ν_A varied from -5.6 to -2.9 in steps of 0.1 .

3.3 Single-Particle Resonances in a Deformed Field.

In this section we will consider formation of resonances in an axially deformed field. The study of resonances in deformed fields has so far only rarely been considered, and for special cases. In reference [83] energy levels and conditions for bound states to become resonances and resonances to become bound states were investigated for an axially deformed Woods-Saxon potential, by solving the radial Schrödinger equation for coupled channels with outgoing asymptotics. However, the coupled channels method used in reference [83] does not easily generalize to the non-resonant continuum. This implies that a complete Berggren basis in a deformed field is difficult to obtain, and all evaluated observables will become complex quantities unless the non-resonant continuum is taken properly into account. In reference [84] a different approach was considered. Their aim was to propose a method to obtain scattering wave functions in the vicinity of a multi-channel resonance on the real axis, then calculate the phase shifts, and investigate whether a resonance condition is met. Further this method allows for evaluation of observables where the continuum is properly taken into account, and the observables become real quantities. Here we propose an alternative method, starting with the momentum space Schrödinger equation given in equation (3.7). The obvious advantage of this, is that the boundary conditions are automatically built into the integral equations. Further, the Contour Deformation Method allows us to obtain a complete set of single-particle states, which subsequently may be used in constructing a complete many-body basis suitable for Gamow Shell Model applications.

We consider an axially symmetric deformed Gaussian potential with no spin and tensor components. In spherical coordinates it is given as

$$V(r, \theta) = V_0 \exp(-r^2(\alpha \cos^2 \theta + \beta \sin^2 \theta)), \quad (3.39)$$

or in Cartesian coordinates,

$$V(x, y, z) = V_0 \exp(-\beta(x^2 + y^2)) \exp(-\alpha z^2), \quad (3.40)$$

here V_0 is the strength of the potential and α and β are shape parameters. Here z is the symmetry axis, and the potential is reflection symmetric in the x, y -plane. In the case $\alpha = \beta$ the potential is just a spherical Gaussian potential. In the case $\alpha > \beta$ the potential field is contracted along the z -axis, and defines an *oblate* shape. In the case $\alpha < \beta$ the potential field is stretched out along the z -axis, and defines a *prolate* shape. Defining a deformation parameter δ by⁵,

$$\delta = 1 - \frac{\alpha}{\beta}, \quad (3.41)$$

equation (3.39) can be written in the form,

$$V(r, \theta; \beta, \delta) = V_0 \exp(-\beta r^2) \exp(\beta \delta r^2 \cos^2 \theta) = V(r; \beta) D(r, \theta; \beta, \delta). \quad (3.42)$$

Here $V(r; \beta)$ is a spherically symmetric formfactor and $D(r, \theta; \beta, \delta)$ a deformation form-factor, $D = 1$ for $\delta = 0$ i.e. $\alpha = \beta$. We require that the volume of the central potential,

⁵Notice that our δ is twice that normally defined in the Nilsson model.

with the shape parameter $\alpha_0 = \alpha = \beta$, is equal to the volume of the axially symmetric deformed ellipsoidal potential. This implies that the shape parameters of the non-central and central Gaussian potential satisfy the following relation,

$$\alpha\beta^2 = \alpha_0^3, \quad (3.43)$$

and the deformation parameter δ may be expressed in terms of α_0 and β by

$$\delta = 1 - \left(\frac{\alpha_0}{\beta} \right)^3. \quad (3.44)$$

In figure 3.3 plots of the isocurves $V(r, \theta) = 0.5$ are shown in the x, z -plane for the deformation parameters $\delta = \pm 0.5$. With potential parameters $\alpha_0 = 1$ and $V_0 = 1$ for the spherically symmetric potential, $\delta = 0.5$ gives the shape parameters $\alpha = 2^{-2/3}$ and $\beta = 2^{1/3}$ for the deformed potential, and $\delta = -0.5$ gives the parameters $\alpha = (3/2)^{2/3}$ and $\beta = (2/3)^{1/3}$, respectively. It is seen that $\delta = 0.5$ corresponds to an *oblate* shape, and for $\delta = -0.5$ the potential takes a *prolate* shape, the symmetry axis being the vertical z -axis. In order to as-

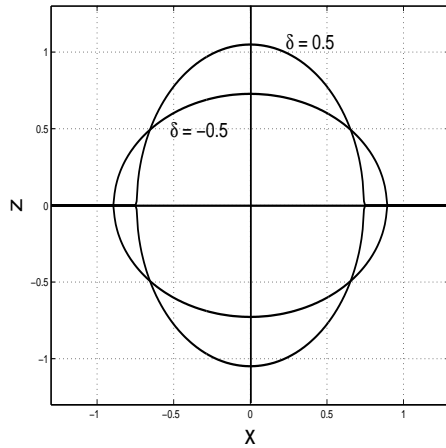


Figure 3.3: Plot of the ellipsoidal isocurves $V(r, \theta) = 0.5$ of the deformed potential for deformation $\delta = \pm 0.5$ with potential strength $V_0 = 1$ in the x, z -plane. For the spherically symmetric potential a shape parameter $\alpha_0 = 1$ was chosen.

sess the shape structure in more detail, it is instructive to study the multipole components of the potential. An axially symmetric potential may be expanded in terms of Legendre polynomials, i.e.

$$V(r, \theta) = \sum_{\lambda} V_{\lambda}(r) P_{\lambda}(\cos \theta). \quad (3.45)$$

Using the orthonormality properties of the Legendre polynomials, the multipole components are given by the integrals

$$V_{\lambda}(r) = \frac{(2\lambda + 1)}{2} V_0 \exp(-\beta r^2) \int_{-1}^1 d\eta \exp(\beta \delta r^2 \eta^2) P_{\lambda}(\eta), \quad (3.46)$$

where $\eta = \cos(\theta)$. Here it is explicitly seen for our reflection symmetric potential, that only *even* multipoles give non-vanishing contributions, since the Legendre polynomials have the property

$$P_\lambda(-\eta) = (-1)^\lambda P_\lambda(\eta),$$

and the potential is an even function in η . The monopole part of the deformed Gaussian

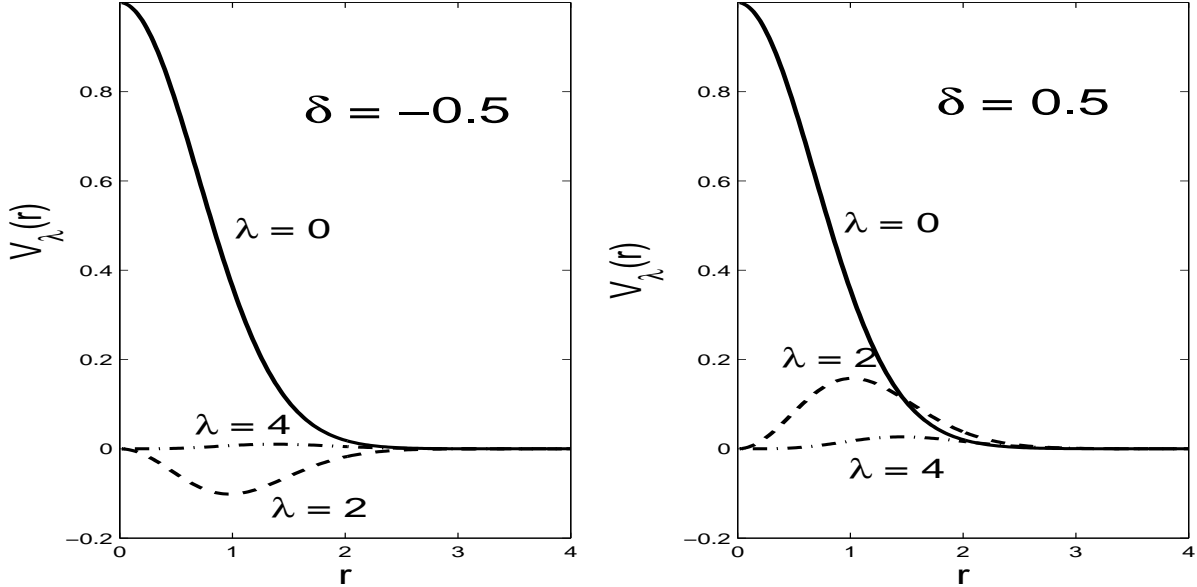


Figure 3.4: Plot of $\lambda = 0, 2, 4$ multipoles of the Gaussian potential with deformation parameters $\delta = 0.5$ (right plot) and $\delta = -0.5$ (left plot) and $\alpha_0 = 1$

potential may be calculated analytically,

$$V_{\lambda=0}(r) = \frac{1}{2}V_0 \exp(-\beta r^2) \int_{-1}^1 d\eta \exp(\beta \delta r^2 \eta^2) = \frac{1}{2}V_0 \exp(-\beta r^2) D_0(r), \quad (3.47)$$

where

$$D_0(r) = \frac{1}{2\sqrt{\tau}} \gamma(1/2, \tau), \quad \tau = -\beta \delta r^2, \quad (3.48)$$

here $\gamma(1/2, \tau)$ is the incomplete gamma function, see e.g. reference [67]. Figure 3.4 gives plots of the $\lambda = 0, 2, 4$ multipoles of the Gaussian potential with deformation parameters $\delta = \pm 0.5$ and the potential parameters $\alpha_0 = 1$ and $V_0 = 1$. It is seen that the radial monopole distribution is more or less identical for $\delta = 0.5$ and $\delta = -0.5$. Further it is seen that the deformed Gaussian potential is nearly a pure quadrupole deformation, since the $\lambda = 4$ multipole is almost vanishing in both cases. This may be understood from considering the exponent of the deformed formfactor in equation (3.42), which can be rewritten in terms of the $Y_{20}(\hat{r})$ spherical harmonic.

Having discussed the shape and multipoles of the deformed Gaussian potential, we now turn to the actual solution of the Schrödinger equation for this potential. We wish to solve the momentum space Schrödinger equation given in equation (3.7). The Fourier transformation of the deformed Gaussian potential in equation (3.40) is,

$$\begin{aligned} V(q_x, q_y, q_z) &= \frac{V_0}{(2\pi)^3} \int dx dy dz \exp(i(q_x x + q_y y + q_z z)) \exp(-\beta(x^2 + y^2) - \alpha z^2) \\ &= \frac{V_0}{8\pi^{3/2}\beta\alpha^{1/2}} \exp\left(-\frac{1}{4\beta}(q_x^2 + q_y^2)\right) \exp\left(-\frac{1}{4\alpha}q_z^2\right), \end{aligned} \quad (3.49)$$

here $q_i = k_i - k'_i$, $i = x, y, z$. In terms of spherical momentum space coordinates k, θ, φ the potential takes the form,

$$\begin{aligned} V(\mathbf{k}, \mathbf{k}') &= \frac{V_0}{8\pi^{3/2}\beta\alpha^{1/2}} \exp\left(-\frac{1}{4\beta}(k^2 \sin^2 \theta + k'^2 \sin^2 \theta') - \frac{1}{4\alpha}(k \cos \theta - k' \cos \theta')^2\right) \\ &\times \exp\left(\frac{1}{2\beta}kk' \sin \theta \sin \theta' \cos(\varphi - \varphi')\right). \end{aligned} \quad (3.50)$$

Due to axial symmetry the dependence of the potential on the azimuthal angles φ, φ' is only on the difference $\omega = \varphi - \varphi'$. The potential may therefore be expanded in a complete set of harmonics, i.e.

$$V(\mathbf{k}, \mathbf{k}') = \sum_{\mu=-\infty}^{\infty} V_{\mu}(\tilde{k}, \tilde{k}') \exp(i\mu\omega), \quad (3.51)$$

here $\tilde{k} = (k, \theta)$. The harmonics $\exp(i\mu\omega)$ obey the orthogonality relation

$$\int_{-\pi}^{\pi} d\omega \exp(-i\mu\omega) \exp(i\mu'\omega) = 2\pi\delta_{\mu,\mu'}, \quad (3.52)$$

the μ 'th harmonic of the potential is therefore given by the integral

$$V_{\mu}(\tilde{k}, \tilde{k}') = \frac{1}{2\pi} \int_{-\pi}^{\pi} d\omega \exp(-i\mu\omega) V(\mathbf{k}, \mathbf{k}'). \quad (3.53)$$

From equation (3.50) it is seen, that for the integral over ω , we have to consider the following integral,

$$I_{\mu}(y) = \frac{1}{2\pi} \int_{-\pi}^{\pi} d\omega \exp(-i\mu\omega) \exp(y \cos \omega) = \frac{1}{\pi} \int_0^{\pi} d\omega \cos(\mu\omega) \exp(y \cos \omega), \quad (3.54)$$

where we have introduced the variable

$$y = \frac{1}{2\beta}kk' \sin \theta \sin \theta'.$$

The integral in equation (3.54) is just the definition of the modified Bessel function of the 1'st kind (see e.g. [74]). The μ 'th harmonic of the potential is thus of analytic form, and given by,

$$V_\mu(\tilde{k}, \tilde{k}') = \frac{V_0}{8\pi^{3/2}\beta\alpha^{1/2}} \times \exp\left(-\frac{1}{4\beta}(k \sin \theta - k' \sin \theta')^2 - \frac{1}{4\alpha}(k \cos \theta - k' \cos \theta')^2\right) \exp(-y) I_\mu(y). \quad (3.55)$$

Inserting the expansion of the potential given in equation (3.51) into the momentum space Schrödinger equation (3.7) and projecting the equation on the harmonics $\exp(i\mu\omega)$, the three-dimensional integral equation has been reduced to an infinite set of two-dimensional integral equations. The μ 'th integral equation is easily solved as a matrix diagonalization problem with dimension $N_r \times N_\theta$. Here N_r is the number of integration points for the radial integral and N_θ the number of integration points for the angle integral. However, the Schrödinger equation can be further reduced to a coupled set of one-dimensional integral equations by projecting on spherical harmonics (see equation (3.10)). The angular momentum projected potential in equation (3.50) then takes the form,

$$\begin{aligned} V_{lm,l'm'}(k, k') &= \int d\hat{k} \int d\hat{k}' Y_{lm}^*(\hat{k}) \left\{ \sum_{\mu=-\infty}^{\infty} V_\mu(\tilde{k}, \tilde{k}') \exp(i\mu\omega) \right\} Y_{l'm'}(\hat{k}') \\ &= 2\pi \int_0^\pi d\theta \sin \theta \int_0^\pi d\theta' \sin \theta' \bar{P}_{lm}(\cos \theta) V_m(\tilde{k}, \tilde{k}') \bar{P}_{l'm}(\cos \theta') \delta_{m,m'}, \end{aligned} \quad (3.56)$$

where $\bar{P}_{lm}(x)$ are the normalized associated Legendre polynomial,

$$\bar{P}_{lm}(x) = \left\{ \frac{2l+1(l-m)!}{2(l+m)!} \right\}^{1/2} P_{lm}(x). \quad (3.57)$$

We wish to study the formation of resonances in the deformed Gaussian potential by the contour deformation method. The 1-dimensional coupled integral equations are then analytically continued from the physical to the non-physical energy sheet by distorting the integration contour. Choosing a suitable inversion symmetric contour L^+ , discussed in the previous section, we end up with the analytically continued coupled integral equations for the axially deformed Gaussian potential,

$$\left(\frac{\hbar^2}{2\mu} k^2 - E_{nlm} \right) \psi_{nlm}(k) = - \sum_{l'} \int_{L^+} dk' k'^2 V_{lm,l'm}(k, k') \psi_{nl'm}(k'). \quad (3.58)$$

As a case study we consider a Gaussian potential which in the spherically symmetric case reproduces the $J^\pi = 3/2^-_1$ resonance in ${}^5\text{He}$. The $J^\pi = 3/2^-_1$ resonance, to be associated with the single-particle orbit $p_{3/2}$, is experimentally known to have a width of $\Gamma \approx 0.60$ MeV. Using the following parameters for the spherically symmetric Gaussian given in equation (3.39),

$$V_0 = -53.5 \text{ MeV}, \quad \alpha_0 = 0.188 \text{ fm}^{-2}, \quad (3.59)$$

the Gaussian potential supports a bound state for the $l^\pi = 0^+$ channel with energy $E = -14.9044\text{MeV}$, and a resonance for the $l^\pi = 1^-$ channel with energy $E = 0.7268 - 0.3096i\text{MeV}$. Here the nucleon spin $s = 1/2$ is neglected since the energy levels are degenerate for $j = l \pm 1/2$, which follows from the spin independence of the Gaussian potential. Table 3.1 gives the convergence of the $m^\pi = 0^+$ ground state energy, for deformation parameters $\delta = \pm 0.9$. It is seen that the deformation $\delta = 0.9$ affects the bound state the most, and the ground state becomes less bound $E = -12.1\text{MeV}$, for the prolate deformation. On the other hand, the oblate deformation $\delta = -0.9$ has little effect on the ground state energy $E = -14.7\text{MeV}$. This may be understood by considering the monopole term of the

l_{\max}	$\delta = 0.9$		$\delta = -0.9$	
	Re[E]	Im[E]	Re[E]	Im[E]
0	-10.5843	0.	-14.4816	0.
2	-11.9041	0.	-14.6533	0.
4	-12.0741	0.	-14.6551	0.
6	-12.0953	0.	-14.6551	0.
8	-12.0979	0.	-14.6551	0.
10	-12.0983	0.	-14.6551	0.

Table 3.1: Convergence of groundstate, $m^\pi = 0^+$, for deformation parameters $\delta = \pm 0.9$ as the number of partial waves increases. In the spherically symmetric case $\delta = 0$ the $l^\pi = 0^+$ Gaussian potential supports a bound state at energy $E = -14.9044\text{MeV}$.

potential, which is the main component in the multipole expansion in equation (3.45). In figure 3.5 a plot of the monopole part of the Gaussian potential with deformation parameters $\delta = \pm 0.9$ is given, together with a plot of the spherically symmetric potential. It is seen that the monopole term for the $\delta = -0.9$ potential is more or less identical to the spherically symmetric potential (slightly less attractive), on the other hand the monopole term for the $\delta = 0.9$ potential is less attractive for $r < 4\text{fm}$, but more attractive at large distances $r > 4\text{fm}$. From this one may conclude that the ground state of the $\delta = -0.9$ potential will be more bound than for the $\delta = 0.9$ potential, since the ground state is deeply bound and the wave function will be mainly located in the interior part of the potential.

The resonant orbit $l^\pi = 1^-$ in the spherically symmetric potential is split into two non-degenerate orbits ($m^\pi = 0^-$ and $m^\pi = 1^-$) in the case of an axially symmetric deformation. This is a characteristic of axially deformed potentials. Table 3.2 gives the convergence of the $m^\pi = 0^-$ and $m^\pi = 1^-$ excited negative parity states in the Gaussian potential, for deformation parameters $\delta = \pm 0.5$. In all cases a satisfactory convergence is obtained with $l_{\max} = 5$. For the states with angular momentum projection along the z -axis ($m = 0$), it is seen that for $\delta = 0.5$ (prolate deformation) the $l^\pi = 1^-$ state has become a bound state with energy $E = -0.680\text{MeV}$. For zero angular momentum projection, the particle moves in an orbit making $\theta = 0$ degrees with the z -axis. So in the case of a prolate deformation, where the field is stretched out along the z -axis, a particle moving in this

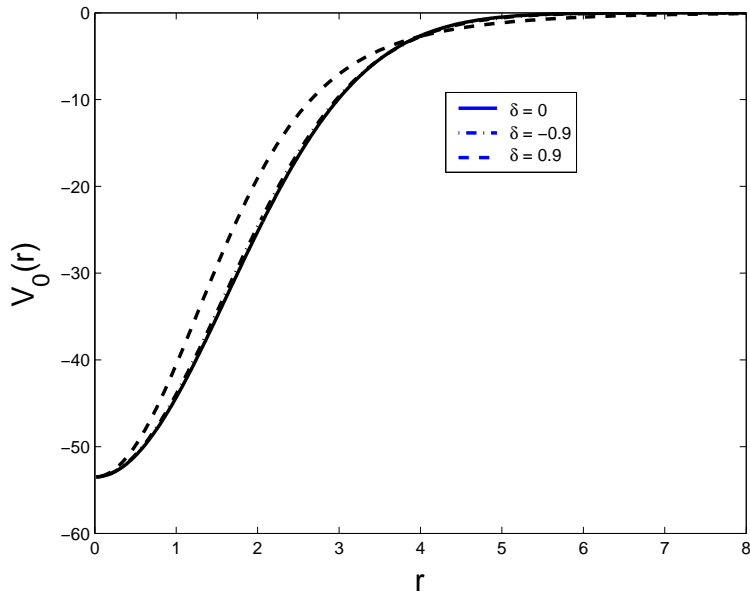


Figure 3.5: Plot of the monopole part of the Gaussian potential with deformation parameters $\delta = 0$ and $\delta = \pm 0.9$.

orbit will “feel” the field more strongly than compared with the spherically symmetric field, and it will become more bound. This explains also why the particle with $m = 0$ becomes more unbound in the case of the oblate deformation $\delta = -0.5$, see Columns 6 and 7 of table 3.2.

For the $m = 1$ case the opposite takes place. In the case of $\delta = 0.5$ the particle becomes more unbound, while for $\delta = -0.5$ the particle becomes more bound. By considering the dipole ($l = 1$) term of the wave function, the particle moves in an orbit making $\theta = \pi/4$ degrees with the z -axis. From this it may be understood that particle gains more binding in the case of an oblate deformation $\delta = -0.5$ and becomes more unphysical in the opposite case $\delta = 0.5$ (see columns 4,5,8 and 9 of table 3.2).

In table 3.3 the squared amplitudes of the wave functions are given for each partial wave l . It is seen that in all cases that the squared amplitudes for the $l = 1$ component of the total wave function, is nearly equal to the norm of the total wave function, while all other partial wave amplitudes are vanishing small. In this sense one may say that the orbital angular momentum is approximately a “good” quantum number.

In figure (3.6) a plot of the bound state energy of the $m^\pi = 0^+$ state are given for the deformation parameter δ taking values between -0.9 and 0.9 . It is seen that the position of the bound state varies much more strongly for a prolate deformation ($\delta > 0$), than for an oblate deformation.

In figure (3.7) a plot of the real (solid line) and imaginary part (dashed line) of the $m^\pi = 0^-$ state are given for the deformation parameter δ taking values between -0.9 and 0.9 . The value for δ in which the resonant state becomes a bound state is given

$\delta = 0.5$				$\delta = -0.5$				
$m^\pi = 0^-$		$m^\pi = 1^-$		$m^\pi = 0^-$		$m^\pi = 1^-$		
l_{\max}	Re[E]	Im[E]	Re[E]	Im[E]	Re[E]	Im[E]	Re[E]	Im[E]
1	-0.5282	0.	1.4865	-1.0177	1.5402	-1.0701	0.3815	-0.1139
3	-0.6772	0.	1.4419	-0.9631	1.5170	-1.0404	0.3602	-0.1042
5	-0.6802	0.	1.4410	-0.9621	1.5168	-1.0402	0.3601	-0.1041
7	-0.6803	0.	1.4410	-0.9620	1.5168	-1.0402	0.3601	-0.1041
9	-0.6803	0.	1.4410	-0.9620	1.5168	-1.0402	0.3601	-0.1041

Table 3.2: Convergence of the $m^\pi = 0^-$ and $m^\pi = 1^-$ energies, for deformation parameters $\delta = \pm 0.5$ with increasing number of partial waves. In the spherically symmetric case ($\delta = 0$) the $l^\pi = 1^-$ Gaussian potential supports a resonance state at energy $E = 0.7268 - 0.3096i$ MeV.

$\delta = 0.5$				$\delta = -0.5$				
$m^\pi = 0^-$		$m^\pi = 1^-$		$m^\pi = 0^-$		$m^\pi = 1^-$		
l_{\max}	Re[ψ_l^2]	Im[ψ_l^2]						
1	0.9947	0.	0.9982	2.31E-03	0.9992	1.1E-03	0.9993	3.E-04
3	5.7E-03	0.	1.8E-03	-2.3E-03	8.E-04	-1.1E-03	7.E-04	-3.E-04
5	5.E-05	0.	2.E-05	-2.E-05	3.E-06	-3.E-06	2.E-06	-9.E-07
7	6.E-07	0.	3.E-07	-2.E-07	2.E-08	-1.E-08	9.E-09	-4.E-09
9	8.E-09	0.	4.E-09	-3.E-09	9.E-11	-7.E-11	4.E-11	-2.E-11

Table 3.3: Convergence of the $m^\pi = 0^-$ and $m^\pi = 1^-$ squared amplitudes of the wave functions for each partial wave l , for deformation parameters $\delta = \pm 0.5$.

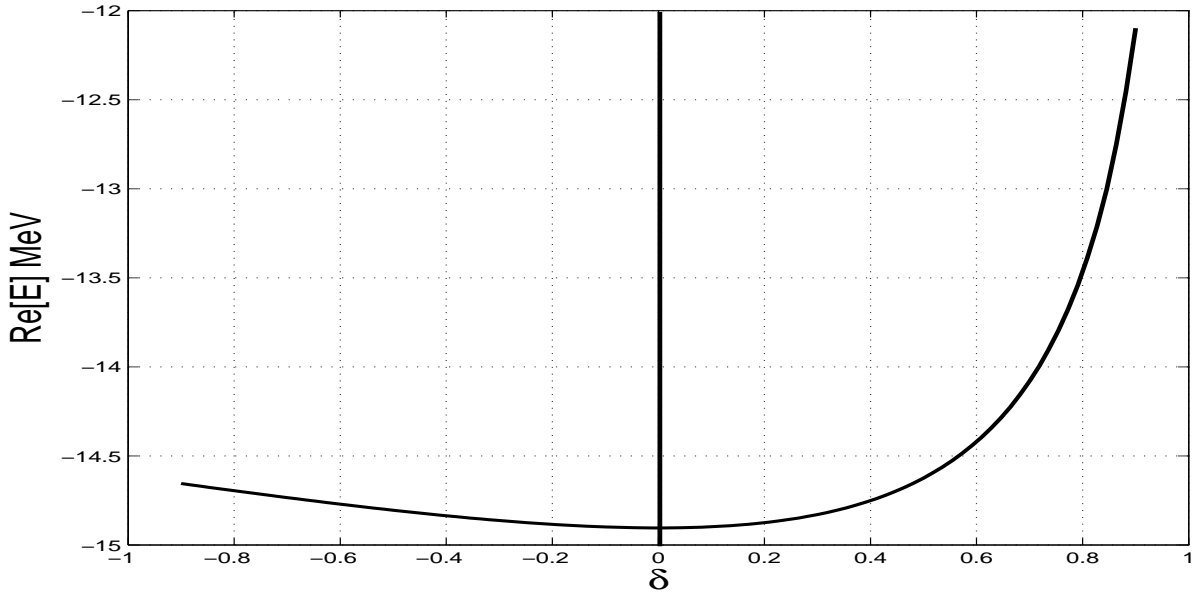


Figure 3.6: Bound state trajectory for the $m^\pi = 0^+$ state in the deformed Gaussian potential. Energy is plotted as function of deformation parameter δ .

when the real energy trajectory meets the imaginary energy trajectory for $\text{Re}[E] < 0$, i.e. $\text{Im}[E] = \text{Re}[E]$. Here it is seen that the resonance for $\delta = 0$ becomes a bound state for $\delta > 0.3$. For $\delta < 0$ the resonance moves further down in the lower half complex k -plane.

In figure (3.8) a plot of the real (solid line) and imaginary part (dashed line) of the $m^\pi = 1^-$ energies are given for the deformation parameter δ taking values between -0.9 and 0.9 . Here the resonance state does not become a bound state for the values of δ considered, $\delta \in (-0.9, 0.9)$. For $\delta \in (-0.9, 0.2)$ the resonance display a weak variation from the $\delta = 0$ resonance, and slowly moves towards the scattering threshold $E = 0$, for $\delta \rightarrow -0.9$. On the other hand, as $\delta \rightarrow 0.9$ the imaginary part of the energy dives into the lower half complex energy plane, and the resonance state becomes strongly unphysical.

In figure (3.9) a combined plot of the real and imaginary parts of the $m^\pi = 0^-$ and $m^\pi = 1^-$ energies are given for the deformation parameter δ taking values between -0.9 and 0.9 . Here the splitting of the $l^\pi = 1^-$ resonant level with respect to the angular momentum projection m is clearly seen. It is also seen that the energy of the $m^\pi = 0^-$ and the $m^\pi = 1^-$ state behave in opposite manner for $\delta > 0$ and for $\delta < 0$. For $\delta \rightarrow 0.9$ the $m^\pi = 0^-$ state becomes more bound while the $m^\pi = 1^-$ becomes more unbound, for $\delta \rightarrow -0.9$ the $m^\pi = 0^-$ state becomes more unbound while the $m^\pi = 1^-$ becomes almost bound.

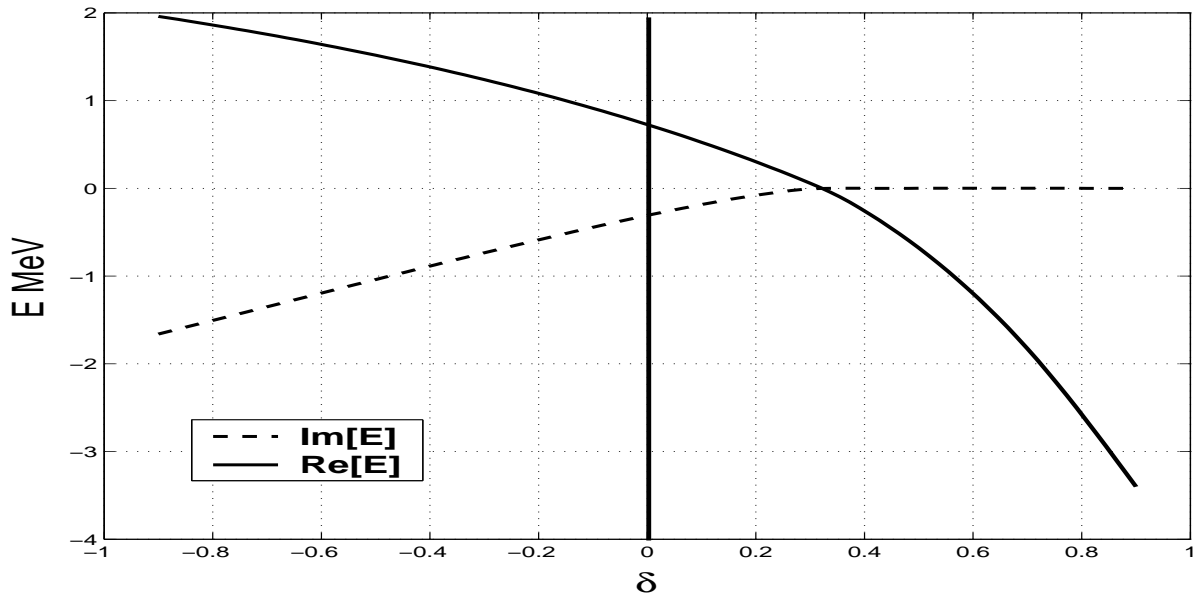


Figure 3.7: Real (solid line) and imaginary part (dashed line) of the $m^\pi = 0^-$ state energy in the deformed Gaussian potential as the deformation parameter δ is varied between -0.9 and 0.9 .

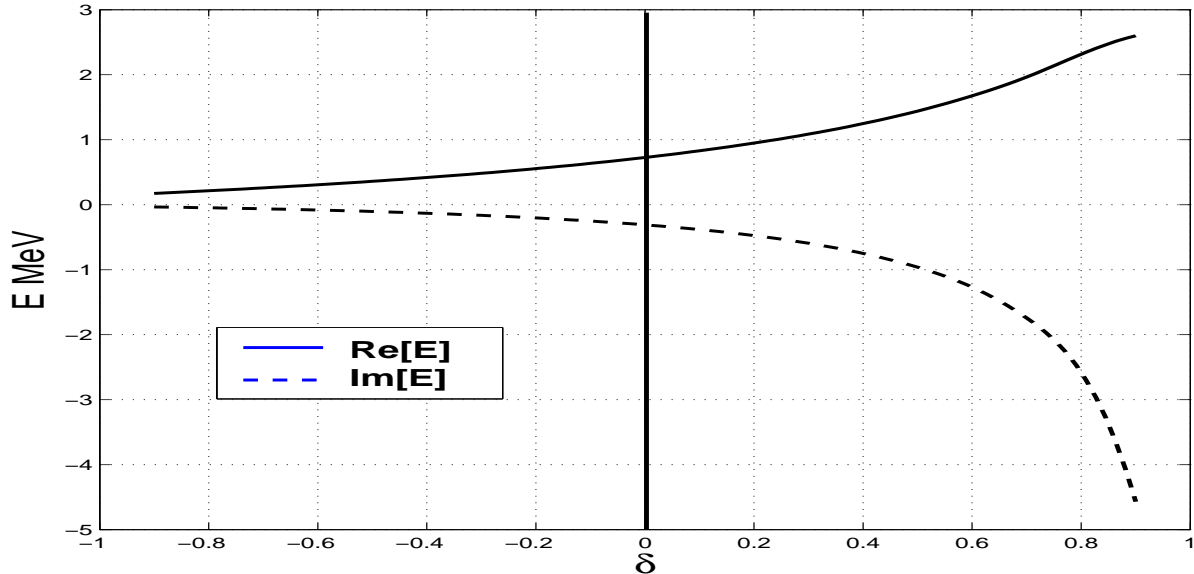


Figure 3.8: Real (solid line) and imaginary part (dashed line) of the $m^\pi = 1^-$ state energy in the deformed Gaussian potential as the deformation parameter δ is varied between -0.9 and 0.9 .

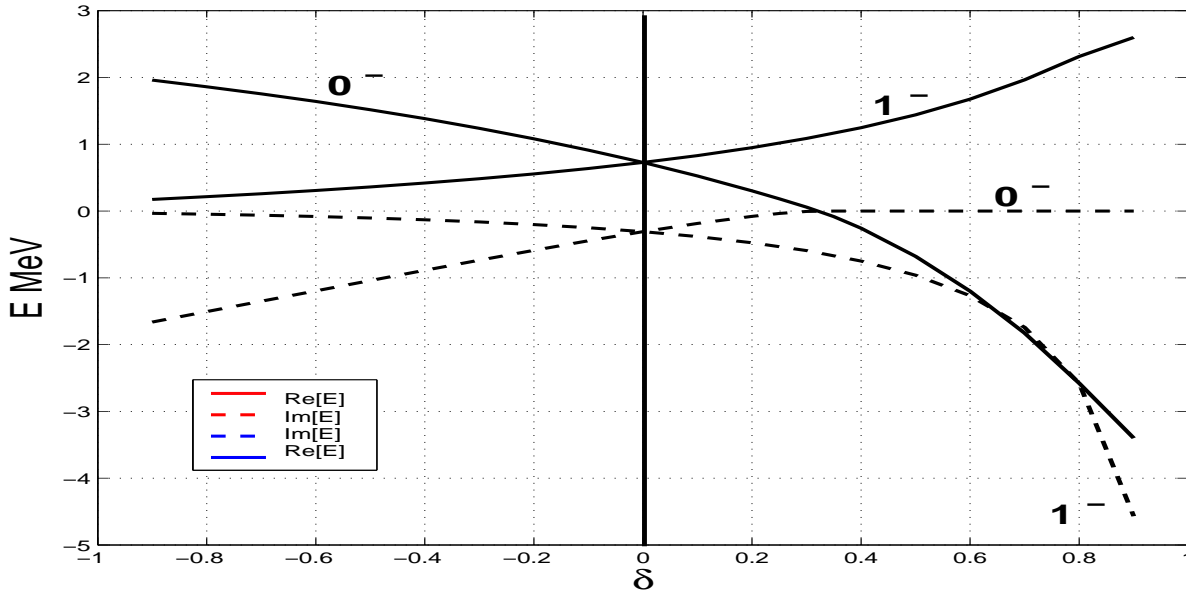


Figure 3.9: Real (solid lines) and imaginary parts (dashed lines) of the $m^\pi = 0^-$ and the $m^\pi = 1^-$ state energies in the deformed Gaussian potential as the deformation parameter δ is varied between -0.9 and 0.9 .

3.4 Two-Particle Resonances and Bound States Embedded in the Continuum in Complex Potentials.

CDM has a number of different applications, in this section scattering from a complex Malfliet-Tjon interaction describing absorptive and emitting processes is considered.⁶ Complex potentials have commonly been used in optical potential models in nuclear and particle physics. Inelastic scattering where the conservation of flux is broken due to the possibility of the particle to be ejected to other exit channels or particles to emerge from them, may be taken into account by a complex absorbing or emitting potentials respectively. Another application of complex potentials, is the nucleon-antinucleon scattering, in which a short range complex annihilation potential may describe how bound- and resonant states are formed such systems.

In letting the interaction strengths be generalized to the complex plane the Schrödinger equation becomes a non-hermitian eigenvalue problem from the very beginning, and the eigenvalues will in general become complex. See references [8, 85] for a more rigorous discussion of complex interactions. Below follows a demonstration that CDM gives accurate calculation of the complete energy spectrum for complex interactions. The pole trajectories

⁶See Paper 1 for a detailed analysis of the structure of the Malfliet-Tjon potential in momentum space, the relevant equations to be solved and the bound, anti-bound and resonant pole distributions as function of the interaction strength.

are studied by varying the absorptive and emissive strengths of the interaction.

In the case of the Malfliet-Tjon interaction two cases are studied. First the attractive strength is scaled by a complex constant $1 + \eta i$, i.e. $V_A \rightarrow (1 + \eta i)V_A$, keeping the repulsive strength V_R real. Since the attractive strength V_A is a negative quantity, absorptive scattering takes place for $\eta > 0$ while emissive scattering takes place for $\eta < 0$. Secondly both the attractive and repulsive interaction strengths are scaled, i.e. $V \rightarrow (1 + \eta i)V$. Starting with $\nu_A = -5$, so for $\eta = 0$ a resonance at $E = 5.1804 - 3.1555i$ MeV corresponding to a pole at $k = 0.3682 - 0.1033i$ fm $^{-1}$ in the complex k -plane appears (see Paper 1) ⁷. In figure 3.10 a plot of the pole trajectory for varying η is given, keeping ν_A fixed. An imaginary part is added to the attractive strength V_A while V_R is kept real. From the figure it is seen

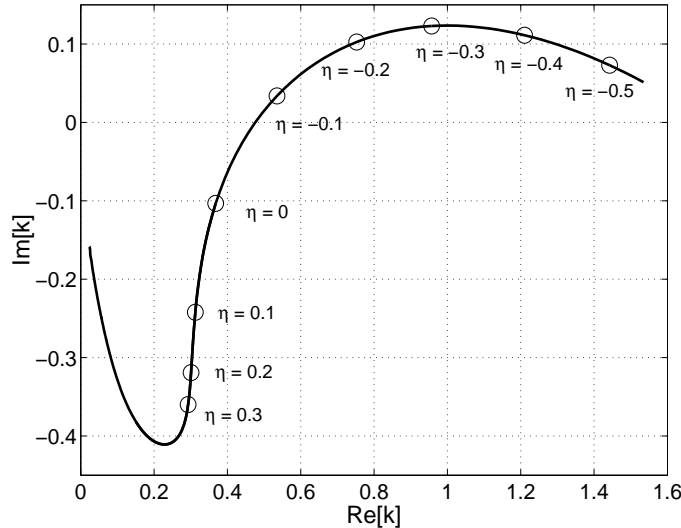


Figure 3.10: Pole trajectory of the $l = 1$ resonance in the $\nu_A = -5$ Malfliet-Tjon interaction, for increasing absorption/emission. Here only the attractive strength of the interaction takes complex values, $V_A \rightarrow (1 + \eta i)V_A$.

that when the probability for finding the particle increases ($\eta < 0$), the resonance pole approaches the real k -axis, and eventually crosses from the non-physical to the physical energy sheet. In the case of absorption ($\eta > 0$) the opposite effect is observed. That the pole becomes “more” physical with a repulsive imaginary part added to the potential, may be understood from the following argument. The resonance is formed inside the potential barrier, with a limited lifetime before it tunnels through the barrier and dies. If more particles are created inside the barrier, the probability of finding a particle inside the barrier should increase with the number of particles added.

In figure 3.11 a plot of the pole trajectory of the resonance at $E = 5.1804 - 3.1555i$ with $\eta = 0$ is given for varying η . Here both attractive and repulsive part are scaled. In scaling both the attractive and repulsive parts of the potential with the same complex con-

⁷Here $V_A = \nu_A \times \hbar c$, see Paper 1 for more details.

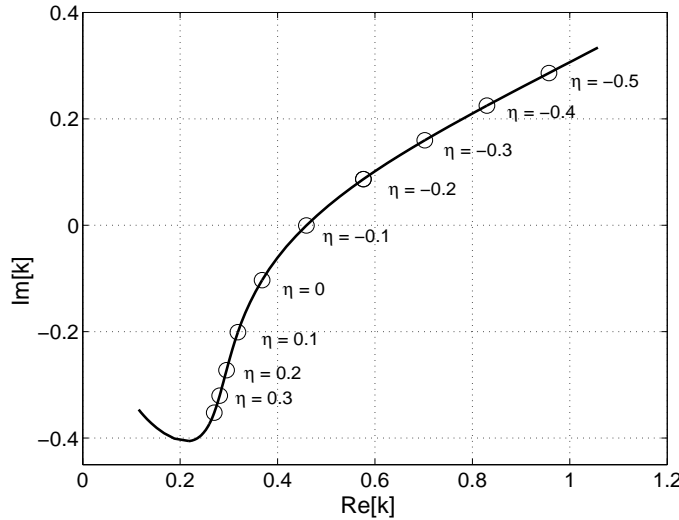


Figure 3.11: Pole trajectory of the $l = 1$ resonance in the $\nu_A = -5$ Malfliet-Tjon interaction, for increasing absorption/emission. Here both attractive and repulsive strengths of the interaction takes complex values, $V \rightarrow (1 + \eta i)V$.

stant $1 + \eta i$, both absorption and emission takes place. However, since the potential is on average more attractive than repulsive, the total effect of letting η become negative will be emission of particles while letting η become positive will result in absorption of particles. This is also seen from the figure 3.11, where the pole moves towards the physical sheet for $\eta < 0$, and becomes more “unphysical” for $\eta > 0$. Since absorption and emission are competing processes in this case, the dependence of the pole position on increasing/decreasing imaginary part of the potential should be weaker than in the former case where only the attractive part was scaled, i.e. pure absorption and emission took place. This is observed by comparing figures 3.10 and 3.11. In figure 3.10 the pole has moved onto the physical energy sheet for $\eta = -0.1$ while it is still on the nonphysical sheet in figure 3.11. The same strong and weak dependence on η is observed for the absorptive process $\eta = 0.1$.

For an assessment of the generality of the results for the Malfliet-Tjon potential obtained above, the pole trajectory for the $l = 1$ Yamaguchi interaction with $\beta = 2 \text{ fm}^{-1}$ and interaction strength $\lambda = 165 \text{ MeV fm}^{-1}$ is considered as well⁸. This interaction supports a resonance at $E = 0.8736 - 0.1285i \text{ MeV}$ for $\eta = 0$. Figure 3.12 gives a plot of the pole trajectory of the resonance for varying η . From the figure it is seen that pole behaves in the same way with increasing emission and absorption as in the Malfliet-Tjon case considered in figures 3.10 and 3.11.

From the above numerical analysis of the resonance pole trajectory for a complex absorbing or emitting potential, one may make the following conclusion. For increasing emission, i.e. $\eta < 0$, the resonant pole in the third quadrant of the complex k -plane moves

⁸See Paper 1 for details on the $l = 1$ Yamaguchi potential.

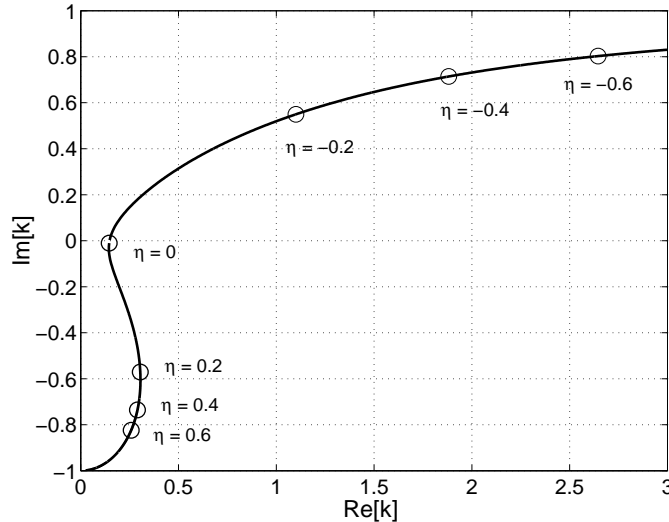


Figure 3.12: Pole trajectory of the resonance at $E = 0.8736 - 0.1285i$ MeV in the Yamaguchi interaction with $\beta = 2 \text{ fm}^{-1}$ and interaction strength $\lambda = 165 \text{ MeVfm}^{-1}$

towards the real k -axis. Eventually the resonant poles move through the unitarity cut and onto the physical energy sheet (upper half complex k -plane). When the pole crosses the cut, the imaginary part of the resonance energy is zero, that is why poles located on the cut are usually defined as *bound states embedded in the continuum*. Poles which are located on the physical energy sheet may be interpreted as unstable bound states. Poles moving onto the physical energy sheet may therefore give a clear signature in physical observables such as phase-shifts and scattering cross sections. For increasing absorption on the other hand, i.e. $\eta > 0$, the resonant pole becomes more and more unphysical in the sense that it moves away from the physical scattering axis. These conclusions apply in the cases considered above, and one may expect them to hold for other potential shapes too.

The illustrations above indicate a general behaviour of decay resonant states when the interaction is scaled by a complex constant. One may ask in a similar fashion in what way the capture resonant states develops as a function of η . Will the symmetry with respect to the imaginary k -axis for capture and decay states prevail? The answer to this is no. It can be seen by considering the symmetry properties of the scattering matrix in the case of a complex interaction. In particular we have the property, see equations (2.14) and (2.15)

$$S_l^*(-k^*, \eta^*) = S_l(k, \eta). \quad (3.60)$$

This implies that if the interaction $(1 + i\eta)V$ supports a resonance at k , the complex conjugated interaction $(1 + i\eta)^*V$ supports a resonance at $-k^*$. The number of poles is invariant with respect to η , the poles only get redistributed as η is varied. The symmetry between decay and capture states is therefore broken. As the capture resonance moves away from the real k -axis in the third quadrant of the complex k -plane the capture state moves toward the real k -axis and eventually into the physical energy sheet. It is quite

interesting that a capture state which for $\eta = 0$ was considered a non-physical state, may become a physical bound state with a finite lifetime for $\eta > 0$.

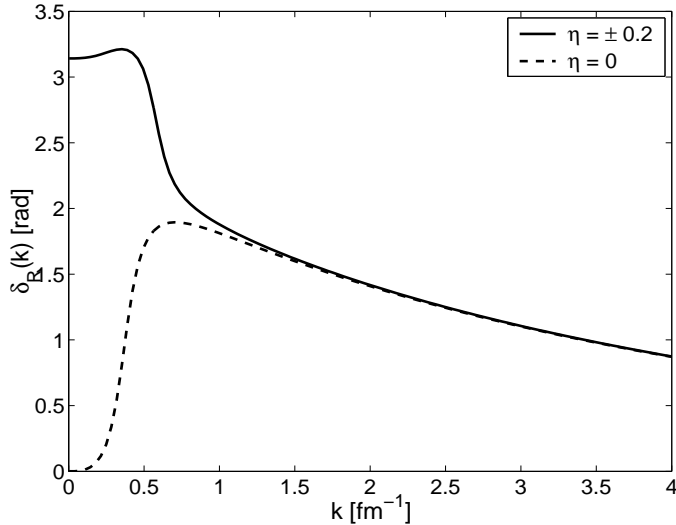


Figure 3.13: Real part of phase shifts for the $l = 1$ Malfliet-Tjon interaction with $\nu_A = -5$. The dashed line gives the phase shifts for $\eta = 0$, while the continuous line give the phase shifts for $\eta \pm 0.2$.

In the case of complex interactions the phase shift is a complex quantity, $\delta = \delta_R + i\delta_I$. The real part δ_R is interpreted as before and describes the elastic scattering while the imaginary part, δ_I , is a measure of the inelastic scattering taking place. Figures 3.13 and 3.14 give plots of the real and imaginary part of the phase shifts for the $l = 1$ Malfliet-Tjon interaction with $\nu_A = -5$ and $\eta = 0, \pm 0.2$. Here only the attractive strength V_A was scaled, keeping the repulsive part V_R real, see figure 3.10 for details on the pole trajectory. In the case $\eta = -0.2$ the decay state has moved onto the physical energy sheet and become a bound state. In the case $\eta = 0.2$ the capture state has moved into the physical energy sheet and become a bound state, while the decay state has become more unphysical. There is no way to differentiate between the real part of the phase shifts for $\eta = \pm 0.2$. The elastic scattering is the same for both cases, which is expected since the real part of the interaction is the same. The imaginary part of the phase shifts are on the other hand different, and is directly related to the sign of η where either an absorption of particles out of the elastic channel or an emission of particles into the elastic channel takes place.

A generalized Levinson theorem may be formulated for the real part of the phase shift [8], $\delta_R(0) - \delta_R(\infty) = n\pi$ where n is the number of poles in the upper half complex k -plane (physical energy sheet). In figure 3.13 we have for $\eta = \pm 0.2$, $\delta(0) = \pi$ which is in accordance with the generalized Levinson' theorem.

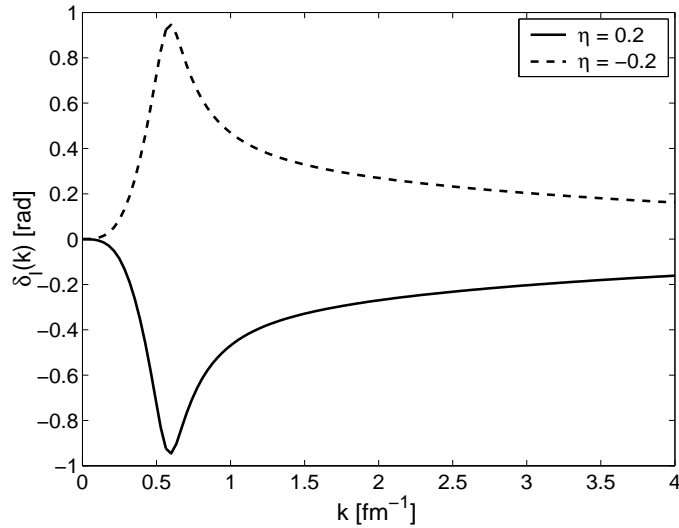


Figure 3.14: Imaginary part of the phase shifts for the $l = 1$ Malfliet-Tjon interaction with $\nu_A = -5$ and $\eta = -0.2$ given by the dashed line and $\eta = 0.2$ by the continuous line.

3.5 Two-Particle Scattering; Isolating Resonance Phenomena by CDM.

In this section we will discuss the solution for the full off-shell t -matrix, and hence the full two-body scattering problem, by expanding the two-body Green's function in a complete set of Berggren states. The Berggren representation of the scattering equations gives an analytic continuation in energy, from the upper rim of the Riemann cut through the cut and into the non-physical energy sheet.

The t -matrix is defined in operator form by

$$t(\omega) = V + Vg^{II}(\omega)V, \quad (3.61)$$

or equivalently

$$t(\omega) = V + Vg_0^{II}(\omega)t(\omega). \quad (3.62)$$

Here ω is the incoming energy, $g^{II}(\omega)$ is the resolvent, commonly known as the Green's operator, and $g_0^{II}(\omega)$ the corresponding free Green's operator. In operator form they are defined by

$$g_0^{II}(\omega) = \frac{1}{\omega - H_0}, \quad (3.63)$$

$$g^{II}(\omega) = \frac{1}{\omega - H}. \quad (3.64)$$

They are related through the Dyson equation

$$g^{II}(\omega) = g_0^{II}(\omega) + g_0^{II}(\omega)Vg^{II}(\omega). \quad (3.65)$$

The term H_0 is the kinetic energy operator and H the full two-body Hamiltonian. The physical interpretation of the Green's functions is that g_0^{II} describes the propagation of two noninteracting particles, while g^{II} describes the propagation of two interacting particles in free space.

3.5.1 Berggren representation of the t -matrix

The Berggren representation of the Green's function is obtained by expanding the unit operator using the completeness relation given in equation (3.33). In this case the Green's operator takes the form

$$g^{II}(\omega) = \sum_{n=a,b,c,d} \frac{|\psi_n\rangle\langle\psi_n^*|}{\omega - E_n} + \int_{L^+} dE \frac{|\psi\rangle\langle\psi^*|}{\omega - E}. \quad (3.66)$$

Here n denotes bound, antibound and resonant states. The integration contour L^+ denotes an arbitrary inversion symmetric contour, see e.g. figure 2.4 in section 2.3 of chapter 2, and gives the non-resonant distorted continuum contribution to the interacting Green's function. If we neglect the non-resonant continuum contribution to the Green's function we get the *resonant state expansion* of the Green's function. Such expansions have been studied over the last decade for finite range potentials, see e.g. [86, 87, 49]. The Green's function given in equation (3.66) is continuous and analytic in energy across the real axis and into the domain \mathbf{C} of the lower part of the complex energy plane. Equation (3.66) is therefore an analytic continuation in energy of the Green's function defined along the real energy axis.

The Berggren representation of the t -matrix is obtained by inserting the interacting Green's function given by equation (3.66) into equation (3.61), giving

$$t(\omega) = V + \Delta t(\omega) = V + \Delta t^R(\omega) + \Delta t^C(\omega). \quad (3.67)$$

Here $\Delta t^R(\omega)$ is the resonant contribution while $\Delta t^C(\omega)$ is the non-resonant distorted continuum contribution to the t -matrix. By projecting $t(\omega)$ on momentum states, and decomposing into partial waves, the t -matrix elements $t_l(k, k'; \omega)$ can be expressed as 1-dimensional integral equations,

$$t_l(k, k', \omega) = V_l(k, k') + \int_{L^+} \int_{L^+} dq dq' q^2 q'^2 V_l(k, q) g^{II}(q, q'; \omega) V_l(q', k'). \quad (3.68)$$

This representation of the t -matrix is valid as long as we do not pass through any singularities of the interaction potential when deforming the real k -axis into the distorted contour L^+ .

In numerically solving equation (3.68), the eigenvalue problem on the discretized contour L^+ given in equation (3.31) has to be solved. Then the interacting Green's function is represented in the discretized complete set of momentum states given in equation (3.33), giving the discretized Green's function,

$$g^{II}(k_i, k_j, \omega) = \sum_n \frac{\psi_{nl}(k_i)\psi_{nl}(k_j)}{\omega - E_{nl}} = \sum_n (\sqrt{w_i w_j} k_i k_j)^{-1} \frac{\psi_{nl}(i)\psi_{nl}(j)}{\omega - E_{nl}}. \quad (3.69)$$

Inserting this discretized form of the interacting Green's function into equation (3.68) and discretizing the integration over q and q' , a discretized version of the t -matrix is obtained. Having obtained $\tilde{g}^{II}(k_i, k_j)$, the full off-shell t -matrix is therefore obtained by the matrix equation

$$t_l(k_i, k_j, \omega) = V_l(k_i, k_j) + \tilde{V}_l^T(i) \tilde{g}^{II}(\omega) \tilde{V}_l(j), \quad (3.70)$$

where $\tilde{V}_l(n)$ is the n 'th column of the potential matrix $V_l(k_i, k_j)$ and $\tilde{g}^{II}(\omega)$ is the symmetric matrix

$$\tilde{g}^{II}(i, j, \omega) = \sqrt{w_i w_j} k_i k_j \sum_n \frac{\psi_{nl}(i) \psi_{nl}(j)}{\omega - E_{nl}}. \quad (3.71)$$

Applying CDM enables us to obtain $t_l(k, k'; \omega)$ for both real and complex energies ω . The integral becomes non-singular on the deformed contour for real and positive input energies ω , resulting in numerically stable solutions for physical two-body scattering. The Berggren representation of the t -matrix also allows for a separate study of the resonant and continuum contributions. The limitation of this method is that most potentials in momentum space have singularities in the complex plane when one argument is real and the other is complex. By applying contour L_1^+ , which is based on rotation into the complex plane, in most cases there will be restrictions on both rotation angle (θ) and maximum incoming and outgoing momentum (k, k'), see for example reference [27].

Using contour L_2^+ we can avoid these limitations by choosing the integration contour in such a way that the potential singularities always will lie outside the integration contour, and therefore do not give any restriction on rotation angle and maximum incoming and outgoing momentum.

3.5.2 Fredholm representation

The partial wave decomposition of equation (3.62) gives the *Fredholm* representation, commonly known as the Lippmann-Schwinger equation

$$t_l(k, k'; \omega) = V_l(k, k') + \frac{2}{\pi} \int_0^\infty \frac{dq q^2 V_l(k, q) t_l(q, k')}{\omega - E(q)}. \quad (3.72)$$

In physical two-body scattering the input energy is real and positive. In this case the *Fredholm* integral equation (3.72) has a singular kernel of Cauchy type. Solving singular integrals can be done by Cauchy's Residue theorem, where we integrate over a closed contour enclosing the poles. There are two ways of doing this, either by letting z lie an infinitesimal distance above the real axis, i.e., $\omega \rightarrow z + i\epsilon$, or by letting ω lie on the real axis. In both cases we must choose a suitable contour enclosing the singularity. If we choose the latter position of the singularity, we get a Cauchy *principal-value* (PV) integral where we integrate up to - but not through - the singularity, and a second contour integral, where the contour can be chosen as a semicircle around the singularity. Equation (3.72) can thus be given in terms of a principal value part and a second term coming from integration over

the semicircle around the pole. The result is

$$t_l(k, k'; \omega) = V_l(k, k') + \frac{2}{\pi} \mathcal{P} \int_0^\infty \frac{dq q^2 V_l(k, q) t_l(q, k')}{\omega - E(q)} - 2i\mu k_0 V_l(k, k_0) t_l(k_0, k'; \omega). \quad (3.73)$$

By rewriting the principal value integral using the relation

$$\mathcal{P} \int_0^\infty dk \frac{f(k)}{k_0^2 - k^2} = \int_0^\infty dk \frac{[f(k) - f(k_0)]}{k_0^2 - k^2}, \quad (3.74)$$

we obtain an equation suitable for numerical evaluation. Equation (3.73) can be converted into a set of linear equations by approximating the integral by a sum over N Gaussian quadrature points ($k_j; j = 1, \dots, N$), each weighted by w_j . The full off-shell t -matrix is then obtained by matrix inversion. This method for solving integral equations is known as the Nystrom method. It is numerically effective and stable, except for the rare case when the incoming energy ω coincides with or is very close to one of the integration points.

So far we have only considered physical input energies in equation (3.72), but it has been shown in reference [8] that the analytically continued Lippmann-Schwinger equation to complex energies takes the same form as equation (3.73). By solving the full off-shell t -matrix for arbitrary complex input energy, we do not have to alter the set of linear equations obtained for physical energy, the only modification is that the energy is complex.

The Lippmann-Schwinger equation for t -matrix (3.72), can be solved by the contour deformation method as well. Using CDM the integral equation given in equation (3.72) has a compact integral kernel (Hilbert-Schmidt kernel) for positive incoming energies ω , thus the principal value (PV) prescription may be avoided. In the first step we calculate the t -matrix elements $t_l(z, k, \omega)$ where k is on the real axis and z is on a suitable deformed contour L^+ . This is obtained by solving the integral equation,

$$t_l(z, k; \omega) = V_l(z, k) + \int_{L^+} \frac{dz' z'^2 V_l(z, z') t_l(z', k)}{\omega - E(z')} \quad (3.75)$$

Here it is seen that for real input energies ω the integral kernel is non-singular since the kinetic energy term $E(z)$ is defined on a deformed contour in the complex k -plane. Having obtained $t_l(z, k; \omega)$ the t -matrix element $t_l(k, k'; \omega)$ is straightforward obtainable by the non-singular integral,

$$t_l(k, k'; \omega) = V_l(k, k') + \int_{L^+} \frac{dz z^2 V_l(k, z) t_l(z, k')}{\omega - E(z)} \quad (3.76)$$

Here k and k' are given along the real k -axis, while z is defined along the deformed integration contour L^+ . This two-step procedure using CDM offers an alternative approach to the numerical solution for the t -matrix. Stable solutions will be obtainable as long as the contour does not pass through any singularities of the potential. Below we consider the solution of the t -matrix for the Malfliet-Tjon potential by CDM and compare results with the standard principal value (PV) prescription. First of all, we have to determine the

singularity structure of the Malfliet-Tjon potential. From equations (3.75,3.68) it is seen that the potential must be defined for one real variable k and one complex variable z given on the contour L^+ . So in conclusion, the contour L^+ must be chosen in such a way that the potential admits analytical continuation from the real k -axis to the complex contour L^+ .

For an illustration we consider two contours C_1 and C_2 . The C_1 contour is just the phase transformation, or complex rotation, $C_1 : |k| \exp(-i\theta)$. The C_2 contour consists of a combination of a rotation and a translation in the complex k -plane⁹. If we integrate along contour C_1 there will always be a singularity on the contour given by

$$z = k_{\max} - i\mu, \quad (3.77)$$

where

$$k_{\max} = \mu / \tan(\theta), \quad (3.78)$$

and $\mu = \min[\mu_A, \mu_B]$ ¹⁰. For $k, k' > k_{\max}$ the contour C_1 will pass through the singularity of the interaction. However, if the interaction, $V_l(k, k')$, is approximately zero for $k, k' > k_{\max}$, or the t -matrix is wanted only in the low momentum regime ($k, k' \ll k_{\max}$), integrating along contour C_1 can be done as long as

$$\theta < \arctan(\mu/k_{\max}). \quad (3.79)$$

In this sense we may call k_{\max} the cutoff momentum. This choice may cause numerical unstable solutions for small values of momenta, since the rotated contour may lie very close to the real k -axis where the integral kernel is singular. The same conclusion has already been pointed out by Nuttal in reference [76].

Here we see the advantage of integrating along contour C_2 . Not only will we be able to reproduce antibound states (see Paper 1), but it yields also accurate results for the t -matrix for real incoming and outgoing momenta. It will always be possible to choose a contour C_2 lying above the nearest singularity $z = \Re[k] - i\mu$, implying no restriction on rotation angle θ irrespective of cutoff momentum k_{\max} . Figure 3.15 gives an illustration.

Figure 3.16 shows a plot of the calculated t -matrix elements $t_l(k, k; E)$ for incoming energy $E = 100$ MeV for the s -wave Malfliet-Tjon interaction, using the contours C_1 and C_2 . In this case we used a rotation angle $\theta = \pi/6$ for both contours, and a translation $b = 300$ MeV for contour C_2 . The Malfliet-Tjon interaction has a singularity along contour C_1 , given by $k_{\max} = \mu / \tan(\theta) = 529.77$ MeV. In this case the interaction is not sufficiently negligible for $k, k' > k_{\max}$, and using contour C_1 will not give an accurate calculation of the t -matrix. This illustrates clearly the advantage of integrating along the contour C_2 instead of C_1 , and the importance of choosing a contour which avoids singularities in the potential.

For a comparison of CDM with the standard PV prescription in solving for the t -matrix numerically we consider the the on-shell unitarity for the S -matrix calculated with both

⁹See Paper 1 for further details. In this particular study natural units are used, i.e. the momentum k is in units of MeV and the potential is in units of MeV^{-2} . In Paper 1 conventional units were used.

¹⁰ μ is here considered as the mass of the pions entering the Yukawa potential; $V(r) = V_0 \exp(-\mu r)/r$

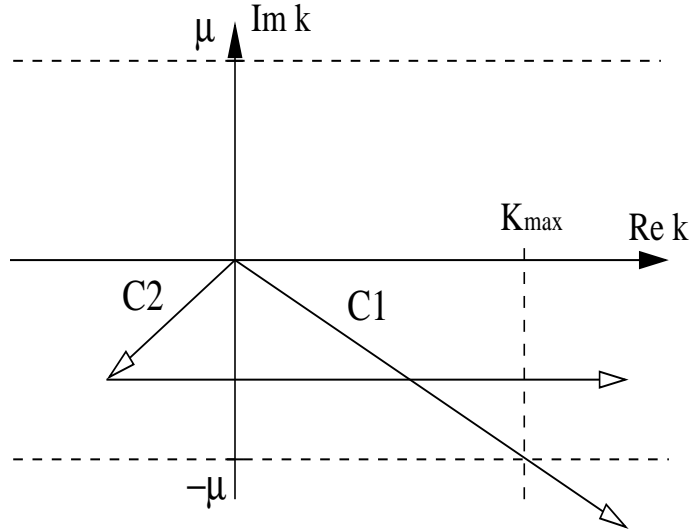


Figure 3.15: Illustration of potential singularities for the Malfliet-Tjon interaction $V_l(k, z)$, where k is real and z complex. Restrictions on the integration contours C_1 and C_2 are clearly seen for given cutoff momentum k_{\max} ($V_l(k, k') \approx 0$ for $k, k' > k_{\max}$).

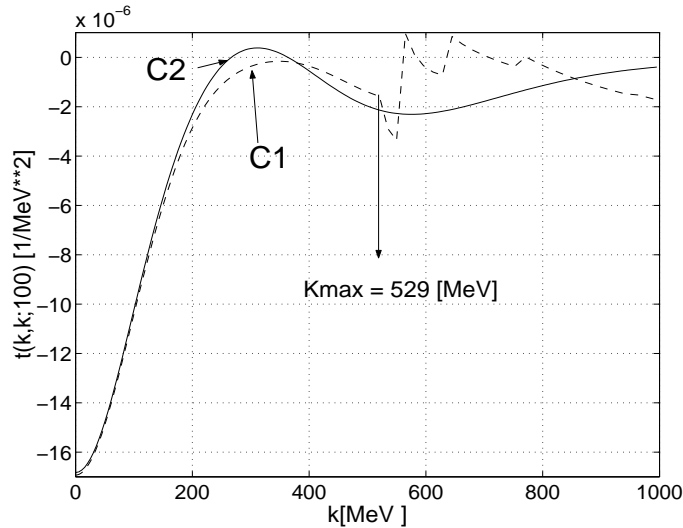


Figure 3.16: Plot of t -matrix elements for the s -wave Malfliet-Tjon interaction using the contour C_1 (dashed line) and the contour C_2 (solid line). The potential singularity along contour C_1 is clearly displayed, and located at $k_{\max} = 529.77$ MeV.

methods. Table 3.4 reports calculations done by the principal value prescription and the contour deformation method C_2 . The calculations used $N = 50$ integration points for the principal value integration, for the contour deformation method we used 30 points along the rotated line and $N_T = 100, 200$ along the translated line. We observe that we need the higher number of integration points along the translated line of C_2 in order to obtain a comparable accuracy with the PV method.

k [MeV]	CDM		
	PV $N = 50$	$N_T = 100$	$N_T = 200$
10.	1.00000000	1.00000811	1.00000811
110.	1.00000000	0.999999940	1.00000000
210.	1.00000000	0.999999940	1.00000000
310.	1.00000000	0.999999881	1.00000000
410.	1.00000000	0.999999881	1.00000000
510.	1.00000000	0.999999881	1.00000000
610.	1.00000000	0.999999881	1.00000000
710.	1.00000000	0.999999821	1.00000000
810.	1.00000000	0.999999821	1.00000000
910.	1.00000000	0.999999821	1.00000000
1010.	1.00000000	0.999999762	1.00000000
1110.	1.00000000	0.999999702	1.00000000
1210.	1.00000000	0.999999702	1.00000000
1310.	1.00000000	0.999999642	1.00000000
1410.	1.00000000	0.999999523	1.00000000
1510.	1.00000000	0.999999642	1.00000000

Table 3.4: Calculations of S -matrix norm, $|S(k)|$, for the s -wave Malfliet-Tjon potential with parameters $V_A = 7.291$ MeV, $\mu_A = 613.69$ MeV, $V_B = -5$ MeV and $\mu_B = 305.86$ MeV. Column 2 gives results for the principal value prescription (PV), while columns 3,4 give results for the contour deformation method (CDM).

3.6 Application of CDM to Resonance-Like Phenomena in nuclear matter.

3.6.1 2p2h Spectral Structures in a Nuclear Medium.

In this section we discuss the application of CDM to nucleon-nucleon scattering in infinite nuclear matter. Of particular interest is the formation and decay of two nucleon bound and resonant states in nuclear matter. In the early 70's Bishop *et. al.* [88, 89] showed that the existence of bound state pairs in a nuclear medium can be directly linked to the singularities of the in-medium t-matrix. The existence of bound pair states in nuclear

medium, is closely related to the concept of *Cooper* pairs. Cooper pairs are considered as the formation of bound electron pairs in a degenerate electron gas, giving rise the phenomenon of *superconductivity*. Treating holes on equal footing with particles, Bishop *et. al.* showed that the pairing effects in nuclear matter were increased when comparing with the standard Bethe-Goldstone approach where only particle propagation is considered, see e.g. reference [90]. Furthermore, in reference [91] it was shown that the BCS gap equation is directly related to the 2p2h bound pair states. Two decades later Dickhoff *et. al.* [92, 93, 94] discussed similar properties of composite pair states in nuclear matter, and formally related the BCS gap equation to the 2p2h (2particle-2hole) self-consistent eigenvalue equation for the bound states. They suggested that strong pairing effects would be present in nuclear matter at certain densities and total momentum, due to the existence of bound pair states.

For a continuous single-particle spectrum these 2p2h bound pair states appear as complex poles of the effective interaction, located around the Fermi energy $2e_f$. These singularities give rise to serious numerical problems when solving the iterated Feynman - Galitskii integral equation for the effective interaction. In reference [94] it was proposed that an introduction of a gap in the single-particle spectrum located at the Fermi surface would resolve this problem. This suggestion was based on the observation that the 2p2h bound state poles become real poles by introducing a gap in the single-particle spectrum at the Fermi surface. If there is no gap in the single-particle energy spectrum, there is no room for the bound states to appear as real excitations, since the hole-hole continuum extends from $-\infty$ to $2e_f$ and the particle-particle continuum extends from $2e_f$ to ∞ . So the 2p and 2h poles appear at complex conjugate energies, $E_{2p} = E_{2h}^*$, around the Fermi energy $2e_f$, this is why the poles of the t -matrix are often called pair-instabilities. By introduction of a minimum gap in the single-particle spectrum this instability will disappear and the poles will position themselves on the real energy axis between $2e_f^+$ and $2e_f^-$. Ultimately this gap at the Fermi surface would be generated self consistently.

The 2p2h bound states are dependent on both the Fermi momentum k_f and the total momentum of the nucleons K . The 2p2h bound states appear only in a specific density region where strong pair correlations are expected, and will eventually dissolve with increasing total momentum of the nucleons. In this case the complete energy spectrum is exposed without analytic continuation of the eigenvalue problem into the complex k -plane. However, with increasing K the 2p2h poles will move towards 2p2h continuum, and one may expect that the 2p2h poles will move into the lower half k -plane (non-physical energy sheet) for K greater than some critical value K_{max} . In close analogy with the free scattering case, these poles may be associated with either virtual or resonant states. In this case CDM may prove to be a reliable and efficient way to calculate these exotic 2p2h states. These 2p2h poles will also appear as singularities in the effective interaction, and may on the same level as the bound state poles cause numerical trouble. One may expect that an introduction of a gap at the Fermi surface will not make these complex poles real poles, since they are located on the non-physical energy sheet. From this observation one may conclude that an introduction of a gap at the Fermi surface does not completely solve the problem associated with pairing instabilities in the iterated effective interaction Γ .

We start by outlining the formalism for 2p2h bound and scattering problems in infinite nuclear matter, and emphasize the relation between the t -matrix and the two-nucleon eigenvalue equation in nuclear matter. Holes and particles are treated on equal footing, hence allowing for hole-hole and particle-particle propagation. Solving for the effective interaction, Γ , the particle - particle and hole - hole ladder diagrams are summed to infinite order. The influence of the surrounding medium is reflected in the Pauli operator and self energy insertions. The two nucleon system is translational invariant, and center of mass motion can be neglected. The ladder summed effective interaction, $\Gamma(\omega)$, is given in operator form

$$\Gamma(\omega) = V + Vg_{II}^{(0)}(\omega)\Gamma(\omega), \quad (3.80)$$

here V is the nucleon-nucleon interaction and $g_{II}^{(0)}(\omega)$ is the non-interacting 2p2h propagator given in terms of a product of two single-particle propagators. The effective interaction can also be given in terms of an interacting 2p2h propagator g_{II} ,

$$\Gamma(\omega) = V + Vg_{II}(\omega)V, \quad (3.81)$$

where $g_{II}(\omega)$ satisfies the Dyson equation

$$g_{II}(\omega) = g_{II}^{(0)}(\omega) + g_{II}^{(0)}(\omega)Vg_{II}(\omega). \quad (3.82)$$

From equation (3.81) it is seen that the singularity structure of the effective interaction $\Gamma(\omega)$ is given in terms of the singularities of the interacting 2p2h propagator $g_{II}(\omega)$. By rewriting equation (3.82) as

$$g_{II}(\omega) = \frac{g_{II}^{(0)}(\omega)}{1 - g_{II}^{(0)}(\omega)V}, \quad (3.83)$$

it is seen that finding the poles of $\Gamma(\omega)$ corresponds to solving the characteristic equation

$$\det \left(1 - g_{II}^{(0)}(\omega)V \right) = 0, \quad (3.84)$$

which is associated with the eigenvalue problem

$$(1 - g_{II}^{(0)}(\omega)V)|\Psi\rangle = 0. \quad (3.85)$$

In the following discussion the propagation of particles and holes is considered with respect to an uncorrelated Fermi sea, which gives the mean field approximation to the 2p2h propagators. In this picture the propagator $g_{II}^{(0)}$ is known as the Feynman - Galitskii [88] propagator, which in turn gives the Feynman - Galitskii integral equation for the effective interaction $\Gamma(\omega)$. In the lab system the Feynman - Galitskii propagator is given by

$$g_{II}^{FG(0)}(p_1, p_2, \omega) = \frac{Q(p_1, p_2)}{\omega - \epsilon(p_1) - \epsilon(p_2)}, \quad (3.86)$$

here $Q = Q_{2p} - Q_{2h}$, the Pauli operator projecting onto the 2p space is given by

$$Q_{2p}(p_1, p_2) = \theta(|\mathbf{p}_1| - k_f)\theta(|\mathbf{p}_2| - k_f), \quad (3.87)$$

and the corresponding 2h projector by

$$Q_{2h}(p_1, p_2) = \theta(k_f - |\mathbf{p}_1|)\theta(k_f - |\mathbf{p}_2|). \quad (3.88)$$

The Pauli operator is an implicit function of the Fermi momentum k_f defining the density of the infinite Fermi sea. The eigenvalue equation (3.85) can now be written

$$\left[H_0 + \begin{pmatrix} Q_{2p} & 0 \\ 0 & -Q_{2h} \end{pmatrix} V \right] \begin{pmatrix} \psi_{2p} \\ \psi_{2h} \end{pmatrix} = E \begin{pmatrix} \psi_{2p} \\ \psi_{2h} \end{pmatrix}, \quad (3.89)$$

here $H_0(p_1, p_2) = \epsilon(p_1) + \epsilon(p_2)$. The single-particle energies ϵ are given by a kinetic energy term and a one-body energy dependent self energy term,

$$\epsilon(p) = \frac{p^2}{2M} + \Sigma(p, \epsilon(p)), \quad (3.90)$$

this gives a self consistent equation for the self energy (Σ).

The normalization and completeness relation for the 2p2h states are given

$$\langle \psi_n | \phi_{n'} \rangle = \delta_{n,n'}, \quad \mathbf{1} = \sum_n |\psi_n\rangle \langle \phi_n|. \quad (3.91)$$

Here the dual states ϕ_{nl} have been introduced. They are solutions of the transposed eigenvalue equation given in equation (3.89), and ϕ_{nl} and ψ_{nl} constitute a bi-orthogonal set of states. The discrete sum is over bound states and in addition the sum implies an integration over the 2p2h continuum. Inserting this complete set of 2p2h states into the Feynman - Galitskii propagator equation (3.82) the spectral representation of the 2p2h interacting propagator is obtained,

$$g_{II}^{FG}(\omega) = \frac{\sum_n |\psi_n\rangle \langle \psi_n|}{\omega - E_n} \quad (3.92)$$

As the nucleon-nucleon interaction is given in relative coordinates it is convenient to transform from the nucleon lab system to relative and center of mass coordinates of the two nucleons,

$$\mathbf{k} = \frac{(\mathbf{p}_1 - \mathbf{p}_2)}{2}, \quad \mathbf{K} = \frac{(\mathbf{p}_1 + \mathbf{p}_2)}{2}. \quad (3.93)$$

Here \mathbf{k} is the relative momentum and $2\mathbf{K}$ the center of momentum of the two interacting nucleons. To allow a partial wave decomposition the standard angle averaged Pauli operator Q and the angle averaged one-body operator \bar{H}_0 are introduced.

A partial wave decomposition of the 2p2h eigenvalue equation (3.89) in relative and center of mass momentum can then be approximated by

$$\bar{H}_0(k, K)\psi_{nl}^\alpha(k, K) + \bar{Q}(k, K; k_f) \int_0^\infty dk' k'^2 V_l(k, k') \psi_{nl}^\alpha(k', K) = E_{nl}^\alpha \psi_{nl}^\alpha(k, K). \quad (3.94)$$

Here α represents the conserved quantum numbers J, S, T while k_f is the Fermi momentum. The normalization integral for the two 2p2h states is

$$\int_0^\infty dk k^2 \psi_{n'l}^*(k, K) \phi_{nl}(k, K) = \delta_{n,n'}, \quad (3.95)$$

where the dual 2p2h states $\phi_{nl}(k, K)$ are given in terms of $\psi_{nl}(k, K)$ by,

$$\phi_{nl}(k, K) = \bar{Q}^{-1}(k, K; k_f) \psi_{nl}(k, K). \quad (3.96)$$

The operator \bar{H}_0 is given by

$$\bar{H}_0 = \frac{k^2}{2\mu} + \frac{K^2}{2\mu} + \bar{\Sigma}_1 + \bar{\Sigma}_2. \quad (3.97)$$

The angle averaged Pauli operator, $\bar{Q} = \bar{Q}_{2p} - \bar{Q}_{2h}$, entering equation (3.94) will in this case depend on both Fermi momentum, k_f , and the momentum K . The hole-hole part \bar{Q}_{2h} for $K < k_f$ is, see reference [95],

$$\bar{Q}_{2h}(k, K; k_f) = \begin{cases} 1 & 0 < k \leq k_a \\ \frac{k_f^2 - K^2 - k^2}{2kK} & k_a < k \leq \sqrt{k_f^2 - K^2} \\ 0 & \text{otherwise,} \end{cases} \quad (3.98)$$

and the particle - particle part, \bar{Q}_{2p} , for $K < k_f$ is

$$\bar{Q}_{2p}(k, K; k_f) = \begin{cases} 0 & 0 < k \leq \sqrt{k_f^2 - K^2} \\ \frac{k^2 + K^2 - k_f^2}{2kK} & \sqrt{k_f^2 - K^2} < k \leq k_b \\ 1 & \text{otherwise,} \end{cases} \quad (3.99)$$

here

$$k_a = k_f - K, \quad k_b = K + k_f. \quad (3.100)$$

In the case $K > k_f$, \bar{Q}_{2h} is zero everywhere. The particle - particle part, \bar{Q}_{2p} , is given by

$$\bar{Q}_{2p}(k, K; k_f) = \begin{cases} 1 & 0 < k \leq k_a \\ \frac{k^2 + K^2 - k_f^2}{2kK} & k_a < k \leq k_b \\ 1 & \text{otherwise,} \end{cases} \quad (3.101)$$

where

$$k_a = K - k_f, \quad k_b = K + k_f. \quad (3.102)$$

Equation (3.94) represents a non-hermitian eigenvalue problem. The general 2p2h energy spectrum will therefore in general be complex. The energy spectrum will depend on both the single-particle energies entering the unperturbed one-body operator \bar{H}_0 and the two nucleon interaction $V_l(k, k')$. For a continuous single-particle spectrum the 2h

continuum extends from $-\infty$ to the Fermi energy $E_f = k_f^2/2m_n$ and the 2p continuum extends from E_f to ∞ . The analytic structure of the integral kernel is the same as for free scattering except for the angle averaged Pauli operator. If we want to search for pole structures on the non-physical energy sheet, an analytical continuation in energy through the branch cut along the real axis, and onto the non-physical energy sheet has to be performed. The Pauli operator is continuous along the whole real k -axis but presents discontinuous derivatives at k_a and k_b . For real k the Pauli operator is therefore analytic only within the domains $k \in [0, k_a]$, $k \in (k_a, k_b]$ and $k \in (k_b, \infty)$. Summarizing; the Pauli operator is nonsingular in the complex k -plane, and analytic within three domains given by $D_1 = |z| \leq k_a$, $D_2 = k_a < |z| \leq k_b$ and $D_3 = |z| > k_b$. Analytical continuation of equation (3.94) onto the non-physical energy sheet (lower half k -plane) can be carried out within each domain where the integral kernel is analytic. Figure 3.17 gives an illustration of regions in the complex plane where the integral kernel is analytic, singularities in the potential are also shown along with a possible choice of deformed integration contour C . The transformed equation (3.94) will on the distorted contour C take the form

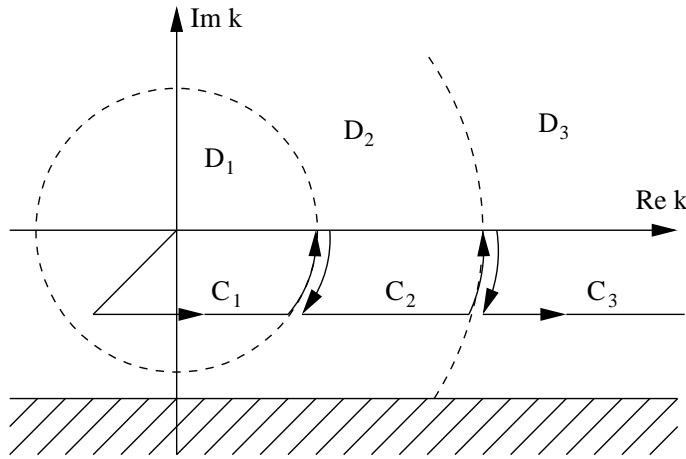


Figure 3.17: D_1 , D_2 and D_3 demarcated by dotted circles define the regions in the complex k -plane where the Pauli operator is analytic. The shaded area represents a region in the complex k -plane where singularities in the potential appear. The optimal deformed contour choice for equation (3.94) is given by $C = C_1 + C_2 + C_3$.

$$\bar{H}_0(k, K)\psi_{nl}^\alpha(k, K) + \bar{Q}(k, K; k_f) \int_C dk' k'^2 V_l(k, k') \psi_{nl}^\alpha(k', K) = E_{nl}^\alpha \psi_{nl}^\alpha(k, K), \quad (3.103)$$

here k and k' are both defined on the contour C , giving a closed integral equation. The Fermi momentum, k_f , and the center of mass momentum, K , are kept real, since equation (3.103) is an integral equation in the relative momentum k only. The normalization of the 2p2h states follow the generalized c -product as described for the free scattering case.

3.6.2 Pair Instabilities for the CD-Bonn interaction.

Here we give a numerical calculation of 2p2h pair states in symmetric nuclear matter using the realistic CD-Bonn [96] nucleon-nucleon interaction. We use a free single-particle spectrum with no gap in the calculations. The 2p2h complex pole trajectories of the virtual states in the 1S_0 channels are considered with increasing Fermi momentum (k_f) and center of mass momentum (K). The 2p2h eigenvalue problem is solved on the contour C consisting of a rotated and a translated part as shown in figure 3.17. The singularity structure of the interaction is the same as for free scattering, the only modification is the angle averaged Pauli operator entering the integral equation ¹¹. Figure 3.18 gives the 1S_0 2p and 2h complex pair states for $K = 0$ MeV and increasing Fermi momentum. Observe that the 2p2h pair states approach the 1S_0 virtual states as $k_f \rightarrow 0$. For $K = 0$ MeV the 2p2h pair states are located in the upper half complex k -plane. In this case integration along the real k -axis will give the complete energy spectrum, see figure 3.18. It is worth noting that the imaginary part of the 2p2h complex energy fits remarkably well with the pairing gap obtained from the BCS gap equation using a free single-particle spectrum, see e.g. reference [97]. This serves to illustrates that the BCS gap equation is an approximate solution of the 2p2h eigenvalue problem as pointed out in reference [92, 93, 94]. Pairing

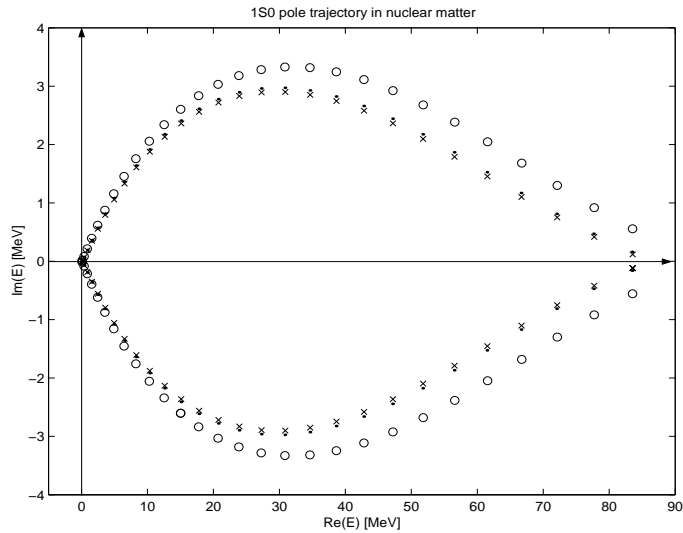


Figure 3.18: 1S_0 2p2h pole trajectory in nuclear matter for $K_{CM} = 0$. Crosses: $t_z = -1$ -channel, dots: $t_z = 1$, circles: $t_z = 0$. $k_f \in [0, 280]$ MeV, $\Delta k_f = 10$ MeV.

correlations may also appear for $K > 0$. Figure 3.19 gives the 1S_0 2p complex pole trajectory for increasing center of mass momentum and fixed Fermi momentum. The complex pole move towards the real energy axis and eventually through the branch cut and onto the non-physical energy sheet with increasing K . Translated to the momentum

¹¹See Paper 1 for a discussion of the singularity structure of the CD-Bonn potential

plane, this implies that the complex pole will move from the upper half k -plane and onto the lower half complex k -plane for a given K_{min} . In the case $K > K_{min}$ the complete 2p2h energy spectrum is no longer obtainable by integrating along the real k -axis. By a suitable choice of contour CDM provides a method for obtaining the complete 2p2h energy spectrum for any $K > K_{min}$. Figure 3.20 gives a sketch of the 1S_0 2p2h pole trajectories

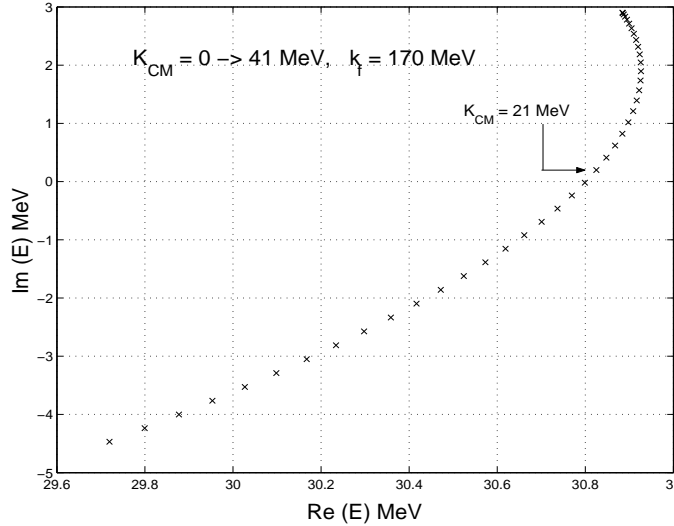


Figure 3.19: Calculated 2p pole trajectory for maximum pairing instability $k_f = 170$ MeV in the 1S_0 neutron - neutron isospin channel as function of K_{CM} . A rotated + translated contour was used in order to obtain the energy spectrum.

in nuclear matter. First K is held fixed and equal $K = 0$ and the Fermi momentum is varied. The 2p and 2h poles will move symmetrically to the imaginary axis in the upper half complex k -plane. Thereafter the Fermi momentum is held fixed and K varied, $K > 0$. In this case the 2p and 2h poles will move towards the real k -axis and for a given K into the lower half complex k -plane.

3.6.3 Calculation of Γ by CDM for the CD-Bonn Nucleon-Nucleon Interaction.

In this section we will discuss a method for solving the full off-shell vertex function (effective interaction), Γ , in a nuclear medium. This method is based on analytic continuation of the integral equations and expansion of the Green's function on a complete set of Berggren states. This is known as the Lehmann representation of the effective interaction Γ .

For two nucleons in free space the vertex function reduces to the t -matrix, and hence the free full two-body scattering problem. In free space the t -matrix can be interpreted as an effective interaction between two nucleons. In a scattering process the t -matrix includes repeated two body interactions to infinite order, i.e. a summation of all ladder diagrams

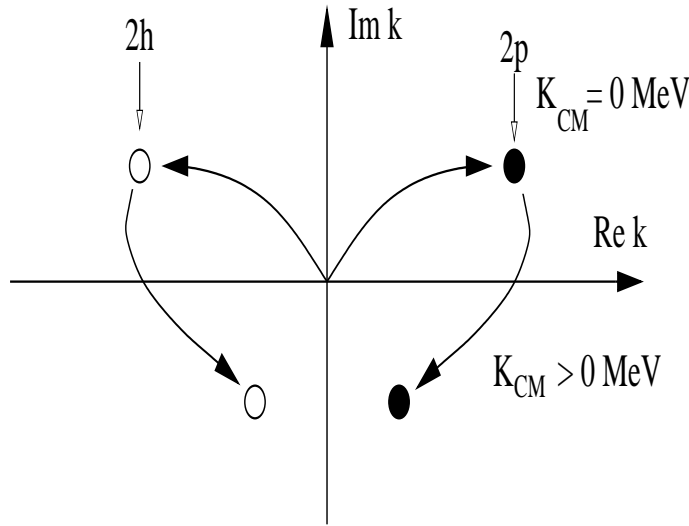


Figure 3.20: Trajectory of 2p2h complex poles (pair instabilities) in nuclear matter for increasing Fermi momentum, k_f , and $K_{CM} = 0$ MeV. The figure also gives the trajectory for increasing center of mass momentum K_{CM} , and k_f held fixed.

to infinite order. In analogue to the free scattering case, we will consider only repeated interactions between either hole or particle states in the medium, giving the 2p2h ladder summed vertex function, Γ .

The integral equation (3.80) for the effective interaction may be written in relative and center of momentum coordinates by

$$\Gamma_l(k, k'; \omega) = V_l(k, k') + \int_0^\infty dq q^2 V_l(k, q) g_{II}^{FG(0)}(q, \omega) \Gamma_l(q, k'; \omega), \quad (3.104)$$

where we introduce the shorthand notation $\Gamma_l(k, k'; \omega) = \Gamma_l(k, k', K, k_f; \omega)$. The non-interacting 2p2h propagator is given,

$$g_{II}^{FG(0)}(k, \omega) = \frac{\bar{Q}(k, K; k_f)}{\omega - H_0(k, K)}. \quad (3.105)$$

In the case of free scattering $Q = 1$, and equation (3.104) reduces to the Lippmann-Schwinger equation for the t -matrix given in equation (3.72). The spectral representation of the effective interaction takes the following form in RCM coordinates

$$\Gamma_l(k, k'; \omega) = V_l(k, k') + \int_0^\infty dq q^2 \int_0^\infty dq' q'^2 V_l(k, q) g_{II}^{FG}(q, q'; \omega) V_l(q', k'), \quad (3.106)$$

where the interacting 2p2h propagator is given by equation (3.92). We will consider the solution of Equation (3.106) for the effective interaction by CDM. Using the completeness relation defined on a distorted contour C , shown in figure 3.17, gives the Berggren

representation of the effective interaction in a nuclear medium,

$$\Gamma_l(k, k'; \omega) = V_l(k, k') + \int_C dz z^2 \int_C dz' z'^2 V_l(k, z) g_{II}^{FG}(z, z'; \omega) V_l(z', k'), \quad (3.107)$$

here the interacting 2p2h propagator are represented in the 2p2h basis obtained by solving the eigenvalue problem in equation (3.103).

By applying CDM and the spectral representation of the effective interaction, we are able to single out the bound and resonant state contribution from the non-resonant 2p2h continuum contribution to the full effective interaction. The effective interaction may be written in the form,

$$\Gamma(\omega) = V + \Delta\Gamma(\omega) = V + \Delta\Gamma^R(\omega) + \Delta\Gamma^C(\omega),$$

here R denotes the discrete bound and resonant states, C denotes the non-resonant continuum contributions. In this way we may study the resonant, $\Delta\Gamma^R$, and non-resonant contributions, $\Delta\Gamma^C$, to the effective interaction separately. In figure 3.21 the effective interaction Γ for the input energy $\omega = (k^2 + K^2)/2m_n$, center of momentum $K = 30\text{MeV}$ and Fermi momentum $k_f = 170\text{MeV}$ is given for the 1S_0 neutron-neutron channel in the CD-Bonn interaction. A sharp peak is observed around the Fermi surface, indicating the existence of bound pair states. In figure 3.22 the non-resonant continuum contribution to the effective interaction is plotted, and it is seen that the peak around the Fermi surface has disappeared. The discontinuities jumps in the non-resonant contribution is due to the analytic structure of the angle averaged Pauli operator given in equations (3.98,3.99, 3.101). In figure 3.23 the resonant contribution to the effective interaction is given. The resonant contribution displays a sharp peak around the Fermi surface, while the resonant contributions are negligible moving away from the Fermi surface.

In conclusion, CDM will enable us to obtain $\Gamma_l(k, k', K; \omega)$ for both real and complex input energies ω . The integral becomes non-singular on the deformed contour for real input energies ω , resulting in numerically stable solutions for two-body scattering in both free space and in a uniform medium. In this perspective, CDM offers an alternative approach to the standard PV prescription in solving for the effective interaction, and offers a valuable tool in describing different contributions to the effective interaction.

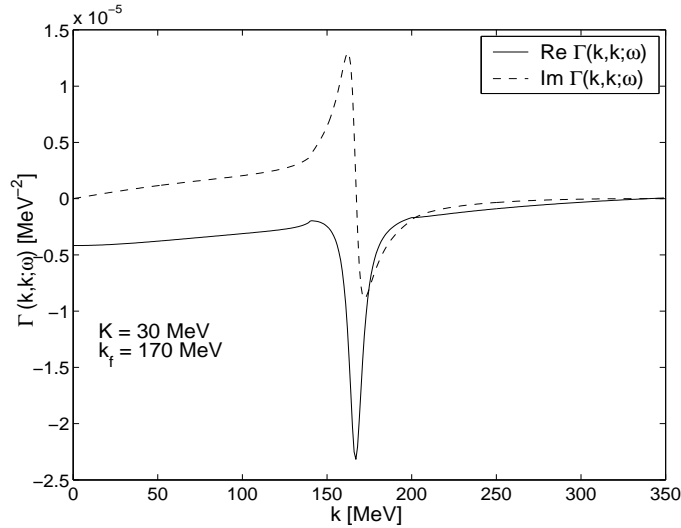


Figure 3.21: Effective interaction $\Gamma(k, k; \omega = (k^2 + K^2)/2m_n)$ for $K = 30$ MeV and $k_f = 170$ MeV for 1S_0 neutron-neutron channel in the CD-Bonn interaction. The peak around the Fermi surface $k \approx 170$ MeV indicates the formation of a pairing instability.

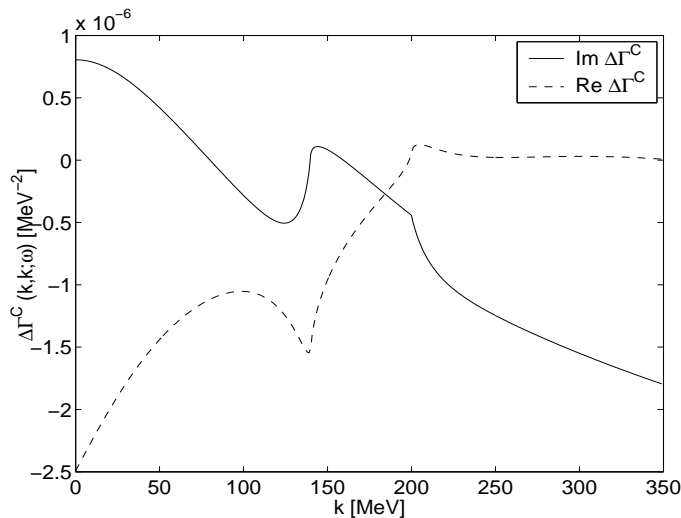


Figure 3.22: Continuum part of effective interaction $\Delta\Gamma(k, k; \omega = (k^2 + K^2)/2m_n)$ for $K = 30$ MeV and $k_f = 170$ MeV for 1S_0 neutron-neutron channel in the CD-Bonn interaction. The peak around $k \approx 170$ MeV has been washed out.

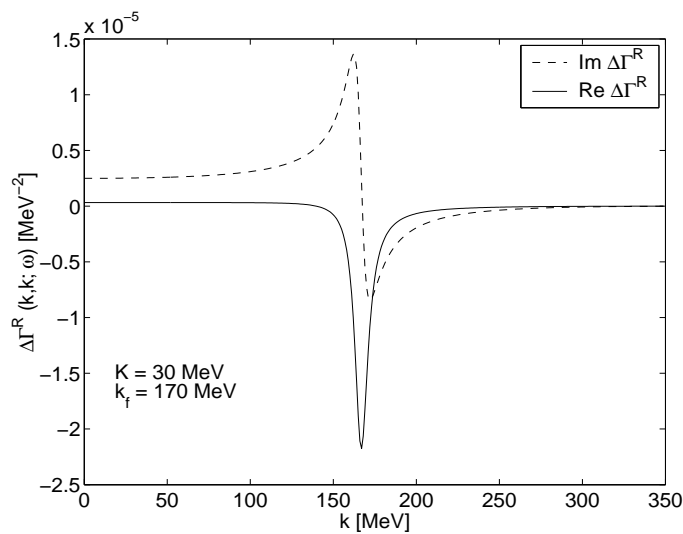


Figure 3.23: Resonant part of effective interaction $\Delta\Gamma(k, k; \omega = (k^2 + K^2)/2m_n)$ for $K = 30$ MeV and $k_f = 170$ MeV for 1S_0 neutron-neutron channel in the CD-Bonn interaction. The resonant part of Γ has is clearly non-negligible around the Fermi surface $k \approx 170$ MeV.

Chapter 4

Effective Interactions and Many-Body Theory for Unstable Nuclei.

4.1 The Gamow Shell Model.

The standard nuclear Shell Model often starts with a harmonic oscillator representation for the single-particle states. Since the harmonic oscillator potential is an infinite potential, the tails in single-particle wave functions fall off too rapidly to describe realistically single-particle motion near the scattering continuum. The harmonic oscillator may therefore be said to work only for deeply bound nucleons. In order for the nuclear Shell Model to be applicable to nuclei far from the valley of stability, the harmonic oscillator picture of single-particle motion has to be abandoned. The proximity of the scattering continuum in loosely bound and unbound nuclei, necessitates a modification and reformulation of the standard nuclear Shell Model.

In the previous sections, it was shown how a single-particle basis consisting of bound, anti-bound and resonant states may be constructed using the Contour Deformation Method in momentum space. Solving the momentum space integral equation on a discretized contour in the complex k -plane a complex symmetric eigenvalue problem for the single-particle states were obtained, from which a complete set of *bi-orthogonal* states follows. Since the basis is discretized on a deformed contour it is possible to assign a unique quantum number to each single-particle state. In the case of harmonic oscillator states we have the usual notation for the quantum numbers (n, l, j) where n is nodal number and (lj) the orbital- and total angular momentum of the single-particle state. In the general case where bound, anti-bound, resonances and non-resonant continuum states are treated on equal footing, the meaning of the quantum number n has to be redefined and clarified. Since all single-particle states have a discrete energy associated with them, it is natural to let n refer to the n 'th discrete energy E_n . Defining n in this manner, all single-particle states have a unique set of quantum numbers n, l, j . figure 4.1 illustrates how N single-particle

Berggren orbitals for a given (lj) partial wave, obtained by solving the momentum space Schrödinger equation on a discretized contour in the complex k -plane, may be organized in an ordered way. The non-resonant continuum orbitals are distinguished from the discrete bound- and resonant orbitals. Having constructed a single-particle Berggren basis, a many-

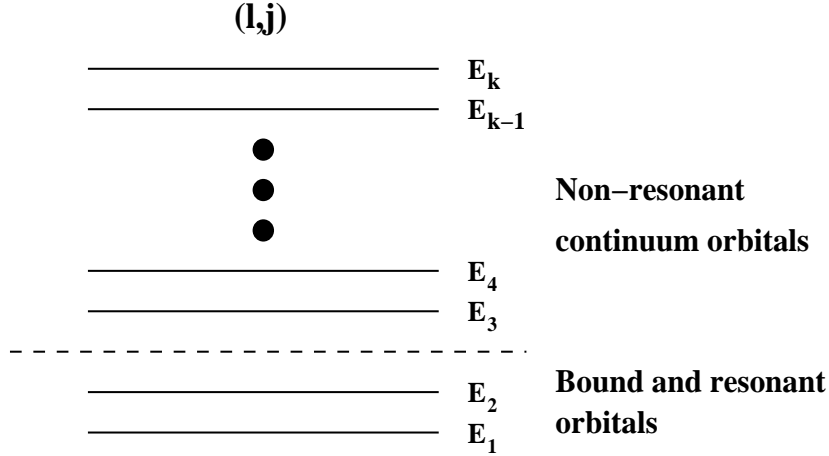


Figure 4.1: Illustration of how the bound, resonant and non-resonant continuum orbitals for a given (lj) single-particle configuration may be organized in an ordered way.

body Berggren basis may be constructed in a completely analogous way as when harmonic oscillator states are used. We construct a complete anti-symmetric N -body basis from the Slater determinants consisting of the Berggren orbitals φ_{nljm} i.e.

$$\Phi_{\alpha_1, \dots, \alpha_N}(1, \dots, N) = \frac{1}{\sqrt{N!}} \begin{vmatrix} \varphi_{\alpha_1}(1) & \dots & \varphi_{\alpha_1}(N) \\ \vdots & & \vdots \\ \varphi_{\alpha_N}(1) & \dots & \varphi_{\alpha_N}(N) \end{vmatrix}, \quad (4.1)$$

where α_i labels the single-particle quantum numbers $(n_i l_i j_i m_i)$. The Slater determinants have eigenvalues $E_i = \varepsilon_{\alpha_1} + \dots + \varepsilon_{\alpha_N}$, which is just the sum of all single-particle energies. Herethe label i subsumes all the different single-particle quantum numbers $\varepsilon_{\alpha_1} + \dots + \varepsilon_{\alpha_N}$. We then have at hand a complete set of Slater determinants, i.e.

$$1 = \sum_i^d |\Phi_i\rangle \langle \Phi_i^*|, \quad (4.2)$$

which the exact many-body wave function may be expanded in. The Shell Model problem then requires the solution of a complex symmetric $N \times N$ matrix eigenvalue equation,

$$H|\Psi_i\rangle = E_i|\Psi_i\rangle, \quad (4.3)$$

with $i = 1, \dots, d$. Representing the Shell Model states in a complete set of Slater determinants, built from the single-particle orbitals with quantum numbers $(nljm)$, is commonly

known as the m -scheme representation. The Slater determinants are antisymmetric and have definite values of the total angular momentum projection $M_J = m_1 + m_2 + \dots + m_n$ and total isospin projection $M_T = \tau_1 + \tau_2 + \dots + \tau_n$, but they are not states with good quantum number of total angular momentum J and isospin T . In standard large-scale Shell Model calculations, using the the m -scheme representation, one is typically interested in the first few low lying energy states. The Lanczos algorithm [98] is an iterative method which has proven to be efficient in solving for a limited set of eigenvalues of large real symmetric matrices.

In the Gamow Shell Model case, the m -scheme and the standard Lanczos iteration technique for solving large eigenvalue problems for real symmetric matrices are not optimal approaches. Firstly, the m -scheme representation of the Shell Model equations does not automatically split the full Shell Model matrix into smaller sub-matrices for different values of the total J and T . In standard Shell Model calculations only bound states appear, whereas in Gamow Shell Model, not only bound states but a rather large set of continuum states are included for each lj configuration. In an m -scheme representation, the dimension of the matrix will, in the Gamow Shell Model case, in most cases be too large to handle numerically. On the other hand, one may construct a many-body basis coupled to definite total J and T , either by the $j - j$ or the $L - S$ coupling scheme. Thereafter the Shell Model equations for a given value of angular momentum and isospin may be diagonalized separately. The dimension of each J, T matrix will then be considerably smaller than the full matrix represented in the m -scheme.

Secondly, the Lanczos iteration method has usually been used for calculation of a set of eigenvalues lowest in real energy. In Gamow Shell Model calculations there may however, be a large number of complex continuum states lying below the physical resonances in real energy. In addition it is difficult to predict where the multi-particle resonances will appear after diagonalization. Direct diganalization procedures has to be abandoned, since the matrices with increasing number of valence particles soon become too large to store and handle on most modern computers. However, as will be shown in the next section, the Lanczos iteration technique may be generalized to complex symmetric matrices. Choosing a reasonable initial Lanczos vector for the multi-particle resonance, it will be demonstrated that the Lanczos iteration procedure gives accurate and converged results for the multi-particle resonance with a fairly small number of iterations.

Choosing to work with Slater determinants coupled to definite J , the N -body anti-symmetric wave function can be constructed viz.,

$$\Psi_{\alpha}^{JM}(1, \dots, N) = \sum_i^d C_i^{JM} \Phi_i^{JM}(1, \dots, N), \quad (4.4)$$

where the indices i represent the various single-particle orbits. Here $\Phi_i^J(1, \dots, N)$ is a normalized N -body anti-symmetric wave function. The Shell Model equation we have to solve is then given by

$$H|\Psi_i^J\rangle = E_i^J|\Psi_i^J\rangle, \quad (4.5)$$

In our Gamow Shell Model studies of ${}^6\text{-}{}^7\text{He}$ in Paper 2, we worked within the $j-j$ coupling scheme. See Appendix B for the derivation of three-body matrix elements in $j-j$ coupling. Table 4.1 gives the various dimensions for the Shell Model matrices with definite angular momentum and parity J^π for the different ${}^{5\text{-}7}\text{He}$ isotopes considered in Paper 2. It is seen that with a valence space of 24 $p_{1/2}$ and 24 $p_{3/2}$ single-particle orbitals, the dimension grows extremely fast with increasing number of valence particles. Even in the case of three valence particles the dimension is too large for direct diagonalization procedures. This problem of the dimensionality of the Gamow Shell Model equations is what we call the *dimensionality problem*. In order to be able to solve for the eigenvalue spectrum of such

${}^5\text{He}$		${}^6\text{He}$		${}^7\text{He}$	
J^π	N	J^π	N	J^π	N
$1/2^-$	24	0^+	600	$1/2^-$	29648
$3/2^-$	24	1^+	1128	$3/2^-$	38896
		2^+	876	$5/2^-$	27072

Table 4.1: Dimension of the Shell Model matrices with definite angular momentum and parity J^π for the ${}^{5\text{-}7}\text{He}$ isotopes.

large complex matrices, effective interaction techniques and matrix perturbation theory generalized for complex symmetric matrices have to be developed and studied. This is the topic of the next sections.

4.2 Lanczos Iteration Scheme for Many-Body Resonances.

The Lanczos iteration technique for finding a limited set of eigenvalues and eigenvectors for large real matrices, has over the years been the dominating approach in solving large-scale Shell Model equations. The method may easily be generalized to apply for complex matrices. This suggest that the method may be a suitable approach for dealing with large complex symmetric matrices which appear in Gamow Shell Model studies. However, we need a reliable prescription for identifying which state is to be associated with the physical multi-particle resonance from the set of eigenvectors obtained from diagonalizing the Lanczos matrix. Below we shall show how such a prescription may be defined. As a test case we consider the bound and resonant spectra of ${}^6\text{He}$, using a Shell Model picture with two valence neutrons moving in $p_{3/2}$ Berggren orbitals outside a ${}^4\text{He}$ core. We use 24 single discretization points for the contour in generating the $p_{3/2}$ single-particle basis of ${}^5\text{He}$. See Paper 2 for further details on the contour, the ${}^4\text{He}$ - n interaction potential and on the residual nucleon-nucleon interaction for the two valence nucleons.

For the Lanczos iteration scheme to converge rapidly, the choice of a 0th order approximation to the multi-particle resonance should resemble the exact multi-particle resonance

as much as possible. Constructing a reasonable starting vector for the Lanczos iteration procedure, is what we have to consider first. Having constructed a complete many-body basis from the single-particle Berggren orbitals, the many-body space may be partitioned into a model space P and an orthogonal complement space Q by some selection procedure. The Shell Model Hamiltonian may then subsequently be divided into two parts,

$$H = \begin{pmatrix} PHP & PHQ \\ QHP & QHQ \end{pmatrix} = \begin{pmatrix} H^{PP} & 0 \\ 0 & 0 \end{pmatrix} + \begin{pmatrix} 0 & H^{PQ} \\ H^{QP} & H^{QQ} \end{pmatrix}. \quad (4.6)$$

The model space P should be constructed in such a way that the most important many-body configurations of the many-body resonance wave function are included in this restricted space. Furthermore, the dimension N_P of the model space P should be small enough so that a full diagonalization of H^{PP} is possible. The 0th order Lanczos vector $|\text{lanc}_0\rangle$, which is the 0th order approximation to the exact wave function, is then obtained by diagonalizing the $N_P \times N_P$ model space matrix H^{PP} . In choosing the model space P it is natural to assume that the most important configurations are those in which all or several particles are in single-particle resonance orbitals. The Q -space consists then of the remaining configurations. In the ${}^6\text{He}$ test case we consider two different model spaces $P = P_1, P_2$. In the first case we let P be given by a single Slater determinant, where both neutrons are in the $p_{3/2}$ single-particle resonance orbital, i.e. $P_1 = |RR\rangle$. In this case the 0th order Lanczos vector is just a single Slater determinant,

$$|\text{lanc}_0\rangle = |\Phi_i^J\rangle = |RR\rangle. \quad (4.7)$$

In the second choice we construct P from all Slater determinants where at least one neutron is in the $p_{3/2}$ single-particle resonance orbital, i.e.

$$P_2 \equiv \{|RR\rangle, |RC\rangle\}, \quad (4.8)$$

and the corresponding model space dimension is $N_{P_2} = 24$. In this case the 0th order Lanczos vector is a linear combination of Slater determinants,

$$|\text{lanc}_0\rangle = \sum_{i=1}^{N_{P_2}} C_{i,j} |\Phi_i^J\rangle. \quad (4.9)$$

Here C is a $N_{P_2} \times N_{P_2}$ orthogonal matrix which diagonalizes H^{PP} . The orthogonal columns j of C have been normalized so that $|\text{lanc}_0\rangle$ is normalized to unity. For each Slater determinant $|\Phi_i\rangle$, $i = 1, \dots, N_{P_2}$ a corresponding amplitude $C_{i,j}$ is assigned. As the diagonalization of the model space matrix H^{PP} gives N_{P_2} possible choices for the 0th order Lanczos vector, we have to determine from this set which is the 0th order approximation to the exact two-particle resonance wave function. This may be done by considering each column j of the matrix C , and determine which of these columns have the largest amplitude $C_{i,j}$ for the Slater determinant where all particles are in single-particle resonance orbitals.

The Lanczos iteration procedure may be summarized by the following steps,

1. Choose an initial Lanczos vector $|\text{lanc}_0\rangle$ (a linear combination of Slater determinants) as the 0th order approximation to the exact multi-particle resonance wave function. See discussion above, on how to choose this starting vector for Gamow Shell Model applications.
2. The next step involves generating a new vector $|\text{new}_{p+1}\rangle$ by letting the full Hamiltonian H act on the p 'th Lanczos vector $|\text{lanc}_p\rangle$, i.e. $|\text{new}_{p+1}\rangle = H|\text{lanc}_p\rangle$. Throughout this process we construct the energy matrix elements of H in this Lanczos basis. The diagonal matrix elements of H are then obtained by

$$\langle \text{lanc}_p^* | H | \text{lanc}_p \rangle = \langle \text{lanc}_p^* | \text{new}_{p+1} \rangle. \quad (4.10)$$

3. The new vector $|\text{new}_{p+1}\rangle$ is then orthogonalized to all previously calculated Lanczos vectors by the Gram-Schmidt procedure

$$|\text{new}'_{p+1}\rangle = |\text{new}_{p+1}\rangle - \sum_{q=0}^p |\text{lanc}_q\rangle \langle \text{lanc}_q^* | \text{new}_{p+1} \rangle, \quad (4.11)$$

and normalized

$$|\text{lanc}_{p+1}\rangle = \frac{1}{\sqrt{\langle \text{new}'_{p+1}^* | \text{new}'_{p+1} \rangle}} |\text{new}'_{p+1}\rangle, \quad (4.12)$$

to give a new normalized Lanczos vector.

4. The off-diagonal matrix elements of H is then obtained by

$$\langle \text{lanc}_{p+1}^* | H | \text{lanc}_p \rangle = \langle \text{lanc}_{p+1}^* | \text{new}'_{p+1} \rangle, \quad (4.13)$$

and all other matrix elements are zero.

5. After p iterations we have an energy matrix of tridiagonal form

$$\begin{bmatrix} H_{0,0} & H_{0,1} & 0 & \dots & 0 \\ H_{1,0} & H_{1,1} & H_{1,2} & \dots & 0 \\ 0 & H_{2,1} & H_{2,2} & \dots & 0 \\ \vdots & \vdots & \vdots & \vdots & H_{p-1,p} \\ 0 & 0 & 0 & H_{p,p-1} & H_{p,p} \end{bmatrix}, \quad (4.14)$$

as the p 'th approximation to the full eigenvalue problem. The number p is a reasonably small number so the matrix can be diagonalized by standard diagonalization routines for sparse matrices of tridiagonal form, to obtain eigenvalues and eigenvectors which are linear combinations of the Lanczos vectors.

6. This process is repeated until a suitable convergence criterion has been reached.

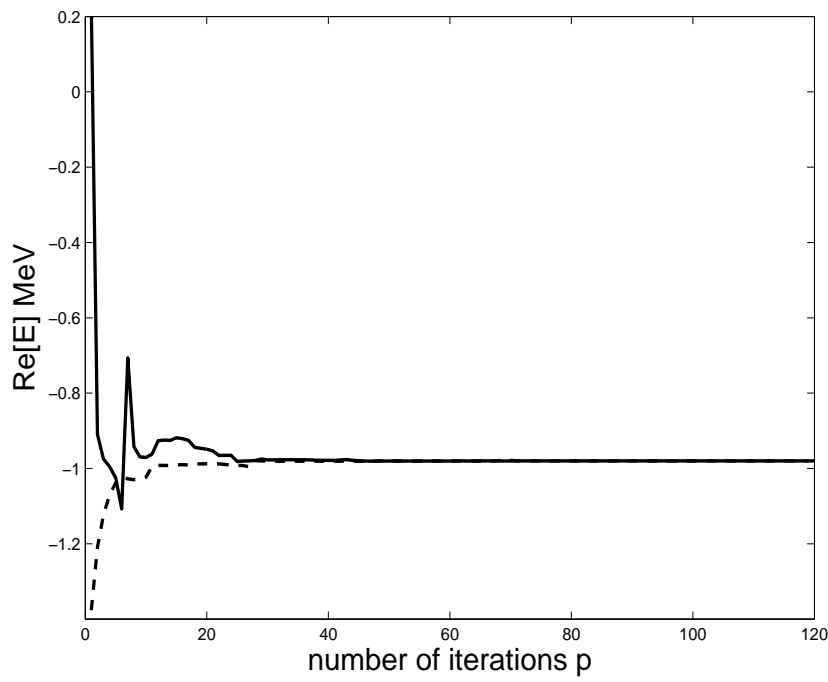


Figure 4.2: Convergence of the real part of the 0^+ ground state energy of ${}^6\text{He}$.

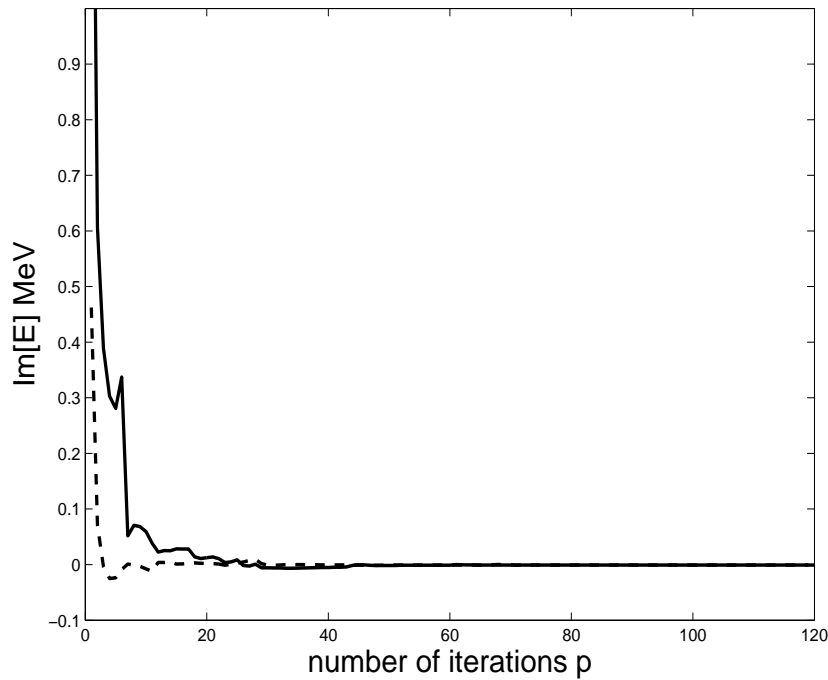


Figure 4.3: Convergence of the imaginary part of the 0^+ ground state energy of ${}^6\text{He}$.

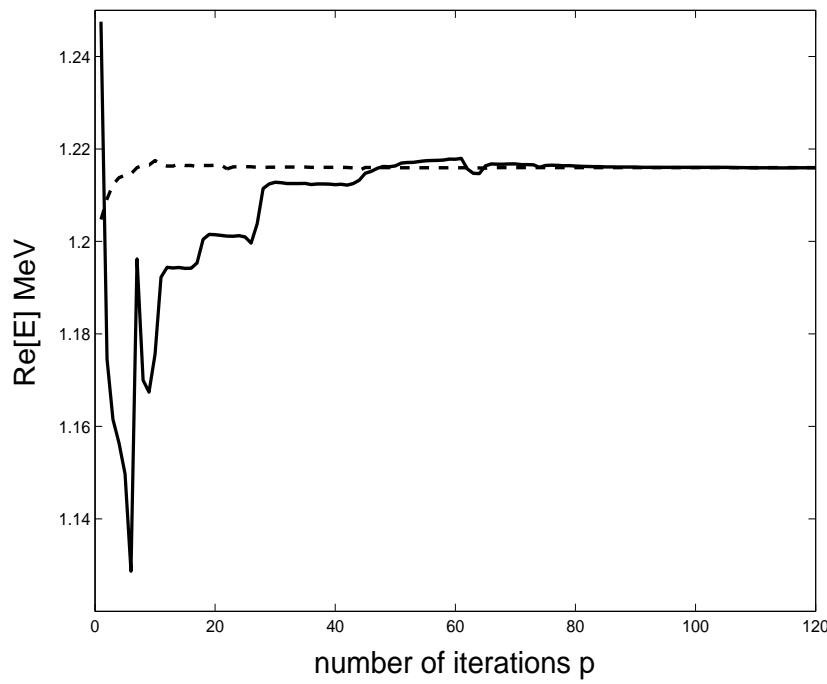


Figure 4.4: Convergence of the real part of the 2^+ resonance energy of ${}^6\text{He}$.

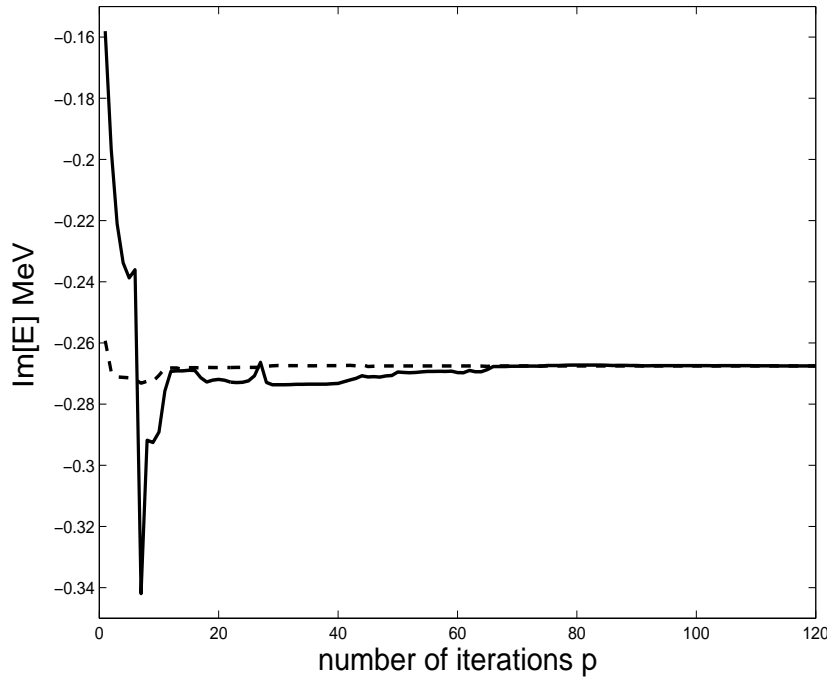


Figure 4.5: Convergence of the imaginary part of the 2^+ resonance energy of ${}^6\text{He}$.

Having determined a converged Lanczos energy matrix, the remaining problem is how to determine which of the states $|\Psi_i(p)\rangle$, $i = 1, \dots, p$ gives the p 'th approximation to the exact multi-particle resonance. This identification may be done unambiguously by determining which state $|\Psi_i(p)\rangle$, $i = 1, \dots, p$ has the largest overlap with the initial Lanczos vector $|lanc_0\rangle$, which is the 0th order approximation to the exact multi-particle resonance.

Figures 4.2 and 4.3 gives the approximate real and imaginary parts of the 0^+ ground state of ${}^6\text{He}$ obtained after p iterations, using the starting vector given in equation (4.7) (solid line) and the starting vector given in equation (4.9) (dashed line). It is seen that both for the real and imaginary parts of the energy, the convergence is faster for the initial Lanczos vector given in equation (4.9) compared with the convergence using the initial vector in equation (4.7). However, it is interesting to see that both choices converge to the exact ground state energy $E(0^+) = -0.98 + 0.00i\text{MeV}$ within the number of iterations p considered. Figures 4.4 and 4.5 give the approximate real and imaginary parts of the 2^+ resonant state of ${}^6\text{He}$ obtained after p iterations, using the starting vector given in equation (4.7) (solid line) and the starting vector given in equation (4.9) (dashed line). Also in this case convergence is faster using equation (4.9) for an initial Lanczos vector. Both choices converge to the exact two-particle resonance energy $E(2^+) = 1.216 - 0.268i\text{MeV}$ for a reasonable small number of iterations p . This test study of the Lanczos iteration procedure applied to Gamow Shell Model studies, is very promising. Both resonances and bound states are reproduced with a small number of iterations, given a reasonable choice for a 0th order approximation to the two-particle resonance wave function.

4.3 Similarity Transformations and Effective Operators for Complex Interactions.

The previous section served to introduce and motivate the application of complex scaling and a Berggren basis in studies of weakly bound nuclear systems. However, employing such a momentum space basis soon exceeds feasible dimensionalities in shell-model studies. To circumvent this problem and to be able to define effective interactions of practical use in shell-model calculations, we introduce effective two-body interactions based on similarity transformation methods. These interactions are in turn employed in Gamow Shell Model calculations. We base our approach on the extensive works of Suzuki, Okamoto, Lee and collaborators, see for example references [99, 100, 101, 102]. This similarity transformation method has been widely used in the construction of effective two- and three-body interactions for use in the No-Core Shell Model approach of Barrett, Navratil, Vary and collaborators, see for example references [38, 39, 40, 41] and references therein. However, since the similarity transformation method has previously only been considered for real interactions, we need to extend its use to Gamow Shell Model calculations, implying a generalization to complex interactions.

We start with the abstract formulation of the Schrödinger equation,

$$(H_0 + V) |\Psi_k\rangle = E_k |\Psi_k\rangle, \quad (4.15)$$

here H_0 includes the single-particle part of the Hamiltonian, kinetic energy and an eventual single-particle potential. The term V is the residual two-body interaction. The Hamiltonian, $H = H_0 + V$, is here a complex symmetric matrix, i.e. $H = H^T$ ¹, since the equations are analytically continued to the complex k -plane, and the eigenvalue problem is no longer Hermitian. The eigenvectors form a complete *bi-orthogonal* set, and are normalized according to the *bi-linear* form,

$$\langle \tilde{\Psi}_k | \Psi_{k'} \rangle = \langle \Psi_k^* | \Psi_{k'} \rangle = \delta_{k,k'}.$$

Here the left eigenvector $\langle \tilde{\Psi}_k |$ is just the transpose of the right eigenvector $|\Psi_k\rangle$, which follows from the fact that the Hamiltonian is complex symmetric (see Appendix A for details).² The Hilbert space is now divided in two subspaces, i.e. a model space and a complement space. The operators which project onto the model space and onto its complement space are labeled P and Q , respectively. The projection operators fulfill the relations

$$P^2 = P, \quad Q^2 = Q, \quad P^T = P, \quad (4.16)$$

and

$$Q^T = Q, \quad P + Q = 1, \quad PQ = 0. \quad (4.17)$$

¹Here H^T means the transpose of H .

²In the following we will use the notation for the bi-orthogonal states $\langle \tilde{\Psi}_k | = \langle \Psi_k^* |$ which are the left eigenvectors of a complex symmetric matrix. This is for distinguishing them from the bi-orthogonal states $\langle \tilde{\phi}_k |$ which are left eigenvectors of non-symmetric matrices, for which it follows that $\langle \tilde{\phi}_k | \neq \langle \phi_k^* |$. See appendix A.

The projection operators are typically chosen to be the eigenprojectors of the one-body operator H_0 , i.e. they are constructed from the basis which diagonalizes H_0 ,

$$\langle \alpha^* | H_0 | \alpha' \rangle = \varepsilon_\alpha \delta_{\alpha,\alpha'}, \quad (4.18)$$

from which they have the explicit form,

$$P = \sum_{\alpha_P} |\alpha_P\rangle\langle\alpha_P^*|, \quad Q = \sum_{\alpha_Q} |\alpha_Q\rangle\langle\alpha_Q^*. \quad (4.19)$$

From this particular choice it follows,

$$\begin{aligned} [H_0, P] &= [H_0, Q] = 0, \\ QH_0P &= PH_0Q = 0. \end{aligned} \quad (4.20)$$

The aim is to construct an effective Hamiltonian within the P -space, for which every eigenvalue of the effective Hamiltonian corresponds to one of the exact eigenvalues of full Hamiltonian H . This can be accomplished by a similarity transformation of the full Hamiltonian,

$$\tilde{H} = X^{-1}HX, \quad |\Phi_k\rangle = X^{-1}|\Psi_k\rangle. \quad (4.21)$$

Representing the Schrödinger equation in the basis of the one-body operator H_0 , it can be rewritten in the 2×2 block structure,

$$\begin{pmatrix} P\tilde{H}P & P\tilde{H}Q \\ Q\tilde{H}P & Q\tilde{H}Q \end{pmatrix} \begin{pmatrix} P\Phi_k \\ Q\Phi_k \end{pmatrix} = E_k \begin{pmatrix} P\Phi_k \\ Q\Phi_k \end{pmatrix}, \quad (4.22)$$

which gives the equations,

$$P\tilde{H}P|\Phi_k\rangle + P\tilde{H}Q|\Phi_k\rangle = E_kP|\Phi_k\rangle \quad (4.23)$$

$$Q\tilde{H}P|\Phi_k\rangle + Q\tilde{H}Q|\Phi_k\rangle = E_kQ|\Phi_k\rangle. \quad (4.24)$$

Where we have used $P^2 = P$ and $Q^2 = Q$. Solving equation (4.24) for $Q|\Phi_k\rangle$, and inserting into equation (4.23), yields an effective eigenvalue problem in the P -space,

$$\left(P\tilde{H}P + P\tilde{H}Q \frac{1}{E_k - Q\tilde{H}Q} Q\tilde{H}P \right) P|\Phi_k\rangle = E_kP|\Phi_k\rangle. \quad (4.25)$$

This effective Hamiltonian depends on the exact eigenvalue E_k of the full problem. However, if a similarity transformation matrix X is chosen such that the decoupling equation,

$$Q\tilde{H}P = Q(X^{-1}HX)P = 0, \quad (4.26)$$

is satisfied, then we end up with an effective Hamiltonian in the P -space which is energy independent, i.e.

$$\left(P\tilde{H}P \right) P|\Phi_k\rangle = E_kP|\Phi_k\rangle. \quad (4.27)$$

There are infinitely many different transformations X which decouple the P - and Q -spaces, see e.g. references [103, 104]. Here we choose the Lee-Suzuki (LS) similarity transformation, see reference [99]. The LS transformation is the simplest transformation, and given by,

$$X = \exp(\omega) \quad (4.28)$$

$$\Rightarrow \tilde{H}_{LS} = \exp(-\omega)H\exp(\omega), \quad |\Phi_k\rangle = \exp(-\omega)|\Psi_k\rangle, \quad (4.29)$$

here ω has the property,

$$\omega = Q\omega P, \quad (4.30)$$

where it is seen that ω acts as a mapping between the P and Q spaces. From equation (4.30) it follows that $\omega^2 = \omega^3 = \dots = 0$ and the transformation operators X and X^{-1} simplify to

$$X = \exp(\omega) = 1 + \omega, \quad X^{-1} = \exp(-\omega) = 1 - \omega, \quad (4.31)$$

for which it immediately derive the effective Hamiltonian and interaction in the P -space,

$$\begin{aligned} P\tilde{H}_{LS}P &= PH(P + \omega), \\ PV_{LS}P &= PH(P + \omega) - PH_0P = PVP + PV\omega = PVP + PVQ\omega. \end{aligned} \quad (4.32)$$

Here we have used the identity $Q\omega = Q\omega P = \omega$.³ The decoupling equation (4.26) becomes,

$$QHP + QHQ\omega - \omega PHP - \omega PHQ\omega = 0. \quad (4.34)$$

The P -space Schrödinger equation (4.27) now becomes,

$$P(H_0 + V_{LS})P|\phi_k\rangle = E_k|\phi_k\rangle, \quad (4.35)$$

where $|\phi_k\rangle = P|\Phi_k\rangle$. The true eigenstate Ψ_k of the original Schrödinger equation (4.15) is related to the P -space eigenstate ϕ_k of equation (4.35) in the following way,

$$|\Psi_k\rangle = XP|\Phi_k\rangle = \exp(\omega)P|\Phi_k\rangle = (P + \omega)|\phi_k\rangle. \quad (4.36)$$

Here it is seen that $\omega|\phi_k\rangle$ is the Q -space component of the true eigenstate $|\Psi_k\rangle$. The eigenvalue problem for the P -space eigenstates in equation (4.35), is of a non-symmetric type. This means that the left and right eigenvectors form a complete bi-orthogonal set. Solving for the left eigenvectors $\langle\tilde{\phi}_k|$ of equation (4.35) which are *bi-orthogonal* to the right eigenvectors (see Appendix A for details) $|\phi_k\rangle$, we get

$$\langle\tilde{\phi}_k|\phi_{k'}\rangle = \delta_{k,k'}, \quad (4.37)$$

³In reference [104] Okamoto *et. al.* classified all energy independent effective interactions in the time independent approach, and formally showed that they may be written as

$$\tilde{H}(m, n) = (P + \omega^\dagger\omega)^{-m}H(P + \omega)(P + \omega^\dagger\omega)^n, \quad (4.33)$$

where m, n are integers of half-integers. For $m = n = 0$ the non-Hermitian Lee-Suzuki effective interaction in equation (4.32), which is the simplest transformation, is obtained.

Using the orthogonality of the true eigenvectors in equation (4.15) we may derive a relationship between the left and right eigenvectors,

$$\langle \Psi_k^* | \Psi_{k'} \rangle = \langle \phi_k^* | (P + \omega^T \omega) | \phi_{k'} \rangle = \delta_{k,k'}, \quad (4.38)$$

from which the following properties follow,

$$\langle \tilde{\phi}_k | = \langle \phi_k^* | (P + \omega^T \omega), \quad (4.39)$$

and

$$(P + \omega^T \omega) = (P + \omega \omega^T). \quad (4.40)$$

Given the left and right eigenvectors of the LS effective Hamiltonian, the formal solution to ω is given by,

$$\omega = \sum_{k=1}^d Q | \Psi_k \rangle \langle \tilde{\phi}_k | P, \quad (4.41)$$

here $d = N_P$ is the dimension of the P -space. The solution to ω is ambiguous in the sense that how to choose the N_P exact eigenstates $|\Psi_k\rangle$ is not unique. The effective interaction will depend on the choice of eigenvectors, and this is why the LS effective interaction is often called a *state-dependent* interaction. With the solution to ω , the N_P eigenvalues of the P -space equation will correspond exactly with the N_P arbitrary chosen eigenvalues of the original Schrödinger equation (4.15). Representing ω in the basis which diagonalizes H_0 (see equation (4.18)), and which defines the projection operators P and Q , we get,

$$\langle \alpha_Q^* | \omega | \alpha_P \rangle = \sum_{k=1}^d \langle \alpha_Q^* | \Psi_k \rangle \langle \tilde{\phi}_k | \alpha_P \rangle. \quad (4.42)$$

The bra states $\langle \tilde{\phi}_k |$ may be obtained from the true eigenstate $|\Psi_k\rangle$. Using the property that the matrix of left eigenvectors is the inverse of the matrix of right eigenvectors for a general matrix (see Appendix A), we get for the matrix of bra states,

$$[\langle \tilde{\phi}_k | \alpha_P \rangle] = [\langle \alpha_P^* | \phi_k \rangle]^{-1} = [\langle \alpha_P^* | \Psi_k \rangle]^{-1}. \quad (4.43)$$

Here [...] refers to the full $N_P \times N_P$ matrix. Then ω in the representation of H_0 is given by the matrix equation,

$$[\langle \alpha_Q^* | \omega | \alpha_P \rangle] = [\langle \alpha_Q^* | \Psi_k \rangle][\langle \alpha_P^* | \Psi_k \rangle]^{-1}. \quad (4.44)$$

It is seen that a solution for ω is obtainable provided the matrix $[\langle \alpha_P^* | \Psi_k \rangle]$ is non-singular. In numerical implementations it is therefore preferable to choose those N_P exact eigenstates $|\Psi_k\rangle$ which have the largest overlap with the P -space, $O_n = \sum_{\alpha_P} |\langle \Psi_n^* | \alpha_P \rangle|^2$. The matrix elements of the LS non-Hermitian Hamiltonian in equation (4.32) in the representation of H_0 (see equation (4.18)) are given by,

$$\langle \alpha_P^* | \tilde{H}_{LS} | \alpha'_P \rangle = \sum_{k=1}^d \left[\langle \alpha_P^* | \Psi_k \rangle E_k \langle \Psi_k^* | \alpha'_P \rangle + \sum_{\alpha_Q} \langle \alpha_P^* | \Psi_k \rangle E_k \langle \Psi_k^* | \alpha_Q \rangle \langle \alpha_Q^* | \omega | \alpha'_P \rangle \right]. \quad (4.45)$$

Here E_k is the exact eigenvalue obtained by diagonalizing the full Hamiltonian given in equation (4.15). When diagonalizing the LS effective Hamiltonian, the E_k , $k = 1, \dots, d$ exact eigenvalues are obtained. The LS effective interaction becomes in the representation of H_0 ,

$$\langle \alpha_P^* | V_{LS} | \alpha'_P \rangle = \langle \alpha_P^* | \tilde{H}_{LS} | \alpha'_P \rangle - \varepsilon_{\alpha_P} \delta_{\alpha_P, \alpha'_P}. \quad (4.46)$$

The LS effective Hamiltonian is non-Hermitian and non-symmetric. It would be preferable to obtain a complex symmetric effective interaction, in order to take advantage of the anti-symmetrization of the two-particle basis. This may be accomplished by a Z -transformation of the P -space states,

$$|\nu_k\rangle = Z|\phi_k\rangle, \quad (4.47)$$

with the following property

$$\langle \tilde{\nu}_k | \nu_{k'} \rangle = \langle \nu_k^* | \nu_{k'} \rangle = \delta_{k, k'}. \quad (4.48)$$

Using again the orthogonality of the true eigenstates $|\Psi_k\rangle$, we get

$$\langle \Psi_k^* | \Psi_{k'} \rangle = \langle \phi_k^* | (P + \omega^T \omega) | \phi_{k'} \rangle = \langle \nu_k^* | (Z^{-1})^T (P + \omega^T \omega) (Z^{-1}) | \nu_{k'} \rangle = \delta_{k, k'}, \quad (4.49)$$

which gives the following condition for the Z -transformation in order for equation (4.48) to be fulfilled,

$$Z^T Z = P + \omega^T \omega. \quad (4.50)$$

Having obtained a solution for Z which obeys equation (4.50), the complex symmetric (CS) effective interaction is given by,

$$V_{CS} = Z(H_0 + V_{LS})Z^{-1} - PH_0P. \quad (4.51)$$

That the Z -transformed LS effective Hamiltonian is complex symmetric follows from the orthogonality in equation (4.48), where the left eigenvector is the transpose of the right eigenvector, which is the case for symmetric matrices only (see Appendix A). References [103, 104] derived and discussed several such Z -transformations for which a Hermitian effective interaction is obtained. One such Z -transformation is,

$$Z = P(1 + \omega^T \omega)^{1/2}P. \quad (4.52)$$

From equation (4.40) it follows that $Z = Z^T$ for this particular choice, and it is easily seen that equation (4.50) is fulfilled. This choice of Z leads to an effective interaction of the Okubo form [105],

$$V_{okb} = P(1 + \omega^T \omega)^{1/2}P(H_0 + V_{LS})P(1 + \omega^T \omega)^{-1/2}P - PH_0P. \quad (4.53)$$

The matrix element of the Okubo effective interaction in the representation of H_0 becomes,

$$\langle \alpha_P^* | V_{okb} | \alpha'_P \rangle = \sum_{\gamma_P} \sum_{\gamma'_P} \langle \alpha_P^* | (P + \omega^T \omega)^{1/2} | \gamma_P \rangle \langle \gamma_P^* | H_{LS} | \gamma'_P \rangle \langle \gamma_P'^* | (P + \omega^T \omega)^{-1/2} | \alpha'_P \rangle - \varepsilon_{\alpha_P} \delta_{\alpha_P, \alpha'_P}. \quad (4.54)$$

To determine V_{okb} , one has to find the square root of the matrix $A = [\langle \alpha^* | (P + \omega^T \omega) | \alpha'_P \rangle]$. In the case of A being real and positive definite the method based on eigenvector decomposition generally gives a stable solution. Using the eigenvector decomposition, with M representing an orthogonal matrix with the eigenvectors of A and D a diagonal matrix composed of the eigenvalues, we have the following

$$A = MDM^T, M^T M = MM^T = 1, D = (D)^{1/2}(D)^{1/2}, \quad (4.55)$$

which gives,

$$A = (MD^{1/2}M^T)(MD^{1/2}M^T), \quad (4.56)$$

the square root of the matrix A is then given by,

$$A^{1/2} = XD^{1/2}X^T. \quad (4.57)$$

For a complex matrix A the procedure based on eigenvector decomposition is generally numerically unstable [106]. An approach suitable for complex matrices is based on properties of the matrix sign function. It can be shown that the square root of a matrix is related to the matrix sign function, see reference [106] for more details. In the case of A being complex and having all eigenvalues in the open right half complex plane, iterations based on the matrix sign function are generally more stable

$$\text{sign} \left(\begin{bmatrix} 0 & A \\ I & 0 \end{bmatrix} \right) = \begin{bmatrix} 0 & A^{1/2} \\ A^{-1/2} & 0 \end{bmatrix}. \quad (4.58)$$

One stable iteration scheme for the matrix sign was derived by Denman and Beavers [107], as a special case of a method for solving the algebraic Riccati equation

$$Y_0 = A, \quad Z_0 = I, \quad (4.59)$$

$$Y_{k+1} = \frac{1}{2}(Y_k + Z_k^{-1}), \quad (4.60)$$

$$Z_{k+1} = \frac{1}{2}(Z_k + Y_k^{-1}), \quad k = 0, 1, 2, \dots, \quad (4.61)$$

and provided A has no non-positive eigenvalues this iteration scheme exhibits a quadratic convergence rate with

$$Y_k \rightarrow A^{1/2}, \quad Z_k \rightarrow A^{-1/2} \quad \text{as } k \rightarrow \infty. \quad (4.62)$$

4.4 Non-Hermitian Many-Body Perturbation Theory.

The former section dealt with the problem of constructing an energy independent effective two-body interaction using similarity transformation methods, generalized to complex interactions. Having constructed an effective interaction in the two-particle model space, this interaction is then the basic ingredient in the many-body problem. However, dealing

with many particles moving in a large valence space, the dimensionality may still be of an order not suitable for a practical solution.

The single-particle resonances have many of the same characteristics as bound states on deformed contours in the complex k -plane, they are discrete square integrable states with a set of definite quantum number. Based on this it is reasonable to assume that in the many-body problem, many-body perturbation theory originally developed for bound states, may be generalized to apply for resonances as well.

The focus in this section will be on the non-Hermitian multi-reference perturbation theory method (MRPTM), which in the Hermitian case has recently been revived in quantum chemistry, see for example references [108, 109, 110]. The MRPTM differs from standard many-body perturbation techniques, in that a set of reference states are constructed by diagonalizing a N -body model-space Hamiltonian exactly. Having constructed a more suitable basis which decouples the P -space, this basis serves as a starting point for a perturbation expansion. It can be shown that this expansion converges much faster than the single-reference perturbation theory, since many higher order terms are already taken into account by the zeroth order term. The chosen N -body model-space P should be of such kind that the coupling of P with the complement space Q is weak, for the perturbation expansion to converge.

For clarity we first outline the standard Many-Body Perturbation Theory where only single references appear. Thereafter we outline the multi-reference theory for non-Hermitian interactions.

4.4.1 Single-Reference Perturbation Theory.

Here we outline the standard many-body perturbation theory, applicable to the case of many-body resonances. We start from the N -body Schrödinger equation,

$$H\Psi = E\Psi, \quad (4.63)$$

where the Hamiltonian is split into an unperturbed part H_0 for which we can obtain exact solution, and a perturbation V , i.e.

$$H = H_0 + V, \quad (4.64)$$

where

$$H_0 = \sum_k (T_k + U_k), \quad V = \sum_{k < l} V_{k,l} - \sum_k U_k. \quad (4.65)$$

The exact solutions of H_0 are given by,

$$H_0\Phi_i = \varepsilon_i\Phi_i, \quad (4.66)$$

where the N -body unperturbed energies ε_i are given by the sum of N single-particle energies obtained by solving the one-body Hamiltonian, $T + U$, and Φ_i is a Slater determinant composed of N -particles occupying the relevant single-particle orbitals. Having obtained

a complete set of many-body Slater determinants, we may define a model space P and complement space Q which project into orthogonal parts of the full space,

$$P = \sum_{i=1}^{N_P} |\Phi_i\rangle\langle\Phi_i^*|, \quad Q = \sum_{i=N_P+1}^N |\Phi_i\rangle\langle\Phi_i^*. \quad (4.67)$$

Here N_P is the dimension of the model space and N is the dimension of the full space. They satisfy the usual equations given in equations (4.16) and (4.17). There are many ways of constructing the many-body P - and Q -spaces. The most usual is to construct them from the single-particle model space, so that P is the space constructed from all single-particles occupying orbits in the single-particle model space p , and Q is the remaining orthogonal space. The exact N -body wave function may then be expanded in this basis,

$$\Psi = \sum_{i=1}^{N_P} C_i \Phi_i + \sum_{i=N_P+1}^N C_i \Phi_i = P\Psi + Q\Psi,$$

and the full Schrödinger equation may be written in the 2×2 block structure given in equation (4.22). An effective eigenvalue problem in the P -space may then be obtained (see previous section),

$$(PHP + PHQG(E_k)QHP) P|\Psi_k\rangle = E_k P|\Psi_k\rangle, \quad (4.68)$$

where we have introduced the complete interacting Green's function in the Q -space,

$$G(E) = \frac{Q}{E - QHQ} = \frac{Q}{E - H_0 - QVQ}, \quad (4.69)$$

Using the operator identity $(AB)^{-1} = B^{-1}A^{-1}$ the interacting Green's function $G(E)$ may be written in the form, neglecting the dependence on E ,

$$G = \frac{Q}{1 - G_0 QVQ} G_0 = G_0 \frac{Q}{1 - QVQG_0}, \quad (4.70)$$

where the non-interacting Green's function G_0 in the Q -space is given by,

$$G_0 = \frac{Q}{E - H_0}. \quad (4.71)$$

By using $(1 - x)^{-1} = 1 + x + x^2 + x^3 + \dots$ we may write

$$\frac{1}{1 - QVQG_0} = 1 + QVQG_0 + (QVQG_0)(QVQG_0) + (QVQG_0)(QVQG_0)(QVQG_0) + \dots, \quad (4.72)$$

which gives for the interacting Q -space Green's function

$$G = G_0(1 + QVQG_0 + (QVQG_0)(QVQG_0) + (QVQG_0)(QVQG_0)(QVQG_0) + \dots), \quad (4.73)$$

which is just the iterated integral equation for $G(E)$,

$$G = G_0 + G_0 Q V Q G. \quad (4.74)$$

Inserting the iterated Q -space Green's function into the equation for the effective Hamiltonian given in equation (4.68), we get the iterated effective interaction,

$$V_{\text{eff}} = PVP + PVQ \frac{1}{E - H_0} QVP + PVQ \frac{1}{E - H_0} QVQ \frac{1}{E - H_0} QVP + \dots, \quad (4.75)$$

where we have used the fact that the operator Q commutes with H_0 , since P and Q are built from the basis which diagonalizes H_0 . The effective interaction given in equation (4.75) still depends on the exact energy, which is to be determined. This problem may be removed by invoking a Taylor expansion in E around the unperturbed energies ε_a of the effective interaction, see references [111, 112] for details. In particular it may be shown that only linked diagrams contribute in the expansion, giving the Goldstone linked-cluster expansion reference [113]. Due to the cancellation of certain diagrams at each order in the perturbation expansion, it is possible to do partial infinite summations of the effective interaction. One such example of infinite partial summation is the ladder equation for the effective interaction,

$$V_{\text{eff}} = V + V \frac{Q}{\varepsilon_a - H_0} V_{\text{eff}}. \quad (4.76)$$

Our focus in this subsection is on the single-reference Rayleigh-Schrödinger perturbation expansion for the energy. Single-reference means that only a single model space state is considered, which gives the projection operators

$$P = |\Phi_a\rangle\langle\Phi_a^*|, \quad Q = \sum_{i \neq a}^N |\Phi_i\rangle\langle\Phi_i^*. \quad (4.77)$$

A perturbative treatment of a single model space state, may only be expected to give convergent results if the coupling with the Q -space is weak. In Gamow Shell Model applications, it is natural to choose the many-body configuration where all particles are in resonant orbitals as the reference state, $|\Phi_a\rangle = |RRR\dots\rangle$, and then add perturbations to this state by taking into account all kinds of excitations to non-resonant continuum states. However, as shown in Paper 2 the coupling with configurations where one or two particles are in non-resonant continuum orbits may not be considered weak in all cases. By projecting the secular equation for the P -space state onto the single model space state Φ_a gives the standard Brillouin-Wigner perturbation expansion for the energy,

$$\begin{aligned} E = \varepsilon_a + \langle\Phi_a^*| &PVP + PVQ \frac{1}{E - H_0} QVP + \\ &PVQ \frac{1}{E - H_0} QVQ \frac{1}{E - H_0} QVP + \dots |\Phi_a\rangle. \end{aligned} \quad (4.78)$$

In the Brillouin-Wigner perturbation expansion the exact energy E , which we wish to determine, appears from second order and to infinity in the energy denominators $E - H_0$.

Equation (4.78) may be rewritten in such a way that only unperturbed energies appear in the denominators, giving the Rayleigh-Schrödinger perturbation expansion. Writing the energy denominator in the form,

$$E - H_0 = \Delta E + \varepsilon_a - H_0,$$

where ΔE is the energy shift we wish to determine, we obtain the following expression,

$$\frac{1}{E - H_0} = \frac{1}{\varepsilon_a - H_0} \left(1 + \frac{\Delta E}{\varepsilon_a - H_0} \right)^{-1} = \frac{1}{a} \left(1 - \frac{\Delta E}{a} + \left(\frac{\Delta E}{a} \right)^2 - + \dots \right), \quad (4.79)$$

where we have defined $a = \varepsilon_a - H_0$. Inserting equation (4.79) into equation (4.78) we get the following equation for the energy shift ΔE ,

$$\begin{aligned} \Delta E = & \langle \Phi_a^* | PVP + PVQ \frac{1}{a} \left(1 - \frac{\Delta E}{a} + \left(\frac{\Delta E}{a} \right)^2 - + \dots \right) QVP + \\ & PVQ \frac{1}{a} \left(1 - \frac{\Delta E}{a} + \left(\frac{\Delta E}{a} \right)^2 - + \dots \right) QVQ \times \\ & \frac{1}{a} \left(1 - \frac{\Delta E}{a} + \left(\frac{\Delta E}{a} \right)^2 - + \dots \right) QVP + \dots | \Phi_a \rangle. \end{aligned} \quad (4.80)$$

Inserting the expression for ΔE back into itself we get order by order correction to the energy by sorting the different powers in V . It may be shown [114] that the n 'th term in the Rayleigh-Schrödinger perturbation expansion for the energy is given by the expansion,

$$E_n = \langle VS_{n-1} \rangle - \sum_{m=1}^{n-1} E_m \langle S_{n-m} \rangle, \quad (4.81)$$

where

$$S_n = \frac{Q}{a} VS_{n-1} - \frac{Q}{a} \sum_{m=1}^{n-1} E_m S_{n-m}, \quad S_0 = 1. \quad (4.82)$$

Here we have introduced the notation $\langle V \rangle = \langle \Phi_a^* | V | \Phi_a \rangle$. By further introducing the quantity $\mathcal{U} = V - \langle V \rangle$, the perturbation expansion up through fifth order may easily be shown to be,

$$\begin{aligned} E_0 &= \varepsilon_a = \langle H_0 \rangle, \\ E_1 &= \langle V \rangle, \\ E_2 &= \left\langle V \frac{Q}{a} V \right\rangle, \\ E_3 &= \left\langle V \frac{Q}{a} \mathcal{U} \frac{Q}{a} V \right\rangle, \end{aligned} \quad (4.83)$$

$$\begin{aligned} E_4 &= \left\langle V \frac{Q}{a} \left[U \frac{Q}{a} U - \left\langle U \frac{Q}{a} U \right\rangle \right] \frac{Q}{a} V \right\rangle, \\ E_5 &= \left\langle V \frac{Q}{a} \left[U \frac{Q}{a} U \frac{Q}{a} U - \left\langle U \frac{Q}{a} U \frac{Q}{a} U \right\rangle - U \frac{Q}{a} \left\langle U \frac{Q}{a} U \right\rangle - \left\langle U \frac{Q}{a} U \right\rangle \frac{Q}{a} U \right] \frac{Q}{a} V \right\rangle. \end{aligned}$$

Here all matrix elements of the form,

$$\left\langle \frac{Q}{a} \text{ or } \frac{Q}{a} \right\rangle = 0, \quad (4.84)$$

since the model space state Φ_a is orthogonal to all states in the complement space Q . The exact energy may then be written as a Taylor series in the perturbation λ , which for $\lambda = 1$ gives the desired result,

$$E = \sum_{n=0}^{\infty} E_n \lambda^n = E_0 + E_1 \lambda + E_2 \lambda^2 + \dots \quad (4.85)$$

A more general and effective approximation which generally gives a more rapid convergence to the exact energy is the Padé approximation [8]. The Padé approximant $E^{[N,M]}$ to the exact energy E is given by the rational fractional expression,

$$E^{[N,M]}(\lambda) = \frac{P_N(\lambda)}{Q_M(\lambda)}, \quad (4.86)$$

where P_N and Q_M are polynomials of degrees N and M respectively. The polynomials P_N and Q_M may be obtained from the coefficients E_n of the Taylor expansion of the exact energy in equation (4.85) by the following formulas,

$$P_N(\lambda) = \begin{vmatrix} E_{N-M+1} & E_{N-M+2} & \dots & E_{N+1} \\ \vdots & \vdots & \vdots & \vdots \\ E_N & E_{N+1} & \dots & E_{N+M} \\ \sum_{j=M}^N E_{j-M} \lambda^j & \sum_{j=M-1}^N E_{j-M+1} \lambda^j & \dots & \dots \sum_{j=0}^N E_j \lambda^j \end{vmatrix}, \quad (4.87)$$

and

$$Q_M(\lambda) = \begin{vmatrix} E_{N-M+1} & E_{N-M+2} & \dots & E_{N+1} \\ \vdots & \vdots & \vdots & \vdots \\ E_N & E_{N+1} & \dots & E_{N+M} \\ \lambda^M & \lambda^{M-1} & \dots & 1 \end{vmatrix}. \quad (4.88)$$

The first few Padé approximants take the following form,

$$\begin{aligned} E^{[0,0]} &= E_0, \\ E^{[1,1]} &= \frac{E_0 E_1 + (E_1^2 - E_0 E_2) \lambda}{E_1 - E_2 \lambda}, \\ E^{[2,1]} &= \frac{E_0 E_2 + (E_1 E_2 - E_0 E_3) \lambda + (E_2^2 - E_1 E_3) \lambda^2}{E_2 - E_3 \lambda}, \end{aligned}$$

$$\begin{aligned}
E^{[1,2]} &= \frac{(E_0^2 E_2 - E_0 E_1^2) + (2E_0 E_1 E_2 - E_0^2 E_3 - E_1^3) \lambda}{(E_0 E_2 - E_1^2) + (E_1 E_2 - E_0 E_3) \lambda + (E_1 E_3 - E_2^2) \lambda^2}, \\
E_{[2,2]} &= [(E_0 E_1 E_3 - E_0 E_2^2) + (E_1^2 E_3 + E_0 E_2 E_3 - E_0 E_2 E_3 - E_0 E_1 E_4 - E_1 E_2^2) \lambda \\
&\quad + (E_1 E_2 E_3 + E_0 E_2 E_4 + E_1 E_2 E_3 - E_1^2 E_4 - E_2^3 - E_0 E_3^2) \lambda^2] / \\
&\quad (E_1 E_3 - E_2^2) + (E_2 E_3 - E_1 E_4) \lambda + (E_2 E_4 - E_3^2) \lambda^2.
\end{aligned} \tag{4.89}$$

In order to clarify the use of single-reference perturbation theory in Gamow Shell Model calculations, we consider the convergence of the Padé approximant $E^{[2,1]}$ versus the standard energy expansion up through third order in energy, for the 0^+ ground state of ${}^6\text{He}$ as the residual nucleon-nucleon interaction is gradually turned on. ${}^6\text{He}$ is here modeled by an inert ${}^4\text{He}$ core with two valence nucleons moving in $24 l j$ orbits $p_{3/2}$, where one is a single-particle resonant orbit and the remaining 23 orbits are in the non-resonant continuum. See Paper 2 for further details on the single-particle potential and the residual nucleon-nucleon interaction. The two-particle model space state is then the configuration where both particles are in resonant orbits, $|RR\rangle$, and the complement space is then all configurations of the type $|RC\rangle, |CC\rangle$, where C labels a non-resonant continuum orbit. Figure 4.6 gives

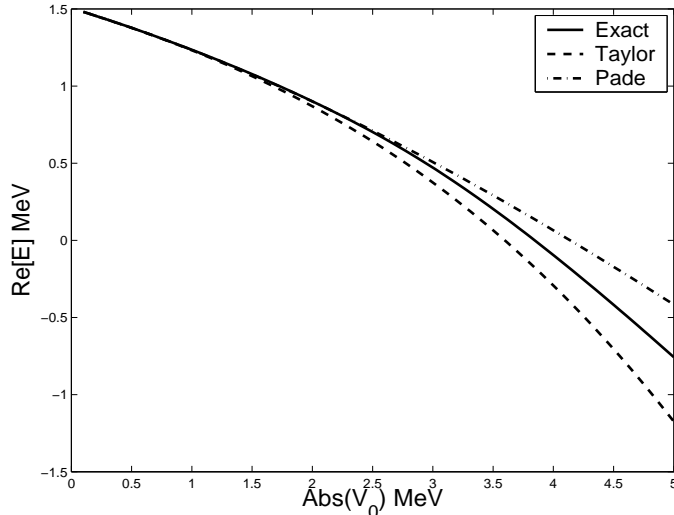


Figure 4.6: Plot of real part of 0^+ energy in ${}^6\text{He}$, for increasing $n-n$ interaction strength V_0 . The solid line gives the exact energy, the dashed line gives the series expansion of the energy up through third order and the dashed-dotted line gives the $E^{[2,1]}$ Padé approximation to the energy.

the real part of the 0^+ energy, while figure 4.7 gives the corresponding imaginary part of the energy, as the interaction strength is gradually turned on. In both cases it is seen that the Padé approximant $E^{[2,1]}$ gives a better fit to the exact energy, than the Taylor expansion up through third order. In both cases the single-reference perturbation theory fails to give satisfactory result for the energy when the interaction strength is that of Paper 2, i.e. $V_0 = -5.315\text{MeV}$. It is also seen that single-reference perturbation theory gives

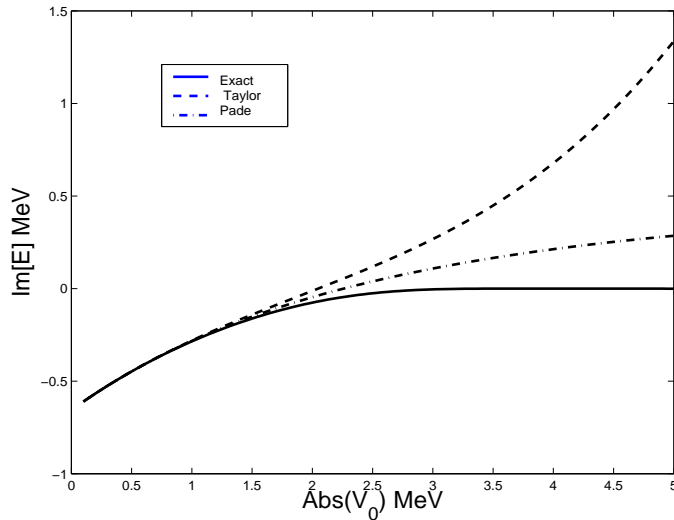


Figure 4.7: Plot of imaginary part of 0^+ energy in ${}^6\text{He}$, for increasing $n - n$ interaction strength V_0 . Solid line gives the exact energy, the dashed line gives the series expansion of the energy up through third order and the dashed-dotted line gives the $E^{[2,1]}$ Padé approximation to the energy.

convergent results in this specific case only for interaction strengths with absolute value less than 1 MeV. One may therefore conclude that single-reference perturbation theory, is not suitable in Gamow Shell Model calculations, since the coupling with the complement space is too strong, for being treated perturbatively.

4.4.2 Multi-Reference Perturbation Theory.

In this section we outline the non-Hermitian multi-reference perturbation theory. We proceed in similar manner to the previous section, and construct a N -body model space P and a complement (orthogonal) space Q according to equation (4.67). The choice of P should be dictated by some intuition on which single-particle configurations play the dominant part in the fully correlated many-body wave function. Having constructed P and Q the many-body wave function and the corresponding Hamiltonian may be represented in this basis. The Hamiltonian may subsequently be partitioned into two parts according to,

$$\begin{pmatrix} PHP & PHQ \\ QHP & QHQ \end{pmatrix} = \begin{pmatrix} H^{PP} & 0 \\ 0 & D^{QQ} \end{pmatrix} + \begin{pmatrix} 0 & H^{PQ} \\ H^{QP} & \tilde{H}^{QQ} \end{pmatrix} = H_0 + H_1. \quad (4.90)$$

Here D^{QQ} is the diagonal part and \tilde{H}^{QQ} the off-diagonal part of QHQ respectively. Written in this form, it is seen that H^0 defines the unperturbed part while H^1 gives the perturbations to H^0 . Provided H^0 is non-singular, the model space block PHP may be

decoupled by constructing a complex orthogonal matrix \mathbf{C} which diagonalizes H^0 , i.e. $\mathbf{C}H^0\mathbf{C}^T = \text{Diag}(E_1^0, E_2^0, \dots, E_N^0)$. Since H^0 is a block diagonal matrix, the matrix \mathbf{C} is given in the form

$$\mathbf{C} = \begin{bmatrix} \chi & \mathbf{0} \\ \mathbf{0} & \mathbf{1} \end{bmatrix}. \quad (4.91)$$

A more convenient many-body basis which decouples (diagonalizes) the reference space is then given by the vectors

$$\Upsilon_i = \sum_{j=1}^{N_P} C_{i,j} \Phi_j = \begin{cases} \sum_{j=1}^{N_P} \chi_{i,j} \Phi_j, & i = 1, N_P \\ \Phi_i, & i = N_P + 1, N \end{cases}, \quad (4.92)$$

and they are solutions of the eigenvalue problem,

$$H_0 |\Upsilon_i\rangle = \tilde{\varepsilon}_i |\Upsilon_i\rangle. \quad (4.93)$$

We assume here that the states $|\Upsilon_i\rangle$ are normalized to unity. The complex orthogonal matrix χ which spans the reference space P , defines our new set of reference states. The states Υ_i , $i = 1, \dots, N_P$ span the same space as the original P -space states Φ_i , but they have been reoriented in space so that they diagonalize PHP . As a measure of how well the zeroth order wave function $\Upsilon_{i=\text{res}}^J$ resembles the exact wave function, one can calculate the complex variance, σ_c^2 see references [15, 115],

$$\begin{aligned} \sigma_c^2 &= \langle \Upsilon_i^J | (H - E_i^0)^2 | \Upsilon_i^J \rangle \\ &= \chi_i^T H^{PQ} H^{QP} \chi_i, \end{aligned} \quad (4.94)$$

where $i = \text{res}$ and χ_i labels the i 'th column of the $N_P \times N_P$ matrix χ . In reference [115] it was proved that the complex variance σ_c provides an upper bound to the exact resonance energy,

$$|E_{\text{res}}^{\text{exact}} - E_{\text{res}}^0| \leq |\sigma_c|. \quad (4.95)$$

Having constructed a new many-body anti-symmetric basis, we develop a perturbation expansion in terms of these eigenvectors of the reference space. Derivation of the Rayleigh - Schrödinger perturbation expansion for the exact energy and wave function follows in exactly the same manner as in previous section. We wish to study how a single reference state Υ_i changes order by order in the Rayleigh-Schrödinger perturbation expansion by adding the perturbation matrix H^1 . So the P -space is a single state and the orthogonal complement is the remaining states

$$\tilde{P} = |\Upsilon_a\rangle\langle\Upsilon_a^*|, \quad \tilde{Q} = \sum_{i \neq a} |\Upsilon_i\rangle\langle\Upsilon_i^*. \quad (4.96)$$

Consider the 1'st order correction to the energy for any state Υ_p in the model space, i.e.

$$E_1(p) = \langle \Upsilon_p^* | H_1 | \Upsilon_p \rangle = \begin{pmatrix} \chi_p^T & 0 \end{pmatrix} \begin{pmatrix} 0 & H^{PQ} \\ H^{QP} & \tilde{H}^{QQ} \end{pmatrix} \begin{pmatrix} \chi_p \\ 0 \end{pmatrix} = 0, \quad (4.97)$$

thus gives zero contribution. This is an extremely nice feature, since all expansion terms where 1'st order matrix elements E_1 appear in a product with more complicated terms give zero contribution. The 1'st order correction to the energy may be said to have been incorporated into the zeroth order energy $\tilde{\varepsilon}_i$. The second order correction to an unperturbed energy $\tilde{\varepsilon}_p$ becomes

$$E_2(p) = \sum_{a \neq p}^N \frac{\langle \Upsilon_p^* | H_1 | \Upsilon_a \rangle \langle \Upsilon_a^* | H_1 | \Upsilon_p \rangle}{\tilde{\varepsilon}_p - \tilde{\varepsilon}_a}. \quad (4.98)$$

From the structure of the perturbation matrix H^1 is easily seen that the sum over Q -space states is restricted to $a > N_P$ by taken into the account $\langle \Upsilon_i^* | H_1 | \Upsilon_j \rangle = 0, i, j \leq N_P$. This illustrates that many excitations from the P - into the Q -space have already been taken into account in the zeroth order wave function. The second order energy term then becomes,

$$\begin{aligned} E_2(p) &= \sum_{a > N_P}^N \frac{\langle \Upsilon_p^* | H_1 | \Upsilon_a \rangle \langle \Upsilon_a^* | H_1 | \Upsilon_p \rangle}{\tilde{\varepsilon}_p - \tilde{\varepsilon}_a} = \sum_{i,j \leq N_P} \sum_{a > N_P} \frac{\chi_{p,i} \langle \Phi_i^* | H_1 | \Phi_a \rangle \langle \Phi_a^* | H_1 | \Phi_j \rangle \chi_{j,p}}{\tilde{\varepsilon}_p - \tilde{\varepsilon}_a} \\ &= \sum_{i,j \leq N_P} \sum_{a > N_P} \frac{\chi_{p,i} H_{i,a}^{PQ} H_{a,j}^{QP} \chi_{j,p}}{\tilde{\varepsilon}_p - D_{a,a}^{QQ}}, \end{aligned} \quad (4.99)$$

and the third order term becomes

$$E_3(p) = \sum_{\substack{a,b > N_P \\ a \neq b}}^N \frac{\langle \Upsilon_p^* | H_1 | \Upsilon_a \rangle \langle \Upsilon_b^* | H_1 | \Upsilon_p \rangle}{(\tilde{\varepsilon}_p - \tilde{\varepsilon}_a)(\tilde{\varepsilon}_p - \tilde{\varepsilon}_b)} = \sum_{i,j \leq N_P} \sum_{\substack{a,b > N_P \\ a \neq b}} \frac{\chi_{p,i} H_{i,a}^{PQ} \tilde{H}_{a,b}^{QQ} H_{b,j}^{QP} \chi_{j,p}}{(\tilde{\varepsilon}_p - D_{a,a}^{QQ})(\tilde{\varepsilon}_p - D_{b,b}^{QQ})}. \quad (4.100)$$

Higher order terms may easily be calculated from the Rayleigh-Schrödinger perturbation expansion given in equation(4.84). Summarizing we get, through fourth order,

$$\begin{aligned} E_0(p) &= \langle \Upsilon_p^* | H^0 | \Upsilon_p \rangle = \tilde{\varepsilon}_p, \\ E_1(p) &= \langle \Upsilon_p^* | H^1 | \Upsilon_p \rangle = 0, \\ E_2(p) &= \langle \Upsilon_p^* | H^1 \frac{Q}{\tilde{\varepsilon}_p - H^0} H^1 | \Upsilon_p \rangle, \\ E_3(p) &= \langle \Upsilon_p^* | H^1 \frac{Q}{\tilde{\varepsilon}_p - H^0} H^1 \frac{Q}{\tilde{\varepsilon}_p - H^0} H^1 | \Upsilon_p \rangle, \\ E_4(p) &= \langle \Upsilon_p^* | H^1 \frac{Q}{\tilde{\varepsilon}_p - H^0} H^1 \frac{Q}{\tilde{\varepsilon}_p - H^0} H^1 \frac{Q}{\tilde{\varepsilon}_p - H^0} H^1 | \Upsilon_p \rangle \\ &\quad - E_2(p) \langle \Upsilon_p^* | H^1 \frac{Q}{(\tilde{\varepsilon}_p - H^0)^2} H^1 | \Upsilon_p \rangle. \end{aligned} \quad (4.101)$$

Where $Q = \sum_{i > N_P} |\Upsilon_i\rangle \langle \Upsilon_i^*|$.

The above perturbation series is a theory which treats one-state-at-a-time, this theory differs from the standard multi-reference perturbation theory which diagonalizes an effective Hamiltonian and solves for all states in the model space simultaneously. The above

perturbation theory sets no restrictions on the choice of many-body reference space, and can in principle be chosen by any suitable selection criterion. The theory also allows for a freely variation of the reference space size, so that it is possible to achieve satisfactory convergent results at a given order in the perturbation series. If the coupling between the reference states is turned off, the perturbation series reduces to the standard single-reference Rayleigh-Schrödinger perturbation theory discussed in the previous section.

In the application of the above multi-reference perturbation theory method to Gamow Shell Model calculations, a reference space which takes into account most of the correlations has to be chosen. Further the size of the P -space should be small enough to allow for a direct diagonalization in order to obtain the reference states Υ_i , $i = 1, \dots, N_P$. The most important configuration in a many-body resonance may be expected to be the pure resonance pole configuration $|RRR\dots\rangle$. We wish then to generate correlations on this unperturbed many-body resonance state, in order to obtain the fully correlated many-body resonance. The correlations are generated by virtual excitations of one or several particles occupying the single-particle resonant orbitals to non-resonant continuum orbitals, induced by the residual nucleon-nucleon interaction. A viable starting point for Gamow Shell Model applications, would be to construct a reference space P consisting of a set of low lying many-body unperturbed states where at least one particle is in a single particle resonance orbital. The orthogonal complement space Q consists then of the remaining states. In Paper 2 where the above perturbation theory was applied to the unbound nucleus ${}^7\text{He}$, the three-particle model space, and corresponding complement space, were defined by

$$P \equiv \left\{ \begin{array}{l} |RRR\rangle, |RRC\rangle, |RCC\rangle, \\ \text{Re}(e_a + e_b + e_c) < E_{\text{cut}}, \\ \text{Im}(e_a + e_b + e_c) > -E_{\text{cut}} \end{array} \right\} \quad Q = 1 - P, \quad (4.102)$$

here the P space is given by configurations where at most two particles move in continuum orbits. In addition, P is further defined by a rectangular cutoff in the complex energy plane. This cutoff in energy is motivated by an assumption that three-particle configurations high in energy play a minor role on the formation of low-lying resonances. Figure 4.8 gives a plot of the $J^\pi = 3/2^-$ unperturbed (non-interacting) three-particle spectrum of ${}^7\text{He}$ used in Paper 2. At most two particles move in complex continuum orbits, and three different cut-offs in energies and corresponding model spaces are shown. Note that only $p_{3/2}$ single-particle orbitals are taken into account. Having constructed a suitable model space P , a full diagonalization is performed. We wish to study the effect of adding the perturbation H^1 to the new many-body resonance wave function. Since the above theory is a one-state-at-a-time theory, the zeroth order resonance $\Upsilon(i = \text{res})$ has to be identified from the zeroth order energy spectrum. This identification may be done by determining which state Υ_i , $i = 1, \dots, N_P$ has the largest overlap with the pure pole configuration $|\Phi_{\text{res}}\rangle = |RRR\dots\rangle$,

$$\text{Max} \left\{ \left| \langle \tilde{\Phi}(\text{res}) | \Upsilon_i \rangle \right| \right\}_{i=1}^{N_P} = \text{Max} \left\{ |\chi_{i,j=\text{res}}| \right\}_{i=1}^{N_P}. \quad (4.103)$$

To make sure that the “correct” physical state is picked out, the complex energy trajectories as the interaction is gradually turned on, may be studied.

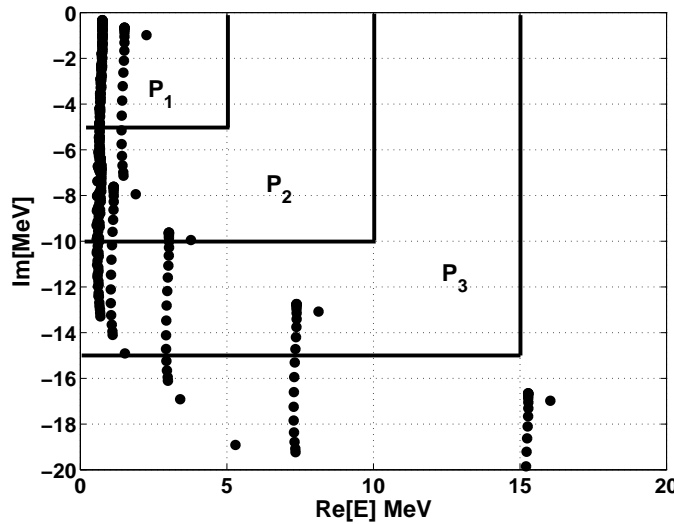


Figure 4.8: Three choices of the model space used in the multi-reference perturbation theory calculations of resonances in ^7He in Paper 2. The three-particle model space states are constructed such that at most two particles move in the non-resonant continuum.

4.5 Effective Interaction Scheme for Gamow Shell Model Calculations.

In the previous sections it was shown that the Lee-Suzuki similarity transformation and the multi-reference perturbation method may be used in the Gamow Shell Model in order to account for the most important correlations of for example a multi-particle resonance. Although the dimensionality of the problem derived either from the similarity transformation method or the multi-reference perturbation method was significantly reduced compared to the full problem, the dimensionality may still be a severe problem when dealing with more than three particles in a large valence space.

The drawback of the multi-reference perturbation method is that one has to store extremely large matrices H^{QQ} if one wishes to go beyond second order in perturbation theory. In the similarity transformation method one does not have to deal with H^{QQ} , as couplings with the Q -space states have been dealt with, in practical calculations at least at the two-body level. Going to systems with larger degrees of freedom, the P -space may nevertheless, at the converged level, be too large for our brute force diagonalization approach.

The aim of this section is to propose an effective interaction and perturbation theory scheme for the Gamow Shell Model. This approach combines the similarity transformation method and the multi-reference perturbation method, so that hopefully multi-particle resonances where several particles move in a large valence space, may be calculated without a diagonalization in the full space. Our algorithm is as follows

1. Choose an optimal set of n_{sp} single-particle orbits, which in turn defines two-body P_{2p} and many-body spaces. In our case these single-particle orbits are defined by selected states in ${}^5\text{He}$.
2. Construct a two-particle effective interaction by the Lee-Suzuki similarity transformation method within the two-particle model space P_{2p} . Such diagonalizations can be done for very large spaces, see for example references [38, 39, 40, 41].
3. The next step is to divide the multi-particle model space P in two smaller spaces P' and Q' , where $P = P' + Q'$ and $N_P = N_{P'} + N_{Q'}$. The choice of P' should be dictated by our knowledge of the physical system. As an example, one may consider those single-particle configurations within the P -space that play the dominant role in the formation of the multi-particle resonance. The number $N_P = N_{P'} + N_{Q'}$ represents the total number of many-body configurations within the P -space.
4. Now that we have divided the P -space in two sub-spaces P' and Q' , we use for example the multi-reference perturbation method to account for excitations from the P' -space to the Q' -space to obtain energy corrections to a specific order. Increase the size of the P' -space until convergence is obtained. In the case $N_{P'} = N_P$ and $N_{Q'} = N_P - N_{P'} = 0$ the multi-reference perturbation expansion terminates at zeroth order, and corresponds to a full diagonalization within the P -space. Another option is to use for example the coupled cluster method as exposed in references [46, 47].
5. Start from top again with a larger set of single-particle orbits, and continue until a convergence criterion is reached.

We illustrate these various choices of model spaces in the following two figures. figure 4.9 defines our model space for the Lee-Suzuki similarity transformation at the two-body level. This corresponds to steps one and two in the above algorithm. The set of single-particle orbits defines the last single-particle orbit in the model space n_{sp} . Note that we could have chosen a model space defined by a cut in energy, as done by the No-Core collaboration, see for example references [38, 39, 40, 41]. These examples serve just to illustrate the algorithm. Figure 4.10 demonstrates again a possible division of the three- and many particle space into the full model space P and a smaller space P' . Again, this figure serves only the purpose of illustrating the method. In our actual calculations we define the smaller space P' via an energy cut in the real and imaginary eigenvalues and selected many-body configurations.

In summary, defining a set of single-particle orbits in order to construct the two-body and many-body model spaces, we obtain first an effective two-body interaction in the space P_{2p} by performing the Lee-Suzuki [99, 100, 101, 102] transformation. This interaction and the pertinent single-particle orbits are then used to define a large many-body space. It is therefore of interest to see if we can reduce this dimensionality through the definition of smaller spaces and perturbative corrections.

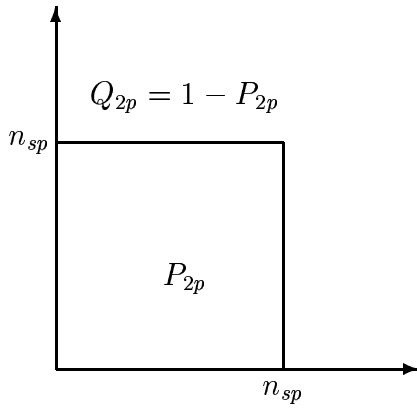


Figure 4.9: Possible definition of the two-body exclusion operator $Q_{2p} = 1 - P_{2p}$ used to compute the Lee-Suzuki similarity transformation and its effective interaction at the two-body level. The border of the model space is defined by the last single-particle orbit n_{sp} .

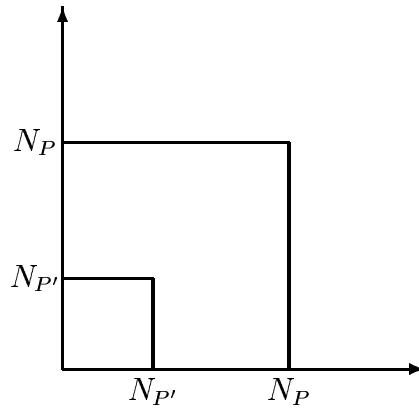


Figure 4.10: Possible definition of many-body space N_P and reduced space N'_P .

4.6 Inclusion of Realistic Nucleon-Nucleon Interactions in Gamow Shell Model Calculations.

In microscopic nuclear many-body calculations, the strong short range repulsion in realistic nucleon-nucleon interactions complicates the calculations considerably since the repulsive core makes a perturbative treatment unsuitable. Therefore we wish to construct a renormalized interaction in a model space, which smoothes out the repulsive core of the bare nucleon-nucleon interaction. Typically, the renormalized nucleon-nucleon interaction has been constructed from the Brueckner G-matrix approach (see reference [111]). The G-matrix is a soft interaction, which is obtained by resumming in-medium particle-particle scattering. The renormalized G-matrix is both energy dependent. It can also be nucleus dependent if one defines a specific closed shell core. This may cause difficulties if one wishes to extend the G-matrix to drip line nuclei.

Recently, an alternative approach which integrates out the high momentum components of the nucleon-nucleon interactions has been proposed [116, 117, 118, 119]. Using a similarity transformation of the two-nucleon Hamiltonian, a Hermitian soft-core effective nucleon-nucleon interaction is obtained in a model space defined by a cutoff Λ in the relative momentum between the nucleons. This effective interaction has become known, as a low-momentum nucleon-nucleon (LMNN) interaction, $V_{\text{low-}k}$. The $V_{\text{low-}k}$ is an energy and nucleus independent effective interaction, which depends only the model space cutoff Λ and the bare nucleon-nucleon interaction. The effective low-momentum interaction ($V_{\text{low-}k}$)

is constructed in such a way that it reproduces exactly the main characteristics of the nucleon-nucleon wave function in the full space. The interaction $V_{\text{low-}k}$ can be a promising approach for nuclei along the drip lines.

Here we show that it is possible to obtain an interaction $V_{\text{low-}k}$ in the complex k -plane, starting with the momentum space Schrödinger equation defined on an inversion symmetric contour L^+ . As an illustration we construct an interaction $V_{\text{low-}k}$ on a purely rotated contour using the realistic CD-Bonn nucleon-nucleon interaction [96]. The effective interaction may then be the basic input in microscopic calculations of many-body resonances or the calculation of specific diagrams such as the Hartree-Fock diagram discussed here.

In the following we outline the procedure for obtaining a complex symmetric interaction $V_{\text{low-}k}$, based on the Lee-Suzuki similarity transformation for complex interactions (see Section 4.3) and the Contour Deformation Method (see Section 3.2). Starting with the transformed momentum space Schrödinger equation,

$$\int_{L^+} dk' k'^2 \langle k^* | T + V | k' \rangle \langle k'^* | \psi_n \rangle = E_n \langle k^* | \psi_n \rangle, \quad (4.104)$$

where the plane wave states are eigenfunctions of the kinetic energy operator and where they form a complete set

$$1 = \int_{L^+} dk k^2 |k\rangle \langle k^*. \quad (4.105)$$

The momentum space Schrödinger equation is solved as a matrix equation by discretizing the integration contour L^+ by some suitable quadrature rule, e.g. Gauss-Legendre quadrature. The discretized Schrödinger equation becomes on the chosen contour

$$\sum_j w_j k_j^2 \langle k_i^* | T + V | k_j \rangle \langle k_j^* | \psi_n \rangle = E_n \langle k_i^* | \psi_n \rangle. \quad (4.106)$$

Here k_i are the integration points and w_i the corresponding quadrature weights. Introducing the modified plane wave kets $|\bar{k}_i\rangle = k_i \sqrt{w_i} |k_i\rangle$, equation (4.106) becomes

$$\sum_j \langle \bar{k}_i^* | T + V | \bar{k}_j \rangle \langle \bar{k}_j^* | \psi_n \rangle = E_n \langle \bar{k}_i^* | \psi_n \rangle. \quad (4.107)$$

where we have

$$1 = \sum_{i=1}^N |\bar{k}_i\rangle \langle \bar{k}_i^*|, \quad \langle \bar{k}_i^* | \bar{k}_j \rangle = \delta_{i,j}. \quad (4.108)$$

The matrix elements of the Hamiltonian becomes in the plane wave basis

$$H_{i,j} = \langle \bar{k}_i^* | T + V | \bar{k}_j \rangle = \frac{k_i^2}{2\mu} \delta_{i,j} + \sqrt{w_i w_j} k_i k_j V_l(k_i, k_j). \quad (4.109)$$

The full space is now divided in a model space P and an orthogonal complement space Q . The model space P consists of the N_P plane wave states lying below some cutoff Λ in momentum, and the Q -space consists of the remaining states, i.e.

$$P = \{|\bar{k}_p\rangle, |k| \leq \Lambda\}, \quad Q = \{|\bar{k}_q\rangle, \Lambda < |k| < \infty\}. \quad (4.110)$$

In order to obtain an effective interaction in the model space P , the decoupling condition in equation (4.26) has to be fulfilled and we have to solve for the transformation operator ω in equation (4.30). Given the transformation matrix ω in the plane wave basis, $\langle \bar{k}_q^* | \omega | \bar{k}_p \rangle$, the low-momentum effective nucleon-nucleon interaction ($V_{\text{low-k}}$), of the Okubo form (see equation (4.53)) is given by

$$\begin{aligned} \langle \bar{k}_p^* | V_{\text{low-k}} | \bar{k}_p' \rangle &= \sum_{k_p''} \sum_{k_p'''} \langle \bar{k}_p^* | (P + \omega^\text{T} \omega)^{1/2} | \bar{k}_p'' \rangle \langle \bar{k}_p'''^* | H_{LS} | \bar{k}_p''' \rangle \langle \bar{k}_p'''^* | (P + \omega^\text{T} \omega)^{-1/2} | \bar{k}_p' \rangle \\ &- \frac{k_p^2}{2\mu} \delta_{k_p, k_p'}, \end{aligned} \quad (4.111)$$

see section 4.3 for further details. The effective interaction in the original plane wave basis $|k_i\rangle$ is then obtained by

$$\langle k_i^* | V_{\text{low-k}} | k_j' \rangle = \frac{\langle \bar{k}_i^* | V_{\text{low-k}} | \bar{k}_j' \rangle}{\sqrt{w_i w_j} k_i k_j}, \quad (4.112)$$

where $\{|k_i\rangle, |k_j\rangle\} \in P$.

The aim is to obtain a realistic effective nucleon-nucleon interaction, which is applicable in microscopic calculations of many-body resonances, an interaction which takes the continuum properly into account. As discussed in detail in the previous sections, the nucleon-nucleon interaction has to be analytically continued onto the second energy sheet, in order to obtain resonances in the calculated spectrum. From a CDM perspective, we wish then to obtain a low-momentum nucleon-nucleon interaction, $V_{\text{low-k}}$, on an inversion symmetric contour in the complex k -plane. Here we illustrate how this may be achieved for the realistic CD-Bonn [96] interaction. A constraint on the theory, is that all low-energy characteristics of the nucleon-nucleon system are conserved. We consider a contour L^+ of the simplest kind, which is just a purely rotated contour in the k -plane. See figure 4.11 for an illustration of the contour.

Having obtained $V_{\text{low-k}}$ by solving equation (4.111), the momentum space Schrödinger equation for the low momentum nucleon-nucleon interaction becomes on the rotated contour $L_\Lambda^+ \equiv \exp(-i\theta)|k|$, $|k| \leq \Lambda$,

$$\int_0^{|k'|=\Lambda} dk' k'^2 \langle k^* | T + V_{\text{low-k}} | k' \rangle \langle k'^* | \psi_n \rangle = E_n \langle k^* | \psi_n \rangle, \quad (4.113)$$

with $k = \exp(-i\theta)|k|$. Discretizing the contour defined from $|k| = 0$ to $|k| = \Lambda$, the matrix equation is obtained

$$\sum_j \langle \bar{k}_i^* | T + V_{\text{low-k}} | \bar{k}_j \rangle \langle \bar{k}_j^* | \psi_n \rangle = E_n \langle \bar{k}_i^* | \psi_n \rangle, \quad (4.114)$$

with the matrix elements of the Hamiltonian given by

$$H_{i,j} = \langle \bar{k}_i^* | T + V_{\text{low-k}} | \bar{k}_j \rangle = \frac{k_i^2}{2\mu} \delta_{i,j} + \sqrt{w_i w_j} k_i k_j V_{\text{low-k}}(k_i, k_j). \quad (4.115)$$

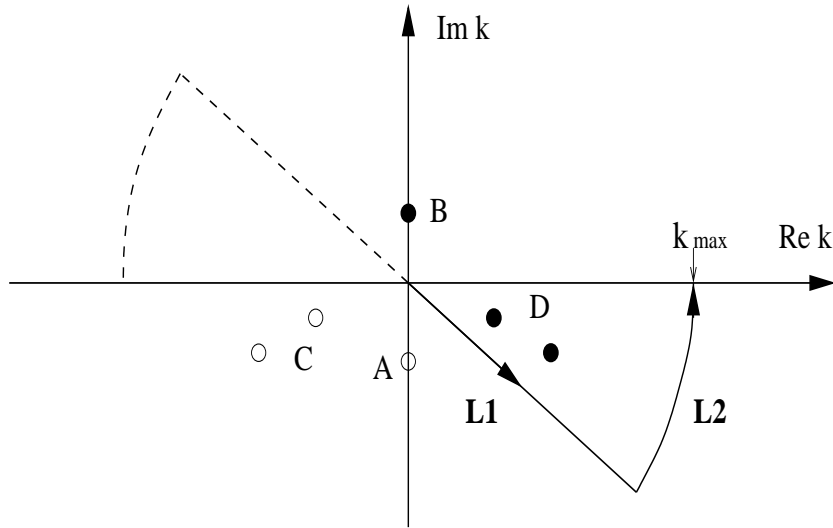


Figure 4.11: Contour $L^+ = L_1 + L_2$ is given by the solid line, while the contour L^- is given by the dashed line. The contour $L = L^+ + L^-$ is clearly *inversion symmetric*. The two body spectrum which is exposed by this contour is marked by filled circles \bullet and the excluded spectrum by open circles \circ . The full spectrum includes bound states (B), antibound (A), decay (D) and capture (C) resonant states.

A two-dimensional interpolation routine is used in order to obtain $V_{\text{low-}k}$ at arbitrary points on the contour L_A^+ . Figure 4.12 gives a plot of the diagonal part of $V_{\text{low-}k}$ (dashed line) interaction, using a cutoff $\Lambda = 2\text{fm}^{-1}$, and the original CD-Bonn (solid line) nucleon-nucleon interaction for the deuteron channel ${}^3S_1 - {}^3D_1$, for the non-scaled case ($\theta = 0$). In references [117, 116] it was shown that the binding energy of the deuteron and the scattering phase shifts below $E_{\text{lab}} < 300\text{MeV}$ using $V_{\text{low-}k}$ for a model space cutoff $\Lambda = 2\text{fm}^{-1}$, reproduce exactly the ones obtained from the original nucleon-nucleon interaction. This is only to be expected since a similarity transformation of the Hamiltonian does not change the energies. However, as shown in reference [117] the D -state probability of the deuteron is not reproduced for momentum cutoffs smaller than $\Lambda \sim 4 - 5\text{fm}^{-1}$, see also table 4.2 for the non-scaled case $\theta = 0$. The exact value of the D -state probability is retained for these values of Λ , by using the corresponding similarity transformed projection operator onto the D -state. In reference [117] the application of $V_{\text{low-}k}$ in calculation of the binding energy of the nuclei ${}^3\text{H}$, ${}^4\text{He}$ and ${}^{16}\text{O}$ where studied. It was found, in comparison with exact calculations using the bare nucleon-nucleon interaction, that a satisfactory convergence for the binding energies were obtained for a momentum cutoff $\Lambda \geq 5\text{fm}^{-1}$. In addition the convergence of the single-particle energies in ${}^{16}\text{O}$ were studied, and also here a satisfactory convergence was obtained for $\Lambda \geq 5\text{fm}^{-1}$.

In table 4.2 we show results for the deuteron binding energy and the D -state probability for different cutoffs Λ , for the non-scaled case ($\theta = 0$) and the complex scaled case ($\theta = \pi/6$). The deuteron binding energy is reproduced for all cutoffs, as expected. It is seen

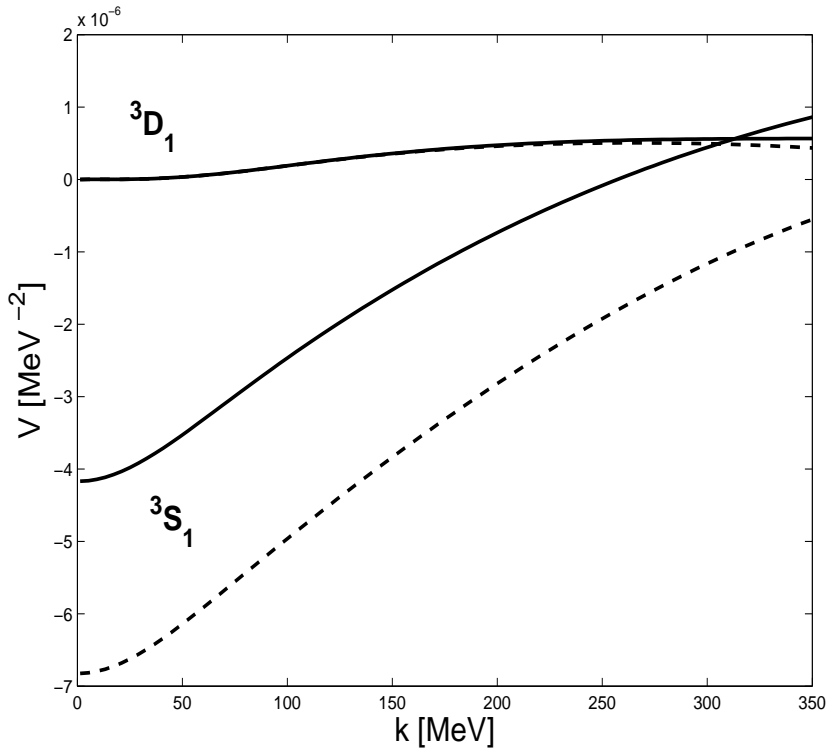


Figure 4.12: Plot of the diagonal part of the $V_{\text{low-}k}$ (dashed line) interaction, using a cutoff $\Lambda = 2\text{fm}^{-1}$, and the original CD-Bonn (solid line) nucleon-nucleon interaction for the deuteron channel $^3S_1 - ^3D_1$, for the non-scaled case ($\theta = 0$). In the plot the momentum k is given in MeV.

that the D -state probability, for the non-scaled case ($\theta = 0$), decreases monotonically for smaller and smaller cutoff Λ . The D -state probability saturates at the exact value for a cutoff $\Lambda \sim 5\text{fm}^{-1}$, this is consistent with the findings in references [117, 118, 119] where the ground state energy of the considered nuclei ${}^3\text{H}$, ${}^4\text{He}$ and ${}^{16}\text{O}$ are converged for a cutoff $\Lambda \geq 5\text{fm}^{-1}$.

It is also seen for the complex scaled case ($\theta = \pi/6$) that the deuteron binding energy is reproduced at all values of Λ . Further it is observed that the D -state probability saturates at the exact value even slower than in the non-scaled case. It is seen that for $\lambda < 5\text{fm}^{-1}$ the D -state probability acquires in addition to the real part, a considerable imaginary part. In this case a satisfactory converged D -state probability is obtained for a cutoff $\Lambda \geq 7\text{fm}^{-1}$. This gives an indication of the cutoff Λ required to give converged results in nuclear structure calculations, using complex scaled low-momentum nucleon-nucleon interactions.

Λfm^{-1}	$\theta = 0$			$\theta = \pi/6$			
	$\text{Re}[E_d]$	$\text{Im}[E_d]$	$P_D(\%)$	$\text{Re}[E_d]$	$\text{Im}[E_d]$	$\text{Re}(P_D(\%))$	$\text{Im}(P_D(\%))$
1.	-2.2246	0.	1.22	-2.2246	-1.5E-05	0.64	-1.39
2.	-2.2246	0.	3.56	-2.2246	-1.5E-05	4.05	-2.11
3.	-2.2246	0.	4.56	-2.2246	-1.6E-05	5.41	-0.58
4.	-2.2246	0.	4.81	-2.2246	-1.1E-05	5.05	8.E-02
5.	-2.2246	0.	4.85	-2.2246	-3.1E-05	4.86	6.E-02
6.	-2.2246	0.	4.85	-2.2246	-1.5E-05	4.84	2.E-02
7.	-2.2246	0.	4.85	-2.2246	-1.5E-05	4.85	-8.E-05
8.	-2.2246	0.	4.85	-2.2246	-1.5E-05	4.85	-3.E-03
9.	-2.2246	0.	4.85	-2.2246	-1.7E-05	4.85	-2.E-03
∞	-2.2246	0.	4.85	-2.2246	-1.5E-05	4.85	-1.E-05
Reference [96]	-2.2246	0.	4.85				

Table 4.2: Deuteron binding energy (in MeV) as function of cutoff Λ (in fm^{-1}), and D -state probability $P_D(\%)$. The non-scaled $\theta = 0$ and complex scaled $\theta = \pi/6$ Hamiltonians are considered.

Figure 4.13 gives a plot of the real (left plot) and imaginary (right plot) parts of the diagonal part of the complex scaled $V_{\text{low-}k}$ (dashed line), using a cutoff $\Lambda = 2\text{fm}^{-1}$, and the corresponding complex scaled CD-Bonn interaction (solid line), for the deuteron channel. It is seen that the imaginary part of $V_{\text{low-}k}$ is far from zero at $k = 0\text{fm}^{-1}$, which imply that the imaginary part of the effective potential in this case does not solely originate from the complex scaled momenta k . The unphysical imaginary part which occur for the D -state probability at $\Lambda = 2\text{fm}^{-1}$ may therefore be traced back to the non-zero imaginary part of $V_{\text{low-}k}$ at $k = 0\text{fm}^{-1}$. Figure 4.14 gives a plot of the real (left plot) and imaginary (right plot) parts of the diagonal part of the complex scaled $V_{\text{low-}k}$ (dashed line), using a cutoff $\Lambda = 7\text{fm}^{-1}$, and the corresponding complex scaled CD-Bonn interaction (solid line), for the

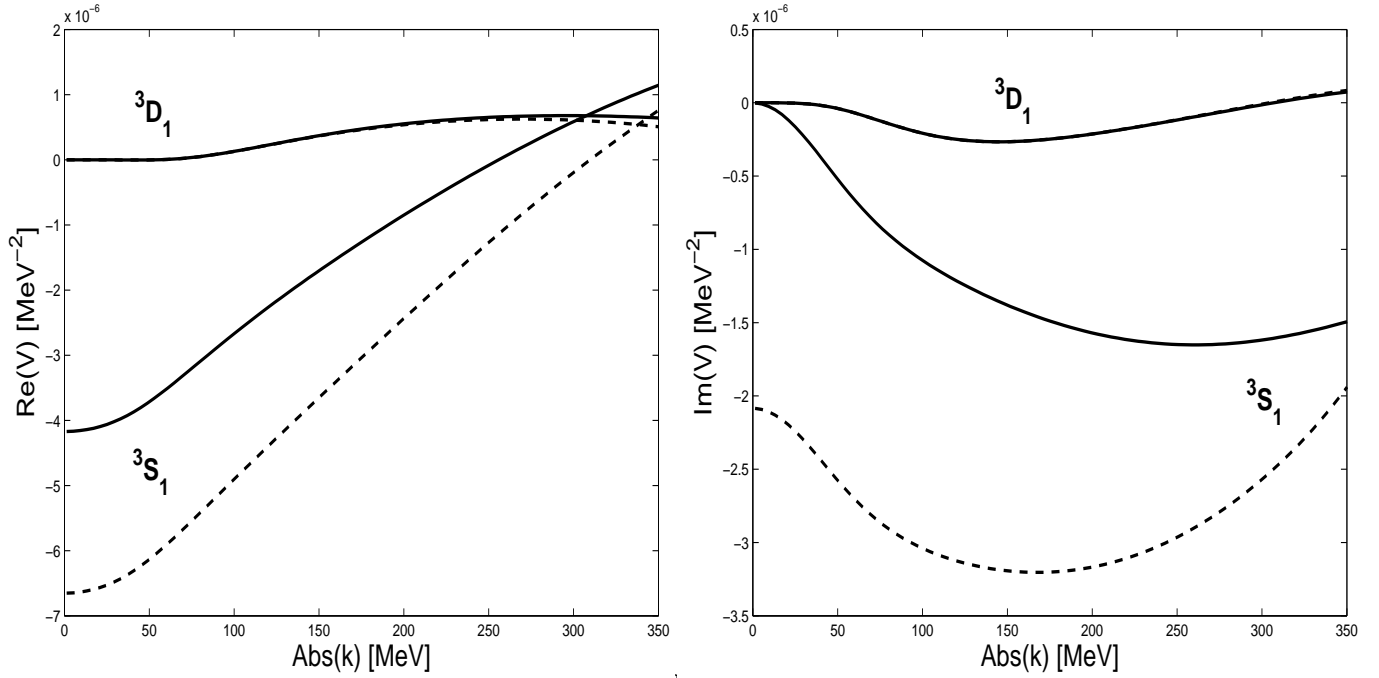


Figure 4.13: Plot of the real (left plot) and imaginary (right plot) part of the complex scaled $\theta = \pi/6$ low-momentum nucleon-nucleon interaction (dashed line), for a model space cutoff $\Lambda = 2\text{fm}^{-1}$. The corresponding complex scaled CD-Bonn interaction is given by the solid line. Here the diagonal part of the interaction for the deuteron channel ${}^3S_1 - {}^3D_1$ is shown. In the plot the momentum k is given in MeV.

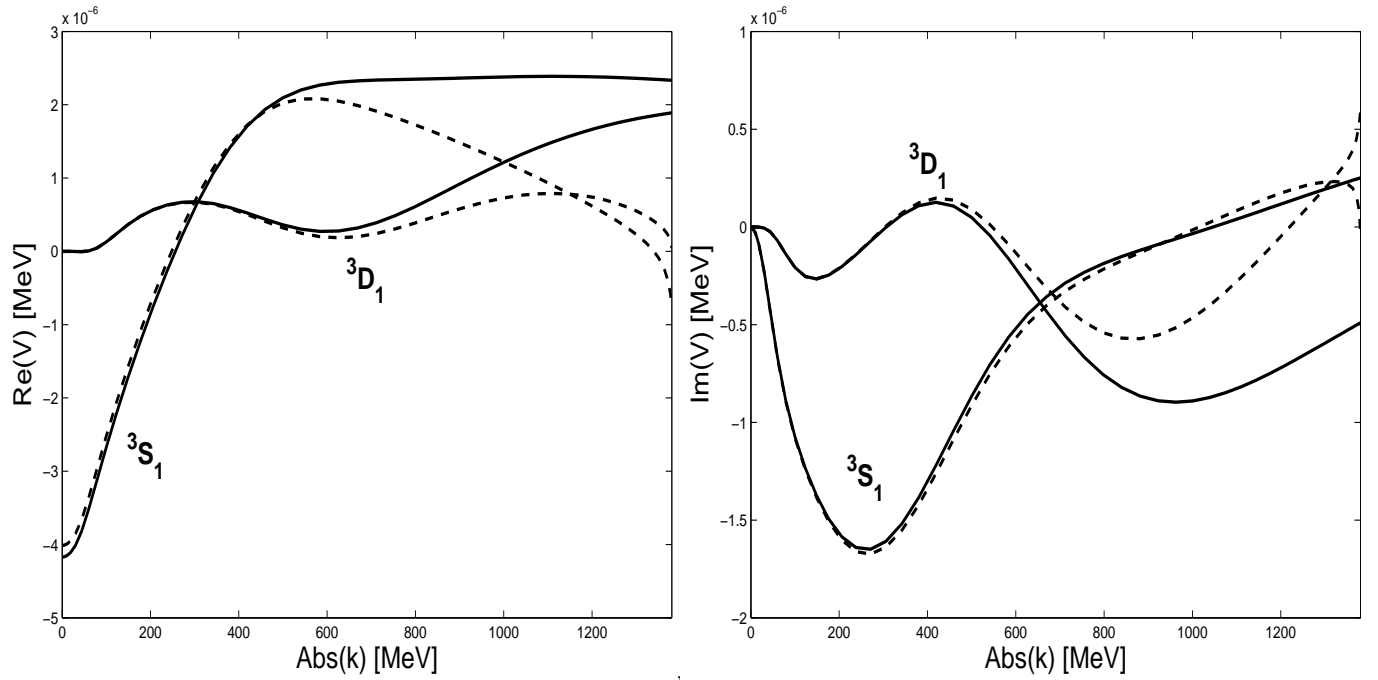


Figure 4.14: Plot of the real (left plot) and imaginary (right plot) parts of the complex scaled $\theta = \pi/6$ low-momentum nucleon-nucleon interaction (dashed line) for a model space cutoff $\Lambda = 7\text{fm}^{-1}$. The corresponding complex scaled CD-Bonn interaction is given by the solid line. Here the diagonal part of the interaction for the deuteron channel ${}^3\text{S}_1 - {}^3\text{D}_1$ is shown. In the plot the momentum k is given in MeV.

deuteron channel. In this case it is seen that the imaginary part of $V_{\text{low-}k}$ is approaching zero for $k \rightarrow 0\text{fm}^{-1}$. This imply that there is no imaginary part in $V_{\text{low-}k}$ except for the complex scaled momenta k . By considering the D -state probability at $\Lambda = 7\text{fm}^{-1}$ we also observe that the exact D -state probability is reproduced in this case. The cutoff Λ at which $V_{\text{low-}k}$ has this property is of course dependent on the complex scaling angle θ . For $\theta \rightarrow 0$ the results for the non-scaled $V_{\text{low-}k}$ is retained. One may conclude from this survey of the properties of complex scaled low-momentum nucleon-nucleon interactions, that one must be careful in choosing a model space cutoff Λ when applying $V_{\text{low-}k}$ in microscopic nuclear structure calculations. However, the present study offers a promising approach for study of resonant structures in nuclear many-body systems, starting with realistically derived nucleon-nucleon interactions. The first application, which is under preparation, is to calculate self consistently Hartree-Fock single-particle energies of loosely bound nuclei using a complex scaled $V_{\text{low-}k}$. This approach, allows for a self-consistent treatment of both single-particle bound states and single-particle resonant states.

Chapter 5

Paper 1.

5.1 Introduction to Paper 1.

Paper 1 discusses how the momentum space Schrödinger equation may be analytically continued to the second energy sheet. The method of analytical continuation is based on deforming (distorting) the integration contour, and this method is commonly known as the Contour Deformation Method (CDM). The rules for analytical continuation of integral equations are discussed, and as an example the Schrödinger equation for the Malfliet-Tjon potential, which is a nucleon-nucleon potential consisting of Yukawa terms, is analytically continued to the second Riemann sheet. It is found, by choosing a suitable deformed contour (rotation+translation), that the analytical structure of the Malfliet-Tjon potential allows for a continuation into the third quadrant of the complex k -plane, and consequently the Contour Deformation Method allows for a study of antibound (virtual) states as well as decaying resonances. Further, CDM is an alternative approach to the full solution of the off-shell scattering amplitude. In the case of potentials consisting of Yukawa terms, choosing a rotated+translated contour which avoids the singularities of the potential, allows for a complete solution of the t -matrix in a large momentum range. Not only does CDM give us information of the complete pole structure of the scattering matrix but also the scattering amplitude is obtainable by expanding the Green's function in a complete set of Berggren states. Expanding the Green's function in a complete set of states, consisting of bound, resonant and non-resonant continuum states allows for a separate study of the resonant contributions to the scattering amplitude. Disentangling the resonant behaviour of the scattering amplitude from the smooth continuum background is gives interesting insights, since the most interesting process taking place in the continuum is the production of resonance phenomena. Finally CDM is applied to the CD-Bonn interaction, which is a realistic nucleon-nucleon potential, and antibound states in the isospin triplet channel 1S_0 are solved for.

5.2 *The contour deformation method in momentum space,
applied to subatomic physics.*

G. Hagen, J. S. Vaagen and M. Hjorth-Jensen

J. Phys. A: Math. Gen., **37**, 8991 (2004).

The contour deformation method in momentum space, applied to subatomic physics

G Hagen¹, J S Vaagen¹ and M Hjorth-Jensen²

¹ Department of Physics and Technology, University of Bergen, N-5000 Bergen, Norway

² Department of Physics and Center of Mathematics for Applications, University of Oslo,
N-0316 Oslo, Norway

E-mail: gaute.hagen@ift.uib.no, jans.vaagen@ift.uib.no and morten.hjorth-jensen@fys.uio.no

Received 5 May 2004

Published 8 September 2004

Online at stacks.iop.org/JPhysA/37/8991

doi:10.1088/0305-4470/37/38/006

Abstract

A generalized contour deformation method (CDM), which combines complex rotation and translation in momentum space, is discussed. CDM gives accurate calculation of two-body spectral structures: bound, antibound, resonant and continuum states forming a Berggren basis. It provides a basis for full off-shell t -matrix calculations both for real and complex input energies. Results for both spectral structures and scattering amplitudes compare perfectly well with exact values for the analytically solvable separable non-local Yamaguchi potential as a testcase. Accurate calculation of antibound states in the Malfliet–Tjon and the realistic CD–Bonn nucleon–nucleon potential are presented. Calculation of antibound states in the CD–Bonn potential are not known to have been given elsewhere.

PACS numbers: 03.65.Nk, 24.30.Gd

(Some figures in this article are in colour only in the electronic version.)

1. Introduction

In nuclear physics, as in atomic physics, the expansion of many-body wavefunctions on single-particle bases, generated by a suitable potential has been a common practice. For a given potential the single-particle eigenstates form a complete set of states,

$$\mathbf{1} = \sum_b |\psi_{nl}\rangle\langle\psi_{nl}| + \frac{1}{2} \int_{-\infty}^{\infty} dk k^2 |\psi_l(k)\rangle\langle\psi_l(k)|. \quad (1.1)$$

A proof of this completeness relation, more precisely known as the *resolution of unity*, is given by Newton [1]. The relation also applies to the binary interaction of say two nucleons and their relative motion. The sum is over the bound states in the system, while the integral is over the positive energy continuum states. The infinite space spanned by this basis is given by all square integrable functions on the real energy axis, known as the L^2 space, which forms

a Hilbert space. In the case of a confining harmonic oscillator potential there is an infinite number of bound states and no continuum integral.

During the last decade the exploration of nuclear driplines has pushed traditional single-particle methods to their limits of applicability. The traditional shell-model with harmonic oscillator single-particle wavefunctions works well in the regime of well-bound nuclei. Moving towards the driplines, however, the nuclei cease to be well bound, and coupling to continuum structures plays an important role. A modification of the shell model where bound, resonant and continuum states are treated on equal footing has been under development the last few years, and has become known as the *Gamow shell model*; see [2–6]. The first attempt to also include antibound states in a realistic nuclear calculation is that of Vertse *et al* [7], where the role of antibound states in the pole RPA description of the giant monopole resonance was investigated. Recently, the role of anti-bound states in the Gamow shell model description of halo nuclei has been discussed [8].

The study of two-body resonant structures has a long history in theoretical physics. There exists a variety of methods described in textbooks; see e.g. [1, 9–11]. Among the more popular methods are those of analytic continuation; the complex scaling method (CSM) and the method based on analytic continuation in the coupling constant (ACCC).

In this work, we consider an approach formulated for integral equations in momentum space. The method is based on deforming contour integrals in momentum space, and is known as the contour deformation or distortion method (CDM). It has been shown in [12] that a *contour rotation* in momentum space is equivalent to a rotation of the corresponding differential equation in coordinate space. The coordinate space analogue is often referred to as the *dilation group transformation* or *complex scaling*. The *dilation group transformation* was first formulated and discussed in [13, 14], and was developed to examine the spectrum of the Green's function on the second energy sheet.

The CDM formulated *in momentum space* is not new in nuclear physics. It was studied and applied in the 1960s and 1970s; see, for example, [15–18], especially in the field of three-body systems. Most of these references applied a *contour rotation* in momentum space. By restricting oneself to a rotated contour certain limitations and restrictions however appear in the equations, determined by the analytical structure of the integral kernels and potentials. In [18] a more sophisticated choice of contour, based on rotation and translation, was applied to the three-nucleon momentum space Faddeev equation for a separable Yamaguchi interaction. This choice of contour made it possible to avoid the logarithmic singularities of the Faddeev kernel and, hence, allowed for a continuation in energy to the non-physical energy sheet.

A revitalizing of the contour deformation method in momentum space is in place, given the new theoretical challenges of dripline physics. CDM is a method which allows for accurate and stable solutions of bound, anti-bound, capture and decay states. We consider a generalized type of contour, allowing for an analytic continuation into the third quadrant of the complex k -plane. Antibound and capture states near the scattering threshold may then be calculated at a specified accuracy. This choice of contour may be regarded as belonging to the *Berggren class* of contours [19]. Berggren [19], and later Lind [20], studied various completeness relations derived by analytic continuation of the completeness relation, stated in equation (1.1), to the complex plane. The Berggren completeness includes discrete summation over resonant as well as bound states. Our choice of contour differs from recent applications of the Berggren formalism (see e.g. [2–6]), in that the contour approaches infinity along complex rays in the complex k -plane as opposed to contours which approach infinity along the real k -axis. We will point out the intimate relationships between complex coordinate scaling, the general Berggren basis and the method of continuation of the scattering equations to the second energy sheet by contour deformation.

Complex scaling *in coordinate space* has for a long time been used extensively in atomic and molecular physics (see [21]). During the last decade it has also been applied in nuclear physics, as interest in loosely bound nuclear halo systems has grown (see e.g. [22–24]). Complex scaling in coordinate space is usually based on a variational method [21], and an optimal variational basis and scaling parameters have to be sought. One of the disadvantages of the coordinate space approach is that the boundary conditions have to be built into the equations, and convergence may be slow if the basis does not mirror the physical outgoing boundary conditions well.

There are several advantages in considering the contour deformation method in momentum space. First, most realistic potentials derived from field theoretical considerations are given explicitly in momentum space. Secondly, the boundary conditions are automatically built into the integral equations. Moreover, the Gamow states (physical resonances) [9] in momentum space are non-oscillating and rapidly decreasing, even for Gamow states with large widths, far from the real energy axis, as opposed to the complex-scaled coordinate space counterpart. The latter states are represented by strongly oscillating and exponentially decaying functions. Finally, numerical procedures are often easier to implement and check. Convergence is easily obtained by just increasing the number of integration points in the numerical integration.

If one restricts the deformation to a rotation of the contour, as studied in [15–17, 25, 26], one is not able to expose antibound states in the energy spectrum, since the maximum allowed rotation angle does not allow rotation into the third quadrant of the complex momentum plane. This limitation is sometimes used as an argument for advocating other approaches, such as the ACCC method; see the recent work of Aoyama [27]. We will show that by distorting the contour by *rotation and translation* into the third quadrant of the complex k -plane, we are able to introduce a new feature to the complex scaling method, namely *accurate calculation of antibound states as well as bound and resonant states*. CDM represents also an alternative to the so-called *exterior complex scaling* method. The *exterior complex scaling* method was just formulated to avoid intrinsic non-analyticities of the potential, and in this way calculation of resonances in *non-dilation* analytic potentials are made possible (see [21] and references therein).

The contour deformation method has also been applied to the solution of the full off-shell scattering amplitude (t -matrix); see [12, 16, 17, 28]. By rotating the integration contour, an integral equation is obtained with a compact integral kernel. This has numerical advantages as the kernel is no longer singular. As discussed in [16], a rotation of the contour gives certain restrictions on the rotation angle and maximum incoming/outgoing momentum in the scattering amplitude. We will again show that our extended choice of contour in momentum space avoids all these limitations and that an accurate calculation of the scattering amplitude can be obtained. Thus, the method we advocate allows us to give an accurate calculation of the full energy spectrum. Moreover, it yields a powerful method for calculating the full off-shell complex scattering amplitude (t -matrix). It is also rather straightforward to extend this scheme to in-medium scattering in, for example, infinite nuclear matter.

In section 2, we outline the CDM in momentum space and discuss its relation to the Berggren completeness, deriving the states of the Malfliet–Tjon nucleon–nucleon interaction as an example. The corresponding Berggren basis is used for convergence studies. As an additional example the states of the CD–Bonn interaction [29] are also calculated, the antibound state for the first time. In section 3, the Berggren representation of the full off-shell t -matrix is given, together with various applications of CDM to the scattering of the Malfliet–Tjon interaction [30]. Section 4 gives expansion of the eigenvalue problem for the analytically solvable separable non-local Yamaguchi [10, 31] interaction on a Malfliet–Tjon Berggren basis. Comparison between analytic and numerical results are given for antibound

and resonant states. Finally, in section 5, we study the expansion of a resonant state generated by a Gaussian interaction on a Berggren basis given by the Malfliet–Tjon interaction. The energy and wavefunction are studied as a function of cutoff in momentum/energy of the complex continuum states entering the Berggren completeness.

2. Berggren spectral decomposition in momentum space

2.1. The contour deformation method

The momentum space Schrödinger equation, for relative motion in partial wave l in a central potential, reads

$$\frac{\hbar^2}{2\mu} k^2 \psi_{nl}(k) + \frac{2}{\pi} \int_0^\infty dq q^2 V_l(k, q) \psi_{nl}(q) = E_{nl} \psi_{nl}(k). \quad (2.1)$$

With real momenta the momentum space Schrödinger equation corresponds to a hermitian Hamiltonian. The energy eigenvalues will in this case always be real, corresponding to discrete bound states ($E_{nl} < 0$) and a continuum of scattering states ($E_{nl} > 0$). Resonant and antibound states can never be obtained by directly solving equation (2.1), as it stands. In a sense, one can say that the spectrum of a hermitian Hamiltonian does not display all information about the physical system.

Generalizing k to the complex k -plane, i.e. $k = \text{Re}[k] + i\text{Im}[k]$, an integral equation for the bound state wavefunctions appearing in equation (2.1) may be written as

$$\psi_{nl}(k) = \frac{1}{E_{nl} - k^2/2\mu} \frac{2}{\pi} \int_0^\infty dq q^2 V_l(k, q) \psi_{nl}(q). \quad (2.2)$$

$\psi(k)$ is analytic in the upper-half complex k -plane corresponding to the physical energy sheet, except for simple poles at the bound state energies (positive imaginary k) and a cut in the complex E -plane along the real energy axis. The interaction between the particles, $V_l(k, q)$ is assumed to be spherically symmetric without tensor components. Our discussion does not involve the particle spins explicitly. The Fourier–Bessel transform of a non-local potential $V_l(r, r')$ in coordinate space is given by

$$V_l(k, k') = \int_0^\infty dr r^2 \int_0^\infty dr' r'^2 j_l(kr) j_l(k'r') V_l(r, r'). \quad (2.3)$$

In the case of a local potential,

$$V_l(r, r') = \frac{\delta(r - r')}{r^2} V_l(r),$$

and equation (2.3) reduces to

$$V_l(k, k') = \int_0^\infty dr r^2 j_l(kr) j_l(k'r) V_l(r). \quad (2.4)$$

The interaction in momentum space is given in units of MeV fm³.

In the following we study and explore the resonant and antibound state spectra by the contour deformation method.

Antibound states are not to be interpreted as physical states, i.e. a quantal system cannot be put in such a state. Nevertheless, antibound states close to the scattering threshold may have impact on observables such as phase shifts. For a system with antibound states close to the scattering threshold, a large enhancement of the scattering cross-section will take place. This enhancement can be understood in terms of the antibound states; see [8] for a discussion of scattering wavefunctions close to threshold in the presence of a nearby bound or antibound

state. From a mathematical point of view an antibound state is defined as a pole of the scattering matrix located on the negative imaginary k -axis.

Resonant states can be divided into two subclasses: decay and capture states. Decay states are associated with poles of the scattering matrix located in the fourth quadrant of the complex k -plane. They have outgoing boundary conditions at infinity. Capture states are on the other hand associated with poles in the third quadrant of the complex k -plane, and have incoming waves at infinity. Naturally only capture states can be given physical meaning. Capture states may be interpreted as quasi-stationary states formed inside a potential barrier in the positive energy regime.

Resonant states will have a definite lifetime before they decay through the barrier. This lifetime varies inversely with the probability of tunnelling through the barrier, and the probability of tunnelling is given by the width Γ of the resonant states. The width is in turn given by the absolute value of the imaginary part of the resonance energy squared. The closer the resonance energy is to the real energy axis, the smaller the width becomes and the lifetime of the quasi-stationary states increases. This indicates that resonant states with energy close to the real energy axis may have larger impact on observable quantities, e.g. phase shifts and scattering cross-sections. Physical decay states are those with positive real energy. Gamow states are to be understood as physical resonant decay states close to the real energy axis, i.e. resonant states with narrow widths. In [9] a more detailed discussion of the interpretation and physical understanding of resonant states is given.

Antibound and resonant states are located on the second (non-physical) energy Riemann sheet. The momentum is a multivalued function of energy; $k(E) = \sqrt{2\mu E}$. Multivalued functions may be represented by Riemann surfaces of branch cuts. The upper-half complex k -plane and the lower-half complex k -plane maps into the same complex energy plane. This problem is resolved by defining a Riemann surface with two sheets. The physical energy sheet (first sheet) is a mapping of the upper-half complex k -plane while the so-called *non-physical* energy sheet (second sheet) is a mapping of the lower-half complex k -plane (see e.g. [1]). To reach into the non-physical energy sheet where antibound and resonant states are to be found one has to analytically continue the scattering equations through the cut along the real energy axis and into the lower-half complex energy plane. We study here the analytic continuation of equation (2.1) into the non-physical sheet by the contour deformation method. Such a transformation of equation (2.1) can be obtained by an analytic continuation of the completeness relation of equation (1.1) to the complex k -plane.

Resonances are not normalizable in the normal sense. Due to their exponentially growing and oscillatory behaviour along the real r -axis the norm integral is divergent. Nevertheless, divergent integrals may be given a definite value by some regularization procedure. Zel'dovich [11] was the first to propose such a regularization procedure for making the norm integrals of resonances definite by adding a convergence factor $\exp(-\epsilon r^2)$ and then taking the limit $\epsilon \rightarrow 0$. This procedure is most convenient in analytic cases; in numerical applications taking the limit $\epsilon \rightarrow 0$ is difficult. Another regularization procedure which is more tractable from a numerical standpoint, is the method proposed by Gyarmati and Vertse [32]; they regularized the norm integrals by a complex rotation in the radial coordinate after a finite radial distance R . This procedure introduces an exponential damping to the growing oscillatory behaviour of the resonant wavefunctions, and numerical implementation of expectation values involving resonant states is made possible.

In the 1960s, Berggren discussed the use of resonant states in eigenfunction expansions of scattering and reaction amplitudes; see [19, 33–35]. He used the regularization procedure by Zel'dovich for resonant states. The resonant states form an incomplete set of states, and for completeness the non-resonant continuum states has to be taken into account. Berggren found

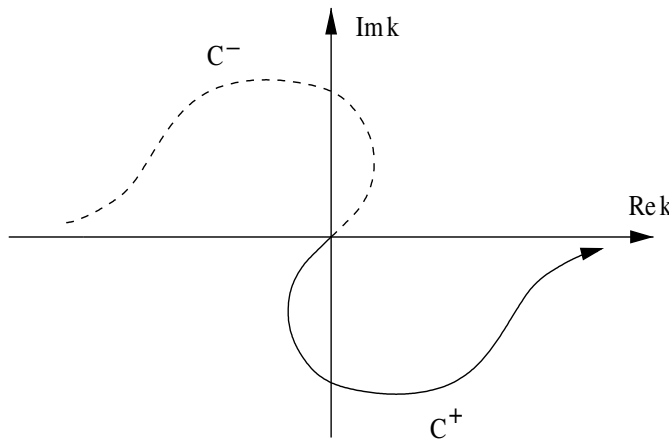


Figure 1. Plot of a general inversion symmetric contour $C = C^+ + C^-$ in the complex k -plane: C^+ is given by the solid line, while C^- is given by the broken line.

that the regularized resonant states along with a set of non-resonant continuum states defined on deformed contours in the complex momentum plane, form a bi-orthogonal set of states. This bi-orthogonal set can in turn be used as expansion basis for various physical quantities, where the resonant character of the system is displayed explicitly.

The method Berggren studied is based on analytic continuation of the completeness relation (see equation (1.1)) to the complex k -plane by deforming the integration contour. We give here a brief summary of the procedure which considers the integral in equation (1.1) as an integral over the contour $\Gamma = S + C$, where the contour C is defined on the real k -axis from $-\infty$ to $+\infty$ and the contour S is given by an infinite semicircle in the upper-half complex k -plane closing the contour Γ . The sum over bound states are then the residues calculated at the poles of the scattering matrix along the positive imaginary k -axis. The integration along the real axis may then be distorted into some *inversion symmetric* contour, meaning that if k is on C , then $-k$ is also on C . By redefining the completeness relation on distorted contours in the complex k plane, one can show by using Cauchy's residue theorem that the summation over discrete states will in general include bound, antibound and resonant states [20, 33]. By this procedure the norm integral of the resonant states is regularized along the distorted contours. In [20] completeness relations for various *inversion symmetric* contours in the complex k -plane were derived and discussed; all inversion symmetric contours will hereafter be labelled *Berggren class* of contours. The eigenfunctions defined along distorted contours form a *biorthogonal* set, and the normalization follows the generalized c -product [20, 21]

$$\langle\langle \psi_{nl} | \psi_{n'l} \rangle\rangle \equiv \langle \psi_{nl}^* | \psi_{n'l} \rangle = \delta_{n,n'}. \quad (2.5)$$

The most general completeness relation on an arbitrary *inversion symmetric* contour (see figure 1) $C = C^+ + C^-$ can then be written as

$$\mathbf{1} = \sum_{n \in C} |\psi_{nl}\rangle \langle \psi_{nl}^*| + \int_{C^+} dk k^2 |\psi_l(k)\rangle \langle \psi_l^*(k)|, \quad (2.6)$$

where C^+ is the distortion of the positive real k -axis, and C^- the distortion of the negative real k -axis.

Here the symmetry of the integrand has been taken into account, that is

$$\int_{C^-} dk k^2 |\psi_l(k)\rangle \langle \psi_l^*(k)| = \int_{C^+} dk k^2 |\psi_l(k)\rangle \langle \psi_l^*(k)|.$$

The summation is over all discrete states (bound, antibound and resonant states) located in the domain \mathbf{C} , defined as the area above the contour C , and the integral is over the non-resonant

complex continuum defined on C^+ . The space spanned by the basis given in equation (2.6) includes all square-integrable functions defined in the domain \mathbf{C} , defining a generalized Hilbert space. The complete basis could then be used to expand other resonant and antibound states (belonging to another Hamiltonian), defined in the region above the distorted contour. Such a complete basis is more flexible than a complete basis defined for only real energies. From the general completeness relation (2.6) one can deduce the corresponding eigenvalue problem, $H|\psi\rangle = E|\psi\rangle$. This eigenvalue problem represents the analytically continued Schrödinger equation onto a general distorted contour C^+ in the complex k -plane. The Hamiltonian will in this case be complex and non-hermitian, as Gamow and antibound states are included in the spectrum.

Above we discussed how a complex and non-hermitian eigenvalue value problem may be obtained by analytic continuation of the completeness relation through the cut and into the second (non-physical) energy sheet. In close analogy with the above discussion on completeness relations, the momentum space Schrödinger equation (2.1), defined on the positive real k -axis, may be directly continued to the lower-half complex k -plane. Thereafter a general completeness relation, like equation (2.6), may be inferred. We must emphasize that the requirement that the distorted contour must be *inversion-symmetric* is not sufficient when continuing the Schrödinger equation (2.1) into the third quadrant of the complex k -plane.

In analytic continuation of integral equations we state the general rule (see e.g. [9]):

Continuing an integral in the complex plane, the moving singularities of the integrand must not intercept the integration contour.

Applying the contour deformation method to the momentum space Schrödinger equation (2.1), we must deform the contour in such a way that an intercept with the singularities is avoided. The only moving singularities of the integral kernel in equation (2.1) are contained in the potential. The analytic continuation of equation (2.1) to the lower-half complex energy plane is a stepwise process where overlapping domains of analyticity are created. Each step of analytic continuation of the Schrödinger equation to the complex energy plane involves the following three steps:

- (i) The analyticity domain, D_1 , for the wavefunction $\psi(k)$ is determined (see equation (2.2)).
Except at the spectrum of the Hamiltonian, the analyticity of $\psi(k)$ is given by the potential $V(k, q)$, where q is real in the first step.
- (ii) Having determined the analyticity region D_1 in the lower-half k -plane, the integration in q along the real axis may be distorted onto a contour C_1^+ in the lower-half complex k -plane.
All points on the contour C_1^+ must be contained in the analyticity domain D_1 .
- (iii) A new analyticity domain D_2 is determined for the wavefunction $\psi(k)$. The domain D_2 is again determined by the singularity structure of the potential $V(k, q)$ where q is now on the distorted contour C_1^+ . If and only if the contour C_1^+ also lies in the new domain of analyticity D_2 , we may choose k on C_1^+ as well. This gives a closed integral equation, and the Schrödinger equation is transformed onto the contour C_1^+ .

This process of analytic continuation may be continued iteratively uncovering larger domains of interest in the complex energy plane. The choice of contour must therefore be based on the following.

- The contour must be *inversion-symmetric*.
- The contour must be located in overlapping domains of analyticity (see step (iii) above) and the wavefunction must admit analytic continuation onto the contour C^+ .
- The choice of contour must be based on an *a posteriori* knowledge of poles in each partial wave of the scattering matrix.

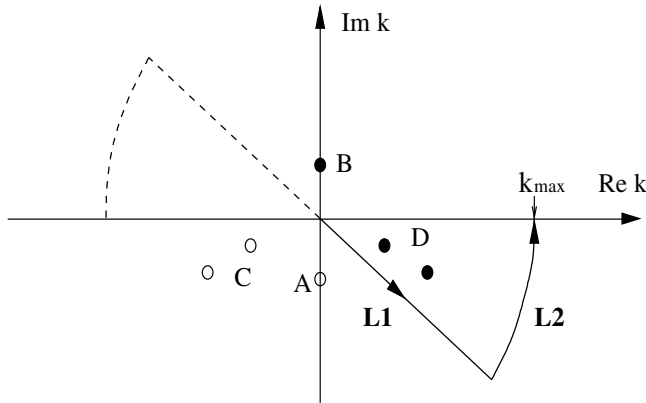


Figure 2. Contour $C_R^+ = L_1 + L_2$ is given by the solid line, while the contour C_R^- is given by the broken line. The contour $C_R = C_R^+ + C_R^-$ is clearly *inversion-symmetric*. The two-body spectrum which is exposed by this contour is marked by filled circles and the excluded spectrum by open circles. The full spectrum includes bound states (B), antibound (A), decay (D) and capture (C) resonant states.

The analytically continued equation (2.1) on a general inversion symmetric contour then takes the form

$$\frac{\hbar^2}{2\mu} k^2 \psi_{nl}(k) + \frac{2}{\pi} \int_{C^+} dq q^2 V_l(k, q) \psi_{nl}(q) = E_{nl} \psi_{nl}(k). \quad (2.7)$$

Here both k and q are defined on the inversion symmetric contour C^+ in the lower-half complex k -plane, giving a closed integral equation. The eigenfunctions satisfy the general completeness relation given in equation (2.6) and are normalized according to the general c -product.

In the following we study two distorted contours C_R^+ and C_{R+T}^+ . These contours can be regarded as a special case of the *Berggren class* of contours. The contour C_R^+ is obtained by a phase transformation (rotation) into the lower-half complex k -plane while the second contour C_{R+T}^+ will be based on rotation followed by translation in the lower-half complex k -plane. These contours approach infinity along complex rays, and not *along* the real k -axis, although as $|k| \rightarrow \infty$ they should approach the real k -axis to define a closed integration contour. It has previously been assumed as a requirement for the choice of distorted contours that they approach infinity along the real k -axis (see e.g. [3]).

First we consider the contour C_R^+ given by two line segments L_1 and L_2 . Line L_1 is given by $k = |k|\exp(-i\theta)$ where $|k| \in [0, k_{\max}]$, L_2 by $k = k_{\max} \exp(-i\theta)$; here k_{\max} is a real and positive constant. One can easily show that for an exponentially bounded potential in coordinate space the integral in equation (2.1) along the arc L_2 will tend to zero for $k_{\max} \rightarrow \infty$. In this case the contour C_R^+ reduces to the line L_1 . Figure 2 shows the contour C_R^+ along with the exposed and excluded two-body spectrum in the complex k -plane, which this choice of contour implies. The contour C_R^+ is part of the *inversion symmetric* contour $C_R = C_R^+ + C_R^-$, also indicated in figure 2.

Most potentials are of such analytic structure; that an analytic continuation into the fourth quadrant of the complex k -plane is possible, except on the imaginary k -axis. One may then uncover arbitrary large portions of the fourth quadrant of the second energy sheet, where resonances may be located. The analytically continued equation (2.7) onto the contour C_R^+ is obtained by the transformation $k = |k|\exp(-i\theta)$ and $q = |q|\exp(-i\theta)$. In this case, equation (2.7) is the momentum space version of the complex-scaled Schrödinger equation in coordinate space, discussed in e.g. [12]. A rotation in momentum space, $|k|\exp(-i\theta)$, is equivalent to the

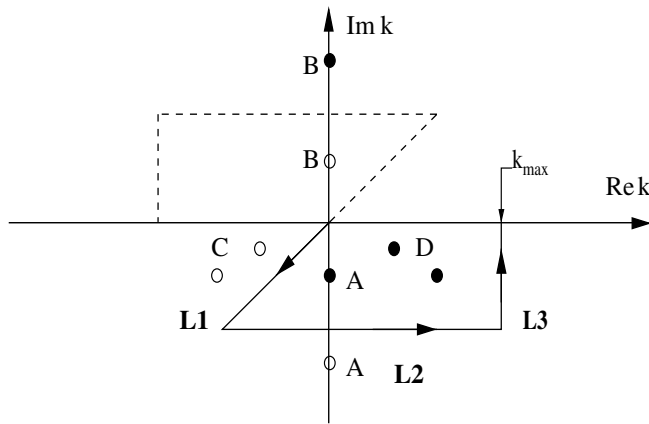


Figure 3. Contour $C_{R+T}^+ = L_1 + L_2 + L_3$ is given by the solid line, while the contour C_{R+T}^- is given by the broken line. The contour $C_{R+T} = C_{R+T}^+ + C_{R+T}^-$ is clearly *inversion-symmetric*. The two-body spectrum which is exposed by this contour is marked by filled circles (\bullet) and the excluded spectrum by open circles (\circ). The full spectrum includes bound states (B), antibound (A), decay (D) and capture (C) resonant states.

complex scaling $r \exp(i\theta)$ in coordinate space. The phase transformation $k \rightarrow |k|\exp(-i\theta)$ turns out to be a similarity transformation (see e.g. [36]). The restriction on the rotation angle θ for the phase transformation may be shown to be $\theta < \pi/2$. This implies that antibound states cannot be included in the spectrum by this choice of contour.

Next we consider the contour obtained by rotation followed by translation in the lower-half complex k -plane. The contour C_{R+T}^+ consists of three line segments. The line segment L_1 is given by a rotation $k = |k|\exp(-i\theta)$ with $|k| \in [0, b]$, whereas L_2 is given by a translation $k = \text{Re}[k] - b \sin(\theta)i$ with $\text{Re}[k] \in [b \cos(\theta), k_{\max}]$ and b determines the translation into the lower-half k -plane and, finally, L_3 is defined by $k = k_{\max} - \text{Im}[k]i$ with $\text{Im}[k] \in [b \sin(\theta), 0]$. For $k_{\max} \rightarrow \infty$, the contribution to the integral in equation (2.1) along the line segment L_3 will vanish, and the contour C_{R+T}^+ reduces to the line segments L_1 and L_2 . Figure 3 shows the contour $C_{R+T}^+ = L_1 + L_2 + L_3$ along with the exposed and excluded two-body spectrum which this choice of contour implies. The contour C_{R+T}^+ is part of the *inversion symmetric* contour $C_{R+T} = C_{R+T}^+ + C_{R+T}^-$ clearly seen in the figure.

Whether one chooses to solve the Schrödinger equation on the contour C_R^+ or on the contour C_{R+T}^+ depends on the problem under consideration. The singularity structure of a general potential is such that an analytic continuation onto a rotated contour in the third quadrant may not be achieved. However, by choosing a modified contour like C_{R+T}^+ which avoids the non-analytic regions of the potential this may be possible. By solving the Schrödinger equation on the distorted contour C_{R+T}^+ rotated into the third quadrant of the complex k -plane, we expose a part of the negative imaginary k -axis where antibound states may be located. In doing this we must emphasize that at the same time we are excluding a part of the positive imaginary k -axis where bound states may be located. This reminds us that the contour should be chosen relative to the partial wave component under study, i.e. a separate analysis has to be made for each partial wave.

2.2. Analyticity of the Malffiet–Tjon interaction in the complex momentum plane

As an illustration we consider the frequently used Malffiet–Tjon nucleon–nucleon (NN) interaction [30], which is a superposition of Yukawa terms. The interaction is in a coordinate

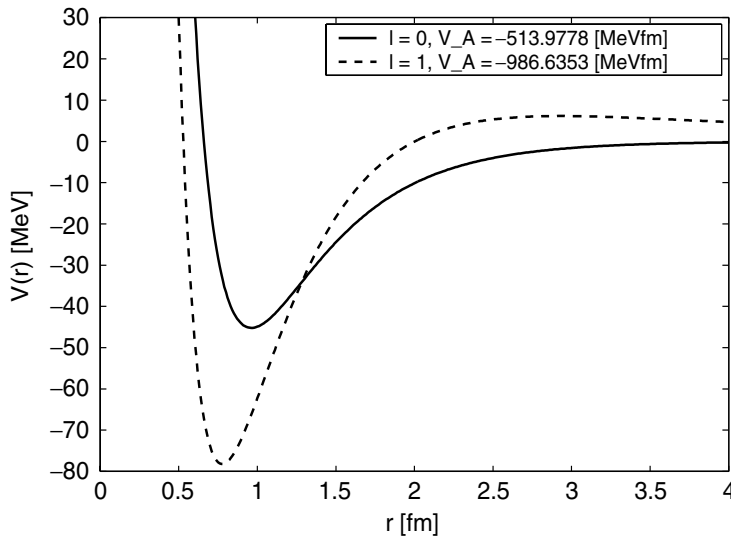


Figure 4. Plot of the $l = 0$ and the $l = 1$ Malfliet–Tjon interaction in coordinate space with angular momentum barrier included.

representation, given by

$$V(r) = V_R \frac{\exp(-\mu_R r)}{r} + V_A \frac{\exp(-\mu_A r)}{r}. \quad (2.8)$$

Here V_R and V_A are the repulsive and attractive strength of the interaction, respectively.

We employ conventional units, i.e. r (fm), k (fm^{-1}), $\mu_{R,A}$ (fm^{-1}) and $V_{R,A}$ (MeV fm). The interaction in coordinate space is given in units of MeV, while in momentum space in units of MeV fm³. The reduced neutron–proton mass is $m_{np}c^2 = 938.926/2$ MeV.

It is known that the 1S_0 channel in the nucleon–nucleon interaction supports an antibound state near the scattering threshold. By choosing interaction parameters

$$V_R = 7.291 \times \hbar c \approx 1438.71 \text{ MeV fm}, \quad \mu_R = 613.69/\hbar c \approx 3.11 \text{ fm}^{-1},$$

$$\mu_A = 305.86/\hbar c \approx 1.55 \text{ fm}^{-1}, \quad V_A = -2.6047 \times \hbar c \approx -513.98 \text{ MeV fm},$$

the Malfliet–Tjon interaction resembles the form of a realistic nucleon–nucleon interaction with attractive and repulsive parts in the 1S_0 channel. It reproduces the 1S_0 phase shift in nucleon–nucleon scattering rather well, and supports an antibound state near the scattering threshold. In the following the parameters V_R , μ_R and μ_A are fixed to the values given above. We will however allow for a variation of the attractive strength V_A . This interaction will then still support bound and antibound states for s-waves, and for higher angular momentum resonances may also appear. Figure 4 gives a plot of the $l = 0$ and the $l = 1$ Malfliet–Tjon interaction in coordinate space with an angular momentum barrier included. For a given partial wave l , the Fourier–Bessel transform of equation (2.8) gives an analytic expression

$$V_l(k, k') = V_R \frac{1}{2kk'} Q_l(x_R) + V_A \frac{1}{2kk'} Q_l(x_A). \quad (2.9)$$

Here $Q_l(x)$ is the Legendre function of the second kind. The arguments of the Legendre function are $x_{R,A} = (k^2 + k'^2 + \mu_{R,A}^2)/2kk'$. Figure 5 gives a plot of the $l = 0$ Malfliet–Tjon interaction in momentum space for the interaction parameters given above.

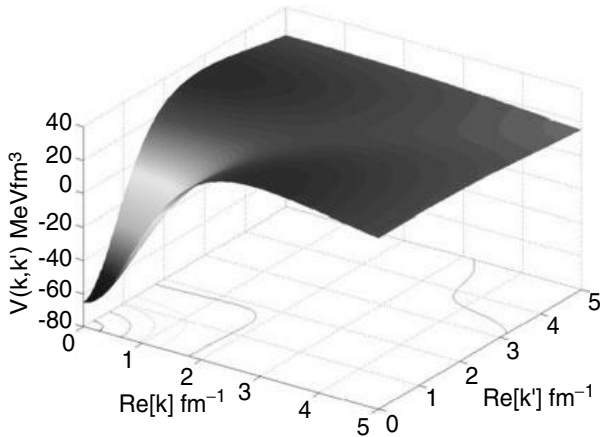


Figure 5. Plot of the $l = 0$ Malfliet–Tjon interaction in momentum space, for real k, k' .

We will give a demonstration of how the momentum space Schrödinger equation for the Malfliet–Tjon interaction may be continued to the non-physical energy sheet, i.e. the lower-half complex k -plane. The only moving singularities of the integral kernel in equation (2.7) are contained in the interaction itself; see equation (2.9). The singularity structure of the interaction is that of the Legendre functions. The Legendre functions are singular for $x = \pm 1$, and this determines the analyticity region of the interaction in the complex k -plane. Thus equation (2.9) is singular for

$$(k - k')^2 + \mu_{R,A}^2 = 0 \quad (2.10)$$

and

$$(k + k')^2 + \mu_{R,A}^2 = 0. \quad (2.11)$$

Equation (2.10) is satisfied for

$$\text{Re}[k] = \text{Re}[k'] \wedge \text{Im}[k] = \pm\mu + \text{Im}[k'],$$

and equation (2.11) for

$$\text{Re}[k] = -\text{Re}[k'] \wedge \text{Im}[k] = \pm\mu_{R,A} - \text{Im}[k'].$$

For k real and k' complex, we see from equation (2.11) that the interaction is singular for $\text{Im}[k'] = \pm\mu_{R,A}$. In the first step of the continuation we keep k real and distort the path of integration into some contour C_1^+ in the analyticity domain $D_1 : -\mu < \text{Im}[k] < \mu$, where we have defined $\mu = \min[\mu_R, \mu_A]$. This defines a new analyticity domain in the complex k -plane, determined by the analytic structure of $V_l(k, k')$, where k' is defined on the contour C_1^+ , i.e. $D_2 : -\mu - C_1 < \text{Im}[k] < \mu - C_1$. If the distorted contour C_1^+ lies in the overlapping domain $D_1 \cap D_2$, k may be defined on the contour C_1^+ as well, giving a closed integral equation. This procedure may be continued ad infinitum, uncovering the complete fourth quadrant of the complex k -plane. Solving the eigenvalue problem by the contour deformation method one may choose a purely rotated contour C_R^+ , or a rotated + translated contour C_{R+T}^+ , where $\theta < \pi/2$. Both contours will expose the resonant structures in the fourth quadrant of the complex k -plane.

For antibound states in the Malfliet–Tjon interaction, one must choose a contour of the type C_{R+T}^+ which consists of a rotation into the third quadrant and a finite translation in the lower-half complex k -plane. It can be easily shown that the translated part of the contour

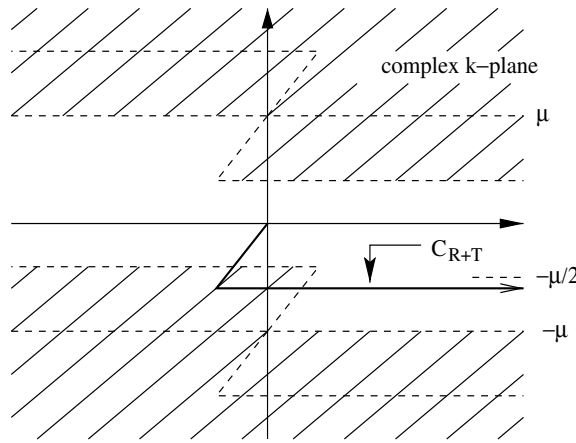


Figure 6. The white area gives the domain of overlapping analyticity for the momentum space Schrödinger equation for a rotated + translated contour, for a translation $|\text{Im}[k]| > \mu/2$. The contour C_{R+T}^+ is partly located outside the overlapping analyticity domain $D_1 \cap D_2$.

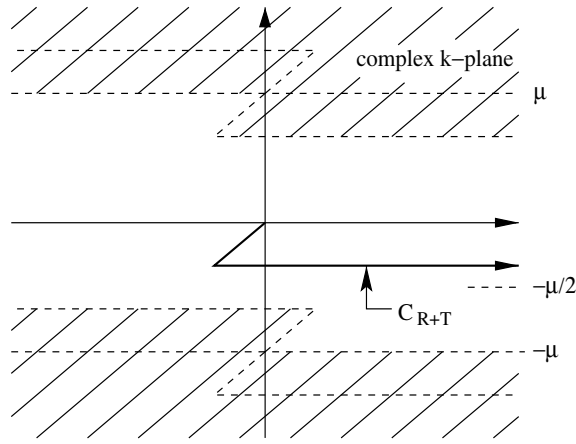


Figure 7. The white area gives the domain of overlapping analyticity for the momentum space Schrödinger equation for the C_{R+T} contour, with a translation $|\text{Im}[k]| < \mu/2$. The contour is located inside the overlapping analyticity domain $D_1 \cap D_2$.

C_{R+T}^+ has to be bounded by $|\text{Im}[k]_{\max}| < \mu/2$. If the translation into the complex k -plane exceeds $\mu/2$, it is not possible to construct overlapping domains of analyticity which contain the distorted contour; see figure 6 for an illustration of this point. Figure 7 shows how the distorted contour C_{R+T}^+ is contained in the overlapping analyticity domains, $D_1 \cap D_2$, for a translation $|\text{Im}[k]| < \mu/2$.

By imposing a lower bound on the translated line segment C_T , given by $|\text{Im}[k]| < \mu/2$, an exploration of antibound states is possible for the Malfliet–Tjon interaction. This limitation of the translation into the lower-half k -plane for the Malfliet–Tjon interaction is related to what is known as the Yukawa cut; in [1] it is shown that the Yukawa interaction has a cut along $\text{Im}[k] \leqslant \mu/2$.

2.3. Antibound and resonant states of the Malfliet–Tjon interaction

Table 1 gives results of a calculation of the antibound neutron–proton s-wave ($l = 0$) state of the Malfliet–Tjon interaction, for increasing strength $V_A = v_A \times \hbar c$, where we have introduced the dimensionless quantity v_A . With our choice of interaction parameters we have

Table 1. Calculation of the neutron–proton antibound state as function of increasing attractive strength v_A for the s-wave Malfliet–Tjon interaction using the deformed integration path C_{R+T}^+ . v_A is dimensionless, and should be multiplied by $\hbar c$ to give the conventional units. The convergence is illustrated by increasing the number of integration points. Column A used $N1 = 30$, $N2 = 50$ integration points; column B used $N1 = 100$, $N2 = 100$ integration points and column C used $N1 = 150$, $N2 = 250$ integration points. Energy E is given in units of MeV.

v_A	CDM			[37]
	A E	B E	C E	
−2.6047	−0.066674	−0.066653	−0.066653	−0.06663
−2.5	−0.310114	−0.310115	−0.310115	−0.31004
−2.3	−1.229845	−1.229845	−1.229845	−1.22970
−2.1	−2.679069	−2.678979	−2.678979	−2.67878

$\mu = \min[\mu_R, \mu_A] = 1.55$ fm, which gives a maximum translation into the lower-half k -plane, $\text{Im}[k]_{\max} = 1.55/2 \approx 0.775$ fm $^{-1}$. This means that all antibound states on the second energy sheet located in the energy domain $E \in [-24.9, 0]$ MeV may be included in the spectrum. For our calculation we use the rotation angle $\theta = 2\pi/3$ and a translation $|\text{Im}[k]| = 0.5 \sin(2\pi/3) \approx 0.433$ fm $^{-1}$. This choice of contour will uncover the portion $E \in [-7.78, 0]$ of the negative energy axis on the second (non-physical) energy sheet. We see that all antibound states which may have an impact on phaseshifts may be included by this choice of contour. The convergence of the calculations is illustrated by increasing the number of integration points. As we obtained convergence of the antibound state energies by increasing the number of integration points, we are led to conclude that our results are stable; furthermore, comparison with the calculations of Elstel *et al* [37] shows only a small difference in the calculated values for the antibound state. In [37] the energy spectrum on the second energy sheet was calculated by analytic continuation of the t -matrix to the second energy sheet, and thereby searching for poles.

In calculating resonant states in the Malfliet–Tjon interaction, any deformed contour in the fourth quadrant of the complex k -plane will do, as long as the resonant states are enclosed by the contour and the real k -axis. The Malfliet–Tjon interaction supports resonant states for angular momentum $l \geq 1$, for which an angular momentum barrier is created and resonant states may be formed inside the barrier.

The $l=1$ partial wave component of the Malfliet–Tjon interaction, supports bound, antibound and resonant states for a given v_A . Figure 8 shows the trajectory of the imaginary part of the bound and antibound state pole in the complex k -plane as a function of interaction strength v_A . The calculations were done on the contour C_{R+T}^+ , rotated into the third quadrant of the complex k -plane. For decreasing interaction strength the bound and antibound states move toward the real axis. It can be seen that for a given interaction strength v_A they are not located symmetrically with respect to the real k -axis, the antibound state being closer to the scattering threshold than the corresponding bound state. This is in agreement with the general rule that, for $l \geq 1$, the number of antibound states between the loosest bound state and the threshold is odd (see e.g. [1]). For $|v_A| \approx 5.47$, the bound and antibound states merge and are both annihilated. This occurs at zero energy ($\text{Im}[k] = 0$ fm $^{-1}$), and is defined as the branching point. For $|v_A| < 5.47$ the bound and antibound states develop into decay and capture resonant states, respectively, moving symmetrically with respect to the imaginary k -axis in the lower-half k -plane.

Figure 9 shows how the bound state of the system approaches the scattering threshold and develop into decay resonant states for decreasing interaction strength v_A . The interaction

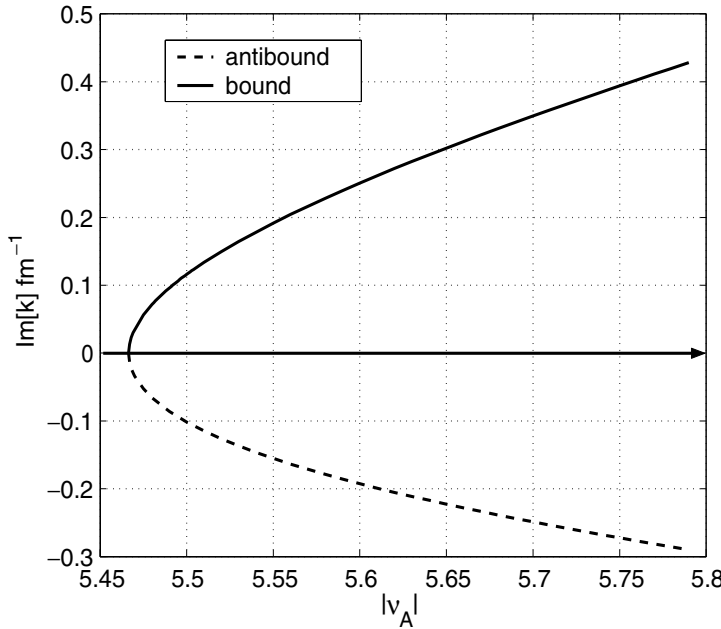


Figure 8. Plot of the bound and antibound state pole trajectory for the $l = 1$ component of Malfliet–Tjon interaction. The location of the poles along the imaginary k -axis is plotted as a function of interaction strength v_A .

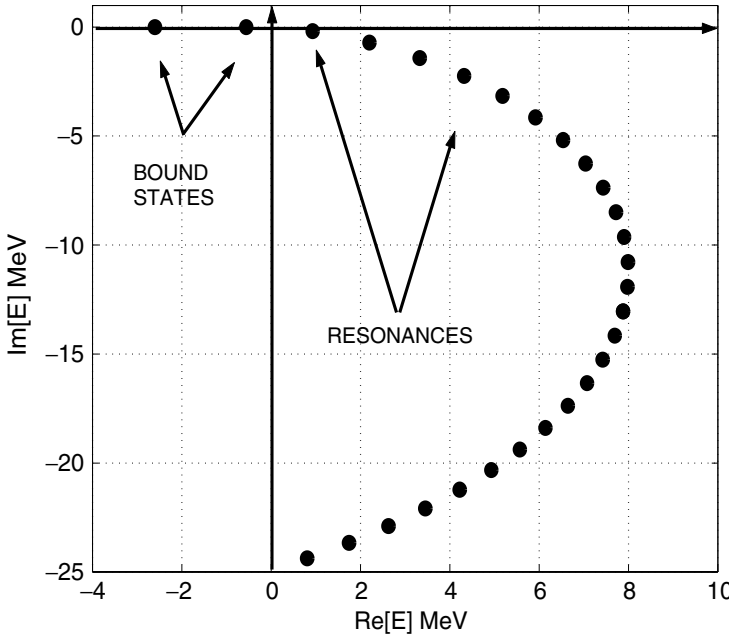


Figure 9. Plot of pole trajectory in the complex energy plane for the $l = 1$ partial wave solution of the Malfliet–Tjon interaction for v_A varied from -5.6 to -2.9 in steps of 0.1 .

strength v_A is varied from -5.6 to -4.1 in steps of 0.1 MeV. For $v_A = -5.6$ and $v_A = -5.5$ we have a bound state. The calculations were performed with the contour C_{R+T}^+ , rotated $\theta = \pi/4$ and translated $|\text{Im}[k]| = 1.5 \sin(\pi/4) \text{ fm}^{-1} \approx 1.06 \text{ fm}^{-1}$ in the fourth quadrant of the complex k -plane. Figures 10 and 11 show plots of the real and imaginary parts

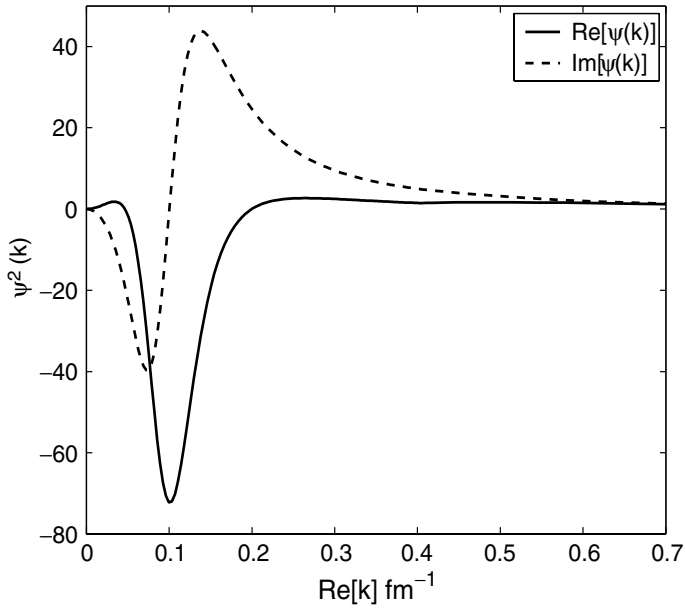


Figure 10. The square of the normalized resonance wavefunction at the resonance energy $E = 0.6554 - 0.1069i$ MeV for an interaction strength $v_A = -5.42$ of the $l = 1$ Malfliet-Tjon interaction. In the complex k -plane this resonant pole is located at $k = 0.1261 - 0.0102i$ fm $^{-1}$. This state is calculated using the contour C_{R+T}^+ with rotation $\theta = \pi/5$ and translation $\text{Im}[k] = -0.5 \times \sin(\theta)$ fm $^{-1}$. We have plotted the real and imaginary parts of the wavefunction as functions of real momenta along the contour C_{R+T}^+ .

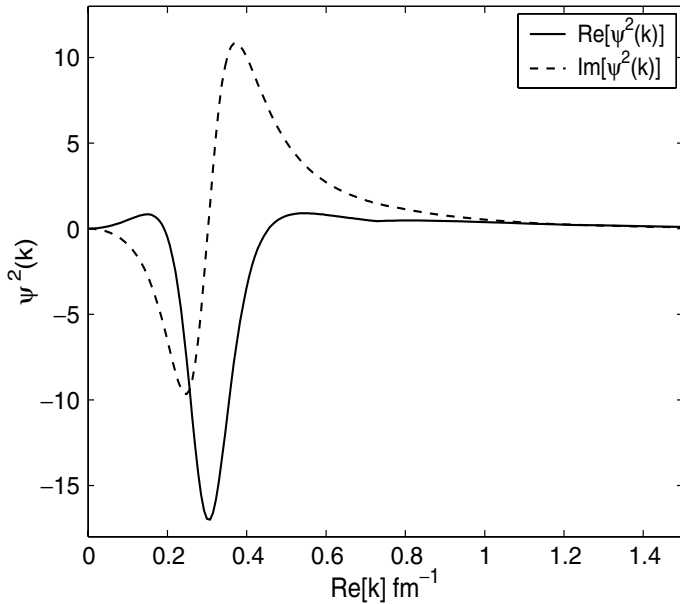


Figure 11. The squared normalized resonance wavefunction at the resonance energy $E = 5.1804 - 3.1555i$ MeV for an interaction strength $v_A = -5$ of the Malfliet-Tjon interaction. In the complex k -plane this resonant pole is located at $k = 0.3682 - 0.1033i$ fm $^{-1}$. This state is calculated using the contour C_{R+T}^+ with rotation $\theta = \pi/5$ and translation $\text{Im}[k] = -0.9 \times \sin(\theta)$. We have plotted the real and imaginary parts of the wavefunction as a function of real momenta along the rotated contour.

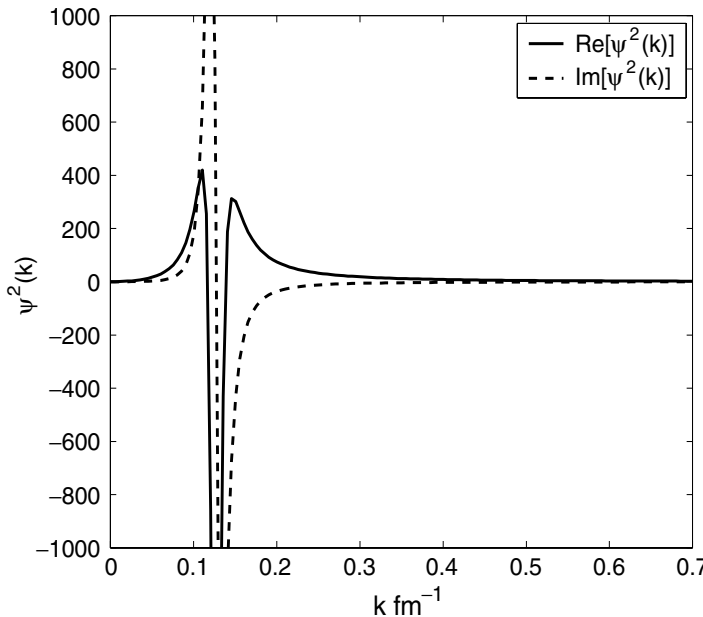


Figure 12. The square of the normalized resonance wavefunction defined along the real k -axis. The resonance energy is $E = 0.6554 - 0.1069i$ MeV for an interaction strength $v_A = -5.42$ in the $l = 1$ Malfliet–Tjon interaction. In the complex k -plane, this resonant pole is located at $k = 0.1261 - 0.0102i$ fm $^{-1}$.

of the squared normalized resonance wavefunction at the resonance energies $E = 0.6554 - 0.1069i$ and $5.1804 - 3.1555i$ MeV corresponding to the interaction strengths $v_A = -5.42$ and -5 , respectively. The wavefunction is plotted as a function of real momenta along the contour C_{R+T}^+ . In the complex k -plane, the resonance energies $E = 0.6554 - 0.1069i$ and $5.1804 - 3.1555i$ MeV corresponds to $k = 0.1261 - 0.0102i$ and $0.3682 - 0.1033i$ fm $^{-1}$, respectively. We see that the peak of real part of the squared resonance wavefunction is located around the real part of the resonant pole in the complex k -plane. The imaginary part of the wavefunction changes sign in the neighbourhood of the resonant pole.

The squared resonance wavefunctions plotted in figures 10 and 11 are not to be interpreted as physical momentum distributions, as they depend on the distorted contour. The physical momentum distribution of a resonant state must be defined along the real k -axis. The Berggren basis contains bound, antibound, resonant and non-resonant continuum states which are defined along the distorted contour. The transformation of these states to the real energy axis is readily done by the integral equation (2.2). All quantities on the right-hand side of equation (2.2) are known, and the integration is over the distorted contour. For k real, we get $\psi_{nl}(k)$ along the real k -axis or equivalently along the real physical energy axis. Figures 12 and 13 show plots of the squared resonance functions for $v_A = -5.42$ and -5 respectively, along the real k -axis. In figure 12, an extreme peaking of the wavefunction is observed at the real energy part of the resonant pole in the complex k -plane. This is due to the small imaginary part of the pole, and the resonant pole is located close to the real k -axis.

On the other hand, for $v_A = -5$, the behaviour of the resonance wavefunction in figure 13 is smooth and well behaved along the real k -axis. In this case, the resonant pole is rather far from the real k -axis, and no singular behaviour is observed. The calculation of resonant states along the real axis become numerically unstable for resonances with narrow widths. This is easily seen from equation (2.2), where the wavefunction becomes ill-behaved for poles close to the real axis.

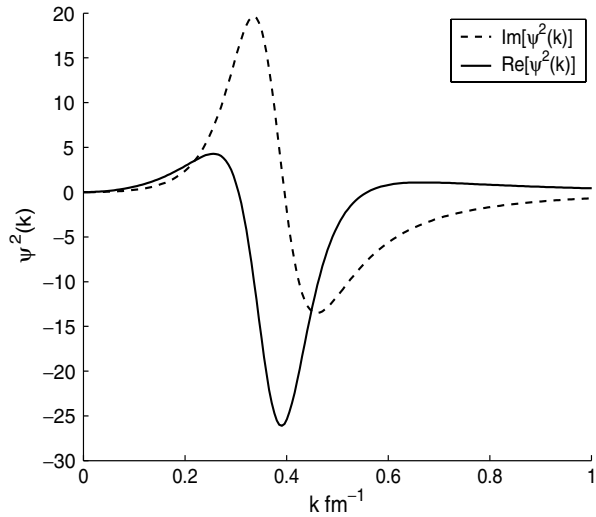


Figure 13. The squared normalized resonance wavefunction defined along the real k -axis. The resonance energy is $E = 5.1804 - 3.1555i$ MeV for an interaction strength $v_A = -5$ of the Malfliet–Tjon interaction. In the complex k -plane, this resonant pole is located at $k = 0.3682 - 0.1033i$ fm $^{-1}$.

2.4. 1S_0 antibound states of the CD–Bonn interaction

As an example of a currently used realistic interaction we present a calculation of the 1S_0 antibound states in the charge-dependent Bonn interaction (CD–Bonn). The CD–Bonn interaction is given in [29]. The tensor component of the CD–Bonn interaction couples angular momentum, $l = j - 1$ and $j + 1$, in the spin triplet channel. It is straightforward to include this coupling in the formalism outlined above.

The realistic nucleon–nucleon interaction does not have a resonant structure in the low energy region $E < 300$ MeV. It does however support antibound states in the 1S_0 isospin triplet channel and a bound state in the coupled isospin singlet channel (the deuteron) ${}^3S_1 - {}^3D_1$. We compare the calculated antibound state locations in the complex k -plane with the values obtained by the effective range approximation (see [1, 9]). In the following, we do not include Coulomb effects when considering the isospin $t_z = -1$ channel (proton–proton scattering).

The effective range approximation for the s-wave poles is given by

$$k = -i \left[\sqrt{\frac{2}{r_{NN}|a_{NN}|}} + \frac{1}{r_{NN}^2} - \frac{1}{r_{NN}} \right]. \quad (2.12)$$

The theoretical (see below) and experimental values [29] for the 1S_0 scattering lengths a_{NN} and effective range r_{NN} are given in table 2.

The antibound state poles are located on the negative imaginary k -axis. Applying CDM in this case, one has to choose a contour which extends into the third quadrant of the complex k -plane. The distorted contour C_{R+T}^+ proves to be suitable contour in this case. To apply CDM by integrating along the contour C_{R+T}^+ the singularities in the CD–Bonn interaction has to be determined.

The CD–Bonn interaction is given explicitly in momentum space. The derivation of the interaction is based on field theory, starting from Lagrangians describing the coupling of the various mesons of interest to nucleons [29]. The one-boson-exchange interaction is

Table 2. Scattering lengths (a) and effective ranges (r) for the 1S_0 channel, in units of fm. For the proton–proton channel Coulomb effects are not included.

	CD–Bonn	Experiment
a_{pp}	−17.4602	
r_{pp}	2.845	
a_{nn}	−18.9680	$−18.9 \pm 0.4$
r_{nn}	2.819	2.75 ± 0.11
a_{np}	−23.7380	$−23.740 \pm 0.020$
r_{np}	2.671	2.77 ± 0.05

Table 3. Calculation of antibound state energies in the 1S_0 isospin triplet channel by the effective range approximation (EFR) and the contour deformation method (CDM), in units of MeV. Convergence is obtained in each isospin channel. Column A used $N1 = 20$, $N2 = 30$ integration points, column B used $N1 = 20$, $N2 = 50$ integration points and column C used $N1 = 30$, $N2 = 80$ integration points. Energy E is given in units of MeV.

T_z	CDM			EFR
	A	B	C	
	E	E	E	E
−1 (pp)	−0.11766	−0.11761	−0.11761	−0.11763
1 (nn)	−0.10070	−0.10069	−0.10069	−0.10070
0 (np)	−0.06632	−0.06632	−0.06632	−0.06632

proportional to

$$V(\mathbf{k}, \mathbf{q}) \propto \sum_{\alpha=\pi^0, \pi^\pm, \rho, \omega, \sigma_1, \sigma_2} \bar{V}_\alpha(\mathbf{k}, \mathbf{q}) F_\alpha^2(\mathbf{k}, \mathbf{q}; \Delta_\alpha). \quad (2.13)$$

Both $\bar{V}_\alpha(\mathbf{k}, \mathbf{q})$ and $F_\alpha^2(\mathbf{k}, \mathbf{q}; \Delta_\alpha)$ contain terms of the form

$$\frac{1}{(\mathbf{k} - \mathbf{q})^2 + m_\alpha^2}, \quad (2.14)$$

which are of the Yukawa type. In a partial wave decomposition these Yukawa terms will be composed of Legendre functions of the second kind, $Q_l(x)$, with $x = (k^2 + q^2 + m_\alpha^2)/2kq$. The analytic structure of the CD–Bonn interaction is then seen to be that of the Malfliet–Tjon interaction, which was discussed above. The poles of the interaction are determined by the various meson masses m_α and cut-off masses Δ_α . Considering the solution of the eigenvalue problem by the contour deformation method using contour C_{R+T}^+ , singularities in the interaction appear for $z = z' = \pm im_\alpha/2$. For a rotation into the third quadrant of the complex k -plane, the maximum translation into the complex k -plane is then determined by the smallest meson mass entering the potential, which is the π -meson, $m_{\pi^0}c^2 = 134.9764$ MeV. For a given rotation into the third quadrant, i.e., $\theta \geq \pi/2$, we get a restriction on the translation; $\text{Im}[k] < -134.9764/2\hbar c \text{ fm}^{-1}$.

Table 3 gives results for the antibound states in the 1S_0 channel by the contour deformation method. A comparison with the effective range calculation of the antibound state poles is also shown. The contour was rotated by an angle $\theta = 2\pi/3$ into the complex k -plane with a subsequent translation transformation given by $\text{Im}[k] = -30 \sin(5\pi/7)/\hbar c \text{ fm}^{-1}$ (or $\text{Im}[k] \approx -0.12 \text{ fm}^{-1}$) in the lower-half k -plane. This is sufficient to reproduce the antibound states in the 1S_0 channel, as they are known to lie very close to the scattering threshold,

$k \approx -0.05i \text{ fm}^{-1}$. By this contour the full energy spectrum is obtainable since it is known *a posteriori* that the 1S_0 channel supports only antibound states near the scattering threshold. The convergence of the numerical calculated values is demonstrated by increasing the number of integration points N .

3. Two-body scattering amplitude in a Berggren representation

3.1. Berggren expansion of the t -matrix

In effective interaction studies for finite nuclei the harmonic oscillator basis has served as a standard expansion basis for the G-matrix. This basis may work well in cases where the nucleons are well bound but less so near the nuclear driplines. The general Berggren basis has an advantage in that it is generated from the Hamiltonian of the examined problem. Expansions in this basis will increase the convergence drastically. In this section we will discuss the solution for the full off-shell t -matrix and, hence, the full two-body scattering problem, by expanding the two-body Green's function in a complete set of Berggren states. The Berggren representation of the scattering equations gives an analytic continuation in energy, from the upper rim of the cut through the cut and into the non-physical energy sheet. This has relevance for nuclear medium studies where the input energy is in general complex. In a nuclear medium calculation the self-consistently determined quasiparticle energies are in general complex.

The t -matrix is defined in operator form by

$$t(\omega) = V + Vg^{II}(\omega)V \quad (3.1)$$

or

$$t(\omega) = V + Vg_0^{II}(\omega)t(\omega). \quad (3.2)$$

Here ω is the incoming energy, $g^{II}(\omega)$ the resolvent, commonly known as the Green's operator, and $g_0^{II}(\omega)$ the corresponding free Green's operator. In operator form they are defined by

$$g_0^{II}(\omega) = \frac{1}{\omega - H_0}, \quad (3.3)$$

$$g^{II}(\omega) = \frac{1}{\omega - H}. \quad (3.4)$$

They are related through the Dyson equation

$$g^{II}(\omega) = g_0^{II}(\omega) + g_0^{II}(\omega)Vg^{II}(\omega). \quad (3.5)$$

The term H_0 is the kinetic energy operator and H the full two-body Hamiltonian. The physical interpretation of the Green's functions is that g_0^{II} describes the propagation of two noninteracting particles, whereas g^{II} describes the propagation of two interacting particles in free space.

By expanding the unit operator on a complete set of physical eigenstates of H given in equation (1.1), we can write the interacting Green's operator as

$$g^{II}(\omega) = \sum_b \frac{|\psi_b\rangle\langle\psi_b|}{\omega - E_b} + \int_0^\infty dE_c \frac{|\psi_c\rangle\langle\psi_c|}{\omega - E_c}. \quad (3.6)$$

This is the spectral decomposition of the Greens's function. Here b denotes the discrete bound state spectrum and c the positive energy continuum. We see from this equation that the interacting Green's function is analytic in the entire complex energy plane, except

at the spectrum of the Hamiltonian including a branch cut along the positive real energy axis. In physical scattering, with outgoing waves at infinity, the energy has to approach the cut from above, i.e. $\omega \rightarrow E + i\eta$. Approaching the cut from below, i.e. $\omega \rightarrow E - i\eta$ corresponds to incoming waves at infinity. The discontinuity of the Green's function across the cut is

$$g^{II}(E + i\eta) - g^{II}(E - i\eta) = -2\pi i |\psi_c\rangle \langle \psi_c|. \quad (3.7)$$

The Berggren representation of the Green's function is obtained by expanding the unit operator using the completeness relation given in equation (2.6). In this case the Green's operator takes the form

$$g^{II}(\omega) = \sum_{\alpha} \frac{|\psi_{\alpha}\rangle \langle \psi_{\alpha}^*|}{\omega - E_{\alpha}} + \int_{C^+} dE \frac{|\psi\rangle \langle \psi^*|}{\omega - E}. \quad (3.8)$$

Here α denotes bound, antibound and resonant states. The integration contour C^+ denotes an arbitrary inversion symmetric contour (see e.g. figure 1), and gives the non-resonant distorted continuum contribution to the interacting Green's function. If we neglect the non-resonant continuum contribution to the Green's function we get the *resonant state expansion* of the Green's function. Such expansions have been studied over the last decade for finite range potentials (see e.g. [7, 38, 20]). The Green's function given in equation (3.8) is continuous and analytic in energy across the real axis and into the domain C of the lower part of the complex energy plane. Equation (3.8) is therefore an analytic continuation in energy of the physical Green's function given in equation (3.6).

The Berggren representation of the t -matrix is obtained by inserting the interacting Green's function given by equation (3.8) into equation (3.1), giving

$$t(\omega) = V + \Delta t(\omega) = V + \Delta t^R(\omega) + \Delta t^C(\omega). \quad (3.9)$$

Here $\Delta t^R(\omega)$ is the resonant contribution while $\Delta t^C(\omega)$ is the non-resonant distorted continuum contribution to the t -matrix. By projecting $t(\omega)$ on momentum states, and decomposing into partial waves, the t -matrix elements $t_l(k, k'; \omega)$ can be expressed as one-dimensional integral equations,

$$t_l(k, k', \omega) = V_l(k, k') + \frac{4}{\pi^2} \int_{C^+} \int_{C^+} dq dq' q^2 q'^2 V_l(k, q) g^{II}(q, q'; \omega) V_l(q', k'). \quad (3.10)$$

This representation of the t -matrix is valid as long as we do not pass through any singularities of the interaction potential by deforming the real k -axis into the distorted contour C^+ . The interacting Green's function on the inversion symmetric contour C^+ is given by

$$g^{II}(k, k'; \omega) = \sum_{\alpha} \frac{\psi_{\alpha}(k)\psi_{\alpha}(k')}{\omega - E_{\alpha}} + \int_{C^+} dE \frac{\psi_E(k)\psi_E(k')}{\omega - E}. \quad (3.11)$$

Equation (3.10) has the same analytic structure as the Green's function of equation (3.8), except for possible singularities in the interaction potential. Using equation (2.2), the on-shell t -matrix may be written as

$$t_l(k, k, \omega = \hbar^2 k^2 / 2m_{np}) = V_l(k, k) + \sum_{\alpha} (\omega - E_{\alpha}) \psi_{\alpha}^2(k) + \int_{C^+} dE (\omega - E) \psi_E^2(k). \quad (3.12)$$

The s -matrix is given in terms of the on-shell t -matrix by

$$s_l(k) = 1 - 2 \frac{m_{np}}{\hbar^2} ik t_l(k, k, \omega). \quad (3.13)$$

Here the resonant and non-resonant wavefunctions defined along the real k -axis enters the equations. The absolute value of the s -matrix is then a valuable test on how accurate our numerical calculations are. Applying CDM enables us to obtain $t_l(k, k'; \omega)$ for both real and complex energies ω . The integral becomes non-singular on the deformed contour for real and positive input energies ω , resulting in numerically stable solutions for physical two-body scattering.

The Berggren representation of the t -matrix also allows for a separate study of the resonant and continuum contributions. The limitation of this method is due to the fact that most potentials in momentum space have singularities in the complex plane when one argument is real and the other is complex. By applying contour C_R^+ , which is based on rotation into the complex plane, in most cases there will be restrictions on both rotation angle (θ) and maximum incoming and outgoing momentum (k, k') (see e.g. [16]). Using a contour of the type C_{R+T}^+ , we can avoid these limitations by choosing the integration contour in such a way that the potential singularities always will lie outside the integration contour and, therefore, do not give any restriction on rotation angle and maximum incoming and outgoing momentum. By an appropriate choice of contour, CDM gives an alternative to the standard principal value prescription in solving for the t -matrix. In addition, it allows for a separate study of the resonant contribution to the full scattering amplitude. In the case of narrow resonances, the resonant contribution to the t -matrix will dominate strongly over the continuum contribution around the resonance energy. This separation is motivated by the fact that the most interesting phenomenon taking place in the continuum is the resonance phenomenon.

3.2. t -matrix for the Malfliet–Tjon interaction using a Berggren basis

In addition to giving accurate calculation of the complete energy spectrum on the second sheet, CDM provides also a basis for a calculation of the fully off-shell two-body scattering amplitude (t -matrix). Here we present calculations of the t -matrix and phase shifts for the Malfliet–Tjon interaction using the C_{R+T}^+ contour. The phase shifts are given in terms of the t -matrix elements by

$$\delta_l(k) = \arctan \frac{\text{Im}[t_l(k, k; \omega)]}{\text{Re}[t_l(k, k; \omega)]}, \quad (3.14)$$

where the input energy ω is given on-shell, i.e. $\omega = \hbar^2 k^2 / 2m_{np}$. If the t -matrix is approximated by the resonant part $t \approx \Delta t^R$, one gets the famous Breit–Wigner approximation to the phase shifts (see e.g. [9])

$$\delta_l(k) \approx \delta^R(k) = \arctan \left(\frac{\Gamma/2}{E - E_R} \right) + \delta^b \quad (3.15)$$

valid for narrow widths Γ and in a small energy range around the resonance energy. The motivation for using the contour C_{R+T}^+ in calculation of the t -matrix is based on the analytic properties of the interaction. For real incoming and outgoing momenta we have to face the problem of avoiding the singularity in the interaction $V(k, k')$, located at $\text{Im}[k] = \pm\mu/2$. By using the contour C_{R+T}^+ this problem is solved, and stable solution of the t -matrix can be obtained. Using the spectral decomposition of the Green's function, a separate analysis

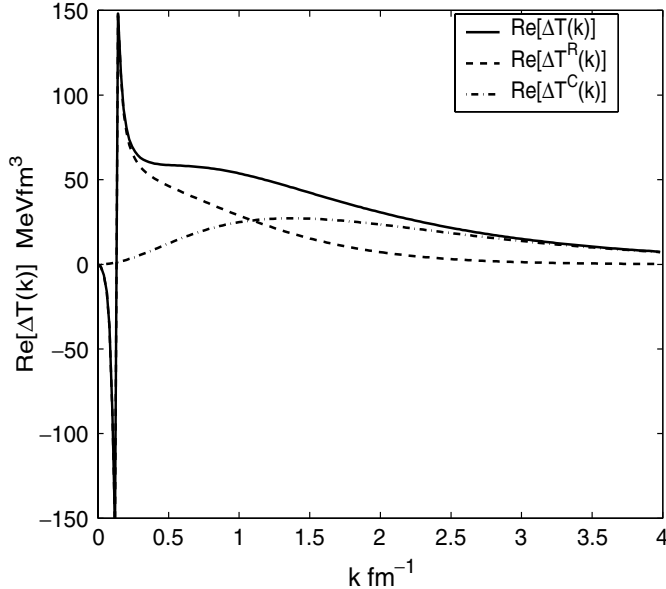


Figure 14. Real part of continuum $\Delta T^C(k)$ and resonant $\Delta T^R(k)$ contributions to the on-shell t -matrix, for the Malfliet–Tjon interaction with strength $v_A = -5.42$ supporting a resonance at energy $E = 0.6554 - 0.1069i$ MeV.

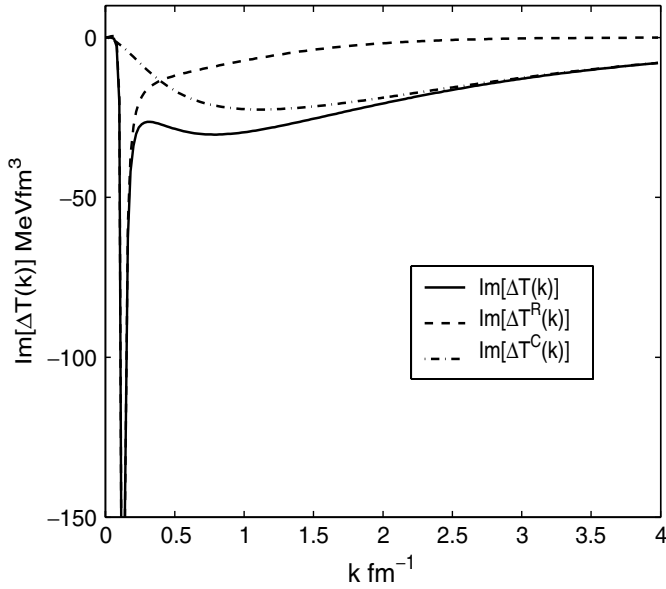


Figure 15. Imaginary part of continuum $\Delta T^C(k)$ and resonant $\Delta T^R(k)$ contributions to the on-shell t -matrix, for the Malfliet–Tjon interaction with strength $v_A = -5.42$ supporting a resonance at energy $E = 0.6554 - 0.1069i$ MeV.

of the resonant and continuum contributions can be performed. We will see below that in the case of a short-range interaction of the Yukawa type, the continuum contribution is non-negligible in most of phase-space, except in a small phase volume around the resonance energy.

Figures 14 and 15 give plots of the real and imaginary parts of Δt , Δt^C and Δt^R . The t -matrix elements were evaluated on-shell. The calculations were done for $v_A = -5.42$ and $l = 1$ Malfliet–Tjon interaction, giving a resonance pole at $k = 0.13 - 1.02i\text{ fm}^{-1}$ in

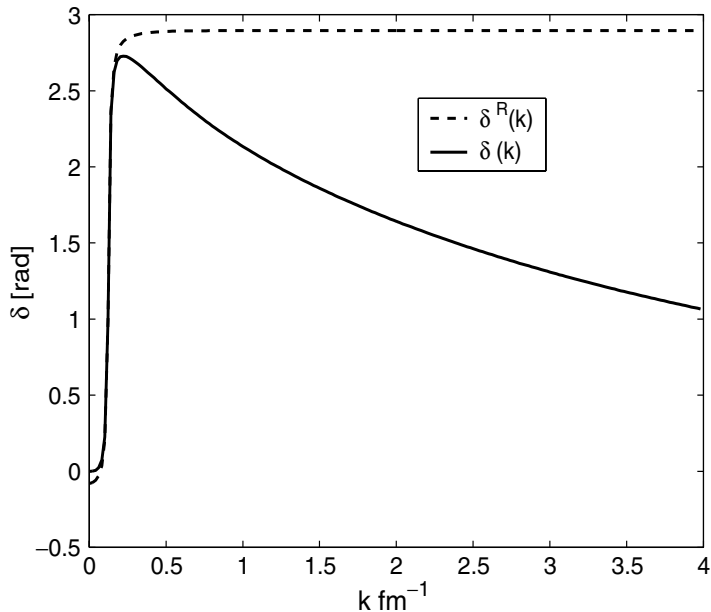


Figure 16. Plot of phase shift for the Malfliet–Tjon interaction with strength $v_A = -5.42$ supporting a resonance at energy $E = 0.6554 - 0.1069i$ MeV. The broken line gives the resonant contribution to the phase shift.

Table 4. Numerical calculations of the absolute value of the s -matrix for various on-shell momenta. The calculations were done with the $l = 1$ Malfliet–Tjon interaction given on the distorted contour C_{R+T}^+ rotated $\theta = \pi/5$ and translated $\text{Im}[k] = -1.5 \sin(\pi/5) \text{ fm}^{-1} \approx -0.8817 \text{ fm}^{-1}$ into the fourth quadrant of the complex k -plane.

$k (\text{fm}^{-1})$	$ s_l(k) $
0.1	0.9999985
1	0.9999999
2	0.9999998
3	0.9999996
4	1.0000017

the complex k -plane. The calculations used a rotation angle $\theta = \pi/5$ and a translation $|\text{Im}[k]| = 1.5 \sin(\pi/5) \approx 0.8817 \text{ fm}^{-1}$, and 50 integration points along the line segments \mathbf{L}_1 and \mathbf{L}_2 , respectively. The resonance energy is located rather close to the real energy axis, and that the resonance part of the t -matrix dominates strongly over the continuum part around the real part of the pole $\text{Re}[k] = 0.13 \text{ fm}^{-1}$. This behaviour justifies the Breit–Wigner approximation to the phase shifts in this energy region.

Figure 16 shows the complete phase shifts, δ , including both non-resonant continuum and resonant contributions, and the resonant contribution, δ^R . In the vicinity of the resonance energy, δ^R gives a good approximation to the full phase shift. Table 4 gives the absolute value of the s -matrix (see equation (3.13)) for various on-shell momenta, and we see that the numerical accuracy is rather good. The accuracy increases with number of integration points used in the calculations.

By decreasing the interaction strength v_A the resonant poles moves further down into the lower-half k -plane. The contribution to the phase shifts and the t -matrix elements from resonances far from the real energy axis is expected to be small. Figure 17 shows the complete

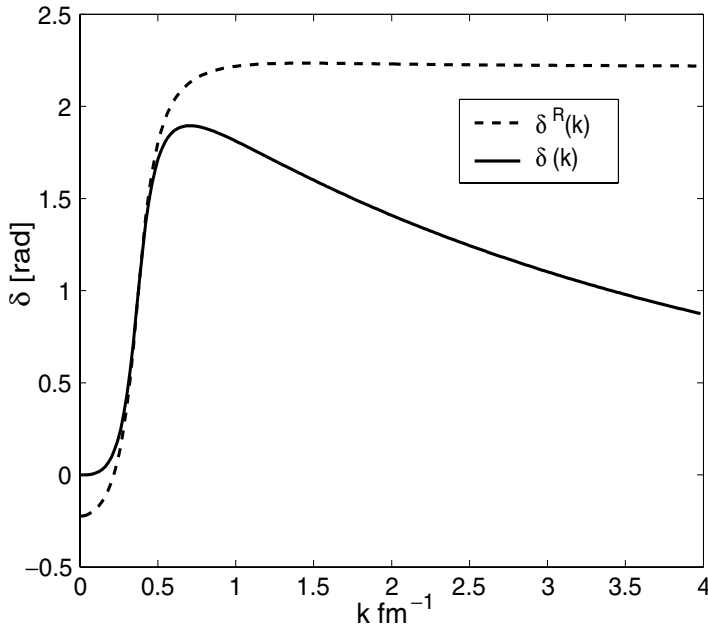


Figure 17. Plot of phase shift for the Malfliet–Tjon interaction with strength $v_A = -5$, supporting a resonance at energy $E = 5.1804 - 3.1555i$ MeV. The broken line gives the resonant contribution to the phase shift.

and the resonant part of phase shifts for the $v_A = 5$ Malfliet–Tjon interaction, for a ‘deep-lying’ resonance.

4. An analytically solvable non-local two-body potential

4.1. Energy spectrum and t -matrix for the Yamaguchi interaction

It is instructive to check the CDM for an analytically solvable case, that of the non-local separable potential given by Yamaguchi [31]; it models s- and p-waves. The coordinate representation of the Yamaguchi interaction is given by a product of two Yukawa terms (see e.g. [10]). A separable interaction in coordinate space gives a separable interaction in momentum space, and is analytically solvable (see e.g. [1] for a demonstration). The Yamaguchi interaction therefore admits analytic solution of the full off-shell t -matrix and the t -matrix poles, corresponding to the energy spectrum. The Yamaguchi s-wave potential supports bound and antibound states, while the Yamaguchi p-wave potential supports bound, antibound and resonant states. The Yamaguchi potential is therefore useful in modelling loosely bound two-body systems which may have a rich resonant state structure, and for checking the numerics in calculations of the t -matrix and the energy spectrum.

The s-wave Yamaguchi potential has the form

$$V_0(k, q) = -\lambda g_0(k)g_0(q), \quad (4.1)$$

where

$$g_0(k) = \frac{1}{k^2 + \beta^2}. \quad (4.2)$$

The full off-shell t -matrix for the s-wave potential reads [1]

$$t_0(k, q; \omega) = -\lambda \frac{g_0(k)g_0(q)}{1 - \Delta_0(\omega)}, \quad (4.3)$$

where we have defined

$$\Delta_0(\omega) \equiv \lambda \frac{2}{\pi} \int_0^\infty dk \frac{k^2(g_0(k))^2}{\hbar^2 k^2/2m - \omega}. \quad (4.4)$$

The integral $\Delta_0(\omega)$ can be evaluated analytically. For $\omega = \hbar^2 k_0^2/2m$ we get

$$\Delta_0(k_0) = \lambda \frac{m}{\hbar^2} \frac{(\beta + ik_0)^2}{\beta(\beta^2 + k_0^2)^2}. \quad (4.5)$$

For bound and antibound states the t -matrix poles are located along the positive and negative imaginary k -axis, respectively. Writing $\kappa = -ik_0$, where κ is a real quantity, we can solve for the t -matrix poles as zeros of the denominator, $1 - \Delta_0(k_0) = 0$, giving in terms of κ ,

$$\kappa = -\beta \pm \sqrt{\frac{\lambda m}{\beta \hbar^2}}, \quad (4.6)$$

and we see that the poles are located along the imaginary k -axis. For $\lambda > \beta^3 \hbar^2/m$, we get a bound ($\kappa > 0$) and an antibound state ($\kappa \leq 0$), and for $\lambda \leq \beta^3 \hbar^2/m$, we get two antibound states.

The separable p-wave interaction is given by

$$V_1(k, q) = -\lambda g_1(k)g_1(q), \quad (4.7)$$

where

$$g_1(k) = \frac{k}{k^2 + \beta^2}, \quad (4.8)$$

and the t -matrix becomes [1]

$$t_1(k, q; E) = -\lambda \frac{g_1(k)g_1(q)}{1 - \Delta_1(k_0)}. \quad (4.9)$$

Here

$$\Delta_1(\omega) \equiv \lambda \frac{2}{\pi} \int_0^\infty dk \frac{k^2(g_1(k))^2}{\hbar^2 k^2/2m - \omega}. \quad (4.10)$$

The integral $\Delta_1(E)$ can be calculated analytically, giving in terms of k_0 ,

$$\Delta_1(k_0) = \lambda \frac{m}{\hbar^2} \frac{\beta^3 + k_0^2(3\beta + 2ik_0)}{(\beta^2 + k_0^2)^2} \quad (4.11)$$

solving for the poles gives in terms of $\kappa = -ik_0$,

$$\kappa = \lambda \frac{m}{\hbar^2} - \beta \pm \sqrt{\lambda \frac{m}{\hbar^2} \left(\lambda \frac{m}{\hbar^2} - \beta \right)}. \quad (4.12)$$

We see that for p-waves the interaction supports bound, antibound and resonant states. The bound state condition is

$$\lambda > \frac{\beta \hbar^2}{m} \quad (4.13)$$

giving in addition an antibound state. The interaction has a branchpoint at $k = 0$, where the bound and antibound states meet and move symmetrically from the imaginary axis into the lower-half k -plane giving capture and decay resonant states. Figure 18 shows the pole trajectory for the Yamaguchi p-wave interaction.

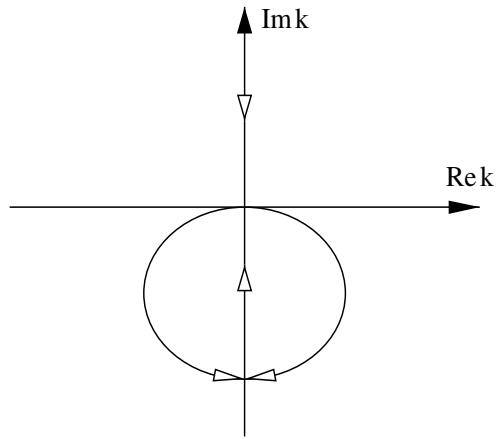


Figure 18. Pole trajectory for the p-wave Yamaguchi interaction in the complex k -plane.

4.2. Expansion of the Yamaguchi eigenvalue problem on a Berggren basis generated from the Malfliet–Tjon interaction

Here we illustrate the flexibility of the Berggren basis as an expansion basis for a more general interaction. The Yamaguchi eigenvalue problem will be expanded on a Berggren basis, again generated from the Malfliet–Tjon interaction. It is interesting to observe the convergence of eigenvalues as the number of non-resonant continuum states increases. Does the fact that the Yamaguchi interaction is non-local whereas the Malfliet–Tjon interaction giving rise to the basis is local, influence the applicability of the Berggren basis, and the convergence of the eigenvalue problem? A numerical investigation of this is carried out below. The numerically determined eigenvalues as a function of basis elements will be compared with the analytical solutions of the eigenvalues.

The Hamiltonian eigenvalue problem expanded on a general Berggren basis takes the abstract form

$$\sum_{\gamma} \langle \varphi_{\alpha}^* | T + V | \varphi_{\gamma} \rangle c_{\gamma} = E \sum_{\gamma} \delta_{\gamma, \alpha} c_{\gamma}, \quad (4.14)$$

where the expansion coefficients c_{γ} fulfil the completeness relation $\sum_{\gamma} c_{\gamma}^2 = 1$. In momentum space, the matrix elements of the kinetic and potential operators take the form

$$\langle \varphi_{\alpha}^* | T | \varphi_{\gamma} \rangle = \frac{2}{\pi} \int_{C^+} dk k^2 \varphi_{\alpha, l}(k) \frac{\hbar^2}{2m} k^2 \varphi_{\gamma, l}(k) \quad (4.15)$$

$$\langle \varphi_{\alpha}^* | V | \varphi_{\gamma} \rangle = \frac{4}{\pi^2} \int_{C^+} dk k^2 \int_{C^+} dk' k'^2 \varphi_{\alpha, l}(k) V_l(k, k') \varphi_{\gamma, l}(k'). \quad (4.16)$$

We consider solutions for the $l = 1$ Yamaguchi interaction with $\beta = 2 \text{ fm}^{-1}$ and varying interaction strength λ . This interaction supports bound states for $\lambda > 2\hbar^2/m \approx 165.883 \text{ MeV fm}^{-1}$. Table 5 gives numerical results for bound and resonant states of the $l = 1$ Yamaguchi interaction. The Berggren basis was generated by the $l = 1$ Malfliet–Tjon interaction given on the distorted contour C_{R+T}^+ rotated $\theta = \pi/5$ and translated $\text{Im}[k] = -\sin(\pi/5) \text{ fm}^{-1} \approx -0.59 \text{ fm}^{-1}$ into the fourth quadrant of the complex k -plane. The calculations used 50 integration points along the rotated and translated parts of the contour.

Table 5. Numerical calculations of bound and resonant states of the $l = 1$ Yamaguchi interaction of strength λ . The Berggren basis was generated by the $l = 1$ Malfliet–Tjon interaction given on the distorted contour C_{R+T}^+ rotated $\theta = \pi/5$ and translated $\text{Im}[k] = -\sin(\pi/5) \text{ fm}^{-1} \approx -0.59 \text{ fm}^{-1}$ into the fourth quadrant of the complex k -plane. Comparison is done with exact energy values for the bound and resonant states. λ is given in units of MeV fm and energy in units of MeV.

λ	CDM		Exact	
	$\text{Re}[E]$	$\text{Im}[E]$	$\text{Re}[E]$	$\text{Im}[E]$
169	−4.09667119	0	−4.09667119	0
166	−0.12337977	0	−0.12337977	0
165	0.87360132	−0.12850277	0.87360132	−0.12850277
164	1.84025247	−0.39895705	1.84025247	−0.39895705
163	2.78279024	−0.75351046	2.78279024	−0.75351046
160	5.46572327	−2.17613872	5.46572327	−2.17613872

Table 6. Numerical calculations of antibound states in the $l = 1$ Yamaguchi interaction. The Berggren basis was generated by the $l = 1$ Malfliet–Tjon interaction given on the distorted contour C_{R+T}^+ rotated $\theta = 2\pi/3$ and translated $\text{Im}[k] = -\sin(2\pi/3) \text{ fm}^{-1} \approx -0.87 \text{ fm}^{-1}$ into the third quadrant of the complex k -plane. Comparison is done with exact energy values for the antibound states. Calculations used 50 integration points along the rotated and translated lines. λ is given in units of MeV fm and energy in units of MeV.

λ	CDM		Exact	
	$\text{Re}[E]$	$\text{Im}[E]$	$\text{Re}[E]$	$\text{Im}[E]$
168	−1.689679639	0	−1.689679639	0
167	−0.948105835	0	−0.948105835	0
166	−0.110946667	0	−0.110946633	0

The singularity structure of the Yamaguchi interaction is particularly simple, having poles only for $\text{Im}[k] = \pm\beta$. Therefore, any contour in the fourth quadrant will do. The interaction parameters for the Malfliet–Tjon interaction, used for the Berggren basis, are the same as in previous sections with $v_A = -5$ supporting a resonance at $E = 5.1804 - 3.1555i \text{ MeV}$.

Table 6 gives numerical results for antibound states in the $l = 1$ Yamaguchi interaction. The Berggren basis was generated by the $l = 1$ Malfliet–Tjon interaction given on the distorted contour C_{R+T}^+ rotated $\theta = 2\pi/3$ and translated $\text{Im}[k] = \sin(\pi/5) \text{ fm}^{-1} \approx 0.87 \text{ fm}^{-1}$ into the third quadrant of the complex k -plane. The calculations again used 50 integration points and the same input as above. The agreement with exact results is convincing for all three cases: bound, resonant and antibound.

5. Expansion of resonances of a Gaussian potential on a Berggren basis generated by the Malfliet–Tjon interaction

We finally consider the frequently used local Gaussian potential

$$V(r) = V_0 \exp(-r^2 \alpha^2), \quad (5.1)$$

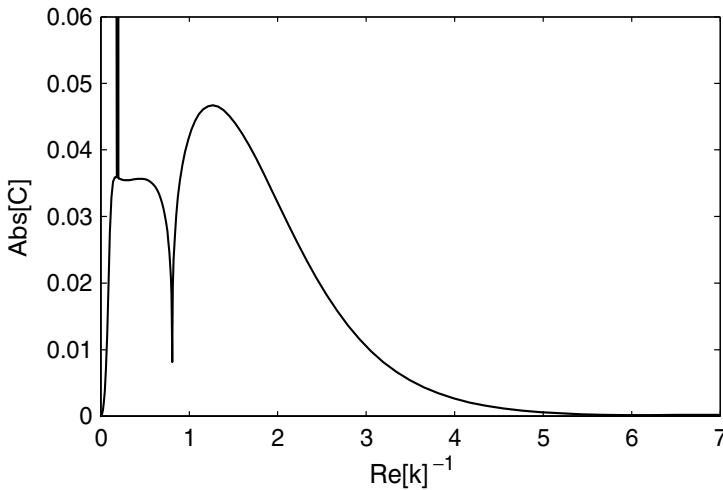


Figure 19. Plot of the absolute value of the coefficients of the Malfliet–Tjon Berggren expansion of a resonant state generated by a Gaussian potential. The coefficients are plotted as a function of $\text{Re}[k] \text{ fm}^{-1}$.

which in momentum space takes the analytic form

$$V_l(k, k') = V_0 \frac{\pi}{4\alpha^2} \frac{1}{\sqrt{kk'}} \exp\left(-\left(\frac{k^2 + k'^2}{4\alpha^2}\right)\right) I_{l+1/2}\left(\frac{kk'}{2\alpha^2}\right). \quad (5.2)$$

Here $I_{l+1/2}(z)$ is a Bessel function of the first kind with complex arguments. In the complex k -plane, the Gaussian potential diverges exponentially for $|\text{Im}[k]| > |\text{Re}[k]|$. Solving the momentum space Schrödinger equation on a rotated contour C_R^+ , we get the restriction $\theta < \pi/4$ on the rotation angle. On the other hand, we may choose a contour of the type C_{R+T}^+ and this problem is resolved, allowing for an continuation in the third quadrant of the complex k -plane.

For a range $\alpha = 1.8 \text{ fm}^{-2}$ and a depth $V_0 = 150 \text{ MeV}$ for the $l = 1$ Gaussian potential, the CDM gives a resonance with energy $E = 0.676131964 - 0.157257363i \text{ MeV}$. This resonance was calculated on the C_{R+T}^+ contour, rotated $\theta = \pi/5$ and translated $\text{Im}[k] = -\sin(\pi/5) \text{ fm}^{-1} \approx 0.5878 \text{ fm}^{-1}$. The Berggren basis was generated from the $l = 1$ Malfliet–Tjon interaction with $v_A = -5.42$ supporting a resonance with energy $E = 0.655473351 - 0.106928706i \text{ MeV}$.

Figure 19 gives the expansion coefficients of the Berggren basis as a function of the real part of the momentum. The spike at $\text{Re}[k] \approx 0.1 \text{ fm}^{-1}$ is due to the large overlap between the resonant wavefunctions of the Malfliet–Tjon and the Gaussian interaction, respectively. The discontinuity around $\text{Re}[k] \approx 0.7 \text{ fm}^{-1}$ has no physical meaning, and is due to the discontinuity in the deformed contour, where the rotated part goes into the translated part. From the distribution of the expansion coefficients one sees that the major contribution from the complex continuum occurs for $\text{Re}[k] < 5 \text{ fm}^{-1}$. On the basis of this observation, one would expect that a cutoff for a given momentum $\text{Re}[k] > 5 \text{ fm}^{-1}$ in the Berggren basis, would not influence the calculation of the resonant state and energy. Table 7 shows the convergence of the resonant energy as a function of cutoff in the Berggren basis. For $\text{Re}[k] > 5 \text{ fm}^{-1}$ the energy has converged satisfactorily.

Figures 20 and 21 show how the corresponding resonant wavefunction converges to the ‘exact’ wavefunction, and the sensitivity of the resonance wavefunction to cutoff in momentum. We observe that for a cutoff in momentum less than 5 fm^{-1} , the tail of the wavefunction is not that well reproduced, even though the resonant energy has converged

Table 7. Resonant energy of the Gaussian potential discussed above as a function of cutoff in momentum/energy in the Berggren basis generated by the Malfliet–Tjon potential. The cutoff momentum is given in units of fm^{-1} and energy in units of MeV.

Cutoff	Re[E]	Im[E]
1	5.32123	0.53077
3	0.74272	-0.02750
5	0.67748	-0.15758
10	0.67698	-0.15742
20	0.67619	-0.15727
30	0.67614	-0.15726
40	0.67613	-0.15725
Exact	0.67613	-0.15725

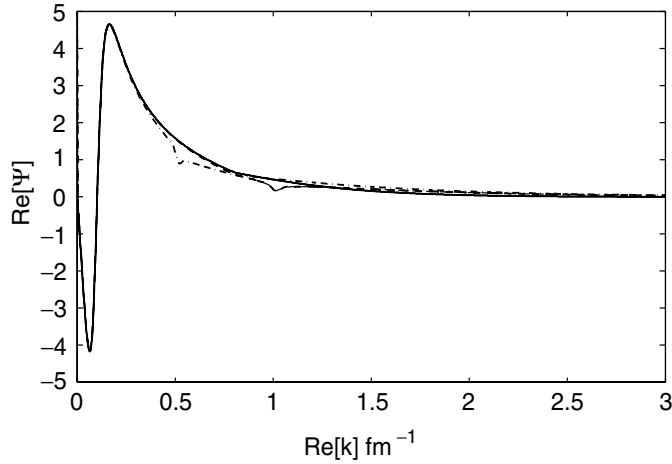


Figure 20. Plot of the real part of the resonant wavefunction generated by the Gaussian potential discussed above. The continuous line is the exact wavefunction, the broken line is the Berggren expanded wavefunction with a cutoff in momentum, $\text{Re}[k] = 1 \text{ fm}^{-1}$ and the dashed-dotted line with a cutoff $\text{Re}[k] = 0.5 \text{ fm}^{-1}$.

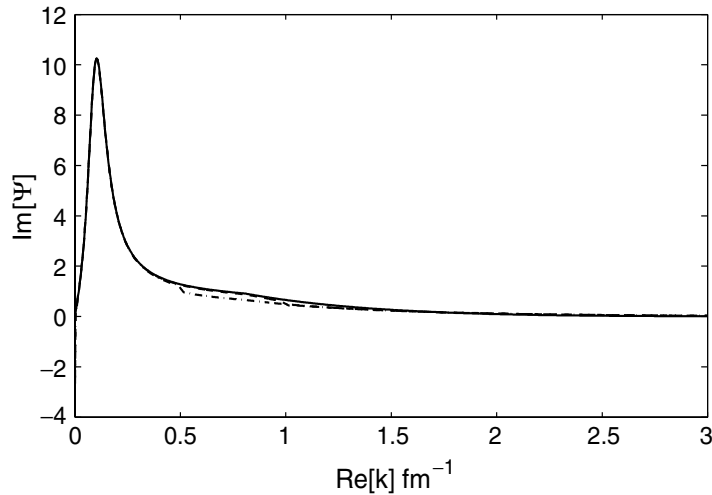


Figure 21. Plot of the imaginary part of the resonant wavefunction generated by the Gaussian potential discussed above. The continuous line is the exact wavefunction, the broken line is the Berggren expanded wavefunction with a cutoff in momentum, $\text{Re}[k] = 1 \text{ fm}^{-1}$ and the dashed-dotted line with a cutoff $\text{Re}[k] = 0.5 \text{ fm}^{-1}$.

satisfactorily for a cutoff $\text{Re}[k] = 5 \text{ fm}^{-1}$. The interior part of the momentum space resonant wavefunction is, on the other hand, well reproduced in both cases considered. Translated into the coordinate space picture, this reflects that in the cases of loosely bound or resonant states the correct tail of the wavefunction is important for reproducing the correct energy.

6. Conclusions and perspectives

A generalized CDM in momentum space has been presented. The deformation of the integration contour is generalized to rotation followed by translation in the complex k -plane. This generalization makes it possible to handle both *dilation* and *non-dilation* invariant potentials. We have, via chosen examples from subatomic physics, shown this to be a powerful procedure for studying resonances and antibound states in two-body systems. The method has also been successfully applied to the calculation of the full off-shell t -matrix.

The CDM allows for stable numerical calculations of binary bound states, resonances and antibound states, in addition to yielding a fully complex on- and off-shell scattering matrix, starting with a realistic nucleon–nucleon interaction. This also allows for several interesting applications and extensions of shell model type formulations. One of the major challenges in the microscopic description of weakly bound dripline nuclei is a proper treatment of both the many-body correlations and the continuum of positive energies and decay channels. Such nuclei pose a tough challenge for traditional nuclear structure methods, based essentially on the derivation of effective interactions and the nuclear shell-model (see e.g. [40] for a review). In the traditional approaches only bound states typically enter the determination of an effective interaction, be it either based upon various many-body schemes or more phenomenologically inspired approaches. Coupled with large-scale shell model studies, several properties of stable nuclei are well reproduced. However, weakly bound nuclei have a strong coupling to unbound states, either resonances or antibound states, as described in, for example, [4–6]. This implies in turn that an effective interaction should reflect such couplings with the continuum, i.e. a consistent many-body scheme should include bound states, resonances and antibound states as well.

The aim of this work has been to establish the formalism for the free scattering case, basing the analysis on schematic and realistic nucleon–nucleon interactions. Work on extension to Borromean halo systems [39] in few-body cluster models with more than two constituents, is in progress.

In forthcoming papers, we will discuss the application of binary CDM to shell model type formulations for dripline nuclei, extensions to few-body halo models and also complex interactions of particular relevance for nuclear reactions.

Acknowledgments

This work has been supported by the Research Council of Norway. We thank Boris V Danilin and Maxime Kartamyshev for stimulating discussions.

References

- [1] Newton R G 1982 *Scattering Theory of Waves and Particles* (New York: Springer)
- [2] Liotta R J, Maglione E, Sandulescu N and Vertse T 1996 *Phys. Lett. B* **367** 1
- [3] Id Betan R, Liotta R J, Sandulescu N and Vertse T 2003 *Phys. Rev. C* **67** 014322
- [4] Michel N, Nazarewicz W, Płoszajczak M and Bennaceur K 2002 *Phys. Rev. Lett.* **89** 042502
- [5] Michel N, Nazarewicz W, Płoszajczak M and Okołowicz J 2003 *Phys. Rev. C* **67** 054311

- [6] Id Betan R, Liotta R J, Sandulescu N and Vertse T 2002 *Phys. Rev. Lett.* **89** 042501
- [7] Vertse T, Curutchet P, Liotta R J and Bang J 1989 *Acta Phys. Hungaria* **65** 305
- [8] Id Betan R, Liotta R J, Sandulescu N and Vertse T 2004 *Phys. Lett. B* **584** 48
- [9] Kukulin V I, Krasnopol'sky V M and Horáček J 1989 *Theory of Resonances* (Amsterdam: Kluwer Academic)
- [10] Sitenko A G 1971 *Lectures in Scattering Theory* (Oxford: Pergamon)
- [11] Baz'A I, Zel'dovich Ya B and Perelomov A M 1966 *Scattering, Reactions and Decay in Nonrelativistic Quantum Mechanics* (Moscow: Fiziko-Matematicheskoi Literatury)
- [12] Afnan I R 1991 *Aust. J. Phys.* **44** 201
- [13] Aguilar J and Combes J M 1971 *Commun. Math. Phys.* **22** 269
- [14] Balslev E and Combes J M 1971 *Commun. Math. Phys.* **22** 280
- [15] Brayshaw D 1968 *Phys. Rev.* **176** 1855
- [16] Nuttall J and Cohen H L 1969 *Phys. Rev.* **188** 1542
- [17] Stelbovics A T 1978 *Nucl. Phys. A* **288** 461
- [18] Glöckle W 1978 *Phys. Rev. C* **18** 18
- [19] Berggren T 1968 *Nucl. Phys. A* **109** 265
- [20] Lind P 1993 *Phys. Rev. C* **47** 1903
- [21] Moiseyev N 1998 *Phys. Rep.* **302** 211
- [22] Csoto A 1994 *Phys. Rev. C* **49** 2244
- [23] Garrido E, Fedorov D V and Jensen A S 2002 *Nucl. Phys. A* **708** 277
- [24] Raskinyte I 2002 Resonances in few-body systems *PhD Thesis* University of Bergen, unpublished
- [25] Nuttall J 1967 *J. Math. Phys.* **8** 873
- [26] Tiktopoulos G 1964 *Phys. Rev.* **136** 275
- [27] Aoyama S 2002 *Phys. Rev. Lett.* **89** 052501
- [28] Pearce B C and Afnan I R 1984 *Phys. Rev. C* **30** 2022
- [29] Machleidt R 2001 *Phys. Rev. C* **63** 024001
- [30] Malfliet R A and Tjon J A 1969 *Nucl. Phys. A* **127** 161
- [31] Yamaguchi K 1954 *Phys. Rev.* **95** 1628
- [32] Gyarmati B and Vertse T 1971 *Nucl. Phys. A* **160** 523
- [33] Berggren T 1971 *Nucl. Phys. A* **169** 353
- [34] Berggren T 1978 *Phys. Lett. B* **73** 389
- [35] Berggren T 1996 *Phys. Lett. B* **373** 1
- [36] Brown L, Fivel D, Lee B W and Sawyer R 1963 *Ann. Phys.* **23** 167
- [37] Elster Ch, Thomas J H and Glöckle W 1998 *Few-Body Systems* **24** 55
- [38] Vertse T, Liotta R J and Maglione E 1995 *Nucl. Phys. A* **584** 13
- [39] Zhukov M V, Danilin B V, Fedorov D V, Bang J M, Thompson I J and Vaagen J S 1993 *Phys. Rep.* **231** 151
- [40] Hjorth-Jensen M, Kuo T T S and Osnes E 1995 *Phys. Rep.* **261** 125

Chapter 6

Paper2.

6.1 Introduction to Paper 2.

Paper 2 deals with the recently developed Gamow Shell Model. Constructing a single-particle Berggren basis in momentum space, generated from the Sack-Biedenharn and Breit (SBB) potential for ${}^5\text{He}$, a complete anti-symmetric two- and three particle basis is constructed. Limiting the discussion to $p_{1/2}$ and $p_{3/2}$ single-particle motion, the energy spectrum of ${}^6\text{He}$ and ${}^7\text{He}$ is solved for, using a phenomenological nucleon-nucleon interaction of a Gaussian type. In using CDM in constructing the single-particle basis, it is shown that convergence of the energy spectrum of ${}^6\text{He}$ with increasing number of non-resonant continuum orbitals is rather fast. However the dimension of the many-body space for nuclei with a larger number of valence particles increases extremely fast, and direct diagonalization methods are no longer possible. This paper deals primarily with this *dimensionality* problem. It is shown how the Lee-Suzuki similarity transformation method may be generalized to complex interactions. Constructing a two-body effective interaction in a reduced space, which exactly reproduce a limited set of eigenvalues of the full Hamiltonian, this is used in the calculation of the resonant energy spectrum of ${}^7\text{He}$. It is shown that the convergence using the similarity transformed interaction is appreciably faster than compared with the bare interaction as the model space is increased. Further, we discuss how a Multi-Reference-Perturbation-Theory-Method (MRPTM), which differs from standard MRPTM in that it is a one-state-at-a-time perturbation theory, may be applied to Gamow-Shell-Model calculations. It is shown that to second order, MRPTM gives satisfactory converged results for ${}^7\text{He}$, and reducing the dimension of the full problem to 8 – 10%. Finally an effective interaction scheme for the Gamow-Shell-Model is discussed, which combines the Lee-Suzuki similarity transformation method with the one-state-at-a-time MRPTM. And converged results for the resonant spectrum of ${}^7\text{He}$ are shown using a model space consisting of both $p_{1/2}$ and $p_{3/2}$ single-particle orbitals. The dimension is in the most severe case, that of the state $J^\pi = 3/2^-$, reduced from ≈ 40000 to ≈ 1600 . This is a promising result, and which may allow for Gamow-Shell-Model studies of nuclei consisting of a larger number of valence particles moving in a large valence space.

6.2 *Effective Interaction Techniques for the Gamow Shell Model.*

G. Hagen, M. Hjorth-Jensen and J. S. Vaagen

Accepted in Phys. Rev. C

Effective Interaction Techniques for the Gamow Shell Model

Gaute Hagen

*Centre of Mathematics for Applications, University of Oslo, N-0316 Oslo, Norway and
Department of Physics and Technology, University of Bergen, N-5007 Bergen, Norway*

M. Hjorth-Jensen

*Department of Physics and Centre of Mathematics for Applications, University of Oslo, N-0316 Oslo, Norway
PH Division, CERN, CH-1211 Geneva 23, Switzerland and
Department of Physics and Astronomy, Michigan State University, East Lansing, MI 48824, USA*

Jan S. Vaagen

*Department of Physics and Technology, University of Bergen, N-5007 Bergen, Norway
(Dated: January 13, 2005)*

We apply a contour deformation technique in momentum space to the newly developed Gamow shell model, using the drip-line nuclei ^5He , ^6He and ^7He as test cases. A major problem in Gamow shell model studies of nuclear many-body systems is the increasing number of many-body configurations due to the large number of resonant and complex continuum single-particle orbits necessary to reproduce multi-particle bound and resonant states. We address this problem using two different effective operator approaches generalized to the complex momentum plane. These are the Lee-Suzuki similarity transformation method for complex interactions and the multi-reference perturbation theory method. We show that a combination of these two approaches results in a drastic truncation of the number of relevant configurations compared with direct diagonalization. This offers interesting perspectives for studies of weakly bound systems.

I. INTRODUCTION

Present and proposed nuclear structure research facilities for radioactive beams will open new territory into regions of heavier nuclei. Such systems pose significant challenges to existing nuclear structure models since many of these nuclei will be unstable or short-lived. How to deal with weakly bound systems and coupling to resonant states is an open and interesting problem in nuclear spectroscopy. Weakly bound systems cannot be properly described within a standard shell-model approach since even bound states exhibit a strong coupling to the single-particle continuum.

It is therefore important to investigate theoretical methods that will allow for a description of systems involved in such element production. Ideally, we would like to start from an ab initio approach with the free nucleon-nucleon interaction and eventually also three-body interactions as the basic building blocks for derivation of an effective shell-model interaction. The newly developed Gamow shell model offers such a possibility, see for example Refs. [1–9]. Similarly, the recently developed Shell Model Embedded in the Continuum, see e.g. Refs. [10–13], conveys similar interesting perspectives. Here we focus on the Gamow shell model, which promises to be a powerful tool in describing and understanding the formation of multi-particle resonances within a shell-model formulation. Representing the shell-model equations using a Berggren basis [14–19], allows for an interpretation of multi-particle resonances in terms of single-particle resonances, as opposed to the traditional harmonic oscillator representation, where resonances never appear explicitly.

Although the Gamow shell model approach is a pow-

erful tool in this respect, there are major computational and theoretical challenges that need to be overcome if we aim at a realistic description of weakly bound and unbound nuclei.

One of the first problems encountered in Gamow shell model calculations, and addressed in Refs. [4, 5], was the problem of identifying the multi-particle resonances on the many-particle energy surface. Refs. [4, 5] related this identification problem to the problem of choosing a contour in the complex k -plane which in the case of two valence particles selects the physical interesting states from the dense distribution of continuum states. In Refs. [4, 5] it was pointed out that using the classical triangular Berggren contour, see e.g. Ref. [14], the unperturbed two-particle energy spectrum would embed the pole configurations in a dense distribution of pole-continuum and continuum-continuum configurations, and an identification based on inspection of the zeroth order energy spectrum is difficult. As a solution the authors employed a “square-well” contour, which in the two-particle case separates the physical states from states belonging to the complex-continuum, making such an identification possible. In this way it is possible to study how the two-particle resonance energy trajectories develop as the nucleon-nucleon interaction is gradually turned on, and in this respect this method is probably the most intuitive. Nevertheless, in the case where more than two particles are present in the shell-model space, the resonant states mix with the complex continuum states, and an identification becomes difficult.

In Refs. [2, 6, 7] the problem of identifying multi-particle resonances was approached from a different angle. The proposed algorithm bears close resemblance

with the Davidson-Liu [20, 21] method. In the first step a diagonalization within the pole space, where all particles are in resonant single particle orbitals, is performed. Secondly a diagonalization within the complete configuration space is performed. Under the assumption of weak coupling of the pole configurations with the configurations where at least one particle moves in a continuum orbital, the physical states may be picked out unambiguously from the states obtained after a full diagonalization, using the criterion of largest overlap with the pole space. Further it was noted in Refs. [2, 6, 7] that the physical states should be invariant with respect to small deformations of the integration contour, and that may serve as an additional identification criterion. This method has its strength in that the identification may in principle be carried out for any number of valence particles, under the assumption that the coupling of pole configurations with continuum configurations is weak. On the other hand this may not always be the case; As pointed out in Ref. [9] for the case of ^{11}Li the two-particle resonances may have a larger continuum component as compared to the pole component, depending on the nucleon-nucleon interaction.

In this work we consider as a test case the light drip-line nuclei $^{5,6,7}\text{He}$, and the formation of resonances in these nuclei starting from a single-particle picture. These nuclei have also been studied with a number of other methods, see for example Refs. [22, 23], and references therein. Our aim is to establish a methodological test case, where some of the basic physics is already known, and where we may try out both two- and three body forces. This paper is restricted to two-body forces and we do not go beyond three valence neutrons. We construct a single-particle basis using the contour deformation method in momentum space, discussed in detail in Ref. [19], see also Ref. [24] for further references on complex scaling. In our case, the identification problem is solved based on inspection of the unperturbed many-particle energy spectrum, as done in Refs. [4, 5]. We show that choosing a rotated plus translated contour in the complex plane, a large portion of the many-particle energy surface is free from complex continuum states, and the basic pole configurations will never be embedded in the dense continuum. Thus it is straightforward to study the resonance trajectories as the nucleon-nucleon interaction is turned on. The geometry of the contour, is of such a simple form (rotation plus translation) that on the many-particle energy surface the locations of complex energy thresholds and multi-particle resonances are easily identifiable. Our procedure tested for ^7He allows for a clear distinction of three-particle resonances from the dense distribution of complex continuum states.

The most severe problem and future challenge is that the shell-model dimension increases dramatically for $n > 2$ particles moving in a large valence space, this is what we henceforth refer to as the dimensionality problem. Using a technique such as the traditional Lanczos iteration method [25] fails in Gamow shell model calculations.

Dealing with large real symmetric matrices, the Lanczos scheme is a powerful method when one wishes to calculate the states lowest in energy. In Gamow shell model calculations there may be a large number of complex continuum states lying below the physical resonances in real energy. In addition it is difficult to predict where the multi-particle resonances will appear after diagonalization. In Refs. [6, 7] this problem was circumvented by choosing a small number of complex continuum orbits in the single-particle basis, five points for the ^{6-9}He isotopes. Taking into account all different kinds of continuum couplings, this was necessary to make the calculations feasible for the heavier He isotopes. It was also pointed out that the results obtained were not converged with respect to the number of single-particle continuum orbits. The results reported in Ref. [2] for the He isotopes used 15 points along the contour. To make calculations feasible for the heavier He isotopes at most two particles where allowed to move in complex continuum orbitals, invoking the lesson from Refs. [6, 7] that configurations with more than two particles in the continuum are of lesser importance. In Ref. [1] this assumption was further justified in GSM calculations of the Li chain. Using an optimal single particle Hartree-Fock basis, it was found in the ^7Li case with three valence particles, that the pure continuum configurations has a considerable smaller amplitude than compared to the remaining amplitudes of other configurations.

As pointed out in Refs. [6, 7], and expanded on in this work, accurate calculations of multi-particle resonances should in general take into account the effect of all kinds of configurations where particles may move in complex continuum orbitals, and correspondingly a quite large number of single particle complex continuum orbitals has to be included to obtain satisfactorily converged results. Our aim in this work is to propose an effective interaction scheme to this end. As a first step, we apply the Lee-Suzuki similarity transformation method [26–29] to Gamow shell-model calculations of the ^6He and ^7He complex energy spectra. The effective interaction is constructed at the two-body level in an optimal single-particle Berggren basis, and it is shown that in the ^7He case convergence is much faster using the effective interaction as compared to the bare interaction. Further, since our choice of contour separates the pole configurations from the dense distribution of complex continuum states in the unperturbed energy spectrum, it allows for a perturbative treatment of the many-particle resonances, since energy denominators $e_a + e_b - (e_k + e_l)$ appearing in the perturbative expansion are never zero. We apply the non-hermitian multi-reference perturbation theory method [30–32], to calculate the ^7He spectrum. In defining a suitable model space which contains the most important configurations, it is found that second order corrections are sufficient to give converged energies, using a rather small model space. Finally, we propose a perturbation theory based scheme which combines the Lee-Suzuki similarity transformation method and the

multi-reference perturbation method to account for couplings with configurations where all single-particles move in complex continuum orbits. We find that the dimensionality of the model space is drastically smaller compared to the full space, at the converged level. This scheme, tested for three valence particles, may then serve as a starting point for Gamow shell model calculations of heavier nuclei.

Up to now Gamow shell model calculations have been performed with phenomenological nucleon-nucleon interactions. A major challenge is to construct effective nucleon-nucleon interactions for drip-line nuclei starting from a realistic nucleon-nucleon interaction. In this paper we focus on the choice of contour and the dimensionality problem. The effective nucleon-nucleon interaction adopted is purely phenomenological. However, the scheme we present, although implemented with a phenomenological nucleon-nucleon interaction, allows to define effective interactions computed with the complex scaled single-particle basis. The problem of constructing an effective interaction based on present interaction models for the nucleon-nucleon force will be considered in a forthcoming work.

The outline of this work is as follows. Sec. II gives a brief description of the contour deformation method in momentum space, and presents calculations of the energy spectrum of the nuclei $^{5,6,7}\text{He}$. Sec. III presents first the Lee-Suzuki transformation method generalized to complex interactions. Thereafter we apply the similarity transformation method to the unbound nucleus ^7He and give a convergence study of the $J^\pi = 3/2^-_1$ resonance, the ground state of ^7He . Sec. IV gives a brief outline of the multi-reference perturbation method, and its application to this state. In Sec. V we present an effective interaction scheme, which combines the Lee-Suzuki similarity transformation and the multi-reference perturbation method, for calculation of multi-particle resonances in weakly bound nuclei. Sec. VI contains an application of our truncation method to the ^7He case. Sec. VII gives the conclusions of the present study and future perspectives and challenges for Gamow shell model calculations.

II. THE GAMOW SHELL MODEL

The newly developed Gamow shell model has promised to become a powerful tool in describing and understanding multi-particle resonances appearing in nuclei near the drip-lines. Here we discuss how two- and three-particle resonances are formed in ^6He and ^7He , and how they are to be understood in terms of a single-particle picture. Our choice of contour in the complex k -plane makes it easy to identify and interpret the multi-particle resonances. In this section no truncations are made, all possible configurations within a model space are used in the shell-model calculations.

A. Berggren Basis in the Momentum Representation

In Ref. [19] we studied the contour deformation method applied to the momentum space Schrödinger equation. It was discussed and shown how the specific choices of contours based on the analytic structure of the potential may allow for a unified description of bound, anti-bound (virtual) and resonant states. We will apply this method to obtain a single-particle Berggren basis for use in Gamow shell model calculations. Here we briefly outline the contour deformation method, and refer the reader to Ref. [19] for a more rigorous discussion.

The analytically continued single-particle Schrödinger equation on a general inversion symmetric contour takes the form

$$\frac{\hbar^2}{2\mu} k^2 \psi_{nl}(k) + \int_{C^+} dq q^2 V_l(k, q) \psi_{nl}(q) = E_{nl} \psi_{nl}(k). \quad (1)$$

Here both k and q are defined on an inversion symmetric contour C^+ in the lower half complex k -plane, resulting in a closed integral equation. The eigenfunctions constitute a complete bi-orthogonal set, normalized according to the Berggren metric [14–19], namely

$$1 = \sum_{n \in C} |\psi_{nl}\rangle \langle \psi_{nl}^*| + \int_{C^+} dk k^2 |\psi_l(k)\rangle \langle \psi_l^*(k)|. \quad (2)$$

In this work we construct a single-particle Berggren ensemble on a rotated plus translated contour, C_{R+T} , in the complex k -plane, studied in detail in Ref. [19]. The contour C_{R+T}^+ is part of the inversion symmetric contour $C_{R+T} = C_{R+T}^+ + C_{R+T}^-$ displayed in Fig. 1. In

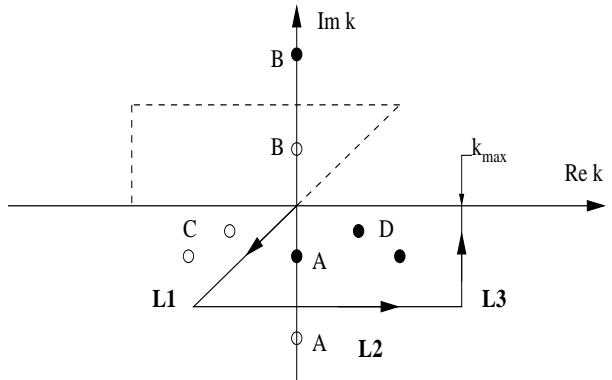


FIG. 1: Contour $C_{R+T}^+ = L_1 + L_2 + L_3$ is given by the solid line, while the contour C_{R+T}^- is given by the dashed line. The contour $C_{R+T} = C_{R+T}^+ + C_{R+T}^-$ is inversion symmetric. The single-particle spectrum which is exposed by this contour is marked by filled circles \bullet and the excluded spectrum by open circles \circ . The full spectrum includes bound states (B), anti-bound (A), decay (D) and capture (C) resonant states.

solving Eq. (1) numerically, we choose a set of N grid

points in k -space by some quadrature rule, for example Gauss-Legendre. The integral is then discretized by $\int dk \rightarrow \sum_{i=1}^N w_i$. On the chosen grid Eq. (1) takes the complex symmetric form

$$\frac{\hbar^2}{2\mu} k_i^2 \psi_{nl}(i) + \sum_j^N \sqrt{w_i w_j} k_i k_j V_l(k_i, k_j) \psi_{nl}(j) = E_{nl} \psi_{nl}(i). \quad (3)$$

Here we have defined $\psi_{nl}(i) \equiv \sqrt{w_i} k_i \psi_{nl}(k_i)$, The norm integral becomes the discrete sum

$$\delta_{n,n'} = \sum_{i=1}^N \psi_{nl}(i) \psi_{n'l}(i) = \sum_{i=1}^N w_i k_i^2 \psi_{nl}(k_i) \psi_{n'l}(k_i). \quad (4)$$

The Berggren completeness given in Eq. (2) takes the discrete form

$$1 = \sum_n^N |\psi_{nl}(i)\rangle \langle \psi_{nl}^*(i)| = \sum_n^N \sum_{i=1}^N \psi_{nl}(i) \psi_{nl}(i). \quad (5)$$

Changing from a continuous to a discrete plane-wave basis, it becomes transparent that the coordinate wave function is an expansion in a basis of spherical-Bessel functions

$$\phi_{nl}(r) = \sqrt{\frac{2}{\pi}} \sum_{i=1}^N \sqrt{w_i} k_i j_l(k_i r) \psi_{nl}(i), \quad (6)$$

where $\psi_{nl}(i)$ are the expansion coefficients. Defining the functions

$$f_l(k_i r) = \sqrt{\frac{2}{\pi}} \sqrt{w_i} k_i j_l(k_i r), \quad (7)$$

and using the discrete representation of the Dirac-delta function

$$\delta(k - k') \rightarrow \frac{\delta_{k_i, k_j}}{\sqrt{w_i w_j}}, \quad (8)$$

we get the expansion

$$\phi_{nl}(r) = \sum_{i=1}^N \psi_{nl}(i) f_l(k_i r), \quad (9)$$

where it is easily seen that the functions $f_l(k_i r)$ are orthogonal for different k_i and normalized

$$\int dr r^2 f_l(k_i r) f_l(k_j r) = \delta_{k_i, k_j}, \quad (10)$$

δ_{k_i, k_j} being the Kronecker delta. The complete and discrete set of single-particle orbits defined by this contour will then include the pole states, i.e., anti-bound, bound and resonant states, and the discretized complex continuum states defined on each point on the contour. This basis serves as our starting point for Gamow shell model calculations.

B. Single-Particle Spectrum of ${}^5\text{He}$

The unbound nucleus ${}^5\text{He}$ may be modeled by an inert ${}^4\text{He}$ core with a neutron moving mainly in the resonant spin-orbit partners $p_{3/2}$ and $p_{1/2}$. The $J^\pi = 3/2^-_1$ resonance, to be associated with the single-particle orbit $p_{3/2}$, is experimentally known to have a width of $\Gamma \approx 0.60$ MeV while the $J^\pi = 1/2^-_1$ resonance, associated with the single-particle orbit $p_{1/2}$, has a large width $\Gamma \approx 4$ MeV. For more information on these systems, see for example the recent review by Jonson [22]. The core-neutron interaction in ${}^5\text{He}$ may be phenomenologically modeled by the SBB (Sack, Biedenharn and Breit) potential [33]. The SBB potential is of Gaussian type with a spin-orbit term, fitted to reproduce the neutron - ${}^4\text{He}$ scattering phase shifts. In momentum space the SBB potential, which consists of a central part c and a spin-orbit term $\vec{\sigma} \cdot \vec{l}$, reads

$$V_{lj}(k, k') = V_{lj}^c(k, k') + (\vec{\sigma} \cdot \vec{l}) V_{lj}^{\sigma l}(k, k'), \quad (11)$$

with

$$V_{lj}^i(k, k') = -g_i \frac{\pi}{4} \frac{a_i^2}{\sqrt{kk'}} \exp\left(\frac{-a_i^2}{4} (k^2 + k'^2)\right) I_{l+1/2}\left(\frac{a_i^2}{2} kk'\right), \quad (12)$$

where the subscripts lj refer to the single-particle orbital and angular momentum quantum numbers l and j , respectively. The term $I_{l+1/2}(z)$ is a Bessel function of the first kind with complex arguments. Fitting this potential

to reproduce the ${}^5\text{He}$ single-particle resonance spectrum and phase-shifts, results in $g_c = 47.4$ MeV, $g_{\sigma l} = 5.86$ MeV and $a_c = a_{\sigma l} = 2.3$ fm.

In the complex k -plane the Gaussian potential diverges exponentially for $|\text{Im}[k]| > |\text{Re}[k]|$. If we apply the complex scaling technique, which consists of solving the momentum space Schrödinger equation on a purely rotated contour, we get the restriction $\theta < \pi/4$ on the clockwise rotation angle. Even for smaller angles we may get a poor convergence, since the Gaussian potential oscillates strongly along the rotated contours. On the other hand, choosing a contour of the type C_{R+T}^+ solves this problem, allowing for a continuation in the third quadrant of the complex k -plane. Furthermore, it yields a faster and smoother decay of the Gaussian potential along the chosen contour.

Since ${}^5\text{He}$ has only resonances in its spectrum, viz., no anti-bound states, there is no need for an analytic continuation in the third quadrant of the complex k -plane, as done in Ref. [19] for the free nucleon-nucleon interaction. We choose a contour of the type C_{R+T}^+ rotated with $\theta = \pi/4$ and translated with $|\text{Im}[k]| = 0.4 \sin(\pi/4) \approx 0.28 \text{ fm}^{-1}$ in the fourth quadrant of the complex k -plane. Figs. 2 and 3 give plots of the single-particle spectrum in ${}^5\text{He}$ for the spin-orbit partners $p_{3/2}$ and $p_{1/2}$ respectively. We have used 50 integration points both along the rotated C_R , and along the translated C_T parts of the contour C_{R+T}^+ in the complex k -plane.

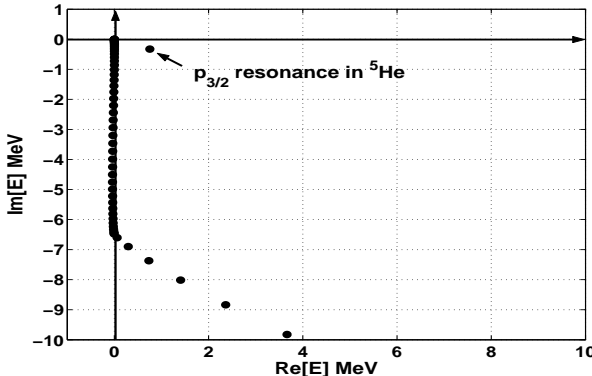


FIG. 2: Plot of the $p_{3/2}$ single-particle spectrum in ${}^5\text{He}$ for a Gaussian single-particle potential. The resonance is well located. The remaining points represent the non-resonant continuum.

Table I gives the convergence of the $p_{3/2}$ and the $p_{1/2}$ single-particle resonances as function of integration points along the contour C_{R+T}^+ . We observe that already with 12 points along the rotated path and 12 points along the translated line, one has a reasonable convergence of the resonance energy, giving in total 48 single-particle states for the valence space consisting of the lj orbits $\{p_{3/2}, p_{1/2}\}$ with their pertinent momenta k defined by the number of mesh points. It is clear that if several particles were to move in this space, the dimensionality would become enormous. It is therefore important, even at the single-particle stage, to optimize the distribution of continuum orbits, in order that the main features of the system are reproduced with a small number

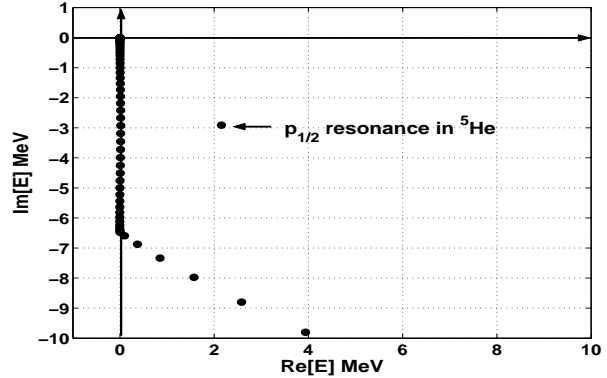


FIG. 3: Plot of the $p_{1/2}$ single-particle spectrum in ${}^5\text{He}$ for a Gaussian single-particle potential. The resonance is well located. The remaining points represent the non-resonant continuum.

of single-particle resonances and complex continuum orbits. Notice also that the calculated width of the $1/2^-$

TABLE I: Convergence of $p_{3/2}$ and $p_{1/2}$ resonance energies in ${}^5\text{He}$ as function of the number of integration points N_R along the rotated C_R and N_T along the translated part C_T of the contour. Energies are given in units of MeV.

			$J^\pi = 3/2^-$	$J^\pi = 1/2^-$	
N_R	N_T	$\text{Re}[E]$	$\text{Im}[E]$	$\text{Re}[E]$	$\text{Im}[E]$
10	10	0.752321	-0.329830	2.148476	-2.912522
12	12	0.752495	-0.327963	2.152992	-2.913609
20	20	0.752476	-0.328033	2.154139	-2.912148
30	30	0.752476	-0.328033	2.154147	-2.912162
40	40	0.752476	-0.328033	2.154147	-2.912162

resonance is somewhat larger (≈ 6 MeV) than the experimental value (≈ 4 MeV), see Ref. [22].

C. Two-Particle Resonances in ${}^6\text{He}$, including $p_{3/2}$ and $p_{1/2}$ orbits.

Next we present results for the resonant spectra of ${}^6\text{He}$. We employ again a shell-model picture with ${}^6\text{He}$ modeled by an inert ${}^4\text{He}$ core and two valence neutrons moving in the lj orbits $\{p_{3/2}, p_{1/2}\}$, ignoring the recoil of the core. The model space consists then of all momenta k defined by the set of mesh points along the various contours, pertinent to these two lj orbits. Using the single-particle wave functions for ${}^5\text{He}$ of Subsec II B, we can in turn construct an anti-symmetric two-body wave function based on these single-particle wave functions, viz.,

$$\Psi_\alpha^{JM}(1, 2) = \sum_{a \leq b} C_{a,b}^{JM} \Phi_{a,b}^{JM}(1, 2), \quad (13)$$

where the indices a, b represent the various single-particle orbits. Here $\Phi_{a,b}^J(1, 2)$ is an anti-symmetric two-particle

basis state in the $j - j$ coupling scheme. The sum over single-particle orbits is limited by $a \leq b$ since we deal with identical particles only. The expansion coefficients fulfill the completeness relation

$$1 = \sum_{a \leq b} (C_{a,b}^{JM})^2, \quad (14)$$

and the two-particle Berggren basis forms a complete set

$$1 = \sum_{a \leq b} |\Phi_{a,b}^{JM}(1,2)\rangle\langle\tilde{\Phi}_{a,b}^{JM}(1,2)|. \quad (15)$$

Here $\langle\tilde{\Phi}_{a,b}^{JM}(1,2)|$ is the complex conjugate of $\langle\Phi_{a,b}^{JM}(1,2)|$. As an effective two-neutron interaction V_{ij} we use a phe-

nomenological interaction of Gaussian type, separable in $\mathbf{r}_i, \mathbf{r}_j$ and with interaction strength V_0 , given by

$$V_{ij}(\mathbf{r}_i, \mathbf{r}_j) = V_0 G(r_i, r_j; a) \sum_{\lambda} (Y_{\lambda}(i) \cdot Y_{\lambda}(j)), \quad (16)$$

where

$$G(r_i, r_j; a) = \exp\left(-\frac{(r_i^2 + r_j^2)}{a^2}\right). \quad (17)$$

The matrix elements of Eq. (16) become

$$\langle\tilde{\Phi}_{a,b}^{JM}(1,2)|V_{12}|\Phi_{c,d}^{JM}(1,2)\rangle = V_0 \frac{\langle\tilde{\Gamma}_{a,b}^{JM}(1,2)|V_{12}|\Gamma_{c,d}^{JM}(1,2)\rangle + (-1)^{J-j_c-j_d+T} \langle\tilde{\Gamma}_{a,b}^{JM}(1,2)|V_{12}|\Gamma_{d,c}^{JM}(1,2)\rangle}{\sqrt{(1+\delta_{ab})(1+\delta_{cd})}}. \quad (18)$$

Here Γ labels non-antisymmetrized two-particle states. Further, the non-antisymmetrized direct matrix elements

are given by

$$\langle\tilde{\Gamma}_{a,b}^{JM}(1,2)|V_{12}|\Gamma_{c,d}^{JM}(1,2)\rangle = \frac{1}{2} (-1)^{j_a+j_c+J} \hat{j}_a \hat{j}_b \hat{j}_c \hat{j}_d F(a, b; c, d) \sum_{\lambda} \{1 + (-1)^{l_a+l_c+\lambda}\} \begin{Bmatrix} j_a & j_b & J \\ j_d & j_c & \lambda \end{Bmatrix} \begin{pmatrix} j_a & \lambda & j_c \\ 1/2 & 0 & -1/2 \end{pmatrix} \begin{pmatrix} j_b & \lambda & j_d \\ 1/2 & 0 & -1/2 \end{pmatrix}. \quad (19)$$

Here $\hat{j} = \sqrt{2j+1}$ and

$$F(a, b; c, d) = \int dr_1 r_1^2 \int dr_2 r_2^2 \phi_a(r_1) \phi_b(r_2) G(r_1, r_2; a) \phi_c(r_1) \phi_d(r_2). \quad (20)$$

By using the expansion of the radial wave functions in spherical Bessel functions, see Eq. (6), the interaction is obtained in the momentum space Berggren basis. Further, the Fourier-Bessel transform of a Gaussian interaction has an analytic form in momentum space, see Eq. (12).

Two model spaces were considered. The first case includes only the $p_{3/2}$ single-particle orbit for various values of the momentum k to be defined below. The second model space includes also the $p_{1/2}$ single-particle orbit

and its relevant momenta. For both model spaces we fit the interaction strength to reproduce the 0^+ binding energy in ${}^6\text{He}$. We have observed that the position of the 2^+ resonance in ${}^6\text{He}$ depends on the range a of the Gaussian interaction, even though we fit the strength so that the 0^+ ground state does not change with a . Unfortunately it turns out that for larger values of a the energy fit is better, but the convergence as function of meshpoints is poorer. Table II gives the 0^+ ground and 2^+ excited state for different values of the Gaussian range a . For each

value of a the strength of the interaction is fitted to reproduce the ground state energy $E(J^\pi = 0^+) \approx -0.98\text{MeV}$. The calculations used 12 integration points along the rotated part and 12 points along the translated part of the contour in all cases. The shape of the contour is also the same in all cases considered in Table II, and is specified in the previous subsection. First of all we observe that for larger values of the gaussian range a the convergence gets systematically poorer, since a small spurious width appears in the ground state energy, this small imaginary part of the 0^+ binding energy in ${}^6\text{He}$ would eventually disappear if the number of integration points is increased. Secondly, and more importantly, it is observed that the larger the range a becomes, the more the 2^+ resonant energy agrees with the experimentally measured values. This demonstrates that the two-particle resonant spectrum depends strongly on the radial shape of the interaction and suggests that we should rather deal with an effective interaction derived from realistic models for the nucleon-nucleon interaction. In our calculations we have chosen a value of a which is a compromise between a small number of mesh points along the contour and a reasonable good fit of the resonant energy spectra.

TABLE II: Dependence of the excited 2^+ state on the Gaussian range a . In all cases the strength V_0 has been fitted to reproduce the 0^+ binding energy of ${}^6\text{He}$. Here only $p_{3/2}$ single-particle orbits are included. The gaussian range a is in units of fm, the interaction strength V_0 in units of MeV and energies are given in units of MeV.

	$J^\pi = 0^+$			$J^\pi = 2^+$		
V_0	a	$\text{Re}[E]$	$\text{Im}[E]$	$\text{Re}[E]$	$\text{Im}[E]$	
-72.684	1.8	-0.980355	0.000047	1.415355	-0.457567	
-17.239	2.8	-0.980205	0.000320	1.333732	-0.355636	
-8.213	3.8	-0.980128	-0.000826	1.271209	-0.301898	
-5.315	4.8	-0.980067	-0.000759	1.215956	-0.267521	
-4.011	5.8	-0.980394	-0.022025	1.165703	-0.246398	
-3.3	6.8	-0.980832	-0.057382	1.038434	-0.173482	

The parameters used in our calculations are $V_0 = -5.315\text{ MeV}$ for the model space involving only the ($p_{3/2}$) states and $V_0 = -4.549\text{ MeV}$ for a model space consisting of both single-particle quantum states $p_{3/2}$ and $p_{1/2}$. We use $a = 4.8\text{ fm}$ for both model spaces.

Figs. 4 and 5 show the 0^+ and 2^+ energy spectrum, respectively, for ${}^6\text{He}$ after a full diagonalization of the two-particle shell-model equation. Here the model space is extended to both $p_{3/2}$ and $p_{1/2}$ single-particle orbits. This model space yields a bound 0_1^+ state as well as a resonant 0_2^+ state. Moreover, we obtain two resonant 2^+ states. Observe that the choice of contour (C_{R+T}^+) separates all physical relevant states from the dense distribution of complex continuum orbits in the energy plane. By this choice of contour the identification of multi-particle resonances is fairly easy, and one may study the resonant

trajectories as the interaction strength is varied.

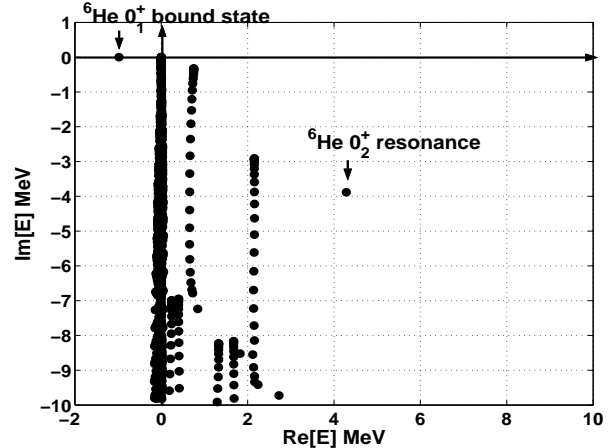


FIG. 4: Plot of the 0_1^+ bound- and 0_2^+ resonant state in ${}^6\text{He}$ for a model space consisting of the $p_{3/2}$ and $p_{1/2}$ single-particle orbits. The bound and resonant states are well located. The remaining points represent the non-resonant continuum.

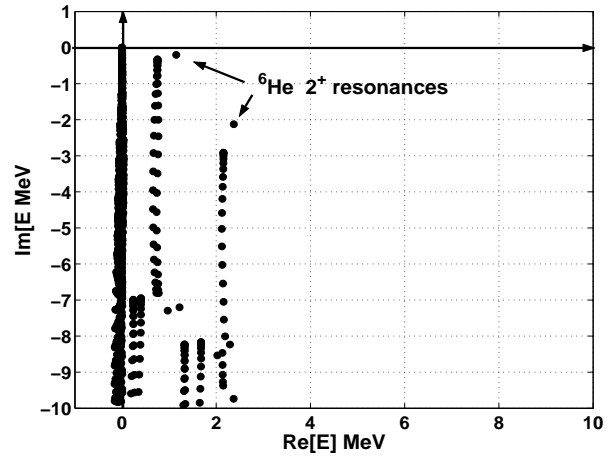


FIG. 5: Plot of 2^+ resonances in ${}^6\text{He}$ for a model space consisting of the $p_{3/2}$ and $p_{1/2}$ single-particle orbits. Both resonant states are well located. The remaining points represent the non-resonant continuum.

The stability of the 0^+ and 2^+ results as function of the number of mesh points is demonstrated in Tables III and IV. Limiting first the attention to a model space consisting only of the $p_{3/2}$ orbit, we note that with $N_R = 12$ integration points along the rotated path C_R and $N_T = 12$ points along the translated line C_T , convergence is satisfactory, i.e. even with a total of only 300 two-particle states.

Tables V, VI and VII repeat the above convergence analysis, but now employing the extended model space consisting of the $p_{3/2}$ and $p_{1/2}$ single-particle orbits, and including also the results for the lowest-lying ${}^6\text{He}$ state

TABLE III: Convergence of the 0_1^+ bound state energy in ${}^6\text{He}$ in terms of the number integration points N_R and N_T along the rotated C_R and the translated part C_T of the contour, respectively. The number N_{2p} gives the dimension of the two-particle anti-symmetrized basis. Here only $p_{3/2}$ single-particle orbits are included. Energies are given in units of MeV.

N_R	N_T	N_{2p}	Re[E]	Im[E]
12	12	300	-0.980067	-0.000759
20	20	820	-0.979508	0.000000
25	25	1275	-0.979509	0.000000

TABLE IV: Convergence of the 2_1^+ resonant state energy in ${}^6\text{He}$ as function of the number of integration points N_R and N_T along the rotated C_R and the translated part C_T of the contour, respectively. The number N_{2p} gives the dimension of the two-particle anti-symmetrized basis. Here only $p_{3/2}$ single-particle orbits are included, and energies are given in units of MeV.

N_R	N_T	N_{2p}	Re[E]	Im[E]
12	12	300	1.215956	-0.267521
20	20	820	1.216495	-0.267745
25	25	1275	1.216496	-0.267745

with quantum numbers $J^\pi = 1^+$. Increasing the model space brings several new features. We note in Table V that the first excited 0_2^+ state is a resonance. The stability of the results as functions of the number of mesh points is comparable to that seen in Tables III and IV. With approximately 12 mesh points we obtain results close to the converged ones. Similar conclusions apply

TABLE V: Convergence of 0_1^+ bound and the 0_2^+ resonant state energy in ${}^6\text{He}$ as function of the number of integration points N_R and N_T along the rotated C_R and the translated part C_T of the contour, respectively. The number N_{2p} gives the dimension of the two-particle anti-symmetrized basis. Here the $p_{3/2}$ and $p_{1/2}$ single-particle orbits are included. Energies are given in units of MeV.

$J^\pi = 0_1^+$				$J^\pi = 0_2^+$			
N_R	N_T	N_{2p}	Re[E]	Im[E]	Re[E]	Im[E]	
12	12	600	-0.980111	-0.000497	4.289194	-3.882119	
20	20	1640	-0.979148	-0.000000	4.286186	-3.882878	
25	25	2550	-0.979148	0.000000	4.286181	-3.882876	

to the 1_1^+ resonance and the two lowest-lying 2^+ resonant states, see Tables VI and VII for more details. We note that the experimental value for the width of the first excited $J^\pi = 2_1^+$ is $\Gamma \approx 113$ keV and the energy is $Re[E]_{2_1^+} = 1797$ keV. Our simplified nucleon-nucleon interaction gives a qualitative reproduction of the data. In a future work we plan to include a realistic nucleon-nucleon interaction for studies of such systems.

We end this subsection by analyzing the squared amplitude of the single-particle configurations

TABLE VI: Convergence of the 1_1^+ resonance as function of the number of integration points N_R and N_T along the rotated C_R and the translated part C_T of the contour, respectively. The number N_{2p} gives the dimension of the two-particle anti-symmetrized basis. Here the $p_{3/2}$ and $p_{1/2}$ single-particle orbits are included. Energies are given in units of MeV.

$J^\pi = 1^+$				
N_R	N_T	N_{2p}	Re[E]	Im[E]
12	12	1128	1.945539	-2.920286
20	20	3160	1.940263	-2.930619
25	25	4950	1.940266	-2.930608

TABLE VII: Convergence of the 2_1^+ and 2_2^+ resonance energy in ${}^6\text{He}$ as function of the number of integration points N_R and N_T along the rotated C_R and the translated part C_T of the contour, respectively. The number N_{2p} gives the dimension of the two-particle anti-symmetrized basis. Here the $p_{3/2}$ and $p_{1/2}$ single-particle orbits are included. Energies are given in units of MeV.

$J^\pi = 2_1^+$				$J^\pi = 2_2^+$			
N_R	N_T	N_{2p}	Re[E]	Im[E]	Re[E]	Im[E]	
12	12	876	1.149842	-0.203052	2.372295	-2.122474	
20	20	2420	1.150527	-0.203060	2.372818	-2.123253	
25	25	3775	1.150527	-0.203060	2.372817	-2.123254	

$|RR\rangle, |RC\rangle, |CC\rangle$ of the $0^+, 1^+$ and 2^+ bound- and resonant wave functions. The results are given in Tables VIII, IX, X, XI and XII. The reason for doing this analysis is due to the fact that our single-particle basis consists of both resonant and continuum single-particle orbits. By performing such an analysis we can disentangle the contribution from for example the non-resonant continuum. In these tables, $|RR\rangle$ stands for both single-particle orbits being in a resonant single-particle orbit, $|RC\rangle$ means that one single-particle orbit is a resonant single-particle orbit and the other a non-resonant continuum single-particle orbit, while for $|CC\rangle$ both single-particle orbits are from the non-resonant single-particle continuum. All the results show that the configurations where both single-particles are resonant orbits, have the largest amplitude in the two-body wave function. It is also seen, that the configurations where both particles are in complex continuum orbits have a small effect on the formation of two-particle resonances in ${}^6\text{He}$. This is a useful result which we will exploit below when we define effective interactions for smaller spaces.

D. Three-Particle Resonances in ${}^7\text{He}$, including $p_{3/2}$ only.

Finally we consider the unbound nucleus ${}^7\text{He}$, which ground state ($J^\pi = 3/2^-$) located ≈ 0.5 MeV above the ${}^6\text{He}$ ground state, and with a measured width $\Gamma \approx 160$

TABLE VIII: Expansion coefficients of the 0_1^+ bound state in ${}^6\text{He}$. The $p_{3/2}$ and $p_{1/2}$ single-particle orbits define the model space. See text for further discussions.

	$(p_{3/2}^2)$		$(p_{1/2}^2)$	
	Re[C ²]	Im[C ²]	Re[C ²]	Im[C ²]
$ RR\rangle$	1.10488	-0.83161	0.22620	-0.16120
$ RC\rangle$	-0.06036	0.88137	-0.19842	0.22423
$ CC\rangle$	-0.09716	-0.04974	0.02486	-0.06305

TABLE IX: Expansion coefficients of the 0_2^+ resonance in ${}^6\text{He}$. The $p_{3/2}$ and $p_{1/2}$ single-particle orbits define the model space. See text for further discussions.

	$(p_{3/2}^2)$		$(p_{1/2}^2)$	
	Re[C ²]	Im[C ²]	Re[C ²]	Im[C ²]
$ RR\rangle$	-0.01136	-0.08003	0.90189	0.33029
$ RC\rangle$	0.04282	-0.03939	0.05966	-0.24478
$ CC\rangle$	0.00617	0.00494	0.00082	0.02896

TABLE X: Expansion coefficients of the 1^+ resonance in ${}^6\text{He}$. The $p_{3/2}$ and $p_{1/2}$ single-particle orbits define the model space. See text for further discussions.

	$(p_{1/2}p_{3/2})$		$(p_{1/2}^2)$		$(p_{3/2}^2)$	
	Re[C ²]	Im[C ²]	Re[C ²]	Im[C ²]	Re[C ²]	Im[C ²]
$ RR\rangle$	0.71068	-0.03739				
$ RC\rangle$	0.00381	-0.06948	0.00016	0.00003	0.02224	0.01171
$ CR\rangle$	0.20647	0.05208	0.00037	0.00071	0.07067	0.03807
$ CC\rangle$	-0.00984	-0.00149	-0.00031	-0.00009	-0.00424	0.00585

TABLE XI: Expansion coefficients of the 2_1^+ resonance in ${}^6\text{He}$. The $p_{3/2}$ and $p_{1/2}$ single-particle orbits define the model space. See text for further discussions.

	$(p_{1/2}p_{3/2})$		$(p_{3/2}^2)$	
	Re[C ²]	Im[C ²]	Re[C ²]	Im[C ²]
$ RR\rangle$	0.11394	-0.00494	0.96962	0.05539
$ RC\rangle$	-0.00474	0.02531	-0.00178	-0.00018
$ CR\rangle$	-0.02776	-0.03796	-0.05069	-0.02708
$ CC\rangle$	0.00229	-0.00772	-0.00089	-0.00282

TABLE XII: Expansion coefficients of the 2_2^+ resonance in ${}^6\text{He}$. The $p_{3/2}$ and $p_{1/2}$ single-particle orbits define the model space. See text for further discussions.

	$(p_{1/2}p_{3/2})$		$(p_{3/2}^2)$	
	Re[C ²]	Im[C ²]	Re[C ²]	Im[C ²]
$ RR\rangle$	0.88847	-0.03742	0.08911	-0.03742
$ RC\rangle$	-0.04888	0.05674	-0.00104	-0.00055
$ CR\rangle$	0.06058	-0.03336	-0.00072	-0.02469
$ CC\rangle$	0.01131	-0.00447	0.00115	-0.00220

keV. Other continuum structures, with tentative spin assignments $J^\pi = 1/2^-$, and $J^\pi = 5/2^-$, have been observed, see for example Ref. [22] for an extensive review of the experimental situation. In this subsection we limit the attention to a model defined by the $p_{3/2}$ single-particle orbits only. We limit the attention to the $J^\pi = 3/2^-$ resonance only. The reason we do not include the $p_{1/2}$ single-particle orbits is that we aim at a diagonalization in the full space, taking into account all complex continuum couplings. This model calculation will serve as a later reference. In the case of 24 mesh points in momentum space for the $p_{3/2}$ single-particle quantum numbers lj , the total dimension d of the ($J^\pi = 3/2^-$) three-particle problem is $d = 9224$. If in addition, we were to include 24 single-particle momenta for the $p_{1/2}$ single-particle quantum numbers lj , we would have roughly $d \sim 40000$ three-body configurations. We will return to the full $p_{3/2}, p_{1/2}$ space in Section VI, using the truncation scheme of the following sections. In Refs. [6] and [7] the dimensionality problem was circumvented by choosing a small number of complex continuum orbits, typically of the order of five, although it was found that a larger number continuum orbits had to be included to obtain converged results. As for ${}^6\text{He}$, we construct a three-body wave function using the single-particle wave functions defined in ${}^5\text{He}$. The three-body wave function is expanded in a three-particle anti-symmetric Berggren basis

$$\Psi_\alpha^{JM}(1, 2, 3) = \sum_{a \leq b \leq c} C_{(a,b)c}^{JM} \Phi_{(a,b)c}^{JM}(1, 2, 3), \quad (21)$$

where the completeness relation reads

$$1 = \sum_{a \leq b \leq c} |\Phi_{(a,b)c}^{JM}(1, 2, 3)\rangle \langle \tilde{\Phi}_{(a,b)c}^{JM}(1, 2, 3)|, \quad (22)$$

with

$$1 = \sum_{a \leq b \leq c} (C_{(a,b)c}^{JM})^2. \quad (23)$$

The two-body nucleon-nucleon interaction is the same as that used for ${}^6\text{He}$. Fig. 6 gives the energy spectrum after a full diagonalization of the three-particle Gamow shell model equation. It is seen that the choice of contour in calculating the single-particle spectrum is again optimal since all physical interesting states are well separated from the dense distribution of complex scattering states. The $J^\pi = 3/2^-$ resonance appears at the energy $E_{3/2^-} = -(0.12 + 0.12i)$ MeV. The $J^\pi = 3/2^-$ energy spectrum of ${}^7\text{He}$ plotted in Fig. 6, shows that the 0^+ and 2^+ states in ${}^6\text{He}$, and the $3/2^-$ state in ${}^5\text{He}$, form complex thresholds. The physical interpretation of these three-particle states is, in the case of the ${}^6\text{He}$ thresholds, that two of the neutrons form either the 0^+ ground state or the 2^+ resonant state, while the third neutron is moving in a complex continuum orbit. In the case of the ${}^5\text{He}$ complex threshold, two neutrons move in complex continuum orbits while the third forms the $3/2^-$ ground state in ${}^5\text{He}$.

A diagonalization within the reduced space, where at most two particles move in continuum orbits gives the resonance energy $-(0.14 + 0.16i)$ MeV, which shows that the effect coming from all particles moving in the continuum is not negligible, but small.

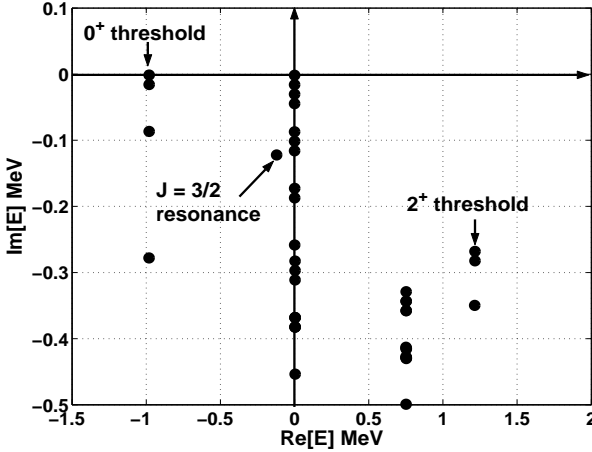


FIG. 6: Plot of the $3/2^-$ complex energy spectrum of ${}^7\text{He}$ for a model space consisting of $p_{3/2}$ single-particle orbits only. The $J^\pi = 3/2^-$ resonance is located at $E_{3/2^-} = -(0.120731 + 0.122211i)$ MeV.

Table XIII gives the squared amplitudes of the various single-particle configurations in the ${}^7\text{He}$ ground state, $\{|RRR\rangle, |RRC\rangle, |RCC\rangle, |CCC\rangle\}$, where again R labels a single-particle resonance and C a complex single-particle continuum orbit. It is seen that the most important configuration, as in the case of ${}^6\text{He}$, is the one where all single-particles are in the $p_{3/2}$ single-particle resonant orbit. The effect of configurations where all particles are in continuum orbits is small, which suggest that the coupling to configurations $|CCC\rangle$ may be taken into account perturbatively. This a feature we will exploit in Secs. III and IV.

In Fig. 6 we note that the $J^\pi = 3/2^-$ ground state in ${}^7\text{He}$ appears at an energy of approximately 0.86 MeV above the ground state in ${}^6\text{He}$, while the experimental value is at approximately 0.5 MeV. This discrepancy with experiment can be understood in terms of the configuration $|RRR\rangle$, and the choice of interaction. Focusing on the first aspect and using coefficients of fractional parentage, we can rewrite the $|RRR\rangle$ configuration as

$$|(p_{3/2})^3; J^\pi = 3/2^-\rangle = \frac{1}{6}|(p_{3/2})_0^2 p_{3/2}; J^\pi = 3/2^-\rangle - \sqrt{\frac{5}{6}}|(p_{3/2})_2^2 p_{3/2}; J^\pi = 3/2^-\rangle. \quad (24)$$

From the geometry one may conclude that the ground state of ${}^7\text{He}$ bears much more resemblance with the 2_1^+ resonance than with the 0_1^+ ground state of ${}^6\text{He}$. In our calculations the 2_1^+ resonance comes at an energy $\approx (1.2 - 0.26i)$ MeV, which is roughly 2.2 MeV above the 0_1^+ ground state of ${}^6\text{He}$, to be contrasted with the experimental value of ≈ 1.8 MeV. This suggests that if we were to increase the attractive strength of the $J^\pi = 2^+$ interaction in ${}^6\text{He}$ and get a better agreement with the experimental value, the $J^\pi = 3/2^-$ resonant ground state of ${}^7\text{He}$ would also get closer to the experimental results.

III. EFFECTIVE INTERACTIONS FOR THE GAMOW SHELL MODEL

A. The Lee-Suzuki Similarity Transformation for Complex Interactions

The previous section served to introduce and motivate the application of complex scaling and a Berggren basis in studies of weakly bound nuclear systems. How-

TABLE XIII: Expansion coefficients of the $J^\pi = 3/2^-$ ground state in ${}^7\text{He}$. Here only $p_{3/2}$ single-particle orbits are included.

	$ p_{3/2}^3\rangle$
	Re[C ²] Im[C ²]
$ RRR\rangle$	1.295549 -0.986836
$ RRC\rangle$	-0.184544 1.099729
$ RCC\rangle$	-0.115738 -0.110375
$ CCC\rangle$	0.004733 -0.002518

ever, employing such a momentum space basis soon exceeds feasible dimensionalities in shell-model studies. To circumvent this problem and to be able to define effective interactions of practical use in shell-model calculations, we introduce effective two-body interactions based on similarity transformation methods. These interactions are in turn employed in Gamow shell model calculations. We base our approach on the extensive works of Suzuki, Okamoto, Lee and collaborators, see for example Refs. [26–29]. This similarity transformation method has been widely used in the construction of effective two-

and three-body interactions for use in the No-Core shell-model approach of Barrett, Navratil, Vary and collaborators, see for example Refs. [34–37] and references therein. However, since the similarity transformation method has previously only been considered for real interactions, we need to extend its use to Gamow shell model calculations, implying a generalization to complex interactions.

To achieve the latter we introduce first the two-body Schrödinger equation

$$H|\Psi_\alpha^J\rangle = (H_0 + V_{12})|\Psi_\alpha^J\rangle = E_\alpha|\Psi_\alpha^J\rangle, \quad (25)$$

which in our specific case represents the ${}^6\text{He}$ shell model equations discussed in detail in Subsec. II C. Here H_0 includes the single-particle part of the Hamiltonian, kinetic energy and an eventual single-particle potential. The term V_{12} is the residual two-body interaction, which we have chosen to be of separable Gaussian form, see Eq. (16). The exact wave function Ψ_α^J is expanded in the anti-symmetric two-particle basis of Eq. (13) generated from the single-particle basis of H_0 , corresponding to the basis from the ${}^5\text{He}$ calculations of Subsec. II B.

The aim is to construct an effective interaction in a reduced two-particle space (model space). The most natural way of defining the two-particle model space is to start from a single-particle formulation. Starting with the single-particle Berggren basis for ${}^5\text{He}$, this space is divided in two sub-spaces, i.e., a single-particle model space (p) and a corresponding complement space (q). These single-particle spaces define in turn our two- (and many-particle) model spaces

$$P = \sum_{a \leq b} |\Phi_{a,b}^J(1,2)\rangle\langle\tilde{\Phi}_{a,b}^J(1,2)|, \quad a, b \in p \quad (26)$$

and the complement space

$$Q = \sum_{a \leq b} |\Phi_{a,b}^J(1,2)\rangle\langle\tilde{\Phi}_{a,b}^J(1,2)|, \quad \begin{cases} a \in p \wedge b \in q \\ a, b \in q \end{cases} \quad (27)$$

The anti-symmetric two-particle basis follows the Berggren metric, and is normalized according to

$$\langle\tilde{\Phi}_{a,b}^J(1,2)|\Phi_{c,d}^J(1,2)\rangle = \frac{\delta_{a,c}\delta_{b,d} - (-1)^{j_a+j_b-J}\delta_{a,d}\delta_{b,c}}{\sqrt{(1+\delta_{a,b})(1+\delta_{c,d})}} \quad (28)$$

The projection operators fulfill the relations

$$P^2 = P, \quad Q^2 = Q, \quad P^T = P, \quad (29)$$

and

$$Q^T = Q, \quad P + Q = 1, \quad PQ = 0, \quad (30)$$

where T indicates the transpose. The first challenge is then obviously how to define a suitable single-particle model space within the Berggren formalism. Ideally the model space should consist of the single-particle orbitals which in the two-, three- and many-body problems give the most important many-body correlations. In defining p within the No-Core Shell Model approach [34–37], one typically selects the n_p lowest oscillator states. Dealing with a single-particle Berggren basis, selecting p is not a straightforward procedure. First, it is rather obvious that the single-particle resonant orbitals should be part of p , on the other hand it is not obvious which non-resonant continuum orbitals should be part of p . One could for example choose the continuum orbitals lowest in real, imaginary or absolute value of the energy, or should one rather choose the non-resonant continuum orbitals closest in energy to the single-particle resonances?

Our prescription of selecting p is based on our knowledge of the physical system, ${}^7\text{He}$, in which we ultimately wish to apply the effective two-body interaction. In Sec. II it was shown that the $J^\pi = 3/2^-$ ground state of ${}^7\text{He}$ has the 2^+ resonance in ${}^6\text{He}$ as an important two-body configuration, see Eq. (24). Based on this result, a viable starting point is to study the single-particle strengths in the 2^+ resonance wave function. To understand the nature of two-particle resonances and how they are formed in a shell-model framework, it is natural to study and analyze the single-particle strengths in the two-particle wave function, and how they are distributed among the single-particle resonances and the various complex continuum orbits, given on a specific contour in the complex k -plane.

The single-particle density operator is given by

$$\hat{n}_i = \sum_j^N |\psi_i(j)\rangle\langle\tilde{\psi}_i(j)|, \quad N = \sum_i \hat{n}_i, \quad (31)$$

where N is the total number of particles, and i represents the single-particle orbit, and their quantum numbers. In the case of ${}^6\text{He}$ with an inert ${}^4\text{He}$ core, $N = 2$. To find the probability, n_i , that either particle 1 or particle 2 is in the single-particle orbit i , we calculate the matrix element of \hat{n}_i with the two-particle resonance wave function,

$$n_i = \langle\tilde{\Psi}_\alpha^J(1,2)|\hat{n}_i|\Psi_\alpha^J(1,2)\rangle = \sum_{a \leq b} \sum_{c \leq d} C_{a,b}^\alpha C_{c,d}^\alpha \left(\frac{1}{(1+\delta_{a,b})(1+\delta_{c,d})} \right)^{1/2} \times \\ \{\delta_{d,i}\delta_{c,i}\delta_{b,d} + (-1)^{j_c+j_i-J+1}\delta_{a,i}\delta_{d,i}\delta_{b,c} + \delta_{b,i}\delta_{d,i}\delta_{a,c} + (-1)^{j_a+j_i-J+1}\delta_{b,i}\delta_{c,i}\delta_{a,d}\}. \quad (32)$$

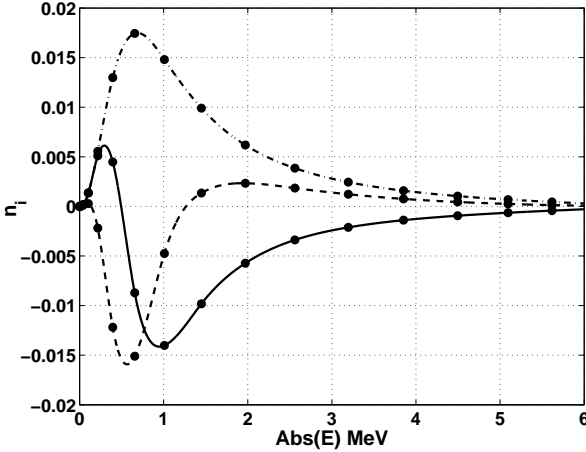


FIG. 7: Plot of the $p_{3/2}$ single-particle complex continuum strength n_i in the two-particle resonance wave function 2_1^+ in ${}^6\text{He}$. The solid line gives the real part, the dotted line the imaginary and the dash-dotted line the absolute value of the strength. The filled circles give the actual location of the complex continuum states in absolute value of energy.

Fig. 7 gives the real, imaginary and absolute values of the single-particle strength among the complex continuum orbits in the 2^+ resonance in ${}^6\text{He}$. The strengths are plotted as a function of the absolute value of the complex continuum energy. Observe that the continuum states near the 2^+ resonance in ${}^6\text{He}$ have the largest strength. This may be understood as an interference effect between the single-particle resonance and the continuum orbits located closest in energy (momentum) to the $p_{3/2}$ single-particle resonance. When defining a single-particle model space, we choose the single-particle resonant and complex continuum orbits with the largest absolute value of the single-particle strength. With this recipe we have a consistent way of defining a single-particle model space, which forms the basis for constructing an effective interaction in the two-particle model space.

Having defined a two-particle model space, we wish to construct an effective two-body interaction within P , which reproduces in the P -space exactly N_P selected eigenvalues of the full Hamiltonian. This can be accomplished by a similarity transformation

$$\tilde{H} = e^{-\omega} H e^{\omega}, \quad (33)$$

where ω is defined by $\omega = Q\omega P$. It follows that $\omega^2 = \omega^3 = \dots = 0$ and $e^\omega = P + Q + \omega$. The two-body shell model equation (25) can then be rewritten in a 2×2 block structure

$$\begin{pmatrix} P\tilde{H}P & P\tilde{H}Q \\ Q\tilde{H}P & Q\tilde{H}Q \end{pmatrix} \begin{pmatrix} P\Psi_\alpha^J \\ Q\Psi_\alpha^J \end{pmatrix} = E_n \begin{pmatrix} P\Psi_\alpha^J \\ Q\Psi_\alpha^J \end{pmatrix}. \quad (34)$$

If $P\tilde{H}P$ is to be the two-particle effective interaction, reproducing exactly N_P eigenvalues of H , the decoupling condition $P\tilde{H}Q = 0$ must be fulfilled. One may show

that the decoupling condition becomes [26, 27]

$$QHP + QHQ\omega - \omega PHP - \omega PHQ\omega = 0, \quad (35)$$

with ω acting as a transformation from the model space P to its complement Q , viz.,

$$\langle \tilde{\Phi}_{c,d}^J | \Psi_\alpha^J \rangle = \sum_{a \leq b} \langle \tilde{\Phi}_{c,d}^J | \omega | \Phi_{a,b}^J \rangle \langle \tilde{\Phi}_{a,b}^J | \Psi_\alpha^J \rangle. \quad (36)$$

With $\Phi_{a,b}^J \in P$ and $\Phi_{c,d}^J \in Q$ respectively. In constructing the two-body effective interaction, one obviously needs the solution for the transformation operator ω . This is obtained in two steps. In the first step the two-body shell model equation (25) is solved exactly, this is done for ${}^6\text{He}$ in SubSec. II C for all relevant spins. Secondly, N_P exact solutions of Eq. (25) are selected, and this set of exact solutions then enters Eq. (36). Now the question arises which N_P exact solutions should be picked out. The effective interaction generated in the model space depends on the N_P exact solutions entering Eq. (36). This is why the effective interaction generated by the similarity transformation method is often referred to as a state dependent effective interaction, and there is no unique solution for ω . From Eq. (36), it is seen that the solution for ω may be obtained as long as the matrix $\langle \tilde{\Phi}_{a,b}^J | \Psi_\alpha^J \rangle$ is invertible and non-singular. Based on this, we choose those N_P exact solutions Ψ_α^J with the largest overlap with the two-particle model space states $\Phi_{a,b}^J$. With the solution ω , the non-hermitian effective interaction R is given by [26, 27]

$$R = P\tilde{H}P - PHP = PV_{12}P + PV_{12}Q\omega. \quad (37)$$

It would be preferable to obtain a complex symmetric effective interaction, in order to take advantage of the anti symmetrization of the two-particle basis. This may be accomplished by a complex orthogonal transformation

$$V_{\text{eff}} = U^{-1}(H_0 + V_{12})U - H_0, \quad (38)$$

where U is complex orthogonal and defined by

$$U = \exp(-S), \quad S = \operatorname{arctanh}(\omega - \omega^T), \quad (39)$$

and

$$U^T U = UU^T = 1, \quad U^T = U^{-1}. \quad (40)$$

Such complex orthogonal transformations preserve the Berggren metric $x^T x$ of any vector $x \in \{C^n\}$. This feature allows us to define a complex symmetric effective two-body interaction

$$V_{\text{eff}} = (P + \omega^T \omega)^{1/2} (PHP + PHQ\omega) (P + \omega^T \omega)^{-1/2} - H_0. \quad (41)$$

In the limit $N_P = N$, where N is dimension of the fully two-body problem, the effective interaction equals the “bare” interaction (V_{12}). To determine V_{eff} numerically, one has to find the square root of the matrix

$A = (P + \omega^T \omega)$. In the case of A being real and positive definite the method based on eigenvector decomposition gives generally a stable solution. For a complex matrix A the procedure based on eigenvector decomposition is generally numerically unstable. An approach suitable for complex matrices is based on properties of the matrix sign function. It can be shown that the square root of the matrix is related to the matrix sign function, see Ref. [38] for more details. In the case of A being complex and having all eigenvalues in the open right half complex plane, iterations based on the matrix sign function are generally more stable. Here we have applied a stable iteration scheme for the matrix sign derived by Denman and Beavers, see Ref. [39] for further details.

Now we have at hand all the tools necessary for the numerical determination of an effective two-body interaction for use in Gamow shell model calculations of ${}^7\text{He}$. Summarizing, the recipe is as follows

- We choose first a set of single-particle orbits and divide them into a single-particle model space (p) and a single-particle excluded space (q).
- The single-particle orbits define in turn a two-body model space (P) and a two-body excluded space (Q).
- We diagonalize thereafter the two-body Schrödinger equation exactly and derive a model space effective interaction V_{eff} by a similarity transformation.
- This two-body effective interaction V_{eff} can in turn be used in a many-body context such as large-scale shell-model diagonalizations.

Below we apply the Lee-Suzuki similarity transformation method to the Gamow shell model calculation of the ground state of ${}^7\text{He}$, for the case of $p_{3/2}$ single particle motion only, fully diagonalized in Subsec II D. The three-particle model space is defined by all single-particle orbits belonging to p in the same way as the two-particle model space was defined in Eq. (26). Having constructed the two-body effective interaction, the equation to be solved for three particles is (see Appendix),

$$(H_0 + \sum_{i < j}^3 V_{\text{eff}}(i, j))|\Psi_\alpha^J\rangle = E_\alpha|\Psi_\alpha^J\rangle, \quad (42)$$

Figs. 8 and 9 show the convergence of the real and imaginary part of the $J^\pi = 3/2^-$ resonance in ${}^7\text{He}$, as the model space is increased. For comparison we plot the results for a diagonalization within the model space using the “bare” interaction. It is seen that results with the effective interaction constructed with the similarity transformation method converges much faster than results obtained with the “bare” interaction. We see that a satisfactory convergence is obtained with 10–11 single-particle Berggren states in the single-particle model space p from ${}^5\text{He}$, corresponding to $\approx 700 - 800$ three-particle

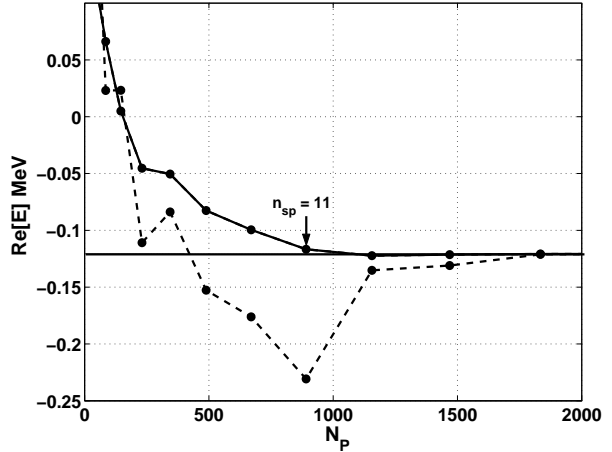


FIG. 8: Convergence of the real part of the $J^\pi = 3/2^-$ resonance in ${}^7\text{He}$ for a space defined by occupation of $p_{3/2}$ single-particle orbits only. The abscissa represents the number of three-particle model space configurations N_P while n_{sp} represents the total number of single-particle momenta for the $p_{3/2}$ single-particle quantum numbers l_j . The solid line corresponds to the effective interaction generated by the Lee-Suzuki similarity transformation method, while the dashed line is obtained using the bare interaction and the same number of three-body configurations. The $3/2^-$ resonance is located at $E = -(0.120731 + 0.122211i)$ MeV. The horizontal line is the real energy obtained in the full space of three-body configurations.

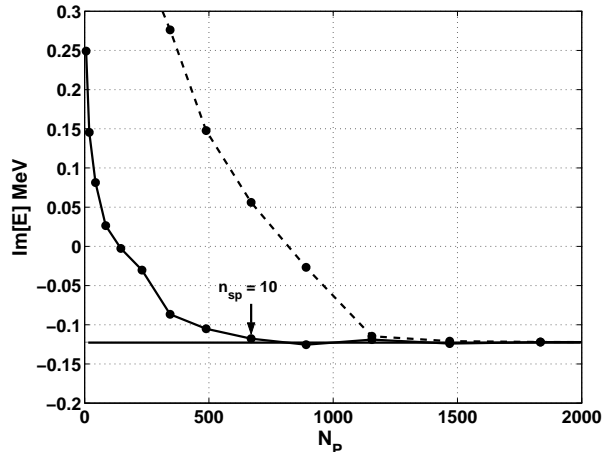


FIG. 9: Same legend as in Fig. 8, but now for the imaginary part.

states N_P . Compared with the full dimension of the three-particle problem, 9224, we have drastically reduced the dimension to about 8% of the full space. This is a considerable benefit which may allow us to extend the Gamow shell model with a complex scaled single-particle basis to heavier systems and realistic effective interactions. However, we can further improve upon this approach by considering perturbative techniques as well.

Perturbative techniques have been widely used in atomic, molecular and nuclear many-body problems. It represents one of many possible approaches for reducing the dimensionality of the many-body problem. Below we focus on recent approaches from quantum chemistry see for example Refs. [30–32]. There the emphasis is on scattering theory and electron decays in many-body systems.

In quantum chemistry the interaction is rather well established and perturbative methods are viable possibilities. In the nuclear many-body problem we need however to renormalize the short range part of the nucleon-nucleon and/or three-body force, in order to obtain an effective interaction which can be used in for example shell-model studies. The Lee-Suzuki scheme has been successfully used for renormalizing the nucleon-nucleon force and its short range behavior. Other techniques such as the two-body G -matrix discussed in Ref. [40] serve much of the same purposes and can be used as effective interactions for nuclear many-body approaches. Such effective interactions, defined for large two-body spaces, are in turn used to generate medium dependent correlations using techniques such as the Coupled Cluster methods [40, 41] or many-body perturbation theory.

Our ultimate goal is thus to marry the Lee-Suzuki approach with either perturbative many-body techniques and/or coupled cluster methods in order to derive many-body correlations not present at the two-body level of Eq. (25).

However, since much progress has been achieved in quantum chemistry for decaying systems based on perturbative many-body methods, we focus on these techniques *only* in the next section.

In Sec. V we bring together the Lee-Suzuki scheme with many-body perturbation theory discussed in Sec. IV and show that the combination of the two, and offers a viable approach to study weakly bound systems.

IV. THE MULTI-REFERENCE PERTURBATION METHOD

The Möller-Plesset multi-reference perturbation theory method (MRPTM) has recently been revived in quantum chemistry, see for example Refs. [30–32], with emphasis on scattering theory and electron decays in many-body systems. Here we only give a brief outline of the method, and refer the reader to Refs. [30–32] for further details. The basic idea of the multi-reference perturbation method is to first diagonalize within a small space (reference space), and then add a perturbation to the reference states by taking into account excitations from the reference space to the complement space. In the application of MRPTM to the formation of three-particle resonances in ${}^7\text{He}$, we first have to define a suitable three-particle reference (model) space. The chosen model-space P should ideally contain most of the correlations in the fully correlated three-particle wave function, hence the coupling of P with the complement space Q should be

weak. Based on our knowledge from the two-particle system ${}^6\text{He}$, studied in Subsec. II C, a reasonable good choice for the complement space, Q , would consist of three-body configurations where all particles move in complex continuum orbits. This is corroborated by studying the squared amplitudes of the three-particle configurations given in Table XIII of the ${}^7\text{He}$ ground state, where it is seen that the amplitudes of configurations where all particles move in continuum orbits are small. In Refs. [6] and [7], where the Helium isotopes ${}^{6-9}\text{He}$ were studied within the Gamow shell model formulation, the authors reached similar conclusions for ${}^6\text{He}$ and ${}^7\text{He}$. The three-particle model space, and corresponding complement space, used in our MRPTM calculations of ${}^7\text{He}$ is then defined by

$$P \equiv \left\{ \begin{array}{l} |RRR\rangle, |RRC\rangle, |RCC\rangle, \\ \text{Re}(e_a + e_b + e_c) < E_{\text{cut}}, \\ \text{Im}(e_a + e_b + e_c) > -E_{\text{cut}} \end{array} \right\} \quad Q = 1 - P, \quad (43)$$

where the P space is given by configurations where at most two particles move in continuum orbits. In addition, P is further defined by a rectangular cutoff in the complex energy plane. This cutoff in energy is motivated by our assumption that three-particle configurations high in energy play a minor role on the formation of low-lying resonances. Note that this way of defining a three-particle model space is different from the one used in the previous section, where the two- and three particle model spaces were dictated by the single-particle model and complement space p and q respectively. In our MRPTM calculations of ${}^7\text{He}$ we start with the complete single particle space $p + q$, and construct all $N = N_P + N_Q$ possible three-particle configurations for given spin and parity. Having constructed a complete three-particle anti-symmetric basis, the three-particle space is divided in a model P and a complement space Q by some given selection criterion, in our case the criterion given in Eq. (43). Fig. 10 gives a plot of the $J^\pi = 3/2^-$ unperturbed (non-interacting) three-particle spectrum of ${}^7\text{He}$, where at most two particles move in complex continuum orbits, three different cut-offs in energies and corresponding model spaces are shown. Note that only $p_{3/2}$ single particle orbitals are taken into account.

Although the coupling with pure continuum configurations turns out to be of a weak character in our study of ${}^7\text{He}$, this may not always be the case. If three-body forces were to be included, one would expect an enhancement in the strengths of amplitudes of the $|CCC\rangle$ configurations, since three-body matrix elements of the type $\langle RRR|V|CCC\rangle$ are no longer vanishing. It may also occur, even at the level of two-body interactions, that the multi-particle resonances have a considerable coupling with pure non-resonant continuum configurations. In Ref. [9] it was found that in the case of two-particle resonances in ${}^{11}\text{Li}$, the continuum contributions play in certain cases a more important role than the single particle resonance orbitals. In principle this does not pose a sig-

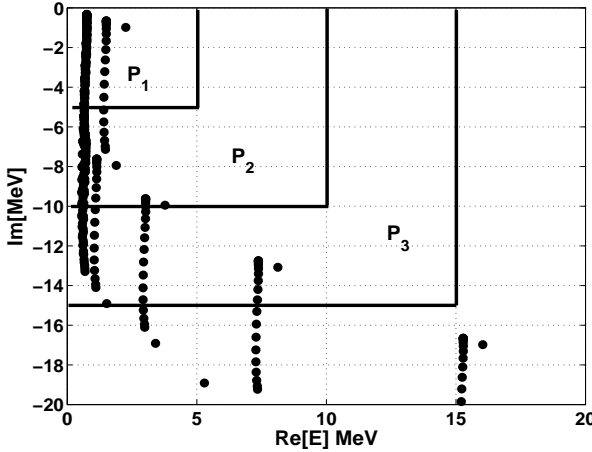


FIG. 10: Three choices of the model space used in the multi-configuration perturbation method. The three-particle model space states are constructed such that at most two particles move in the non-resonant continuum.

nificant problem regarding the applicability of MRPTM in Gamow shell-model calculations. The three-particle model space originally defined by Eq. (43) may be rede-

fined to include any number of pure non-resonant continuum configurations $|CCC\rangle$, say for example the N_C configurations $|CCC\rangle$ closest to the three-particle break-up threshold ($E = 0$ MeV).

Representing the Hamiltonian in the three-particle anti-symmetric basis (22), and having defined a suitable three-particle model-space, the shell model equation may be written in a block structure

$$\begin{pmatrix} H^{PP} & H^{PQ} \\ H^{QP} & H^{QQ} \end{pmatrix} \begin{pmatrix} P\Psi_\alpha^J \\ Q\Psi_\alpha^J \end{pmatrix} = E_\alpha^J \begin{pmatrix} P\Psi_\alpha^J \\ Q\Psi_\alpha^J \end{pmatrix}, \quad (44)$$

where the matrix elements of the model space block are given by

$$H_{i,j}^{PP} = \langle \tilde{\Phi}_i^J | H | \Phi_j^J \rangle = \langle \tilde{\Phi}_{(ab)c}^J | H | \Phi_{(de)f}^J \rangle, \quad (45)$$

with $\tilde{\Phi}_{(ab)c}^J \in P$ and $\Phi_{(de)f}^J \in P$. The matrix elements of the remaining blocks are given in the same form, with $\Phi_{(ab)c}^J$ belonging either to P or Q . See the Appendix for details on the evaluation of three-body matrix elements with two-body forces in $j-j$ coupling. Thereafter the full Hamiltonian is divided in two parts

$$\begin{pmatrix} H^{PP} & H^{PQ} \\ H^{QP} & H^{QQ} \end{pmatrix} = \begin{pmatrix} H^{PP} & 0 \\ 0 & D^{QQ} \end{pmatrix} + \begin{pmatrix} 0 & H^{PQ} \\ H^{QP} & \tilde{H}^{QQ} \end{pmatrix} = H^0 + H^1. \quad (46)$$

Here D^{QQ} is the diagonal part and \tilde{H}^{QQ} the off-diagonal part of H^{QQ} respectively. Written in this form, it is seen that H^0 defines the unperturbed part while H^1 gives the perturbations to H^0 . Provided H^0 is non-singular, the model space block H^{PP} may be decoupled by constructing a complex orthogonal matrix \mathbf{C} which diagonalizes H^0 , i.e. $\mathbf{C}H^0\mathbf{C}^T = \text{Diag}(E_1^0, E_2^0, \dots, E_N^0)$. Since H^0 is a block diagonal matrix, the matrix \mathbf{C} is given in the form

$$\mathbf{C} = \begin{bmatrix} \chi & \mathbf{0} \\ \mathbf{0} & \mathbf{1} \end{bmatrix}. \quad (47)$$

A more convenient three-particle basis which decouples the reference space is then given by

$$\Upsilon_i^J = \sum_{j=1}^N C_{i,j} \Phi_j^J = \begin{cases} \sum_{j=1}^{N_P} \chi_{i,j} \Phi_j^J, & i = 1, N_P \\ \Phi_i^J, & i = N_P + 1, N \end{cases}. \quad (48)$$

The complex orthogonal matrix χ which spans the reference space P , defines our new set of reference states.

Identifying the reference state Υ_i^J , $i \in (1, \dots, N_P)$, which gives the zeroth order approximation of the exact three-particle resonance, may be done by determining which state Υ_i^J has the largest overlap with the pure

pole configuration $|\Phi_{\text{res}}^J\rangle = |RRR\rangle$,

$$\text{Max} \left\{ |\langle \tilde{\Phi}_{\text{res}}^J | \Upsilon_i^J \rangle| \right\}_{i=1}^{N_P} = \text{Max} \{ |\chi_{i,j=\text{res}}| \}_{i=1}^{N_P}. \quad (49)$$

In our MRPTM calculation of ${}^7\text{He}$ we used the algorithm defined in Eq. (49) as identification method. To make sure that we picked out the “correct” physical state, we studied the complex energy trajectories as the interaction was gradually turned on. As a measure of how well the zeroth order three-particle resonance wave function $\Upsilon_{i=\text{res}}^J$ resembles the exact resonance wave function, one can calculate the complex variance σ_c^2 see Refs. [24, 42],

$$\begin{aligned} \sigma_c^2(i=\text{res}) &= \langle \Upsilon_i^{J*} | (H - E_i^0)^2 | \Upsilon_i^J \rangle \\ &= \chi_i^T H^{PQ} H^{QP} \chi_i, \end{aligned} \quad (50)$$

where χ_i labels the i ’th column of the $N_P \times N_P$ matrix χ . The reference states Υ_i^J are normalized. In Ref. [42] it was proved that the complex variance σ_c provides an upper bound to the exact resonance energy,

$$|E_{\text{res}}^{\text{exact}} - E_{\text{res}}^0| \leq |\sigma_c|. \quad (51)$$

The upper bound provides us with a valuable tool for determining how close the approximated resonance energy

is to the exact resonance energy, especially since in most practical applications the exact resonance energy is not known. However, in this particular case we know the exact position of the resonance energy from the full diagonalization in Sec. II D, so we can compute $|E_{\text{res}}^{\text{exact}} - E_{\text{res}}^0|$ and compare with $|\sigma_c|$. Table XIV gives the zeroth order resonance energy and corresponding upper bounds $|\sigma_c|$ of the $J^\pi = 3/2^-$ ground state of ${}^7\text{He}$, using the three-particle model space defined in Eq. (43) for several different cutoffs in energy.

TABLE XIV: Convergence of the zeroth order energy of the $J^\pi = 3/2^-$ ground state of ${}^7\text{He}$, for increasing energy cutoffs within the reference space, see Eq. (43). The corresponding upper bounds $|\sigma_c|$ of the exact ground state energy are also given. The numbers N_P and N_Q gives the dimensions of the three-particle model space P and complement space Q respectively. The full dimensionality with $n_{sp} = 24$ is $N = N_P + N_Q = 9224$.

E_{cut}	N_P	N_Q	$\text{Re}[E_{\text{res}}^0]$	$\text{Im}[E_{\text{res}}^0]$	$ E_{\text{res}}^{\text{exact}} - E_{\text{res}}^0 $	$ \sigma_c $
0	1	9223	0.970	1.505	1.959	2.722
10	305	8919	-0.292	-0.045	0.188	1.891
20	403	8821	-0.198	-0.183	0.098	1.479
30	469	8755	-0.145	-0.153	0.039	0.841
50	479	8745	-0.136	-0.157	0.038	0.618
100	543	8681	-0.135	-0.157	0.038	0.600
1000	1083	8141	-0.135	-0.157	0.038	0.600

As Table XIV indicates, a diagonalization within a model space where at most two particles move in continuum orbits, does not provide us with a satisfactory approximation of the exact ground state energy of ${}^7\text{He}$ within our model. Having obtained the zeroth order approximation to the exact three-particle resonance, after full diagonalization of the unperturbed Hamiltonian H^0 , a standard perturbation expansion in energy may be performed, to take into account couplings with configurations where all particles move in continuum orbits. Using intermediate normalization, the energy corrections up to third order for a given state Υ_i^J , $i \in (1, \dots, N_P)$ may be shown to be [30–32],

$$E_i^0 = \chi_i^T H^{PP} \chi_i, \quad E_i^1 = 0, \quad (52)$$

$$E_i^2 = \sum_{j=1}^{N_Q} \frac{M_{i,j}^2}{E_i^0 - D_{j,j}^{QQ}}, \quad (53)$$

$$E_i^3 = \sum_{j,k=1}^{N_Q} \frac{M_{i,j} \tilde{H}_{j,k}^{QQ} M_{i,k}}{(E_i^0 - D_{j,j}^{QQ})(E_i^0 - D_{k,k}^{QQ})} \quad j \neq k, \quad (54)$$

where we have defined the $N_P \times N_Q$ matrix $\mathbf{M} = \chi^T H^{PQ}$, and χ_i means the i 'th column of the matrix χ . For the perturbation series to converge, the reference energies E_i^0 must be separated from the diagonal elements $D_{k,k}^{QQ}$. This can in principle always be enforced by enlarging the model space P , for example by including a set of pure complex continuum configurations in P .

Observe that there is no first order correction to the energy, meaning that it has been accounted for by the reference states and energies, Υ_i^J, E_i^0 . Note also that we have used the bare two-body interaction of Eq. (16). This is to be contrasted to the method outlined in the next section where we use the Lee-Suzuki transformation in order to define an effective interaction.

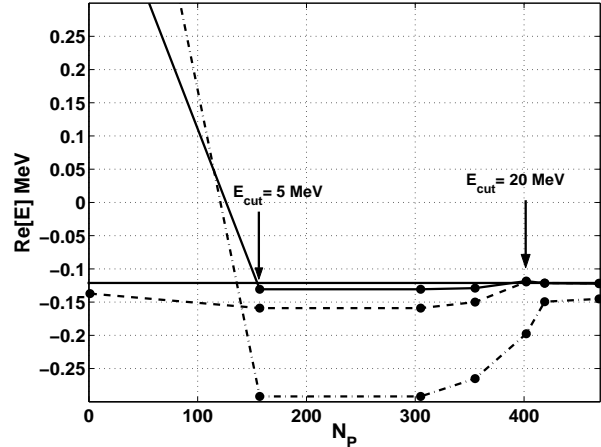


FIG. 11: Convergence of the real part of the $J^\pi = 3/2^-$ resonance in ${}^7\text{He}$, as the dimension of three-particle model space increases with increasing cutoff in energy. The cutoff in energy is increased in steps of 5 MeV, i.e. $E_{\text{cut}} = 0, 5, \dots, 30$, and given by the filled circles. The horizontal line indicates the real part of the $J^\pi = 3/2^-$ resonance located at $E = -(0.120731 + 0.122211i)$ MeV. The dashed-dotted line is the zeroth order energy, the dashed line represents the second-order energy while the solid line is the third-order energy.

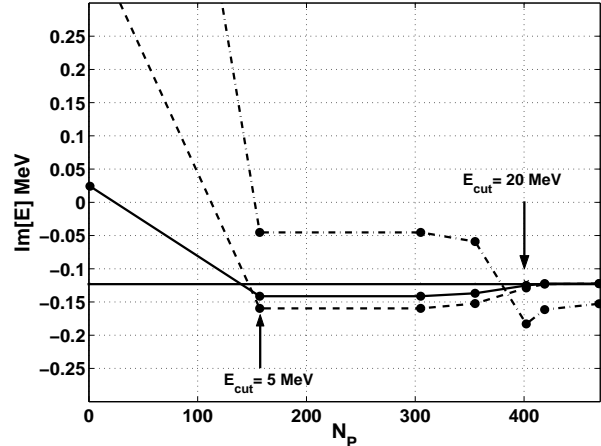


FIG. 12: Same legend as in Fig. 11 but for the imaginary part of the $J^\pi = 3/2^-$ resonance in ${}^7\text{He}$.

Figs. 11 and 12 show the convergence of the real and imaginary part of the three-particle resonance energy in the multi-reference perturbation method up to third order, see Eqs. (52), (53) and (54). The model space used

here is given in Eq. (43), and the calculations were done for increasing cutoffs in energy, $E_{\text{cut}} = 0, 5, \dots, 30$ MeV. Here only $p_{3/2}$ single particle orbitals were considered, and the calculations used 24 integration points in the construction of the single-particle basis for ${}^5\text{He}$, giving in total $N = N_P + N_Q = 9224$ three particle configurations for ${}^7\text{He}$, with spin and parity $J^\pi = 3/2^-$. The convergence of the ground state energy is plotted with respect to the number of three-particle model-space states N_P for each energy cutoff. From Figs. 11 and 12 one notes that a satisfactory convergence is obtained with $N_P \approx 400$, corresponding to the energy cutoff $E_{\text{cut}} = 20$ MeV. Excitations of model space configurations located above $E_{\text{cut}} \approx 5$ MeV yield small contributions to the second- and third-order corrections to the resonance energy, as expected. Observe that the second- and third-order terms converge at the same number of model space states, which indicates that second-order corrections in energy are apparently sufficient for our applications. This is also an advantage from a numerical point of view. In second order one has to store only the diagonal part of the block H^{QQ} , while in third order the complete block H^{QQ} has to be stored, which may be extremely large in many cases. The zeroth order energy, which corresponds to diagonalization within P , does not saturate at the exact resonance energy with increasing N_P , which again shows that possible couplings with the Q -space have to be accounted for, if one aims at accurate calculations.

Summing up these results, we see that we obtain stable results with approximately $N_P \approx 400$ three-body configurations within the multi-reference perturbation method, while the similarity transformation method of Sec. III gives stable results for $N_P \approx 800$ three-body configurations for the same problem. The question now is whether we can marry these two approaches in our quest for smaller Gamow shell model spaces. Such a combined approach forms also the standard approach in nuclear shell-model studies, either based on no-core approaches or with effective interactions for valence systems.

This is the topic of the next section.

V. EFFECTIVE INTERACTION SCHEME FOR THE GAMOW SHELL MODEL

In the previous sections it was shown that the Lee-Suzuki similarity transformation and the multi-reference perturbation method may both be used in the Gamow shell model in order to account for the most important correlations of a multi-particle resonance. Although the dimensionality of the problem derived either from the similarity transformation method or the multi-reference perturbation method was significantly reduced compared to the full problem, it may still be a severe problem when dealing with more than three particles in a big valence space.

The drawback of the multi-reference perturbation method is that one has to store extremely large matrices

H^{QQ} if one wishes to go beyond second order in perturbation theory. In the similarity transformation method one does not have to deal with H^{QQ} , as couplings with the Q -space states have been dealt with, in practical calculations at least at the two-body level. Going to systems with larger degrees of freedom, the P -space may nevertheless, at the converged level, be too large for our brute force diagonalization approach.

The aim of this section is to propose an effective interaction and perturbation theory scheme for the Gamow shell model. This approach combines the similarity transformation method and the multi-reference perturbation method, so that multi-particle resonances where several particles move in large valence spaces, may be calculated without a diagonalization in the full space. Our ultimate goal is to derive effective interactions for weakly bound systems to be used with the Coupled Cluster methods [40, 41].

Our algorithm is as follows

1. Choose an optimal set of n_{sp} single-particle orbits, which in turn defines two-body P_{2p} and many-body spaces. In our test case these single-particle orbits are defined by selected states in ${}^5\text{He}$.
2. Construct a two-particle effective interaction by the Lee-Suzuki similarity transformation method within the two-particle model space P_{2p} . Such diagonalizations can be done for very large spaces, see for example Refs. [34–37].
3. The next step is to divide the multi-particle model space P in two smaller spaces P' and Q' , where $P = P' + Q'$ and $N_P = N_{P'} + N_{Q'}$. The choice of P' should be dictated by our knowledge of the physical system. As an example, one may consider those single-particle configurations within the P -space that play the dominant role in the formation of the multi-particle resonance. The number $N_P = N_{P'} + N_{Q'}$ represents the total number of many-body configurations within the P -space.
4. Now that we have divided the P -space in two subspaces P' and Q' , we use for example the multi-reference perturbation method to account for excitations from the P' -space to the Q' -space to obtain energy corrections to a specific order. Increase the size of the P' -space until convergence is obtained. In the case $N_{P'} = N_P$ and $N_{Q'} = N_P - N_{P'} = 0$ the multi-reference perturbation expansion terminates at zeroth order, and corresponds to a full diagonalization within the P -space. Another option is to use for example the coupled cluster method as exposed in Refs. [40, 41].
5. Start from top again with a larger set of single-particle orbits, and continue until a convergence criterion is reached.

We illustrate these various choices of model spaces in the following two figures. Fig. 13 defines our model space

for the Lee-Suzuki similarity transformation at the two-body level. This corresponds to steps one and two in the above algorithm. The set of single-particle orbits defines the last single-particle orbit in the model space n_{sp} . Note that we could have chosen a model space defined by a cut in energy, as done by the No-Core collaboration, see for example Refs. [34–37]. These examples serve just to illustrate the algorithm. Fig. 14 demonstrates again a possi-

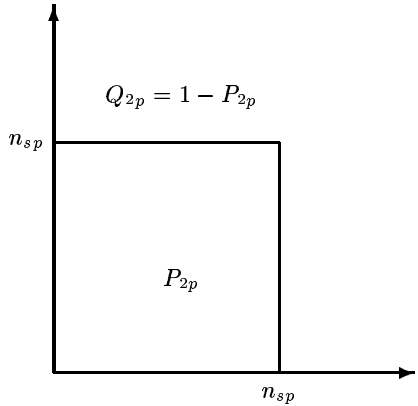


FIG. 13: Possible definition of the two-body exclusion operator $Q_{2p} = 1 - P_{2p}$ used to compute the Lee-Suzuki similarity transformation and its effective interaction at the two-body level. The border of the model space is defined by the last single-particle orbit n_{sp} .

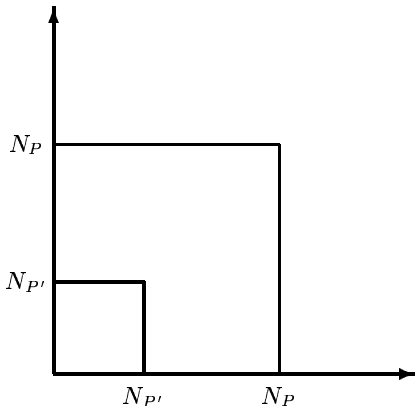


FIG. 14: Possible definition of many-body space N_P and reduced space $N'_{P'}$.

ble division of the three- and many particle space into the full model space P and a smaller space P' . Again, this

figure serves only the purpose of illustrating the method. In our actual calculations we define the smaller space P' via an energy cut in the real and imaginary eigenvalues and selected many-body configurations.

In summary, defining a set of single-particle orbits in order to construct the two-body and many-body model spaces, we obtain first an effective two-body interaction in the space P_{2p} by performing the Lee-Suzuki [26–29] transformation. This interaction and the pertinent single-particle orbits are then used to define a large many-body space. It is therefore of interest to see if we can reduce this dimensionality through the definition of smaller spaces and perturbative corrections.

We present here as a test case, the calculation of the $J^\pi = 3/2^-$ three-particle resonance within the perturbation scheme outlined above. A number of 24 single-particle orbits for the lj configuration $p_{3/2}$ are included, giving a total dimension of $d = 9224$ for the $J = 3/2$ three-particle basis.

We define five different three-particle model spaces P , given by the total number of three-body configurations N_P . The number of single-particle orbits and three-body states are listed in Table. XV. The single-particle model space, defining P , is constructed according to the prescription outlined in Section III.

TABLE XV: Five different P -spaces defined for increasing number of single-particle model space orbits n_{sp} consisting of the lj configuration $p_{3/2}$. The number N_P gives the dimension of the three-particle model space P for $J^\pi = 3/2^-$ with a full dimensionality with $n_{sp} = 24$ of $N = 9224$.

	P	P_1	P_2	P_3	P_4	P_5
n_{sp}	8	10	12	14	16	
N_P	344	670	1156	1834	2736	

For each three-particle model space P listed in Table XV, a division in two smaller subspaces P' and Q' is performed, i.e., $P = P' + Q'$. The subspace P' which defines a *proper subset* of each model space P , is defined by

$$P' \equiv \left\{ \begin{array}{l} |RRR\rangle, |RRC\rangle, |RCC\rangle \\ \text{Re}(e_a + e_b + e_c) < E_{\text{cut}} \\ \text{Im}(e_a + e_b + e_c) > -E_{\text{cut}} \end{array} \right\} \subset P_i. \quad (55)$$

Having defined the spaces P, Q, P' and Q' we write the Hamiltonian within the P -space in the form

$$\begin{pmatrix} H^{P'P'} & H^{P'Q'} \\ H^{Q'P'} & H^{Q'Q'} \end{pmatrix} = \begin{pmatrix} H^{P'P'} & 0 \\ 0 & D^{Q'Q'} \end{pmatrix} + \begin{pmatrix} 0 & H^{P'Q'} \\ H^{Q'P'} & \tilde{H}^{Q'Q'} \end{pmatrix} = H^0 + H^1. \quad (56)$$

Where $H^{P'P'} = P'H^{PP}P'$, $H^{P'Q'} = P'H^{PP}Q'$, $H^{Q'P'} = Q'H^{PP}P'$ and $H^{Q'Q'} = Q'H^{PP}Q'$. Then a matrix C which diagonalizes H^0 is constructed, and which defines our reference states within P' , see Sec. IV for further details. Corrections to the reference states coming from correlations contained in H^1 are then added perturbatively up to third order in our case, see Eqs. (52), (53) and (54). Tables XVI,XVII, XVIII, XIX and XX give the ground state energy of ${}^7\text{He}$ up to second and third order in our MRPTM calculations within each model space P_i given in Table XV. The reader should note that for each space P_1 , P_2 and so forth, listed in Table XV, we compare the results from this perturbative analysis with those from the exact diagonalization done in these spaces.

TABLE XVI: Resonance energy to second (E^2) and third (E^3) order in the multi-reference perturbation expansion, for the model space P_1 given in Table XV. The subspaces P'_1 are defined for different energy cutoffs, increased in steps of 10 MeV. The last line gives the exact energy within P_1 . Energies are given in units of MeV.

$N_{P_1} = 344$			$N_{P'_1 \max} = 113$		
$N_{P'_1}$	$N_{Q'_1}$	E_{cut}	$\text{Re}[E^2]$	$\text{Im}[E^2]$	$\text{Re}[E^3]$
1	343	0	0.066	0.322	0.606
113	231	10	0.041	-0.075	0.041
Exact within P_1 :			0.042	-0.076	

TABLE XVII: Same legend as in Table XVI but for the model space P_2 and the subspaces P'_2 .

$N_{P_2} = 670$			$N_{P'_2 \max} = 181$		
$N_{P'_2}$	$N_{Q'_2}$	E_{cut}	$\text{Re}[E^2]$	$\text{Im}[E^2]$	$\text{Re}[E^3]$
1	669	0	-0.053	0.357	0.562
157	513	10	-0.078	-0.110	-0.079
181	489	20	-0.082	-0.110	-0.083
Exact within P_2 :			-0.081	-0.110	

TABLE XVIII: Same legend as in Table XVI but for the model space P_3 and the subspaces P'_3 .

$N_{P_3} = 1156$			$N_{P'_3 \max} = 265$		
$N_{P'_3}$	$N_{Q'_3}$	E_{cut}	$\text{Re}[E^2]$	$\text{Im}[E^2]$	$\text{Re}[E^3]$
1	1155	0	-0.099	0.378	0.561
205	951	10	-0.114	-0.134	-0.114
265	891	20	-0.117	-0.130	-0.118
Exact within P_3 :			-0.116	-0.130	

As the number of reference states $N_{P'}$ increases with increasing cutoff E_{cut} in energy, one reaches a maximum of reference states $N_{P' \max}$ within each P -space. From the definition of the reference space P' in Eq. (55), it will never coincide with the P -space as one exhausts the number of configurations $|RRR\rangle$, $|RRC\rangle$, $|RCC\rangle$ within

TABLE XIX: Same legend as in Table XVI but for the model space P_4 and the subspaces P'_4 .

$N_{P_4} = 1834$			$N_{P'_4 \max} = 365$		
$N_{P'_4}$	$N_{Q'_4}$	E_{cut}	$\text{Re}[E^2]$	$\text{Im}[E^2]$	$\text{Re}[E^3]$
1	1833	0	-0.134	0.397	0.532
253	1581	10	-0.155	-0.160	-0.130
347	1487	20	-0.119	-0.127	-0.120
365	1469	30	-0.122	-0.123	-0.123
Exact within P_4 :			-0.121	-0.124	

TABLE XX: Same legend as in Table XVI but for the model space P_5 and subspaces P'_5 .

$N_{P_5} = 2736$			$N_{P'_5 \max} = 419$		
$N_{P'_5}$	$N_{Q'_5}$	E_{cut}	$\text{Re}[E^2]$	$\text{Im}[E^2]$	$\text{Re}[E^3]$
1	2735	0	-0.137	0.399	0.530
253	2483	10	-0.159	-0.160	-0.131
347	2389	20	-0.120	-0.129	-0.118
409	2327	30	-0.122	-0.122	-0.122
419	2317	40	-0.122	-0.122	-0.122
Exact within P_5 :			-0.121	-0.122	

P , since by definition one never includes the configurations $|CCC\rangle$, i.e. $\{|P'\rangle\} \subset \{|P\rangle\}$. The perturbation scheme for a reference space P' given by Eq. (55), will therefore only yield convergent results as long as our assumption that the configurations $|CCC\rangle$ play a minor role compared to the reference states holds. Although the configurations $|CCC\rangle$ turn out to play a minor role for the states we have considered in this work, there is no a priori reason for this to be the case when considering other multi-particle resonances. If no convergence is observed, one should simply choose another reference space P' , based for example on the single-particle model space, see Figs. 13 and 14.

To give a graphical illustration of the perturbation scheme outlined above, Figs. 15 and 16 exhibit the results obtained in Tables XVI,XVII, XVIII, XIX and XX. Fig. 15 gives plot of the real part of the ground state energy of ${}^7\text{He}$ up to third order, i.e. column six in Tables XVI,XVII, XVIII, XIX and XX, as the number of reference states $N_{P'_i}$ increases with increasing cutoff in energy E_{cut} . Fig. 16 gives corresponding results for the imaginary part of the energy, i.e. column seven of Tables XVI,XVII, XVIII, XIX and XX. From the plots and the tables we conclude that convergence is obtained for a small number of reference states $N_{P'} \sim 350 - 400$.

In the approach considered above, the dimension of the Q' -space is considerably smaller than the dimension of the complement space $Q = 1 - P$. This makes it much less time and memory consuming to compute the matrix elements of $H^{Q'Q'}$. We have seen from the above calculations that a termination of the perturbation expansion at second order compares well with the rate of convergence

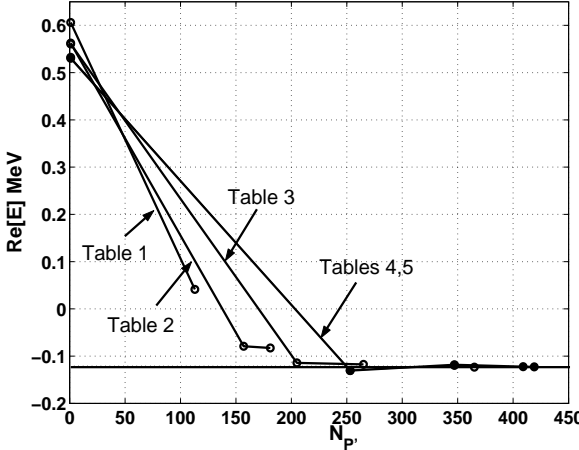


FIG. 15: Convergence of the real part of the $J^\pi = 3/2^-$ resonance energy in ${}^7\text{He}$ up to third order within the perturbative scheme outlined in the text, for the different model spaces P given in Table XV. The open circles along the different solid lines gives the calculations within each P_i . $N_{P'}$ gives the number of reference states in P' , which is a subspace of P . The horizontal line is the the real part of the $J^\pi = 3/2^-$ resonance located at $E = -(0.120731 + 0.122211i)$ MeV.

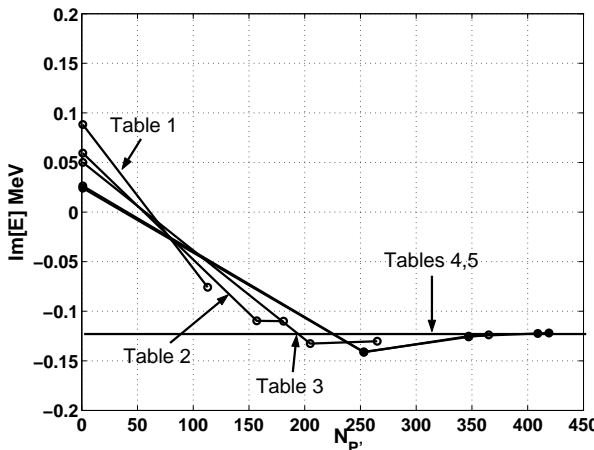


FIG. 16: Same legend as in Fig. 15 but now for the imaginary part.

for the third-order expansion. This makes it numerically feasible to treat systems where several particles move in a large valence space, within the perturbative scheme outlined above combined with an effective two-bdy interaction derived from the Lee-Suzuki scheme. As such we have a recipe for weakly bound systems which preserves much of the same methodology as is used in deriving effective interactions for the nuclear shell model.

VI. APPLICATION TO ${}^7\text{He}$ INCLUDING BOTH $p_{1/2}$ AND $p_{3/2}$

As shown in the previous sections, the effective interaction and perturbation scheme reduces the dimensionality of the shell-model equations drastically. Concluding this work, we apply the perturbation scheme to the calculation of the three-particle resonances in ${}^7\text{He}$, where 24 single-particle orbits for each of the lj single-particle orbits $p_{1/2}$ and $p_{3/2}$ now are included. The Hamiltonian for the $J^\pi = 1/2^-, 3/2^-$ and $J^\pi = 5/2^-$ states for ${}^7\text{He}$ implies dimensions $N_P = 29648$, 38896 and $N_P = 27072$, respectively. The main components of the ${}^7\text{He}$ resonant wave functions turn out to be the of $|RRR\rangle$ type, in the non-interacting limit corresponding to energies and wave functions;

$$\begin{aligned} |(p_{3/2})^3; J^\pi = 3/2_1^- \rangle, E_0 &= (2.26 - 0.98i) \text{ MeV} \\ |p_{1/2}(p_{3/2})_0^2; J^\pi = 1/2_1^- \rangle, E_0 &= (3.66 - 3.57i) \text{ MeV} \\ |p_{1/2}(p_{3/2})_2^2; J^\pi = 3/2_2^- \rangle, E_0 &= (3.66 - 3.57i) \text{ MeV} \\ |p_{1/2}(p_{3/2})_2^2; J^\pi = 5/2_1^- \rangle, E_0 &= (3.66 - 3.57i) \text{ MeV} \\ |(p_{1/2})_0^2 p_{3/2}; J^\pi = 3/2_3^- \rangle, E_0 &= (5.06 - 6.15i) \text{ MeV} \end{aligned}$$

We report here only the converged results, which gives the ${}^7\text{He}$ resonances,

$$\begin{aligned} E(3/2_1^-) &= (0.02 - 0.08i) \text{ MeV} \\ E(1/2_1^-) &= (0.39 - 3.98i) \text{ MeV} \\ E(3/2_2^-) &= (2.43 - 1.95i) \text{ MeV} \\ E(5/2_1^-) &= (2.75 - 0.89i) \text{ MeV} \\ E(3/2_3^-) &= (3.85 - 3.06i) \text{ MeV} \end{aligned}$$

For the $J^\pi = 3/2^-$ case, which has the most severe dimensionality, the converged values reported above was obtained with a reference space of dimension $N_{P'} \approx 1400 - 1800$. So for the $J^\pi = 3/2^-$ case, the dimension has been drastically reduced from 38896 to $1400 - 1800$. Fig. 17 shows a plot of the calculated energy levels for the nuclei ${}^{5-7}\text{He}$ within our truncation procedure. The non-interacting energy levels for ${}^6\text{He}$ and ${}^7\text{He}$ are also shown, and serve to illustrate how the two- and three-particle resonances develop when the nucleon-nucleon interaction from Eq. (16) is turned on.

There are several interesting features to be seen from Fig. 17. The 0^+ - and 2^+ -states in ${}^6\text{He}$ are formed within our model due to a strong pairing effect between the two neutrons moving in equivalent orbits. Thus, when the nucleon-nucleon interaction is turned on, we observe that the 0_1^+ and 2_1^+ dive down drastically in energy, and one becomes bound, the other almost bound. On the other hand, the $(p_{1/2} \otimes p_{3/2}) 1^+$ state in ${}^6\text{He}$ exhibits weak pairing effects. Our preliminary calculation of ${}^7\text{He}$ exhibits a richer continuum structure than so far seen in experiment, see the review [22], and references therein. In Ref. [22] two excited states with tentative

spins $J^\pi = 1/2^-$ and $J^\pi = 5/2^-$ are reported to exist above the ${}^7\text{He}$ ground state, at excitation energies 0.57 MeV and 2.87 MeV respectively. The main decay channel of the resonance at 2.87 MeV is $\alpha + 3n$. From this decay channel, Ref. [22] concludes that the configuration $[p_{1/2} \ (p_{3/2})_2^2; J^\pi = 5/2^-]$, involving the ${}^6\text{He}$ 2_1^+ state, is the most probable one, which also is our finding. The $J^\pi = 1/2^-$ resonance exhibits a peculiar behaviour, it moves way down towards the threshold in real energy when the nucleon-nucleon interaction is turned on, on the other hand the width increases slightly. However, these results must be gauged with the fact that we are

using a purely phenomenological nucleon-nucleon interaction model. The inclusion of a realistic interaction is the topic for a future work. The $1/2^-$ state is certainly not a simple spin-orbit partner to the $3/2^-$ ground state. We will return to a comprehensive discussion of the ${}^7\text{He}$ spectrum in a forthcoming paper, making comparisons with other procedures, see for example Ref. [43]. A realistic calculation has also to account for the recoil of the α -particle. The main issue here was however to demonstrate how to derive effective interactions for the Gamow shell model, with a considerable reduction in dimensionality.

VII. CONCLUSION AND FUTURE PERSPECTIVES

In this work we have applied the contour deformation method in momentum space, with a single-particle basis in momentum space serving as starting point for Gamow shell model calculations of loosely bound nuclei.

The main purpose of this work was to propose an effective interaction scheme for Gamow shell model calculations. One of the most severe difficulties regarding Gamow shell model calculations is the dramatic growth of dimension when dealing with several valence particles moving in a large shell-model space. This dimensionality problem is even more severe than in the harmonic oscillator representation used in traditional shell-model equation studies. In the Berggren representation a large number of complex-continuum orbits has to be included as well. The clear distinction of the non-interacting resonances from the dense distribution of complex continuum states, allows for a perturbation treatment, when configuration mixing is taken into account. For perturbation expansions to converge, the unperturbed states have to be well separated from the Q -space states, or else the propagators will contain poles which make a perturbative treatment difficult. We have shown that the Lee-Suzuki similarity transformation combined with the multi-reference perturbation method, reduces the necessary basis to about 3 – 4% that of the full problem.

To test the procedure, the resonant spectra of the drip-line nuclei ${}^{5-7}\text{He}$ have been studied and described using phenomenologically derived nucleon-nucleon interactions. We have shown that our choice of contour gives a good convergence for various resonant multi-nucleon states, and in addition allows for a clear distinction between physical states and the remaining complex continuum states.

Treating the many-particle problem in a perturbation scheme, requires finding a reference (model) space which contains most of the many-body correlations. The method and scheme outlined here, allows for a perturba-

tive treatment of many-body states in which also anti-bound states play an important role, such as in the drip-line nuclei ${}^{11}\text{Li}$.

The location and width of multi-particle resonances also depend on the effective interaction used between valence nucleons. The next step is to derive a realistic effective interaction for Gamow shell model calculations, and self-consistent Hartree-Fock single-particle energies for loosely bound nuclei, starting from a realistic nucleon-nucleon force. Using the Berggren representation may give an underlying understanding of many-body resonances from a microscopic point of view. Moreover, in our algorithm of Sec. V we employed the multi-reference perturbation method. Our future plans involve replacing the perturbative treatment by the more flexible Coupled Cluster approaches, as discussed in Refs. [40, 41]. The substantial challenge of computing other observables than energy is also being addressed, with inspirations drawn from few-body studies using hyper-harmonics see for example Refs. [44, 45].

Acknowledgments

Support by the Research Council of Norway is greatly acknowledged. G. H. also greatly acknowledges support by the Centre of Mathematics for Applications at the University of Oslo. Discussions with M. Kartamyshev, B. V. Danilin and S. N. Ershov have been helpful.

APPENDIX: THREE-BODY MATRIX ELEMENTS IN $j - j$ COUPLING.

The matrix element of a two-body interaction with anti-symmetric three-body Berggren states in $j - j$ coupling, may be written in terms of anti-symmetric two-body matrix elements as

$$\begin{aligned}
& \langle \tilde{\Phi}_{(ab)c}(123) | V | \Psi_{(de)f}(123) \rangle = \langle \tilde{a}b | v | de \rangle_{J_{ab}}^{AS} \delta_{c,f} \delta_{J_{ab}, J_{de}} + \\
& \left(\frac{1 + \delta_{d,f}}{1 + \delta_{d,e}} \right)^{1/2} (-1)^{j_d - J_{de} + J_{ab} - J} U(j_e j_d J j_f; J_{de} J_{ab}) \langle \tilde{a}b | v | df \rangle_{J_{ab}}^{AS} \delta_{c,e} - \\
& \left(\frac{1 + \delta_{e,f}}{1 + \delta_{d,e}} \right)^{1/2} (-1)^{j_d + J_{ab} - J} U(j_d j_e J j_f; J_{de} J_{ab}) \langle \tilde{a}b | v | ef \rangle_{J_{ab}}^{AS} \delta_{c,d} + \\
& \left(\frac{1 + \delta_{b,c}}{1 + \delta_{a,b}} \right)^{1/2} (-1)^{j_a + J_{de} - J} U(j_a j_b J j_c; J_{ab} J_{de}) \langle \tilde{b}c | v | de \rangle_{J_{de}}^{AS} \delta_{a,f} +
\end{aligned}$$

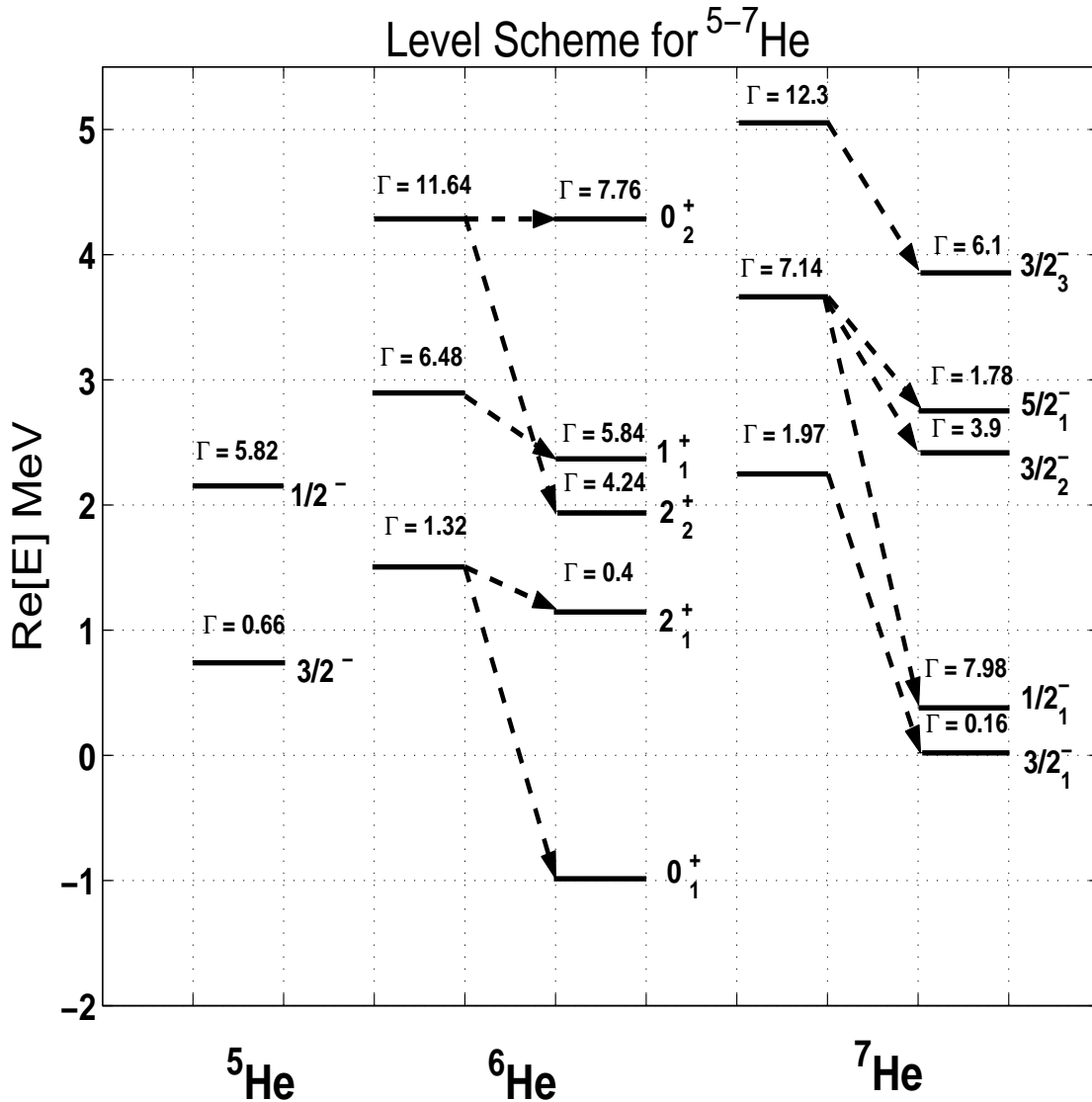


FIG. 17: Energy levels for ${}^6\text{He}$ and ${}^7\text{He}$ for interacting and non-interacting valence neutrons, based on our computed ${}^5\text{He}$ single-particle spectrum, including both $p_{1/2}$ and $p_{3/2}$ orbits. The non-interacting energy levels for ${}^6\text{He}$ and ${}^7\text{He}$ are shown to the left in each case.

$$\begin{aligned}
& \left(\frac{1 + \delta_{b,c}}{1 + \delta_{a,b}} \right)^{1/2} \sum_{J_{bc}} (-1)^{j_a + j_d - 2J} U(j_a j_b J j_c; J_{ab} J_{bc}) \times \\
& \left\{ \left(\frac{1 + \delta_{d,f}}{1 + \delta_{d,e}} \right)^{1/2} (-1)^{J_{de}} U(j_e j_d J j_f; J_{de} J_{bc}) \langle \tilde{b}c | v | df \rangle_{J_{bc}}^{AS} \delta_{a,e} + \right. \\
& \quad \left. \left(\frac{1 + \delta_{e,f}}{1 + \delta_{d,e}} \right)^{1/2} U(j_d j_e J j_f; J_{de} J_{bc}) \langle \tilde{b}c | v | ef \rangle_{J_{bc}}^{AS} \delta_{a,d} \right\} + \\
& \left(\frac{1 + \delta_{a,c}}{1 + \delta_{a,b}} \right)^{1/2} (-1)^{j_a - J_{ab} + J_{de} - J} U(j_b j_a J j_c; J_{ab} J_{de}) \langle \tilde{a}c | v | de \rangle_{J_{de}}^{AS} \delta_{b,f} + \\
& \quad \left(\frac{1 + \delta_{a,c}}{1 + \delta_{a,b}} \right)^{1/2} \sum_{J_{ac}} (-1)^{j_a + j_d - J_{ab} - 2J} U(j_b j_a J j_c; J_{ab} J_{ac}) \times \\
& \quad \left\{ \left(\frac{1 + \delta_{d,f}}{1 + \delta_{d,e}} \right)^{1/2} (-1)^{J_{de}} U(j_e j_d J j_f; J_{de} J_{ac}) \langle \tilde{a}c | v | df \rangle_{J_{ac}}^{AS} \delta_{b,e} + \right. \\
& \quad \quad \left. \left(\frac{1 + \delta_{e,f}}{1 + \delta_{d,e}} \right)^{1/2} U(j_d j_e J j_f; J_{de} J_{ac}) \langle \tilde{a}c | v | ef \rangle_{J_{ac}}^{AS} \delta_{b,d} \right\} \tag{A.1}
\end{aligned}$$

Here $U(j_a, j_b, J, j_c; J_{ab}, J_{bc})$ is the normalized Racah coefficient, and $\langle \tilde{a}b \rangle = \langle ab^* \rangle$ due to the Berggren metric.

In the case where all the single particle orbits in the ket (bra) are equivalent, i.e., $d = e = f$, one needs co-

efficients of fractional parentage in order to make the three-body wave function totally anti-symmetric in $j - j$ coupling. The anti-symmetric three-body matrix element then takes the form,

$$\begin{aligned}
\langle \tilde{\Phi}_{(ab)c}(123) | V | \Phi_{ddd}(123) \rangle &= \sqrt{3} \langle j_d^2 J_{ab}, j_d | \} j_d^3 J \rangle \langle \tilde{a}b | v | dd \rangle_{J_{ab}}^{AS} \delta_{c,d} + \\
&\quad \sqrt{3} (-1)^{j_a + j_d - 2J} \sum_K \langle j_d^2 K, j_d | \} j_d^3 J \rangle \times \\
& \quad \left\{ \left(\frac{1 + \delta_{b,c}}{1 + \delta_{a,b}} \right)^{1/2} \sum_{J_{bc}} U(j_a j_b J j_c; J_{ab} J_{bc}) U(j_d j_d J j_d; K J_{bc}) \langle \tilde{b}c | v | dd \rangle_{J_{bc}} \delta_{a,d} + \right. \\
& \quad \quad \left. \left(\frac{1 + \delta_{a,c}}{1 + \delta_{a,b}} \right)^{1/2} \sum_{J_{ac}} (-1)^{J_{ab}} U(j_b j_a J j_c; J_{ab} J_{ac}) U(j_d j_d J j_d; K J_{ac}) \langle \tilde{a}c | v | dd \rangle_{J_{bc}} \delta_{b,d} \right\} \tag{A.2}
\end{aligned}$$

where $\langle j_d^2 J_{ab}, j_d | \} j_d^3 J \rangle$ is the coefficient of fractional parentage.

-
- [1] N. Michel, W. Nazarewicz, and M. Płoszajczak, Phys. Rev. C **70**, 064313 (2004).
 - [2] N. Michel, W. Nazarewicz, M. Płoszajczak, and J. Rotureau, nucl-th/0401036 (2004).
 - [3] J. Dobaczewski, W. N. N. Michel, M. Płoszajczak, and M. V. Stoitsov, nucl-th/0401034 (2004).
 - [4] R. J. Liotta, E. Maglione, N. Sandulescu, and T. Vertse, Phys. Lett. B **367**, 1 (1996).
 - [5] R. IdBetan, R. J. Liotta, N. Sandulescu, , and T. Vertse, Phys. Rev. C **67**, 014322 (2003).
 - [6] N. Michel, W. Nazarewicz, M. Płoszajczak, and K. Bennaceur, Phys. Rev. Lett. **89**, 042502 (2002).
 - [7] N. Michel, W. Nazarewicz, M. Płoszajczak, and J. Okołowicz, Phys. Rev. C **67**, 054311 (2003).
 - [8] R. IdBetan, R. J. Liotta, N. Sandulescu, and T. Vertse, Phys. Rev. Lett. **89**, 042501 (2002).
 - [9] R. IdBetan, R. J. Liotta, N. Sandulescu, and T. Vertse, Phys. Lett. B **584**, 48 (2004).

- [10] K. Bennaceur, F. Nowacki, J. Okolowicz, and M. Płoszajczak, Nucl. Phys. A **651**, 289 (1999).
- [11] K. Bennaceur, F. Nowacki, J. Okolowicz, and M. Płoszajczak, Nucl. Phys. A **671**, 203 (2000).
- [12] J. Okolowicz, M. Płoszajczak, and I. Rotter, Phys. Rep. **374**, 271 (2003).
- [13] A. Volya and V. Zelevinsky, Phys. Rev. C **67**, 054322 (2003).
- [14] T. Berggren, Nucl. Phys. A **109**, 265 (1968).
- [15] T. Berggren, Nucl. Phys. A **169**, 353 (1971).
- [16] T. Berggren, Phys. Lett. B **73**, 389 (1978).
- [17] T. Berggren, Phys. Lett. B **373**, 1 (1996).
- [18] P. Lind, Phys. Rev. C **47**, 1903 (1993).
- [19] G. Hagen, J. S. Vaagen, and M. Hjorth-Jensen, J. Phys. A: Math. Gen. **37**, 8991 (2004).
- [20] E. R. Davidson, Comput. Phys. Commun. **53**, 49 (1989).
- [21] E. R. Davidson, Comput. Phys. **5**, 519 (1993).
- [22] B. Jonson, Phys. Rep. **389**, 1 (2004).
- [23] M. V. Zhukov, B. V. Danilin, D. V. Fedorov, J. M. Bang, I. J. Thompson, and J. S. Vaagen, Phys. Rep. **231**, 151 (1993).
- [24] N. Moiseyev, Phys. Rep. **302**, 211 (1998).
- [25] R. R. Whitehead, A. Watt, B. J. Cole, and I. Morrison, Adv. Nucl. Phys. **9**, 123 (1977).
- [26] K. Suzuki and S. Y. Lee, Progr. Theor. Phys. **64**, 2091 (1980).
- [27] K. Suzuki, Progr. Theor. Phys. **68**, 246 (1982).
- [28] K. Suzuki and R. Okamoto, Progr. Theor. Phys. **93**, 905 (1995).
- [29] S. Fujii, E. Epelbaum, H. Kamada, R. Okamoto, K. Suzuki, and W. Glöckle, Phys. Rev. C **70**, 024003 (2004).
- [30] C. Butch, R. Santra, and L. S. Cederbaum, Phys. Rev. A **69**, 032505 (2004).
- [31] F. Chen, E. R. Davidson, and S. Iwata, Int. J. Quantum Chem. **86**, 256 (2002).
- [32] R. Santra and L. S. Cederbaum, Phys. Rep. **368**, 1 (2002).
- [33] S. Sack, L. C. Biedenharn, and G. Breit, Phys. Rev. **93**, 321 (1954).
- [34] P. Navrátil and B. R. Barrett, Phys. Rev. C **57**, 562 (1998).
- [35] P. Navrátil, J. P. Vary, and B. R. Barrett, Phys. Rev. Lett. **84**, 5728 (2000).
- [36] P. Navrátil, J. P. Vary, and B. R. Barrett, Phys. Rev. C **62**, 054311 (2000).
- [37] P. Navrátil, G. P. Kamuntavicius, and B. R. Barrett, Phys. Rev. C **61**, 044001 (2000).
- [38] N. J. Higham, Num. Algorithms **15**, 227 (1997).
- [39] E. D. Denman and A. N. Beavers, Appl. Math. Comput. **2**, 63 (1976).
- [40] D. J. Dean and M. Hjorth-Jensen, Phys. Rev. C **69**, 054320 (2004).
- [41] K. Kowalski, D. J. Dean, M. Hjorth-Jensen, T. Papenbrock, and P. Piecuch, Phys. Rev. Lett. **92**, 132501 (2004).
- [42] E. R. Davidson, E. Engdahl, and N. Moiseyev, Phys. Rev. A **33**, 2436 (1986).
- [43] S. C. Pieper, R. B. Wiringa, and J. Carlson, nucl-th/0409012 (2004).
- [44] S. N. Ershov, B. V. Danilin, and J. S. Vaagen, Phys. Rev. C **64**, 064609 (2001).
- [45] B. V. Danilin, T. Rogde, J. S. Vaagen, I. J. Thompson, and M. V. Zhukov, Phys. Rev. C **69**, 024609 (2004).

Chapter 7

Summary and perspectives.

The main purpose of this thesis has been to investigate and develop methods suitable for study of resonance phenomena in nuclear and subatomic physics. Emphasis has been on the momentum space formulation of the Schrödinger equation. It has been shown, starting from the integral formulation of the Schrödinger equation, that an efficient way of obtaining a complete set of states including bound-, antibound and resonant states is through the Contour Deformation Method. The strength of the Contour Deformation Method has been illustrated by studying a wide range of different cases in subatomic physics where resonance phenomena appear. These applications ranges from the case of a single-particle moving in a spherically symmetric field to the case of strong deformations of the field. Further, it has been studied how resonances may be solved for in complex potentials which models absorptive and emissive processes, using the Contour Deformation Method. The results obtained in these specific applications, strongly favour the Contour Deformation Method in comparison with other methods such as complex coordinate scaling and analytic continuation in the coupling strength. The most appealing feature of CDM is that, not only does it give accurate results for resonances and anti-bound states, but in addition it provides us with a complete set of states which may be used in many different eigenfunction expansions. The only limitation of CDM is that the analytic structure of the potential has to be known, since the choice of contour is dictated by the singularity structure of the potential. The revival and study of CDM applied to nuclear physics, may be considered the main issue of the first part of this thesis, and is also the topic of Paper 1.

In the second part of this thesis, the focus was directed towards the issue of how resonance phenomena may be understood in nuclei, when several valence particles are present. The newly developed Gamow Shell Model is a promising approach in the study of loosely bound and unbound nuclei along the drip lines. The main ingredient in the Gamow Shell Model is the construction of a complete set of many-body Slater determinants built up from a single-particle Berggren basis. It has been shown in this work that a viable starting point in Gamow Shell Model studies is to obtain a single-particle basis by the Contour Deformation Method in momentum space. The results displayed in Paper 2, indicate rapid convergence for many-body resonances using a single-particle basis in momentum space.

The challenge for present and future Gamow Shell Model calculations is how to deal with the extreme growth of the number of Slater determinants in the many-body expansion basis. This topic was the main issue of the second part of the thesis. The basic idea was to modify standard effective interaction theory and many-body perturbation theory, so that their range of applicability encompass the complex interactions and matrices which follow from the generalization of the standard Shell Model to the complex energy plane. Further, the extreme dimension of the Shell Model Hamiltonian matrix requires development of large-scale matrix diagonalization routines which can handle both real and complex matrices. In this thesis it was shown how the Lanczos iteration method may be generalized to complex energy matrices. It was further shown, that by choosing a reasonable initial Lanczos vector for the 0th order multi-particle resonance, the multi-particle resonance may be unambiguously picked out from the set of states obtained from diagonalization at each iteration, by identifying the state which has the largest overlap with the 0th order Lanczos vector.

Another important result was the generalization of the Lee-Suzuki similarity transformation to include complex interactions. The emphasis was on the derivation of effective interactions for loosely bound or unbound nuclei which have a strong coupling with the continuum. We demonstrated by a numerical study in Paper 2, that the construction of an effective two-body interaction based on the Lee-Suzuki similarity transformation method, leads to a drastic reduction of the Gamow Shell Model dimensionality for more than two particles. Furthermore it was shown in Paper 2 that the one-state-at-a-time Multi-Reference-Perturbation-Theory combined with the construction of an effective two-body interaction, reduces drastically the dimension of Shell Model space. This result is very promising when extending the Gamow Shell Model to applications in structure calculations of heavier dripline nuclei, with a larger number of valence particles moving in a large valence space.

With further progress in computational power one may hope that *ab initio* calculations of light and medium size nuclei within the Berggren representation may become possible in the near future. Coupled-Cluster techniques have proven to be a promising method for calculations of medium size nuclei. Very recently [46, 47, 48], converged Coupled-Cluster results for the ground- and first excited state of ^{16}O were reported, using modern nucleon-nucleon interactions derived from effective field-theory. A promising way of approach would be to generalize the Coupled-Cluster method to complex interactions, and at the first stage see how resonant structures are formed in light nuclei starting from an *ab initio* approach. As this thesis only deals with a phenomenological residual nucleon-nucleon interaction, the next step is to include a realistic and microscopically derived effective nucleon-nucleon interaction in Gamow Shell Model calculations. Constructing a single-particle Berggren basis by solving the Hartree-Fock equation self-consistently with an effective nucleon-nucleon interaction constructed from the G-matrix approach or with the recently developed low-momentum nucleon-nucleon interaction ($V_{\text{low-}k}$), and then calculating matrix elements of the effective interaction in this basis, is a future challenge for the Gamow Shell Model. How single-particle resonances are formed from the underlying nucleon-nucleon interaction is a very interesting study in itself, and work along these lines are in progress using a

renormalized nucleon-nucleon interaction of the $V_{\text{low-}k}$ type, generalized to the complex k -plane.

Bibliography

- [1] I. Tanihata, H. Hamagaki, O. Hashimoto, Y. Shida, and N. Yoshikawa. Measurements of interaction cross sections and nuclear radii in the light p-shell region. *Phys. Rev. Lett.*, 55:2676, 1985. pages 7
- [2] V. Zhukov, B.V. Danilin, D.V. Fedorov, J.M. Bang, I.J. Thompson, and J.S. Vaagen. Bound state properties of borromean halo nuclei: ${}^6\text{He}$ and ${}^{11}\text{Li}$. *Phys. Rep.*, 231:151, 1993. pages 8
- [3] B. Jonson. Light dripline nuclei. *Phys. Rep.*, 389:1, 2004. pages 9
- [4] J.S. Vaagen, G. Hagen, B.V. Danilin, S.N. Ershov, and I.J. Thompson. *Structure and Dynamics of Elementary Matter*, volume 166. Kluwer Academic Publishers, 2004. pages 9
- [5] G. A. Gamow. unknown. *Zs. f. Physik*, 51:204, 1928. pages 10
- [6] G. Breit and E. P. Wigner. Capture of slow neutrons. *Phys. Rev.*, 49:519, 1936. pages 10
- [7] R. G. Newton. *Scattering Theory of Waves and Particles*. Springer-Verlag, New York, 1982. pages 11, 19, 20, 21, 28, 42, 43
- [8] V. I. Kukulin, V. M. Krasnopol'sky, and J. Horáček. *Theory of Resonances*. Kluwer Academic publishers, Amsterdam, 1989. pages 11, 42, 56, 60, 64, 98
- [9] A. G. Sitenko. *Lectures in scattering theory*. Pergamon Press Ltd. Oxford, 1971. pages 11, 19, 20, 22
- [10] Y. B. Zel'dovich. *JETP (Sov. Phys.)*, 39:776, 1960. pages 11, 12, 25
- [11] J. Aguilar and J. M. Combes. Class of analytic perturbations for one-body schrödinger hamiltonians. *Commun. Math. Phys.*, 22:265, 1971. pages 11
- [12] E. Balslev and J. M. Combes. Spectral properties of many-body schrödinger operators with dilatation-analytic interactions. *Commun. Math. Phys.*, 22:280, 1971. pages 11
- [13] N. Moiseyev and C.T. Corcoran. Autoionizing states of H_2 and using the complex scaling method. *Phys. Rev. A*, 20:814, 1979. pages 11

- [14] N. Moiseyev. Resonance states by the generalized complex variational method. *Mol. Phys.*, 47:582, 1982. pages 11
- [15] N. Moiseyev. Quantum theory of resonances: Calculating energies, widths and cross-sections by complex scaling. *Phys. Rep.*, 302:211, 1998. pages 11, 28, 43, 101
- [16] B. Gyarmati and A.T. Kruppa. Complex scaling in the description of nuclear resonances. *Phys. Rev. C*, 34:95, 1986. pages 11
- [17] A. Csoto. Three-body resonances by complex scaling. *Phys. Rev. C*, 49:2244, 1994. pages 11
- [18] T. Myo, K. Kato, S. Aoyama, and K. Ikeda. Analysis of ${}^6\text{He}$ coulomb breakup in the complex scaling method. *Phys. Rev. C*, 63:054313, 1998. pages 11
- [19] E. Garrido, D. V. Fedorov, and A. S. Jensen. Dipole excited states in ${}^{11}\text{Li}$ with complex scaling. *Nucl. Phys. A*, 708:277, 2002. pages 11
- [20] I. Raskinyte. Resonances in few-body systems. *PhD Thesis University of Bergen 2002, unpublished*, 2002. pages 11
- [21] S. A. Rakityansky, S. A. Sofianos, and K. Amos. A method for calculating the jost function for analytic potentials. *Il Nuovo Cimento*, 111B, N.3:363, 1996. pages 11
- [22] S. A. Sofianos and S. A. Rakityansky. Exact method for locating potential resonances and regge trajectories. *J. Phys. A: Math. Gen.*, 30:3725, 1997. pages 11
- [23] S. Aoyama. Theoretical prediction for the ground state of ${}^{10}\text{He}$ with the method of analytic continuation in the coupling constant. *Phys. Rev. Lett.*, 89:052501, 2002. pages 11
- [24] G. Hagen, J. S. Vaagen, and M. Hjorth-Jensen. The contour deformation method in momentum space, applied to subatomic physics. *J. Phys. A: Math. Gen.*, 37:8991, 2004. pages 12, 16
- [25] I. R. Afnan. Resonances in few-body systems. *Aust. J. Phys.*, 44:201, 1991. pages 12
- [26] D. Brayshaw. Off- and on-shell analyticity of three-particle scattering amplitudes. *Phys. Rev.*, 176:1855, 1968. pages 12
- [27] J. Nuttall and H. L. Cohen. Method of complex coordinates for three-body calculations above the breakup threshold. *Phys. Rev.*, 188:1542, 1969. pages 12, 41, 63
- [28] A. T. Stelbovics. On the application of contour rotation to three-body amplitudes. *Nucl. Phys. A*, 288:461, 1978. pages 12

- [29] W. Glöckle. S-matrix pole trajectory in a three-neutron model. *Phys. Rev. C*, 18:18, 1978. pages 12
- [30] T. Berggren. On the use of resonant states in eigenfunction expansions of scattering and reaction amplitudes. *Nucl. Phys. A*, 109:265, 1968. pages 12, 29, 33
- [31] B.S. Pudlinger, V.R. Pandharipande, J. Carlson, and R. Wiringa. Quantum monte carlo calculations of $A \leq 6$ nuclei. *Phys. Rev. Lett.*, 74:4396, 1995. pages 13
- [32] B. S. Pudlinger, V. R. Pandharipande, J. Carlson, Steven C. Pieper, and R. B. Wiringa. Quantum monte carlo calculations of nuclei with $A < 7$. *Phys. Rev. C*, 56:1720, 1997. pages 13
- [33] R. B. Wiringa, Steven C. Pieper, J. Carlson, and V. R. Pandharipande. Quantum monte carlo calculations of $A = 8$ nuclei. *Phys. Rev. C*, 62:014001, 2000. pages 13
- [34] Steven C. Pieper and R. B. Wiringa. Quantum monte carlo calculations of light nuclei. *Ann. Rev. Nucl. Part. Sci.*, 51:53, 2001. pages 13
- [35] Steven C. Pieper, V. R. Pandharipande, R. B. Wiringa, and J. Carlson. Realistic models of pion-exchange three-nucleon interactions. *Phys. Rev. C*, 64:014001, 2001. pages 13
- [36] Steven C. Pieper, K. Varga, and R. B. Wiringa. Quantum monte carlo calculations of $A = 9, 10$ nuclei. *Phys. Rev. C*, 66:044310, 2002. pages 13
- [37] Steven C. Pieper, R. B. Wiringa, and J. Carlson. Quantum monte carlo calculations of excited states in $A = 6 - 8$ nuclei. *nucl-th/0409012*, 2004. pages 13
- [38] P. Navrátil and B. R. Barrett. Shell-model calculations for the three-nucleon system. *Phys. Rev. C*, 57:562, 1998. pages 13, 88, 105
- [39] P. Navrátil, J. P. Vary, and B. R. Barrett. Properties of ^{12}C in the ab initio nuclear shell model. *Phys. Rev. Lett.*, 84:5728, 2000. pages 13, 88, 105
- [40] P. Navrátil, J. P. Vary, and B. R. Barrett. Large-basis ab initio no-core shell model and its application to ^{12}C . *Phys. Rev. C*, 62:054311, 2000. pages 13, 88, 105
- [41] P. Navrátil, G. P. Kamuntavicius, and B. R. Barrett. Few-nucleon systems in a translationally invariant harmonic oscillator basis. *Phys. Rev. C*, 61:044001, 2000. pages 13, 88, 105
- [42] F. Coester. Bound states of a many-particle system. *Nuclear Phys.*, 7:421, 1958. pages 14
- [43] F. Coester and H. Kümmel. Short-range correlations in nuclear wave functions. *Nuclear Phys.*, 17:477, 1960. pages 14

- [44] P. Piecuch, P. D. Fan, K. Jedziniak, and K. Kowalski. Exactness of two-body cluster expansions in many-body quantum theory. *Phys. Rev. Lett.*, 90:113001, 2003. pages 14
- [45] K. Kowalski and P. Piecuch. Extension of the method of moments of coupled-cluster equations to excited states: The triples and quadruples corrections to the eomccsd energies. *J. Chem. Phys.*, 116:7411, 2002. pages 14
- [46] D. J. Dean and M. Hjorth-Jensen. Coupled-cluster approach to nuclear physics. *Phys. Rev. C*, 69:054320, 2004. pages 14, 105, 176
- [47] K. Kowalski, D. J. Dean, M. Hjorth-Jensen, T. Papenbrock, and P. Piecuch. Coupled cluster calculations of ground and excited states of nuclei. *Phys. Rev. Lett.*, 92:132501, 2004. pages 14, 105, 176
- [48] M. Wloch, D. J. Dean, J. R. Gour, M. Hjorth-Jensen, K. Kowalski, T. Papenbrock, and P. Piecuch. Ab initio couplec-cluster study of ^{16}O . *nucl-th/0501067*, 2005. pages 14, 176
- [49] P. Lind. Completeness relations and resonant state expansions. *Phys. Rev. C*, 47:1903, 1993. pages 14, 29, 30, 31, 62
- [50] R. J. Liotta, E. Maglione, N. Sandulescu, and T. Vertse. A representation to describe nuclear processes in the continuum. *Phys. Lett. B*, 367:1, 1996. pages 14, 16
- [51] H. Feshbach. A unified of nuclear reactions. *Ann. Phys.*, 5:357, 1958. pages 15
- [52] H. Feshbach. A unified of nuclear reactions.II. *Ann. Phys.*, 19:287, 1962. pages 15
- [53] U. Fano. Effects of configuration interaction on intensities and phase shifts. *Phys. Rev.*, 124:1866, 1961. pages 15
- [54] K. Bennaceur, F. Nowacki, J. Okolowicz, and M. Ploszajczak. Study of the $^7\text{Be}(p, \gamma)^8\text{B}$ and $^7\text{Li}(n, \gamma)^8\text{Li}$ capture reactions using the shell model embedded in the continuum. *Nucl. Phys. A*, 651:289, 1999. pages 15
- [55] K. Bennaceur, F. Nowacki, J. Okolowicz, and M. Ploszajczak. Analysis of the $^{16}\text{O}(p, \gamma)^{17}\text{F}$ capture reaction using the shell model embedded in the continuum. *Nucl. Phys. A*, 671:203, 2000. pages 15
- [56] J. Okolowicz, M. Ploszajczak, and I. Rotter. Dynamics of quantum systems embedded in a continuum. *Phys. Rep.*, 374:271, 2003. pages 15
- [57] A. Volya and V. Zelevinsky. Non-hermitian effective hamiltonian and continuum shell model. *Phys. Rev. C*, 67:054322, 2003. pages 15
- [58] N. Michel, W. Nazarewicz, and M. Płoszajczak. Proton-neutron coupling in the gamow shell model: the lithium chain. *nucl-th/0407110*, 2004. pages 16

- [59] N. Michel, W. Nazarewicz, M. Płoszajczak, and J. Rotureau. Gamow shell-model description of weakly bound and unbound nuclear states. *nucl-th/0401036*, 2004. pages 16
- [60] J. Dobaczewski, W. Nazarewicz N. Michel, M. Płoszajczak, and M. V. Stoitsov. Structure of exotic nuclei. *nucl-th/0401034*, 2004. pages 16
- [61] R. IdBetan, R. J. Liotta, N. Sandulescu, , and T. Vertse. Shell model in the complex energy plane and two-particle resonances. *Phys. Rev. C*, 67:014322, 2003. pages 16
- [62] N. Michel, W. Nazarewicz, M. Płoszajczak, and K. Bennaceur. Gamow shell model description of neutron-rich nuclei. *Phys. Rev. Lett.*, 89:042502, 2002. pages 16
- [63] N. Michel, W. Nazarewicz, M. Płoszajczak, and J. Okołowicz. Gamow shell model description of weakly bound nuclei and unbound nuclear states. *Phys. Rev. C*, 67:054311, 2003. pages 16
- [64] R. IdBetan, R. J. Liotta, N. Sandulescu, and T. Vertse. Two-particle resonant states in a many-body mean field. *Phys. Rev. Lett.*, 89:042501, 2002. pages 16
- [65] R. IdBetan, R. J. Liotta, N. Sandulescu, and T. Vertse. A shell model representation with antibound states. *Phys. Lett. B*, 584:48, 2004. pages 16, 17
- [66] G. H. Hardy. *Divergent Series*. Clarendon Press, 2nd edition, 1956. pages 25
- [67] M. L. Boas. *Mathematical Methods in the Physical Sciences*. John Wiley and Sons, Inc, 2nd edition, 1983. pages 25, 48
- [68] B. Gyarmati and T. Vertse. On the normalization of gamow functions. *Nucl. Phys. A*, 160:523, 1971. pages 26
- [69] B. Gyarmati, F. Krisztinkovics, and T. Vertse. On the expectation value in gamow state. *Phys. Lett. B*, 41:110, 1972. pages 33
- [70] T. Berggren. On the interpretation of complex cross sections for production of resonant final states. *Phys. Lett. B*, 73:389, 1978. pages 33
- [71] T. Berggren. Expectation value of an operator in a resonant state. *Phys. Lett. B*, 373:1, 1996. pages 33
- [72] L. C. Biedenharn and H. Van Dam. *Quantum theory of angular momentum : a collection of reprints and original papers*. New York : Academic Press, 1965. pages 39
- [73] I. S. Gradshteyn and I. M. Ryzhik. *Table of Integrals Series and Products*. Academic Press Inc., 4th edition, 1963. pages 39, 43

- [74] M. Abramowitz and I. A. Stegun. *Handbook of mathematical functions*. Dover Publications, Inc., New York, 1972. pages 39, 50
- [75] G. Tiktopoulos. Euclidean approach to the bethe-salpeter equation for scattering. *Phys. Rev.*, 136:275, 1964. pages 41
- [76] J. Nuttall. Analytic continuation of the off-energy shell scattering amplitude. *J. Math. Phys.*, 8:873, 1966. pages 41, 65
- [77] J. Nuttall. Contour distortions in relativistic three-particle scattering functions. *Phys. Rev.*, 160:1459, 1967. pages 41
- [78] G. C. Wick. Properties of bethe-salpeter wave functions. *Phys. Rev.*, 96:1124, 1954. pages 41
- [79] T. Berggren. On the treatment of resonant final states in direct reactions. *Nucl. Phys. A*, 169:353, 1971. pages 43
- [80] I. Bar-On and V. Ryaboy. Fast diagonalization of large and dense complex symmetric matrices, with applications to quantum reaciton dynamics. *Scientific Computing*, 44:1412, 1997. pages 43
- [81] I. Bar-On and M. Paprzycki. An efficient algorithm for finding eigenvalues of complex symmetric matrices. *Computer Assisted Mechanics and Engineering Sciences*, 5:85, 1998. pages 43
- [82] I. Bar-On and M. Paprzycki. High performance solution of the complex symmetric eigenproblem. *Numerical Algorithms*, 18:195, 1998. pages 43
- [83] L.S. Ferreira, E. Maglione, and R. J. Liotta. Nucleon resonances in deformed nuclei. *Phys. Rev. Lett.*, 78:1640, 1997. pages 46
- [84] K. Hagino and Nguyen Van Giai. Structure of positive energy states in a deformed mean-field potential. *Nucl. Phys. A*, 735:55, 2004. pages 46
- [85] L. P. Kok and H. van. Haeringen. On the theory of complex potential scattering. *Ann. of Phys.*, 131:426, 1981. pages 56
- [86] T. Vertse, P. Curutchet, R. J. Liotta, and J. Bang. On the role of anti-bound states in the rpa description of the giant monopole resonance. *Acta Physica Hungaria*, 65:305, 1989. pages 62
- [87] T. Vertse, R. J. Liotta, and E. Maglione. Exact and approximate calculation of giant resonances. *Nucl. Phys. A*, 584:13, 1995. pages 62
- [88] R.F. Bishop, M. R. Strayer, and J. M. Irvine. Singularities in the galitskii-feynmann t matrix. *Phys. Rev. A*, 10:2423, 1974. pages 67, 69

- [89] R.F. Bishop, H. B. Ghassib, and M. R. Strayer. Composite pairs and effective two-body scattering in a many-body medium. *Phys. Rev. A*, 13:1570, 1976. pages 67
- [90] M. I. Haftel and F. Tabakin. Nuclear saturation and smoothness of nucleon-nucleon potentials. *Nucl. Phys. A*, 158:1, 1970. pages 68
- [91] A. Goldberg and R. D. Puff. Bose condensation of fermion composites. *Phys. Rev. Lett.*, 30:869, 1973. pages 68
- [92] W. H. Dickhoff. Connection between brueckner ladders and pairing correlations. *Phys. Lett. B*, 210:15, 1988. pages 68, 73
- [93] W. H. Dickhoff, C. C. Gearhart, B. E. Vonderfecht, A. Polls, and A. Ramos. A new state of nuclear matter. *Recent Progress in Many-Body Theories*, 2:141, 1990. pages 68, 73
- [94] B. E. Vonderfecht, C.C. Gearhart, and W. H. Dickhoff. Bound pair states in nuclear matter. *Phys. Lett. B*, 253:1, 1991. pages 68, 73
- [95] A. Ramos, A. Polls, and W. H. Dickhoff. Single-particle properties and short-range correlations in nuclear matter. *Nucl. Phys. A*, 503:1, 1989. pages 71
- [96] R. Machleidt. The high-precision, charge-dependent bonn nucleon-nucleon potential (cd-bonn). *Phys. Rev. C*, 63:024001, 2001. pages 73, 107, 108, 111
- [97] D.J. Dean and M. Hjorth-Jensen. Pairing in nuclear systems: from neutron stars to finite nuclei. *Rev. Mod. Phys.*, 75:607, 2003. pages 73
- [98] R. R. Whitehead, A. Watt, B. J. Cole, and I. Morrison. *Adv. Nucl. Phys.*, 9:123, 1977. pages 81
- [99] K. Suzuki and S. Y. Lee. Convergent theory for effective interaction in nuclei. *Progr. Theor. Phys.*, 64:2091, 1980. pages 88, 90, 105
- [100] K. Suzuki. Construction of hermitian effective interaction in nuclei — general relation between hermitian and non-hermitian forms —. *Progr. Theor. Phys.*, 68:246, 1982. pages 88, 105
- [101] K. Suzuki and R. Okamoto. Effective operators in time-independent approach. *Progr. Theor. Phys.*, 93:905, 1995. pages 88, 105
- [102] S. Fujii, E. Epelbaum, H. Kamada, R. Okamoto, K. Suzuki, and W. Glöckle. Low-momentum nucleon-nucleon interaction and its application to few-nucleon systems. *Phys. Rev. C*, 70:024003, 2004. pages 88, 105
- [103] Jason D. Holt, T.T.S. Kuo, and G.E. Brown. Family of hermitian low-momentum nucleon interactions with phase shift equivalence. *Phys. Rev. C*, 69:034329, 2004. pages 90, 92

- [104] R. Okamoto, S. Fujii, and K. Suzuki. Formal relation among various hermitian and non-hermitian effective interactions. *Int. J. Mod. Phys. E*, 14:1, 2005. pages 90, 92
- [105] S. Okubo. unknown. *Prog. Theor. Phys.*, 12:603, 1954. pages 92
- [106] N. J. Higham. Stable iterations for the matrix square root. *Num. Algorithms*, 15:227, 1997. pages 93
- [107] E. D. Denman and A. N. Beavers. The matrix sign function and computations in systems. *Appl. Math. Comput.*, 2:63, 1976. pages 93
- [108] C. Butth, R. Santra, and L. S. Cederbaum. Non-hermitian rayleigh-schrdinger perturbation theory. *Phys. Rev. A*, 69:032505, 2004. pages 94
- [109] F. Chen, E. R. Davidson, and S. Iwata. New time-independent perturbation theory for the multireference problem. *Int. J. Quantum Chem.*, 86:256, 2002. pages 94
- [110] R. Santra and L. S. Cederbaum. Non-hermitian electronic theory and applications to clusters. *Phys. Rep.*, 368:1, 2002. pages 94
- [111] M. Hjorth-Jensen, Thomas T. S. Kuo, and Eivind Osnes. Realistic effective interactions for nuclear systems. *Phys. Rep.*, 261:125, 1995. pages 96, 106
- [112] P. J. Ellis and E. Osnes. An introductory guide to effective operators in nuclei. *Rev. Mod. Phys.*, 49:777, 1977. pages 96
- [113] B. H. Brandow. Linked-cluster expansions for the nuclear many-body problem. *Rev. Mod. Phys.*, 39:771, 1967. pages 96
- [114] K. A. Brueckner. Many-body problem for strongly interacting particles. ii. linked cluster expansion. *Phys. Rev.*, 100:36, 1955. pages 97
- [115] E. R. Davidson, E. Engdahl, and N. Moiseyev. New bounds to resonance eigenvalues. *Phys. Rev. A*, 33:2436, 1986. pages 101
- [116] Scott Bogner, T. T. S. Kuo, L. Coraggio, A. Covello, and N. Itaco. Low momentum nucleon-nucleon potential and shell model effective interactions. *Phys. Rev. C*, 65:051301, 2002. pages 106, 109
- [117] S. Fujii, E. Epelbaum, H. Kamada, R. Okamoto, K. Suzuki, and W. Glöckle. Low-momentum nucleon-nucleon interaction and its application to the few-nucleon systems. *Phys. Rev. C*, 70:024003, 2004. pages 106, 109, 111
- [118] S. Fujii, H. Kamada, R. Okamoto, and K. Suzuki. Dependence of nuclear binding energies on the cutoff momentum of low-momentum nucleon-nucleon interaction. *nucl-th*, page 0406082, 2004. pages 106, 111
- [119] Andreas Nogga, Scott K. Bogner, and Achim Schwenk. Low-momentum interaction in few-nucleon systems. *Phys. Rev. C*, 70:061002, 2004. pages 106, 111

Appendix A

Left and right eigenvectors and bi-orthogonal sets.

Given the eigenvalue equation,

$$A^T y = \lambda y, \quad (\text{A.1})$$

where the $n \times n$ matrix A^T is of general form, and T indicates transposition. The eigenvalues λ are determined by the characteristic equation,

$$\det(A^T - \lambda I) = \det(A - \lambda I) = 0, \quad (\text{A.2})$$

which shows that the eigenvalues of A^T are the same as those of A . Consider the eigenvalue equation for the i 'th eigenvector,

$$A^T y_i = \lambda_i y_i, \quad (\text{A.3})$$

then the transpose of this equation gives,

$$y_i^T A = \lambda_i y_i^T, \quad (\text{A.4})$$

here y_i^T is the left eigenvector of A corresponding to the eigenvalue λ_i . The eigenvalue equation for A is

$$Ax_j = \lambda_j x_j, \quad (\text{A.5})$$

where it is seen that x_j is the right eigenvector of the matrix A corresponding to the eigenvalue λ_j . Now multiply Eq. (A.4) with x_j from the right and Eq. (A.5) with y_i^T from the left, and subtract to obtain,

$$\lambda_j y_i^T x_j = \lambda_i y_i^T x_j, \quad (\text{A.6})$$

$$\Rightarrow (\lambda_j - \lambda_i) y_i^T x_j = 0, \quad (\text{A.7})$$

$$\Rightarrow y_i^T x_j = 0 \text{ if } \lambda_i \neq \lambda_j, \quad (\text{A.8})$$

where it is customary to say that the left y_i^T and right x_j eigenvectors of a matrix A are *bi-orthogonal* to each other. If all n eigenvalues of the matrix A are distinct, then $y_i^T x_j = 0$

for $i, j = 1, 2, \dots, n$, $i \neq j$, but $y_i^T x_i \neq 0$. This implies that the right and left eigenvectors can be scaled so they form a complete set of *bi-orthogonal* vectors.

$$Y^T X = 1. \quad (\text{A.9})$$

Here Y^T is a matrix whose rows are $y_i^T, i = 1, \dots, n$ and X is a matrix whose columns are $x_i, i = 1, \dots, n$, and $y_i^T x_j = \delta_{i,j}$. This shows explicitly that Y^T is the inverse of X . It is clear that this works for any matrix which has a complete set of linearly independent eigenvectors (a nondefective matrix) regardless of whether the eigenvalues are distinct. As we have seen before, we can write in this case

$$X^{-1} A X = \text{diag} [\lambda_i].$$

Indeed, if we can find any matrix Z such that $Z^{-1} A Z$ is diagonal, then the columns of Z are the right eigenvectors of A , and the rows of Z^{-1} are the left eigenvectors of A , while the diagonal entries of $Z^{-1} A Z$ are the eigenvalues of A . Defective matrices have an incomplete set of eigenvectors, and the theory requires their reduction to Jordan normal form.

In the special case of A being a complex symmetric matrix, which is often the case in physical applications, then the left eigenvectors are just the transpose of the right eigenvectors. In this case it is sufficient to solve the right eigenvalue equation, and a complete set of *bi-orthogonal* vectors are obtained directly.

Appendix B

Three-body matrix elements in $j-j$ coupling

Throughout this section the anti-symmetric three- and two-body wave functions are written as $\bar{\Psi}$ and $\bar{\Phi}$ respectively, while the non-anti-symmetrized functions are without the bar. The single-particle wave functions are given by ϕ . The anti-symmetric three-body wave function may be written

$$\bar{\Psi}_{(ab)c}^{JM}(123) = \frac{1}{\sqrt{3}} \{ \Psi_{(ab)c}^{JM}(123) - \Psi_{(ab)c}^{JM}(132) + \Psi_{(ab)c}^{JM}(231) \}, \quad (\text{B.1})$$

here $(ab)c$ labels all relevant single particle quantum numbers $a = n_a, l_a, j_a$, and the coupling rule $(j_a \otimes j_b)_{J_{ab}} \otimes j_c$ is indicated. The wave function in equation (B.1) is anti-symmetric only in case where at least two of the orbits abc are different. In the case $a = b = c$ one has to make use of coefficients of fractional parentage to make the three-body wave function anti-symmetric. The non anti-symmetrized wave functions $\Psi_{(ab)c}^{JM}(123)$ are given by

$$\Psi_{(ab)c}^{JM}(123) = \left[\bar{\Phi}_{ab}^{J_{ab}}(12) \otimes \phi_c(3) \right]_{JM}. \quad (\text{B.2})$$

Here $\bar{\Phi}_{ab}^{J_{ab}}(12)$ is an anti-symmetric two-particle wave function.

$$\bar{\Phi}_{ab}^{J_{ab}}(12) = \frac{1}{\sqrt{2(1 + \delta_{ab})}} \sum_{m_a, m_b} \langle j_a m_a, j_b m_b | J_{ab} M_{ab} \rangle (\phi_a(1)\phi_b(2) - \phi_a(2)\phi_b(1)). \quad (\text{B.3})$$

In the following derivation the total spin and projection JM will be suppressed for notational economy.

Consider a matrix element of the three-body wave function in equation (B.1) with a general interaction consisting of only two-body terms $V = V_{12} + V_{13} + V_{23}$.

$$\langle \bar{\Psi}_{(ab)c}(123) | V | \bar{\Psi}_{(de)f}(123) \rangle = \quad (\text{B.4})$$

$$\frac{1}{\sqrt{3}} \langle \Psi_{(ab)c}(123) - \Psi_{(ab)c}(132) + \Psi_{(ab)c}(231) | V | \bar{\Psi}_{(de)f}(123) \rangle, \quad (\text{B.5})$$

from the anti-symmetry follows

$$\langle \Psi_{(ab)c}(123) | V | \bar{\Psi}_{(de)f}(123) \rangle = \langle -\Psi_{(ab)c}(131) | V | \bar{\Psi}_{(de)f}(123) \rangle \quad (\text{B.6})$$

$$= \langle \Psi_{(ab)c}(231) | V | \bar{\Psi}_{(de)f}(123) \rangle, \quad (\text{B.7})$$

and henceforth

$$\langle \bar{\Psi}_{(ab)c}(123) | V | \bar{\Psi}_{(de)f}(123) \rangle = \sqrt{3} \langle \Psi_{(ab)c}(123) | V | \bar{\Psi}_{(de)f}(123) \rangle = \quad (\text{B.8})$$

$$\langle \Psi_{(ab)c}(123) | V_{12} | \Psi_{(de)f}(123) - \Psi_{(de)f}(132) + \Psi_{(de)f}(231) \rangle + \quad (\text{B.9})$$

$$2 \langle \Psi_{(ab)c}(123) | V_{23} | \Psi_{(de)f}(123) - \Psi_{(de)f}(132) + \Psi_{(de)f}(231) \rangle. \quad (\text{B.10})$$

Starting with the matrix element of V_{12} , one has

$$\langle \Psi_{(ab)c}(123) | V_{12} | \Psi_{(de)f}(123) - \Psi_{(de)f}(132) + \Psi_{(de)f}(231) \rangle = V_{12}^1 + V_{12}^2 + V_{12}^3, \quad (\text{B.11})$$

where

$$V_{12}^1 = \langle ab | V_{12} | de \rangle_{J_{ab}}^{AS} \delta_{c,f} \delta_{J_{ab}, J_{de}}, \quad (\text{B.12})$$

and

$$V_{12}^2 + V_{12}^3 = \langle \Psi_{(ab)c}(123) | V_{12} | - (\Psi_{(de)f}(132) - \Psi_{(de)f}(231)) \rangle, \quad (\text{B.13})$$

recoupling $1, 3 \rightarrow 1, 2$ in $\Psi_{(de)f}(132)$ and $2, 3 \rightarrow 2, 1$ in $\Psi_{(de)f}(231)$ one may show by angular momentum algebra that

$$- (\Psi_{(de)f}(132) - \Psi_{(de)f}(231)) = \quad (\text{B.14})$$

$$\left(\frac{1 + \delta_{d,f}}{1 + \delta_{d,e}} \right)^{1/2} \sum_{J_{df}} (-1)^{j_d + J_{df} - J_{de} - J} U(j_e j_d J j_f; J_{de} J_{df}) \Psi_{(df)e}(123) \quad (\text{B.15})$$

$$- \left(\frac{1 + \delta_{e,f}}{1 + \delta_{d,e}} \right)^{1/2} \sum_{J_{ef}} (-1)^{j_d + J_{ef} - J} U(j_d j_e J j_f; J_{de} J_{ef}) \Psi_{(ef)d}(123), \quad (\text{B.16})$$

here $U(j_a j_b J j_c; J_{ab} J_{bc})$ are the normalized Racah coefficients. It follows that the terms V_{12}^2 and V_{12}^3 are given by

$$V_{12}^2 = \left(\frac{1 + \delta_{d,f}}{1 + \delta_{d,e}} \right)^{1/2} \sum_{J_{df}} (-1)^{j_d + J_{df} - J_{de} - J} U(j_e j_d J j_f; J_{de} J_{df}) \times \langle ab | V_{12} | df \rangle_{J_{ab}}^{AS} \delta_{c,e} \delta_{J_{ab}, J_{df}} \quad (\text{B.17})$$

$$V_{12}^3 = - \left(\frac{1 + \delta_{e,f}}{1 + \delta_{d,e}} \right)^{1/2} \sum_{J_{ef}} (-1)^{j_d + J_{ef} - J} U(j_d j_e J j_f; J_{de} J_{df}) \times \langle ab | V_{12} | ef \rangle_{J_{ab}}^{AS} \delta_{c,d} \delta_{J_{ab}, J_{ef}}. \quad (\text{B.18})$$

Calculating the matrix element of V_{23} one first recouple $1, 2 \rightarrow 2, 3$ in the $\langle \text{bra} |$.

$$\Psi_{(ab)c}(123) = \left(\frac{1}{2(1 + \delta_{a,b})} \right) \times \quad (\text{B.19})$$

$$\left\{ \sum_{J_{bc}} (-1)^{j_a + J_{bc} - J} U(j_a j_b J j_c; J_{ab} J_{bc}) \Psi \left(\Phi_{bc}^{J_{bc}}(23) \phi_a(1) \right) + \right. \quad (\text{B.20})$$

$$\left. \sum_{J_{ac}} (-1)^{j_a - J_{ab} + J_{ac} - J} U(j_b j_a J j_c; J_{ab} J_{ac}) \Psi \left(\Phi_{ac}^{J_{ac}}(23) \phi_b(1) \right) \right\}, \quad (\text{B.21})$$

here $\Phi_{bc}^{J_{bc}}$ and $\Phi_{ac}^{J_{ac}}$ are non anti-symmetric two-body wave functions. Anti-symmetric two-body matrix elements may be expressed in terms non anti-symmetric matrix elements by

$$\langle \bar{\Phi}_{ab}(12) | V_{12} | \bar{\Phi}_{cd}(12) \rangle = \left(\frac{2}{(1 + \delta_{ab})} \right)^{1/2} \langle \Phi_{ab}(12) | V_{12} | \bar{\Phi}_{cd}(12) \rangle. \quad (\text{B.22})$$

Evaluating the matrix element of V_{23} one has to evaluate the following matrix elements

$$\langle \Psi_{(bc)a}(231) | V_{23} | \Psi_{(de)f}(123) - \Psi_{(de)f}(132) + \Psi_{(de)f}(231) \rangle, \quad (\text{B.23})$$

and

$$\langle \Psi_{(ac)b}(231) | V_{23} | \Psi_{(de)f}(123) - \Psi_{(de)f}(132) + \Psi_{(de)f}(231) \rangle, \quad (\text{B.24})$$

which are evaluated in the same manner as the evaluation of V_{12} in equation (B.11). After some angular momentum recoupling algebra in the $| \text{ket} \rangle$, one ends up with the final expressions

$$\begin{aligned} \langle \bar{\Psi}_{(ab)c}(123) | V | \bar{\Psi}_{(de)f}(123) \rangle &= \langle ab | V_{12} | de \rangle_{J_{ab}}^{AS} \delta_{c,f} \delta_{J_{ab}, J_{de}} + \\ &\left(\frac{1 + \delta_{d,f}}{1 + \delta_{d,e}} \right)^{1/2} (-1)^{j_d - J_{de} + J_{ab} - J} U(j_e j_d J j_f; J_{de} J_{ab}) \langle ab | v | df \rangle_{J_{ab}}^{AS} \delta_{c,e} - \\ &\left(\frac{1 + \delta_{e,f}}{1 + \delta_{d,e}} \right)^{1/2} (-1)^{j_d + J_{ab} - J} U(j_d j_e J j_f; J_{de} J_{ab}) \langle ab | v | ef \rangle_{J_{ab}}^{AS} \delta_{c,d} + \\ &\left(\frac{1 + \delta_{b,c}}{1 + \delta_{a,b}} \right)^{1/2} (-1)^{j_a + J_{de} - J} U(j_a j_b J j_c; J_{ab} J_{de}) \langle bc | v | de \rangle_{J_{de}}^{AS} \delta_{a,f} + \\ &\left(\frac{1 + \delta_{b,c}}{1 + \delta_{a,b}} \right)^{1/2} \sum_{J_{bc}} (-1)^{j_a + j_d - 2J} U(j_a j_b J j_c; J_{ab} J_{bc}) \times \\ &\left\{ \left(\frac{1 + \delta_{d,f}}{1 + \delta_{d,e}} \right)^{1/2} (-1)^{J_{de}} U(j_e j_d J j_f; J_{de} J_{bc}) \langle bc | v | df \rangle_{J_{bc}}^{AS} \delta_{a,e} + \right. \\ &\left. \left(\frac{1 + \delta_{e,f}}{1 + \delta_{d,e}} \right)^{1/2} U(j_d j_e J j_f; J_{de} J_{bc}) \langle bc | v | ef \rangle_{J_{bc}}^{AS} \delta_{a,d} \right\} + \end{aligned}$$

$$\begin{aligned}
& \left(\frac{1 + \delta_{a,c}}{1 + \delta_{a,b}} \right)^{1/2} (-1)^{j_a - J_{ab} + J_{de} - J} U(j_b j_a J j_c; J_{ab} J_{de}) \langle ac | v | de \rangle_{J_{de}}^{AS} \delta_{b,f} + \\
& \left(\frac{1 + \delta_{a,c}}{1 + \delta_{a,b}} \right)^{1/2} \sum_{J_{ac}} (-1)^{j_a + j_d - J_{ab} - 2J} U(j_b j_a J j_c; J_{ab} J_{ac}) \times \\
& \left\{ \left(\frac{1 + \delta_{d,f}}{1 + \delta_{d,e}} \right)^{1/2} (-1)^{J_{de}} U(j_e j_d J j_f; J_{de} J_{ac}) \langle ac | v | df \rangle_{J_{ac}}^{AS} \delta_{b,e} + \right. \\
& \left. \left(\frac{1 + \delta_{e,f}}{1 + \delta_{d,e}} \right)^{1/2} U(j_d j_e J j_f; J_{de} J_{ac}) \langle ac | v | ef \rangle_{J_{ac}}^{AS} \delta_{b,d} \right\}. \quad (B.25)
\end{aligned}$$

In the case $a = b = d = e \neq c = f$ and $J_{ab} = J_{aa}, J_{de} = J'_{aa}$ are even, equation (B.25) simplifies to

$$\begin{aligned}
& \langle \bar{\Psi}_{(aa)c}(123) | V | \bar{\Psi}_{(aa)c}(123) \rangle = \langle aa | v | aa \rangle_{J_{aa}}^{AS} \delta_{J_{aa}, J'_{aa}} + \\
& 2 \sum_{J_{ac}} (2J_{ac} + 1) \sqrt{(2J_{aa} + 1)(2J'_{aa} + 1)} \left\{ \begin{array}{ccc} j_a & j_a & J_{aa} \\ j_c & J & J_{ac} \end{array} \right\} \left\{ \begin{array}{ccc} j_a & j_a & J'_{aa} \\ j_c & J & J_{ac} \end{array} \right\} \langle ac | v | ac \rangle_{J_{ac}},
\end{aligned}$$

where the normalized Racah coefficients are expressed in terms of $6 - j$ symbols. Next consider the case where all the single particle orbits in the ket are equivalent, i.e. $d = e = f$, in this case one has to make a coefficients of fractional parentage expansion to make the three-body wave function totally anti-symmetric in the $j - j$ coupling scheme;

$$\bar{\Psi}_{ddd}(123) = \sum_K \langle j_d^2 K, j_d | \} j_d^3 J \rangle \Psi_{(dd)d}(123). \quad (B.26)$$

In this way the wave function is expressed in terms of anti-symmetric two-particle wave functions, and one may proceed in the same manner as for the case considered above. After some angular momentum recouplings, one ends up with the final expression for the matrix element,

$$\begin{aligned}
& \langle \bar{\Psi}_{(ab)c}(123) | V | \bar{\Psi}_{(dd)d}(123) \rangle = \sqrt{3} \langle j_d^2 J_{ab}, j_d | \} j_d^3 J \rangle \langle ab | v | dd \rangle_{J_{ab}}^{AS} \delta_{c,d} + \\
& \sqrt{3} (-1)^{j_a + j_d - 2J} \sum_K \langle j_d^2 K, j_d | \} j_d^3 J \rangle \times \\
& \left\{ \left(\frac{1 + \delta_{b,c}}{1 + \delta_{a,b}} \right)^{1/2} \sum_{J_{bc}} U(j_a j_b J j_c; J_{ab} J_{bc}) U(j_d j_d J j_d; K J_{bc}) \langle bc | v | dd \rangle_{J_{bc}} \delta_{a,d} + \right. \\
& \left. \left(\frac{1 + \delta_{a,c}}{1 + \delta_{a,b}} \right)^{1/2} \sum_{J_{ac}} (-1)^{J_{ab}} U(j_b j_a J j_c; J_{ab} J_{ac}) U(j_d j_d J j_d; K J_{ac}) \langle ac | v | dd \rangle_{J_{bc}} \delta_{b,d} \right\}. \quad (B.27)
\end{aligned}$$